Study on the Mode of Action of Marine Natural Product Aplyronine A by Using Novel Chemical Probes

Kozo YONEDA

February 2016

Study on the Mode of Action of Marine Natural Product Aplyronine A by Using Novel Chemical Probes

Kozo YONEDA

Doctoral Program in Chemistry

Submitted to the Graduate School of

Pure and Applied Sciences

in Partial Fulfillment of the Requirements

for the Degree of Doctor of Philosophy in

Science

at the

University of Tsukuba

Acknowledgment

My current and past associates in Kigoshi group:

Dr. Takayuki Ohoyoshi

Dr. Kenichi Kobayashi

Dr. Yosuke Sato

Dr. Takuma Takemura

Mr. Tomoya Ishitsuka

Mr. Yuta Ebihara

Ms. Yumi Ochiai

Mr. Nozomi Ogihara

Ms. Miyuki Sugiyama

Mr. Keisuke Tomita

Dr. Yuichiro Hirayama

Mr. Yamato Miyazawa

Mr. Takuya Yamada

Dr. Baro Gise

Mr. Akihiro Usui

Mr. Yuto Onozaki

Mr. Shinichi Kobayashi

Ms. Yuki Saito

Mr. Satoshi Tanabe

Mr. Eri Yaguchi

Mr. Yuhsuke Sakai

Mr. Koichi Takeno

Mr. Ryosuke Fujisawa

Mr. Shota Funakubo

Ms. Mami Shimanuki

Mr. Yuhei Sone

Mr. Masaki Tsunoda

Mr. Tomomi Nakamura

Mr. Keisuke Niida

Ms. Maiko Matsuki

Ms. Sachiko Matsumoto

Mr. Satoru Inomata

Mr. Ogura Tomotaka

Mr. Takahiro Kaneko

Mr. Kizuku Kimura

Mr. Shuya Shioda

Mr. Kenta Tanabe

Mr. Kota Tsuchiya

Mr. Masahiro Hida

Ms. Miho Komai

Dr. Yuko Kato

Mr. Hirotaka Oka

Mr. Atsushi Kawamura

Mr. Ryo Nakajima

Mr. Kota Yamagishi

Mr. Seiji Ogawa

Mr. Atsuhiro Takano

Mr. Keita Saito

Mr. Kazuaki Suzuki

Mr. Taiki Sunaba

Mr. Kentaro Futaki

Mr. Fumitaka Ichimura

Mr. Masami Okamura

Mr. Yu Seguchi

Ms. Ayaka Taniguchi

Mr. Shun Watanabe

Ms. Yaping Hu

Ms. Mayu Namiki

Ms. Momoko Takahashi

Mr. Hiroki Nakane

Mr. Rei Watanabe

Mr. Hikaru Tano

Graduate School of Pure and Applied Sciences

University of Tsukuba

February 2014

Kozo Yoneda

Table of Contents

List of Abbreviation

Ac	acetyl	F-actin	fibrous actin
ADP	adenosine diphosphate	FBS	fetal bovine serum
ApA	aplyronine A	FCM	flow cytometry
ApC	aplyronine C	FKBP	FK506-binding protein
AP	alkyl-linker photoaffinity pyrene probe	FL	fluorescent probe
Apy-Su	amidopyrene succinate	G-actin	globular actin
aq	aqueous	GFP	green fluorescent protein
Arp	actin-related protein	GTP	guanosine triphosphate
ATP	adenosine triphosphate	HBSS	hanks balanced saline solution
Boc	*tert*-butoxycarbonyl	HOBt	1-hydroxy-benzotriazol
BODIPY	boron-dipyrromethene	HPLC	high performance liquid chromato-
BRB80	Brinkley Rassembly Buffer 80		graphy
BSA	bovine serum albumin	HRMS	high resolusion mass spectrometry
CBB	Coomassie brilliant blue	HRP	horseradish peroxidase
CHCA	α-cyano-4-hydroxycinnamic acid	HU	hydroxyurea
CyD	cytochalasin D	IC_{50}	inhibitory concentration 50%
DAPI	4',6-diamidino-2-phenylindole	ICT	intramolecular charge transfer
DIPEA	*N,N*-diisopropylethylamine	I.D.	internal diameter
DMF	dimethylformamide	IgG	immunoglobulin G
DMSO	dimethylsulfoxide	IR	infrared spectroscopy
DNA	deoxyribonucleic acid	LaA	latrunculin A
DTT	dithiothreitol	LA-LDI	label-assisted laser
EBV	Epstein-barr virus		desorption/ionization
EC_{50}	effective concentration 50%	MALDI	matrix-assisted laser
EDC	*N*-(3-dimethylaminopropyl)-*N'*-		desorption/ionization
	ethylcarbodiimide	Me	methyl
EDTA	ethylenediaminetetraacetic acid	MS	mass spectrometry
EGFP	enhanced green fluorescence protein	MTT	3-(4,5-dimethyl-2-thiazolyl)-2,5-
EGTA	ethyleneglycoltetraacetic acid		diphenyltetrazolium bromide
E-MEM	eagle's minimal essential medium	MyB	mycalolide B
ESI	electrospray ionization	NHS	*N*-hydroxy succinimide
Et	ethyl	NMR	nuclear magnetic resonance

ODS	octadodecylsilyl	PP	PEG-linker photoaffinity pyrene probe
PAGE	polyacrylamide gel electrophoresis	PPI	protein-protein interaction
PAH	polycyclic aromatic hydrocarbon	SDS	sodium dodecyl sulfate
PaP	PEG-linker photoaffinity amidopyrene probe	SLF	synthetic ligand of FKBP
		S/N	signal-to-noise
PB	photoaffinity biotin probe	TAMRA	tetramethylrhodamine
PBS	phosphate buffered saline	T/C	test/control
PBS-T	PBS containing 0.1 % Tween 20	TFA	trifluoroacetic acid
PEG	polyethylene glycol	TOF	time of flight
Phth	phthalimide	Tris	tris(hydroxymethyl)amino-methane
PIPES	piperazine-N,N'-bis (2-ethane-sulfonic acid)	UV	ultraviolet
		Vis	visible
PET	photoinduced electron transfer	WB	Western blotting
PMF	peptide mass fingerprinting	w/w	wet weight
pNA	paranitroaniline		

Chapter 1. General introduction

1-1. Natural Product Chemistry and Drug Discovery

Natural products chemistry is the study that includes the purification of bioactive compounds produced by living organisms, the determination of their structures, syntheses, and the clarification of their modes of action. The products of living organisms are distinguished between primary metabolites and secondary metabolites. Primary metabolites are essential and universally existed in living organisms, such as amino acids, sugars, lipids and nucleic acids. Secondary metabolites are the compounds produced by specific biological reactions of living organisms, such as terpenoides, steroids and polyphenols, and are advantageous to survive or control the living system of another species.

Achievements in natural products chemistry have been applied for our lives. Especially, secondary metabolites have been used as medicinal drugs from a long time ago.[1] For example, penicillin isolated from *Penicillium* in 1928, is utilized as an antibiotic, and morphine isolated from opium in 1806 as an analgesic drug (Figure 1-1).
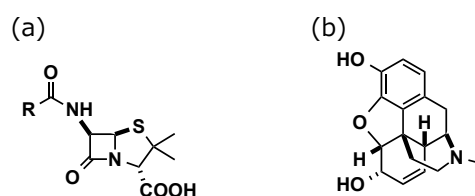
Figure 1-1. Natural products applied for medicinal drugs. (a) The core structure of penicillin, "R" is the variable group. (b) Structure of morphine.

Recently, natural products obtained from marine organisms, such as sponge, sea squirt, nudibranch and microorganism, have been focused as well as those from terrestrial organisms, such as fungi and plants. Marine covers over the 70% of earth's surface, and abundant variety of living organisms live there. The environment of marine remarkably differs from the terrestrial one. To adapt this environment, marine organisms have developed different metabolic and defense systems from terrestrial ones. Therefore, secondary metabolites produced by marine organisms are expected to have unique structures and interesting bioactivity, which is not found in the compounds obtained from terrestrial organisms.

Actually, many researchers have conducted the study on drug discovery of various marine natural products, and some of them are currently used as drugs. Examples are described as follow (Figure 1-2). Conotoxin[2], isolated from a cone snail, is neurotoxic at high concentration, but shows more analgesic effect than morphine at low concentration. Conotoxin is a general term of several structural isomers. One of them is referred as ziconotide, and was approved in 2004 as the useful drug for pain relief without addiction. Holotoxin[3], isolated from a sea cucumber, shows antifungal activity, and is used as the treatment of trichophytosis. Compared with antibacterial drugs, antifungal drug with high selectivity is rare because the cell components of fungus are more similar to those of human than bacteria. The case of holotoxin indicates that marine natural product is also useful for antifungal drug, which is generally difficult to be developed.

(a)

H–Cys–Lys–Gly–Lys–Gly–Ala–Lys–

Cys–Ser–Arg–Leu–Met–Tyr–Asp–

Cys–Cys–Thr–Gly–Ser–Cys–Arg–

Ser–Gly–Lys–Cys–NH₂

Conotoxin
Analgetic drug

(b)

Holotoxin
Antifungal drug
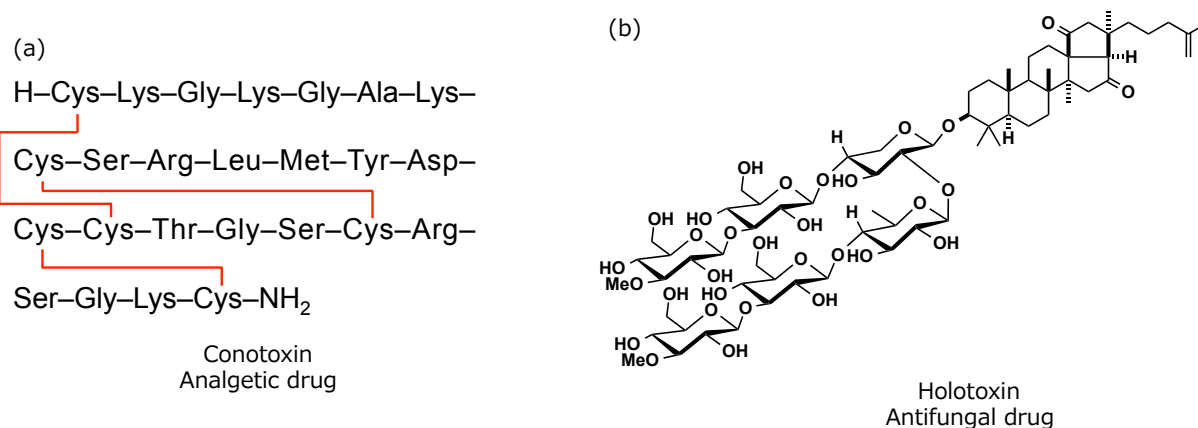
Figure 1-2. Medicinal drugs from marine origin. (a) Sequence of conotoxin (ziconotide), red lines show disulfide bonds. (b) Structure of holotoxin.

Halichondrin B[4] (Figure 1-3a), isolated from the marine sponge *Halichondria okadai* by Hirata and Uemura group, is a microtubule-targeting compound, and was recently applied for an antitumor drug. In this case, eribulin[5] (Figure 1-3b), which is an important unit for the bioactivity of halichondrin B, was developed due to the high cost of total synthesis and the tiny isolated amount of natural compound. Eribulin was approved as the therapeutic agent of metastatic breast cancer in 2010. This case indicates that simplifying the structures of natural products is highly important for the development of medicinal drugs.

Thus, marine natural products provide us with considerable benefit, and additional development of marine natural products chemistry is expected.
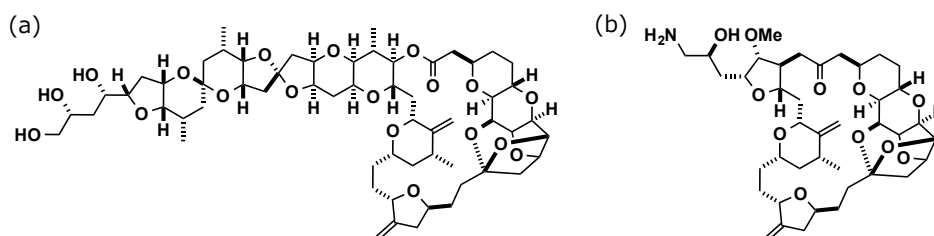
Figure 1-3. Marine natural product applied for antitumor drug. Structures of (a) halichondrin B and (b) eribulin.

1-2. Mode of Action and Target proteins of Natural Products

Recently, the modes of action of natural products that show unique bioactivity, has been focused in order to develop natural product research for medicinal drugs, agrochemicals, and research tools. To clarify their modes of action, information about target proteins, such as cellular localization or effect, are needed to be clarified. As the analytical methods of mode of action studies, there are several biological approaches, such as screening using proteins, cells, and animal disease models, but currently different methods are developing.

For example, Schreiber's group converted a FK506, isolated from *Streptmyces tsukubaensis*[6] and is currently used as an immunosuppressant drug, to the FK506−resin conjugate (Figure 1-4).[7] By using this conjugate, an FK506-binding protein (FKBP) was purified as a target protein from bovine thymus and human spleen. After this report, many researches about the mode of action of FK506 have been reported. And it was clarified that FK506−FKBP complex interacts with calcineurin, which is a calcium-sensitive serine/threonine phosphatase, and the formation of the ternary complex plays critical roles for the immunosuppressant activity of FK506.[8] So, identification of target proteins is important for the analysis of modes of action. Additionally, this case shows that the analytical method using chemical modification is one of the effective methods to search the target molecules of natural products. This approach possibly leads to the discovery of an interesting compound, which shows the novel mode of action.
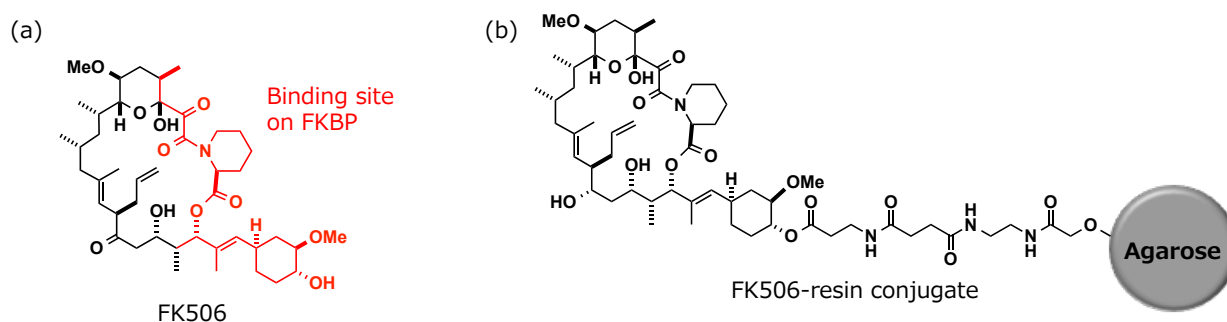
Figure 1-4. Structures of (a) FK506 and (b) the FK506-resin conjugate.

Furthermore, binding mode analysis is important for further development of natural products chemistry. In the case of FK506, binding mode on target proteins was established by X-ray crystallography, and the right-half part of FK506 molecule was found to be important for the interaction with FKBP (Figure 1-4, red line). Based on this information, many artificial analogs, which have the simplified structures of FK506, were synthesized.[9] One of them, SLF (synthetic ligand of FKBP, Figure 1-5), is commercially available and contributes to a number of pharmacological or biological studies on FKBP.
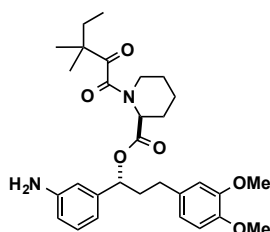
Figure 1-5. Structure of SLF.

It has been shown that important pharmacological tools as well as pharmaceutical lead compounds could be developed by the target identification of natural products and the clarification of their binding modes. Therefore, study on the mode of action of natural products is expected to make impact on medicinal chemistry, agriculture, pharmaceutical sciences, and so on.

1-3. Chemical Biology

Besides molecular biology approach, chemical approach collaborated with biology as described above is recently developing to analyze the mode of action, and this study is referred to chemical biology. "Chemical probes" are widely used as the research tools of chemical biology. In general, they have bioactive compound moieties (ligands), detecting groups, and reacting groups.

For example, chemical probe possessing a fluorescent group as a detecting group is referred as a fluorescent probe, and is generally used for the observation of cellular behavior of the ligand. There are various fluorescent groups, such as coumarin, fluorescein, boron-dipyrromethene (BODIPY), and tetramethylrhodamine (TAMRA) (Figure 1-6).[10] They have different fluorescence property. A typical example of a fluorescent probe is rhodamine-phalloidin that has a TAMRA group (Figure 1-7).[11] This probe utilizes the effect of phalloidin to stabilize cytoskeletal microfilament (actin filament) and is able to stain microfilament. This fluorescent probe is widely available for cellular and molecular biology studies.

Coumarin
Blue fluorescence

Fluorescein
Green fluorescence

BODIPY
Green fluorescence

TAMRA
Red fluorescence
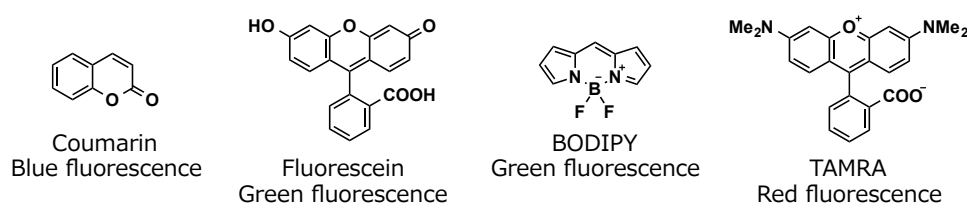
Figure 1-6. Typical fluorescent groups.

Rhodamine-phalloidin

20 μm
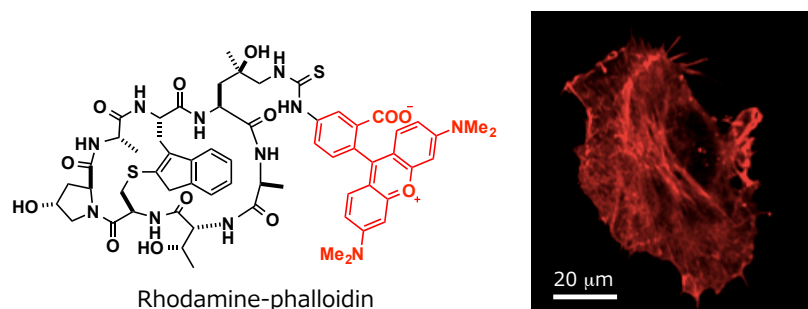
Figure 1-7. Structure of rhodamine-phalloidin (left) and stained actin filament (right).

A chemical probe which has a biotin group as a detecting group is referred as biotin probe, and is available for the affinity purification of target proteins that interact with the ligand moiety by the avidin-loaded resin, because avidin strongly binds to biotin (Figure 1-8a). So, target proteins specifically interact with biotin probe that is pretreated with an avidin resin (Figure 1-8b). After washing the probe−resin conjugate, the target proteins that interact with the ligand moiety can be purified from the protein mixture.
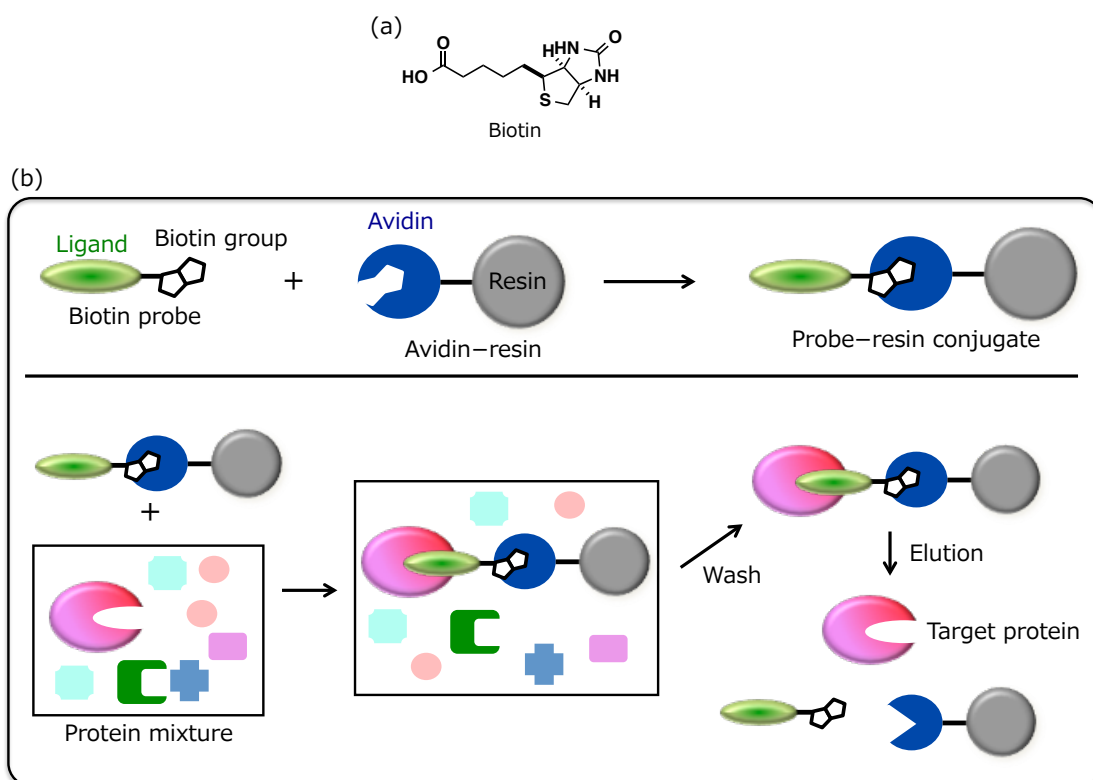
Figure 1-8. Outline of biotin probe. (a) Structure of biotin. (b) Purification method of target proteins by using biotin probe.

Furthermore, a chemical probe that has a reacting group is particularly useful to study the target proteins, in which the interaction with a ligand is weak. The reason is that the reacting group is able to form a stable covalent bond between target protein and chemical probe (Figure 1-9). Various reacting groups have been well developed (Figure 1-10).[12] For example, an *N*-hydroxy succinimide (NHS) ester moiety and a maleimide group are used to form covalent bonds to particular amino acids. The former reacts with the ε-amino group of a lysine residue because the NHS ester easily reacts with primary and secondary amines. The latter reacts with a cysteine residue because the 1,4-addtion of the thiol to the maleimide group occurs. Photoreacting groups, such as benzophenone, azide and diazirine can form covalent bonds with various adjacent molecules because the reacting species (ketyl radical, nitrene and carbene) are generated by UV irradiation. This type of chemical probes possessing a reacting group makes a covalent bond with any adjacent functional groups of the ligand-bound target proteins. So, these chemical probes are applicable for the binding mode analysis of the ligands with the target proteins as well as the identification of target proteins, by analyzing the amino acid residues bound to the reacting groups.
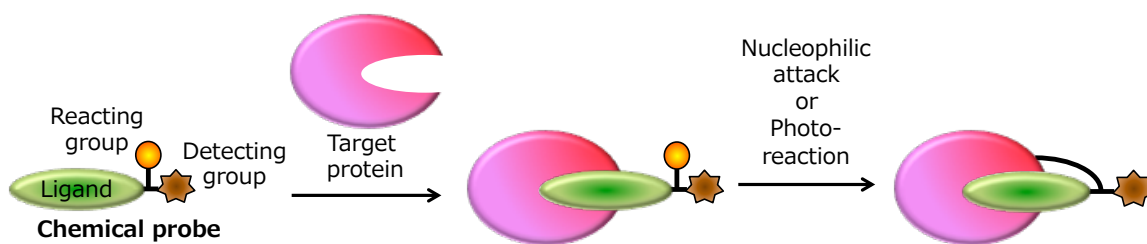
Figure 1-9. Labeling of the target protein by using a chemical probe.
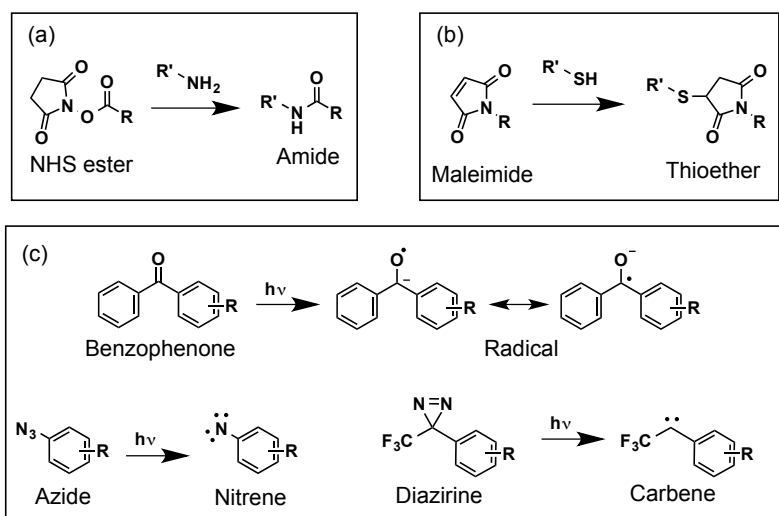
Figure 1-10. Structures and reactions of reacting groups.
(a) NHS ester, (b) maleimide, (c) photoreacting groups.

Thus, chemical probe is a useful tool to analyze the mode of action of bioactive compounds, and has been contributed to the chemical biology research aimed at the drug discovery of natural products.

1-4 Aplyronine A

1-4-1. Isolation and Bioactivities of Aplyronine A

　　　　Development of chemical biology has facilitated the study on the mode of action of various natural products. However, there are a number of natural products whose modes of action are unknown even though they show unique bioactivities. One of the compounds is a marine natural product aplyronine A (ApA, **1**).

　　　　ApA (**1**) is a 24-membered macrolide (Figure 1-11) isolated in 1993 from the Japanese sea hare *Aplysia kurodai* (Figure 1-12).[13] ApA (**1**) has two modified amino acid moieties, *N,N,O*-trimethylserine and *N,N*-dimethylalanine, and the C24-34 side-chain moiety with a terminal *N*-methyl enamide group. ApA (**1**) shows potent cell-growth inhibitory activities against HeLa S3 cells, a human cervical carcinoma cell line (IC$_{50}$ 0.010 nM), and exhibits remarkable antitumor activities *in vivo* against P388 murine leukemia cells (T/C 545%, 0.08 mg/kg) and several cancers (Table 1).[13a] This antitumor activity is more potent than many cancer drugs. Additionally, ApA (**1**) interacts with a cytoskeletal protein, actin, and depolymerizes fibrous actin (F-actin) to globular molecule (G-actin) (EC$_{50}$ 1.6 μM against 3 μM actin). So, the study on the mode of action of ApA is expected to lead to the development of novel cancer drugs targeting actin.
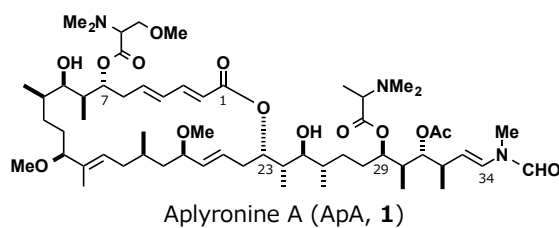
Cell-growth inhibitory activity against HeLa S3 cells	IC$_{50}$ 0.010 nM
Antitumor activity	see Table 1
Actin-depolymerizing activity against 3 μM actin	EC$_{50}$ 1.6 μM

Figure 1-11. Structure and bioactivities of aplyronine A.

Figure 1-12. *Aplysia kurodai.*

Table 1. Antitumor activities of aplyronine A (**1**).

Tumor	Dose (mg/kg/day)	Life prolong effect test/control (%)
P388 murine leukemia	0.08	545
Colon C26 carcinoma	0.08	255
Lewis lung carcinoma	0.04	556
B16 melanoma	0.04	201
Ehrlich carcinona	0.04	398

1-4-2. Actin and Actin-targeting Compounds

Actin is a cytoskeletal protein, and shows the equilibrium between G-actin and F-actin in cells. By the dynamic equilibrium, actin controls various cell functions, such as cell division, cell motility, muscle contraction, and cytokinesis. So, the compounds that interact with actin are expected to show a variety of bioactivities because they directly affect the above cell functions. Actually, many actin-targeting compounds show cell-growth inhibitory activity. Examples are described as follows. Phalloidin as shown above and jasplakinolide[14] facilitate actin-polymerization by binding to F-actin (Figure 1-13). In contrast, latrunculin A[15] and cytochalasin D[16] are known to inhibit actin-polymerization (Figure 1-14). Bistramide A[17], and various macrolides, such as swinholide A[18], mycalolide B[19], kabiramide C[20], and reidispongiolide A[21], depolymerize F-actin as with ApA (Figure 1-15). All of them show potent cell-growth inhibitory activity.

Thus, many actin-targeting compounds that inhibit cell-growth of tumor cells have been reported, but their modes of action are hardly clarified.

Phalloidin   Jasplakinolide
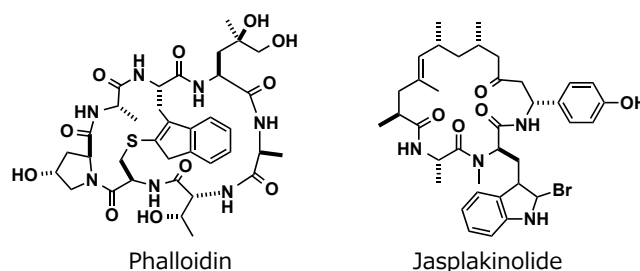
Figure 1-13. Structures of F-actin stabilizing compounds.

Latrunculin A   Cytochalasin D
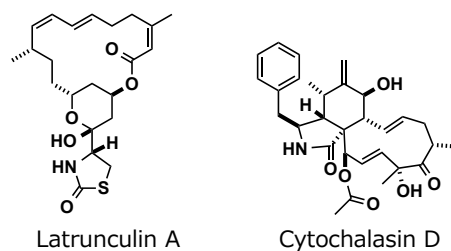
Figure 1-14. Structures of typical actin-polymerization inhibitors.

Bistramide A

Swinholide A

Mycalolide B

Kabiramide C

reidispongiolide A
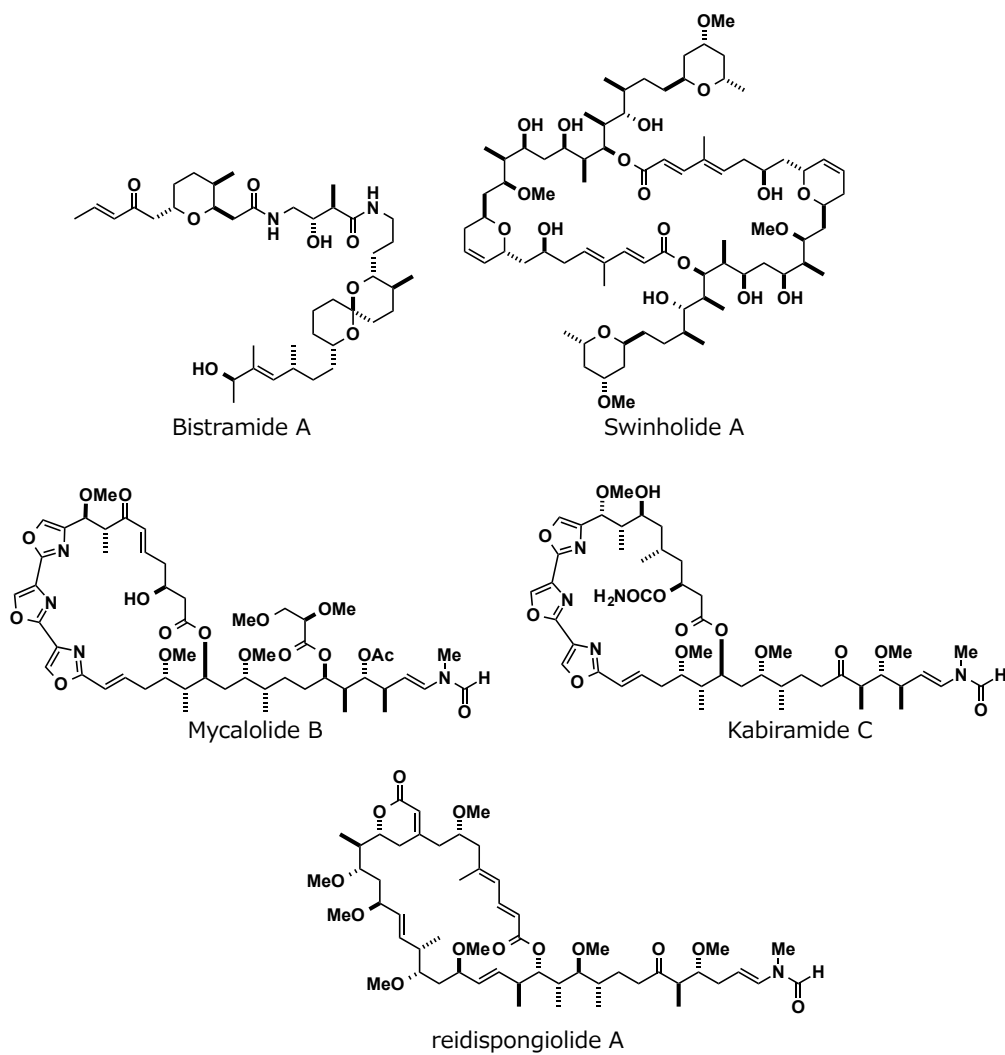
Figure 1-15. Structures of actin-depolymerizing compounds.

1-4-3. Difference of Aplyronine A from Other Actin-targeting Compounds

Interestingly, the side-chain of ApA is similar to the above actin-targeting macrolides (Figure 1-15). So, in all cases of these macrolides, the side-chain moiety is thought to be important for the interaction with actin. Figure 1-16 shows the X-ray crystal structures of the actin–aplyronine A complex[22] and the actin–kabiramide C complex[23] (Figure 1-16a,b). Both ApA and kabiramide C insert their side-chain moieties into the hydrophobic cleft between the subdomains 1 and 3 of actin to form 1:1 complexes. Additionally, it was reported that mycalolide B, reidispongiolide A and swinholide A also show the same binding modes on actin as with ApA. However, cell-growth inhibitory activity of ApA is much more potent than other actin-targeting compounds. This reason is thought to be due to the difference of macrolactone structure. Therefore, the roles of macrolactone should be clarified to understand the mode of action of ApA.

When the actin-ApA complex is looked from the side view, trimethylserine group on the macrolactone ring of ApA is protruded from the actin surface (Figure 1-16c). So, trimethylserine group may have unique effects on cells, which are different from the interaction with actin.
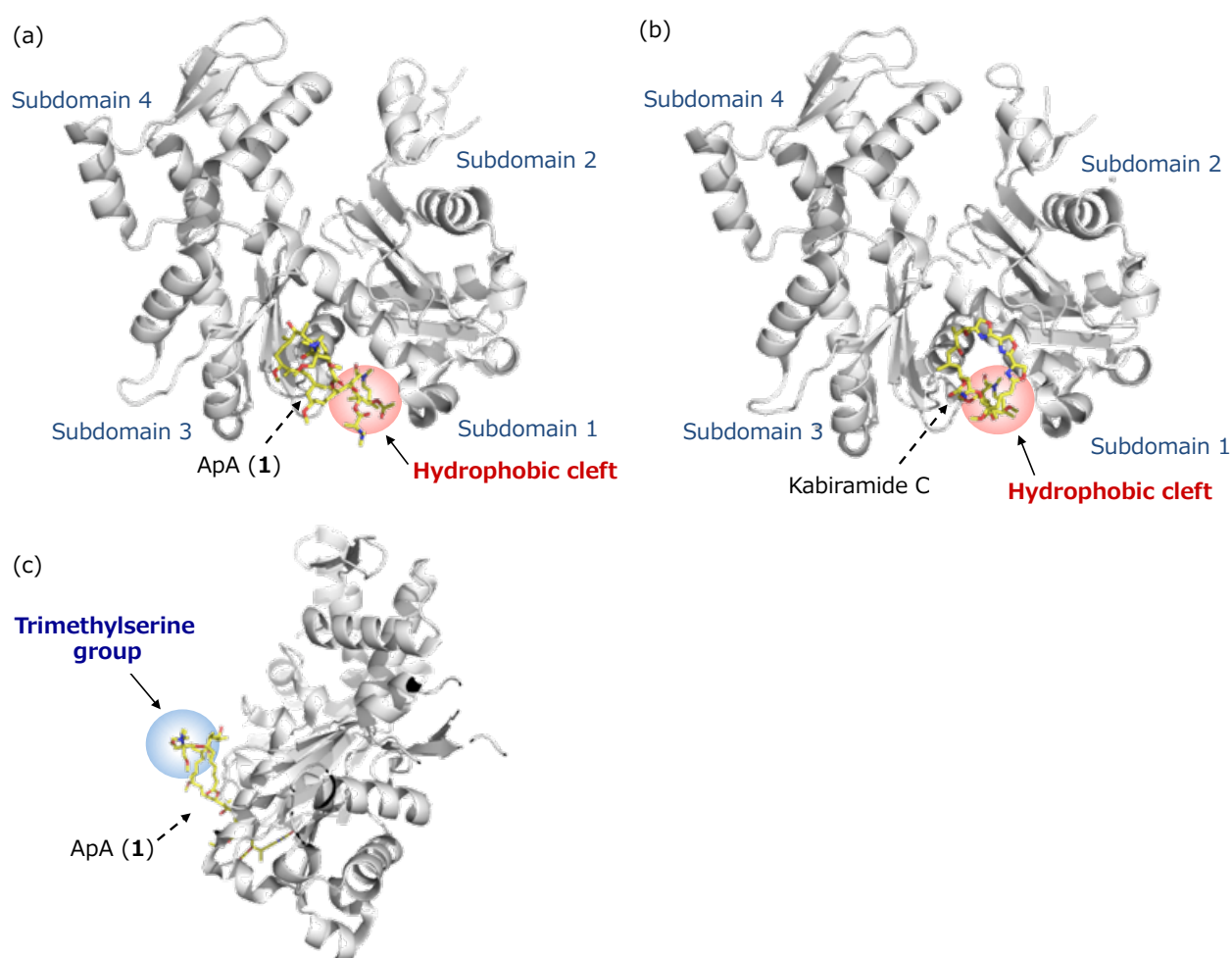
Figure 1-16. X-ray crystal structures of (a,c) the actin−ApA complex (1WUA), and (b) the actin−kabiramide C complex (1QZ5). (a,b) Front views. (c) Side view.

1-4-4. Structure–activity Relationships of Aplyronine A

The total synthesis of ApA was completed in 1996, and studies on structure–activity relationships have been performed.[24] For example, it was shown that the ApA side-chain derivative **2** exhibits no cell-growth inhibitory activity in spite of possessing one-tenth of actin-depolymerizing activity of ApA (Figure 1-17). Therefore, functional group on macrolactone moiety is expected to play an important role for the potent activity of ApA. However, neither macrolactone analogs **3** nor **4** show both activities. These results indicate that the effect of side-chain moiety on actin is necessary but not sufficient for the potent cell-growth inhibitory activity of ApA, and both effects of the side-chain and the macrolactone moieties are essential.

	2	**3, 4**
Cell-growth inhibitory activity against HeLa S3 cells	inactive	**3**: R = Me IC_{50} = 2100 nM
Actin-depolymerizing activity against 3 μM actin	EC_{50} = 7.9 μM	**4**: R = H inactive
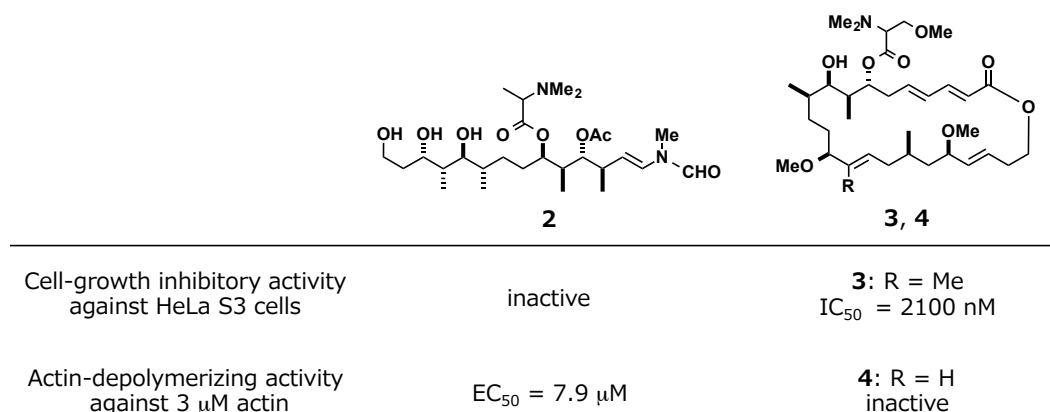
Figure 1-17. Examples of structure-activity relationship of ApA.

Furthermore, aplyronine analogs isolated from *Aplysia kurodai* have provided us perspectives about the reason for strong bioactivity of ApA. Especially, aplyronine C (ApC, **5**), lacks only the C7 trimethylserine moiety of ApA, has approximately 1000-fold less cell-growth inhibitory activity than ApA while it has comparative actin-depolymerization activity of ApA (Figure 1-18). This result suggests that the trimethylserine ester moiety particularly plays a key role for the potent cell-growth inhibitory activity, which ApC and other typical actin-depolymerizing compounds lack.

Aplyronine C (ApC, **5**)

Cell-growth inhibitory activity against HeLa S3 cells	IC_{50} = 17 nM
Actin-depolymerizing activity against 3 μM actin	EC_{50} = 1.4 μM
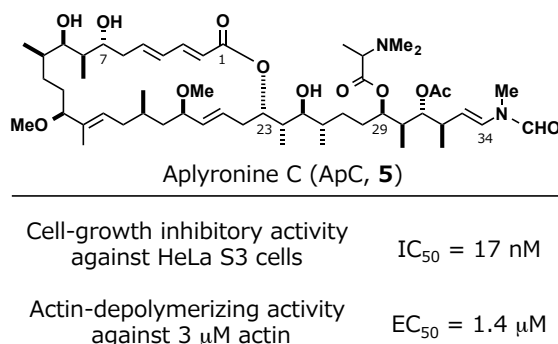
Figure 1-18. Structure and bioactivities of aplyronine C (ApC, **5**).

1-4-5. Hypotheses of the Mode of Action of Aplyronine A

The author made two hypotheses about the relationship of potent bioactivity of ApA with its structural properties of the side-chain and the macrolactone moieties (Figure 1-19). The first one is that ApA more highly accumulates in tumor cells by the effects of C7 trimethylserine ester moiety, and then actin-depolymerization is caused by the side-chain moiety. As a result, ApA shows potent cell-growth inhibitory activity compared with other actin-targeting compounds. The second one is that ApA first binds to actin by its side-chain moiety, then the actin-ApA complex interacts with the second target protein(s) through the functional group on macrolactone moiety, such as trimethylserine ester moiety.
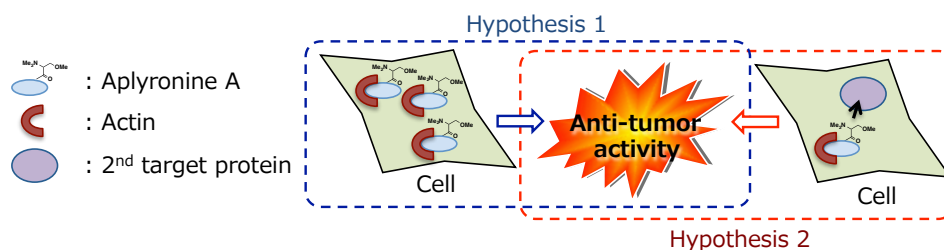
Figure 1-19. Hypotheses of the mode of action of ApA.

In order to confirm these hypotheses, chemical probes were designed to examine the accumulation of ApA and to search for the second target proteins.

References

1. (a) Keller, N. P.; Turner, G.; Bennett, J. W. *Nat. Rev. Microbiol.* **2005**, *3*, 937−947. (b) Hartmann, T. *Phytochem.* **2007**, *68*, 2831−2846. (c) Rishton, G. M. *Am. J. Cardiol.* **2008**, *101(10A)*, 43D−49D.

2. (a) Olivera, B. M.; McIntosh, J. M.; Cruz, L. J.; Luque, F. A.; Gray, W. R. *Biochemistry* **1984**, *23*, 5087−5090. (b) Olivera, B. M.; Gray, W. R.; Zeikus, R.; McIntosh, J. M.; Varga, J.; Rivier, J.; de Santos, V.; Cruz, L. J. *Science* **1985**, *230*,1338−1343.

3. Shimada, S. *Science* **1969**, *163*,1462.

4. Hirata, Y.; Uemura, D. *Pure Appl. Chem.* **1986**, *58*, 701−710.

5. (a) Wang, Y.; Habgood, G. J.; Christ, W. J.; Kishi, Y.; Littlefield, B. A.; Yu, *J. M. Bioorg. Med. Chem. Lett.* **2000**, *10*, 1029−1032. (b) Kim, D. S.; Dong, C. G.; Kim, J. T.; Guo, H.; Huang, J.; Tiseni, P. S.; Kishi, Y. *J. Am. Chem. Soc.* **2009**, *131*, 15636−15641.

6. Tanaka, H.; Kuroda, A.; Marusawa, H.; Hatanaka, H.; Kino, T.; Goto, T.; Hashimoto, M. *J. Am. Chem. Soc.* **1987**, *109*, 5031−5033.

7. Harding, M. W.; Galat, A.; Uehling, D. E.; Schreiber, S. L. *Nature* **1989**, *341*, 758−760.

8. Liu, J.; Farmer, J. D. Jr.; Lane, W. S.; Friedman, J.; Weissman, I.; Schreiber, S. L. *Cell* **1991**, *66*, 807−815.

9. Keenan, T.; Yaeger, D. R.; Courage, N. L.; Rollins, C. T.; Pavone, M. E.; Rivera, V. M.; Yang, W.; Guo, T.; Amara, T. F.; Clackson, T.; Gilman, M.; Holt, D. A. *Bioorg. Med. Chem.* **1998**, *6*, 1309−1335.

10. (a) Wagner, B. D. *Molecules* **2009**, *14*, 210−237. (b) Urano, Y.; Kamiya, M.; Kanda, K.; Ueno, T.; Hirose, K.; Nagano, T. *J. Am. Chem. Soc.* **2005**, *127*, 4888−4894. (c) Loudet, A.; Burgess, K. *Chem. Rev.* **2007,** *107*, 4891−4932. (d) Beija, M.; Afonso, C. A. M.; Martinho, J. M. G. *Chem. Soc. Rev.* **2009**, *38*, 2410−2433.

11. Faulstich, H.; Zobeley, S.; Rinnerthaler, G.; Small, J. V. *J. Muscle Res. Cell Motil.* **1988**, *9*, 370−383.

12. (a) Kotzyba–Hibert, F.; Kapfer, I.; Geoldner, M. *Angew. Chem., Int. Ed. Engl.* **1995**, *34*, 1296–1312. (b) Hatanaka, Y.; Sadakane, Y. *Curr. Top Med. Chem.* **2002**, *2*, 271–288. (c) Vodovozova, E. L. *Biochemistry (Moscow)* **2007**, *72*, 1–20. (d) Böttcher, T.; Pitscheider, M.; Sieber, S. A. *Angew. Chem., Int. Ed.* **2010**, *49*, 2680–2698.

13. (a) Yamada, K.; Ojika, M.; Ishigaki, T.; Yoshida, Y.; Ekimoto, H.; Arakawa, M. *J. Am. Chem. Soc.* **1993**, *115*, 11020–11021. (b) Ojika, M.; Kigoshi, H.; Ishigaki, T.; Yamada, K. *Tetrahedron Lett.* **1993**, *34*, 8501−8504. (c) Ojika, M.; Kigoshi, H.; Ishigaki, T.; Nishiwaki, M.; Tsukada, I.; Mizuta, K.; Yamada, K. *ibid*. **1993**, *34*, 8505−8508. (d) Ojika, M.; Kigoshi, H.; Ishigaki, T.; Nishiwaki, M.; Tsukada, I.; Tsuboshi, T.; Ogawa, T.; Yamada, K. *J. Am. Chem. Soc.* **1994**, *116*, 7441−7442. (e) Saito, S.; Watabe, S.; Ozaki, H.; Kigoshi, H.; Yamada, K.; Fusetani, N.; Karaki, H. *J. Biochem.* **1996**, *120*, 552−555. (f) Ojika, M.; Kigoshi, H.; Yoshida, Y.; Ishigaki, T.; Nishiwaki, M.; Tsukada, I.; Arakawa, M.; Ekimoto, H.; Yamada, K. *Tetrahedron* **2007**, *63*, 3138−3167. (g) Yamada, K.; Ojika, M.; Kigoshi, H.; Suenaga, K. *Nat. Prod. Rep.* **2009**, *26*, 27−43.

14. Bubb, M. R.; Senderowicz, A. M. J.; Sausville, E. A.; Duncan, K. L. K.; Korn, E. D.; *J. Biol. Chem.* **1994**, *269*, 14869−14871.

15. (a) Kashman, Y.; Groweiss, A.; Shmueli, U.; *Tetrahedron Lett.* **1980**, *21*, 3629−3632. (b) Sector, I.; Shochet, N. R.; Kashman, Y.; Groweiss, A. *Science* **1983**, *219*, 493−495. (c) Morton, W. M.; Asycough, K. R.; Maclaughlin, P. *Nat. Cell Biol.* **2000**, *2*, 376−378.

16. Aldridge, D. C.; Armstrong, J. J.; Speake, R. N.; Turner, W. B. *Chem. Commun (London).* **1967**, 26−27.

17. Blard, J. F.; Roussakis, C.; Kornprobst, J. M.; Barbin, D. G.; Verbist, J. F. *J. Nat. Prod.* **1994**, *57*, 1336-1345.

18. Carmely, S; Kashman, Y. *Tetrahedron Lett.* **1985**, *26*, 511−514.

19. Fusetani, N.; Yasumuro, K.; Matsunaga, S.; Hashimoto, K. *Tetrahedron Lett*. **1989**, *30,* 2809−2812.

20. Matsunaga, S.; Fusetani, N.; Hashimoto, K. *J. Am. Chem. Soc*. **1986**, *108*, 847−849.

21. D'Auria, M. V.; Paloma, L. G.; Minale, L.; Zampella, A. Verbist, J. F.; Roussakis, C.; Debitus, C.; Patissou, J.; *Tetrahedron* **1994**, *50*, 4829−4834.

22. Hirata, K.; Muraoka, S.; Suenaga, K.; Kuroda, T.; Kato, K.; Tanaka, H.; Yamamoto, M.; Tanaka, M.; Yamada, K. *J. Mol. Biol.* **2006**, *356*, 945−954.

23. Klenchin, V. A.; Allingham, J. S.; King, R.; Tanaka, J.; Marriott, G.; Rayment, I. *Nat. Struct. Mol. Biol.* **2003**, *10*, 1058−1063.

24. (a) Kigoshi, H.; Suenaga, K.; Mutou, T.; Ishigaki, T. Atsumi, T.; Ishiwata, H.; Sasakura, A.; Ogawa, T.; Ojika, M.; Yamada, K. *J. Org. Chem.* **1996**, *61*, 5326−5351. (b) Suenaga, K.; Kamei, N.; Okugawa, Y.; Takagi, M.; Akao, A.; Kigoshi, H.; Yamada, K. *Bioorg. Med. Chem. Lett.* **1997**, *7*, 269−274. (c) Kigoshi, H.; Suenaga, K.; Takagi, M.; Akao, A.; Kanematsu, K.; Kamei, N.; Okugawa, Y.; Yamada, K. *Tetrahedron* **2002**, *58*, 1075−1102.

Chapter 2.

Analysis of the Mode of Action of Aplyronine A with Chemical Probes

Abstract

To clarify the mode of action of anti-tumor macrolide aplyronine A, several fluorescent probes and photoaffinity biotin probes were synthesized. By using fluorescent probe, it was indicated that aplyronine A bound to cytoplasmic actin and accumulates into tumor cells. On the photolabeling experiment by using photoaffinity biotin probe, tubulin was specifically purified along with actin as the target proteins of aplyronine A. And, C7 trimethylserine moiety of aplyronine A was important for the interaction with tubulin. Furthermore, the author established that aplyronine A inhibits normal spindle formations in tumor cells and cell cycle progression at the cell-growth inhibitory concentration. And, aplyronine A induces apoptosis. These effects are expected to be deeply related to the potent anti-tumor activity of ApA, and this study would lead to further clarification of the mode of action of aplyronine A.

2-1. Introduction

In the past, some chemical probes of aplyronine A (ApA, **1**) have been developed. For example, fluorescent photoaffinity probe **6** possessing the side-chain of ApA as a ligand was reported in 2006 to analyze binding mode on actin,[1] and an ApA biotin probe **7** in 2011 to search for the target proteins of ApA.[2] By using probe **6**, it was revealed that the side-chain of ApA binds to the same site of actin as mycalolide B, but not as cytochalasin D. This result corresponds to the X-ray crystal structure of the actin−ApA complex.[3] And actin-related proteins 2,3 (Arp 2, 3) were purified from the whole cell lysate of tumor cells (HeLa S3) with biotin probe **7**. Furthermore, fluorescent microscopy analysis showed that probe **7** distributed in the cytoplasm.
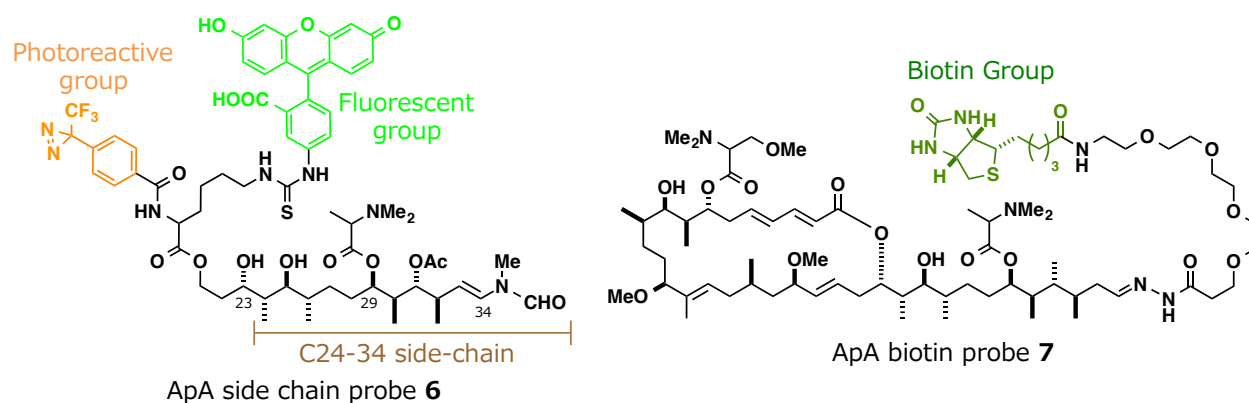
Figure 2-1. Structures of synthesized ApA probes in the past.

In this manner, the analyses with chemical probes provide us with much information on target proteins and bioactive ligands. So, the author designed different type probes to analyze the mode of action of ApA in this chapter.

2-2. Analysis of the Behavior of Cells Treated with Aplyronine A Fluorescent Probes

2-2-1. Syntheses of Fluorescent Probes

Modification of bioactive ligands without loss of activity is very important to get useful probes. Inappropriate modification may lead to the loss of bioactivities and the change of interactions with target proteins. In the case of probe **7**, it was known that ApA C34 *N*-methyl enamide moiety can be replaced with hydrogen bond acceptors without a significant loss of activity.[4]   And, there is a space behind the C34 enamide moiety based on the X-ray analysis of an actin–ApA complex (Figure 2-2). Actually, probe **7** showed actin-depolymerizing activity comparable to ApA (**1**) and only 10-fold less cell-growth inhibitory activity than ApA.[2] Thus, the author planned to synthesize new chemical probes by elongation of the C34 enamide moiety.
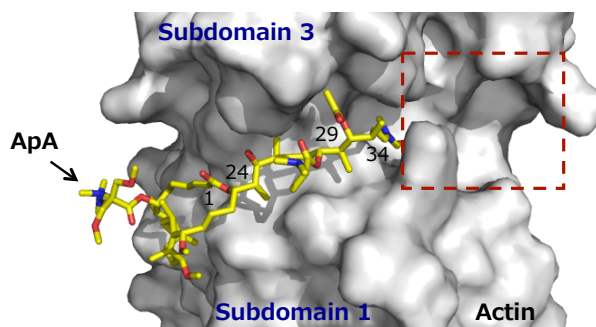
Figure 2-2. Binding mode of ApA to actin.

In order to analyze cellular behavior of ApA in more detail, an aplyronine A fluorescent probe (ApA-FL, **8**) was designed (Figure 2-3). TAMRA was selected as a fluorescent group. TAMRA is a red fluorophore, and its fluorescence hardly depends on pH, and its photobleaching is less than other fluorescent groups, such as fluorescein. TAMRA group was planned to conjugate via the oxime bond with ApA ligand. The oxime bond would be formed in mild condition with an aldehyde obtained by the hydrolysis of ApA and an oxyamine. ApC fluorescent probe (ApC-FL, **9**) was also designed to compare with **8**.
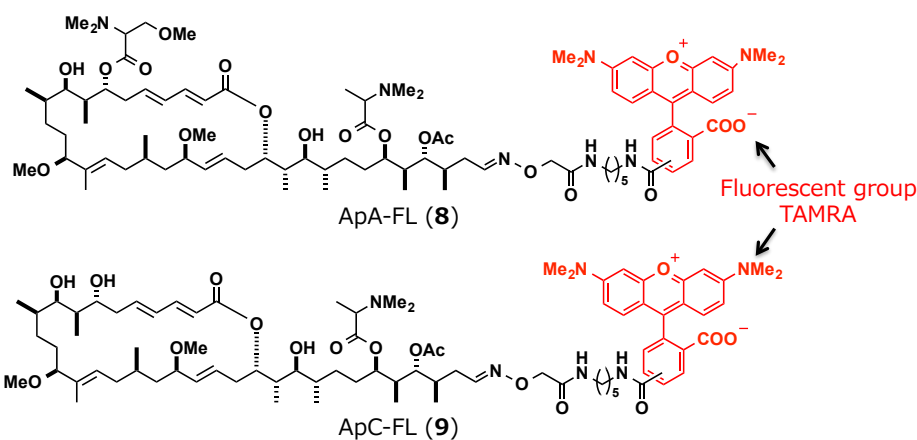
Figure 2-3. Structures of ApA-FL (**8**) and ApC-FL (**9**).

First, ApA (**1**) and ApC (**5**) were isolated from the sea hare *Aplysia kurodai* in $2.6 \times 10^{-5}\%$ and $2.6 \times 10^{-7}\%$ yields, respectively. But the amount of ApC (**5**) was not enough to synthesize ApC probe for futher investigations. So, to prepare ApC probe, conversion from ApA (**1**) to ApC (**5**) was examined (Scheme 2-1). After trials, ApC (**5**) was found to be yielded from ApA (**1**) by selective methanolysis in mild basic condition [0.1% triethylamine, in MeOH at 50 °C] in 60% yield.
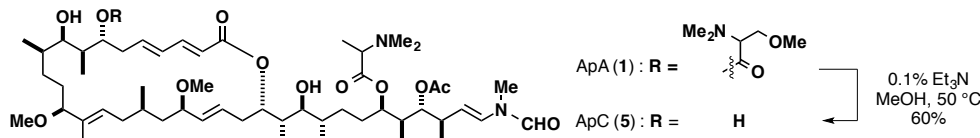
Scheme 2-1. Derivatization of ApA (**1**) into ApC (**5**).

ApA-FL (**8**) was synthesized as shown in Scheme 2-2. ApA (**1**) was hydrolyzed in acidic condition to give the C34 aldehyde **10**[5]. An aminooxy-5(6)-TAMRA (**12**) was condensed with **10** to afford ApA-FL (**8**, 66% in 2 steps). Similarly, ApC-FL (**9**) was prepared from ApC (**5**, 44% in 2 steps). For comparison, a TAMRA-conjugate of mycalolide B (MyB-FL, **15**) was designed. Mycalolide B (MyB, **13**) binds to the same site of actin as with ApA and shows actin-depolymerizing activity, which is comparable to that of ApA. An aldehyde **14** [6] was obtained from the hydrolysis of MyB (Wako), followed by the oximation with **12** to give MyB-FL (**15**) (15% in 2 steps, Scheme 2-3). Additionally, a model TAMRA analogue **16** that has no natural ligands was also synthesized from 3-phenylpropanal in 85% yield (Scheme 2-4).
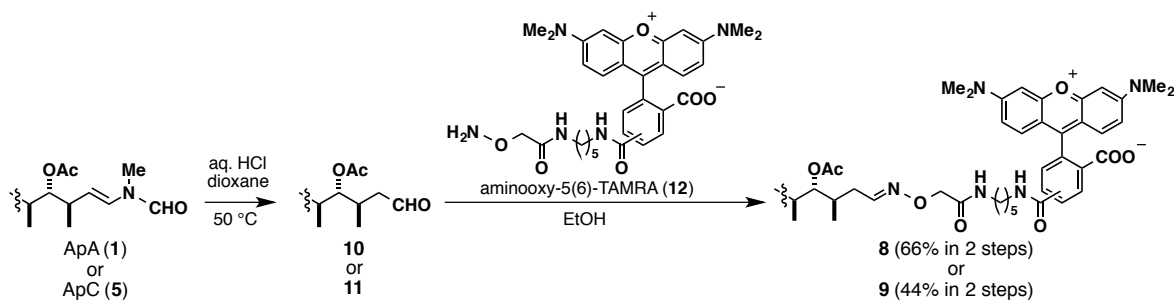
Scheme 2-2. Syntheses of ApA-FL (**8**) and ApC-FL (**9**).
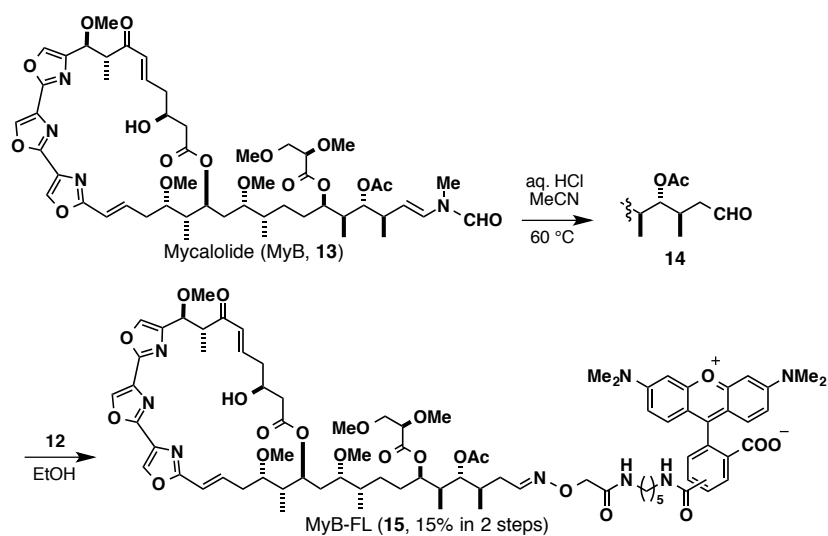
Scheme 2-3. Syntheses of MyB-FL (**15**).

3-phenylpropanal   12 / EtOH → **16** (85%)
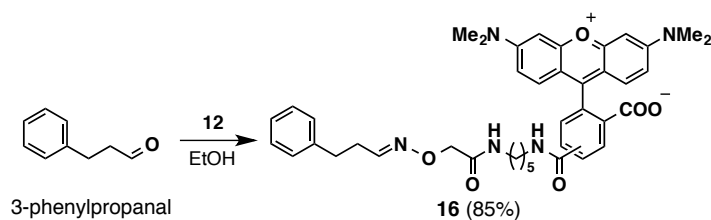
Scheme 2-4. Synthesis of model probe **16**.

2-2-2. Bioactivities of Fluorescent Probes

Cell-growth inhibitory activities of fluorescent probes were compared with those of natural products (Table 2-1). The activity of ApA-FL (**8**) and MyB-FL (**15**) were only about 10-fold weaker than each natural product, while ApC-FL (**9**) showed the activity as much as ApC. ApA-FL (**8**) exhibited potent cell-growth inhibitory activity, which was ca. 30 and 840 times stronger than ApC-FL (**9**) and MyB-FL (**15**). Model probe **16** hardly showed cytotoxicity compared with other probes. It was thought that the cell-growth inhibitory activities of fluorescent probes reflected the activity of each natural ligand.

Table 2-1. Cell-growth inhibitory activity of fluorescent probes.

Compound	IC_{50} against HeLa S3 cells (nM)
ApA-FL (**8**)	0.37
ApA (**1**)	0.010
ApC-FL (**9**)	11
ApC (**5**)	17
MyB-FL (**15**)	310
MyB (**13**)	21
Model **16**	10000

The author next checked the stability of ApA-FL in cells. After HeLa S3 cells treated with ApA-FL (**8**) for 1.5 h were washed, **8** were extracted from the cells with dimethylsulfoxide (DMSO), and the extract was analyzed by HPLC (Figure 2-4). As a result, only two fluorescent peaks were detected in the lysate sample (Figure 2-4b), and these retention times corresponded to those of pure 6- and 5-TAMRA derivatives of ApA-FL (Figure 2-4c). These observations confirmed that ApA-FL (**8**) was not metabolized and modified in cells at that treating time. This result suggested that **8** exhibits high bioavailability as well as the stability of the oxime bond. Therefore, IC_{50} of ApA-FL did not attribute to a ligand resulted from the cleavage of oxime bond, but to the probe itself.
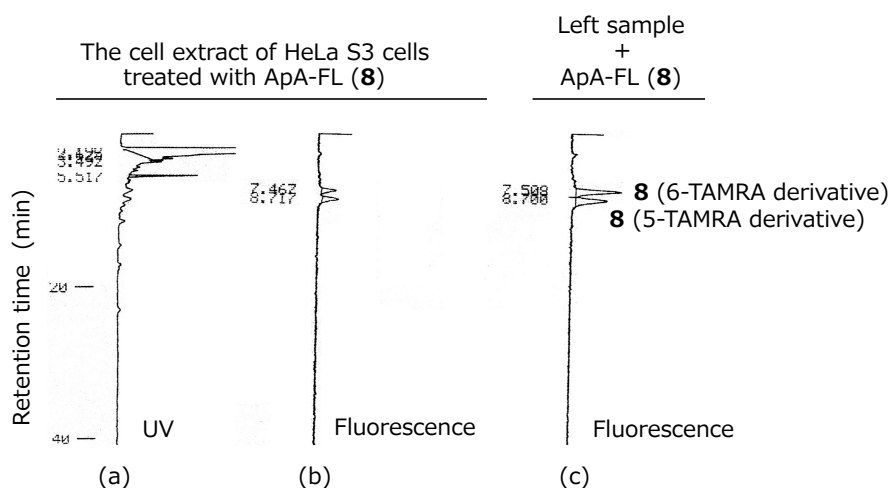
Figure 2-4. HPLC analysis of the recovered ApA-FL from cells. Detection: (a) UV absorbance (254 nm) and (b) fluorescence (λ_{ex} 565 nm, λ_{em} 580 nm). In (c), the mixture of **8** and the cell extract of HeLa S3 cells treated with **8** was analyzed and detected by fluorescence (λ_{ex} 565 nm, λ_{em} 580 nm).

In vitro actin-depolymerizing assay was next examined by using a pyrene-labeled actin[7] since its fluorescent intensity increases along with the polymerization (Figure 2-5). First, pyrenyl F-actin was prepared by the addition of Mg^{2+}, an actin-polymerizing promoter, to the 9:1 mixture of actin and pyrene-labeled actin monomers. After adding fluorescent probes to pyrenyl F-actin in portions, their 50% effective concentrations (EC_{50}) of actin-depolymerization were calculated from the decreasing fluorescent intensity.

ApA-FL (**8**) significantly reduced the fluorescence of pyrenyl F-actin (EC_{50} 0.8 μM against 3 μM actin), which was 1.6 times stronger than **1** (EC_{50} 1.3 μM). Meanwhile. model compound **16** scarcely exhibited this activity even at 2.5 μM (Figure 2-6). Pyrenyl actin is prepared by the labeling of cysteine 374 residue of actin with *N*-(1-pyrene) iodoacetamide[7]. This cysteine residue exists in the subdomain 1 of actin, and is near from the ApA-binding site. Therefore, fluorescence resonance energy transfer potentially occurred from the pyrene group to TAMRA moiety, and the fluorescence of pyrene might apparently decrease. This might explain the reason that the EC_{50} value of **8** was apparently lower than that of ApA. Thus, actin-depolymerizing assay using pyrenyl actin was improper to evaluate the activity of **8**. A coworker checked actin-depolymerizing activity of **8** by ultracentrifugation method. As a result, **8** showed strong activity compared with ApA[8]. Then the author planned to check the actin-depolymerizing activity *in situ* (on cells).
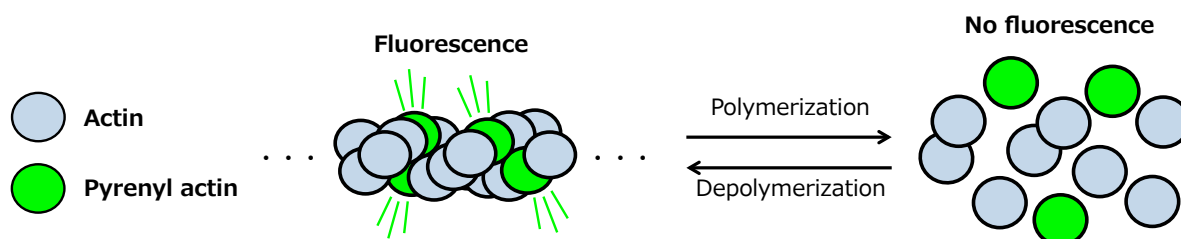
Figure 2-5. Relationship between pyrenyl actin and its fluorescence.
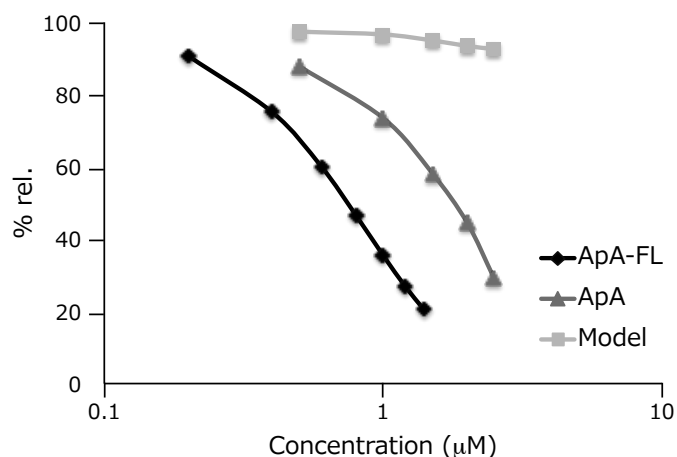
Figure 2-6. Actin-depolymerizing activities of probes. ApA-FL (**8**), ApA (**1**) and model **16** were shown in diamond, trigona, and square shapes, respectively.

To visualize actin-depolymerization in tumor cells, ApA-FL (**8**, 3 μM) was added to the HEp-2 cells that expressed a green fluorescent protein (GFP)-actin fusion protein. HEp-2 cells are a kind of the epithelioid carcinoma cells of human cervix uteri, and more suitable for cellular observation than HeLa S3 cells due to the wide spread cytoplasm. Treatment of **8** for 1-2 h raised the GFP fluorescence around nucleus, suggesting that the cytoplasmic actin aggregated (Figure 2-7). This is a common phenotype with various actin-targeting agents[9]. Since GFP-actin was initially included in the actin cytoskeleton, GFP fluorescence of the untreated cells was localized only in the cytoplasm. However, after the cells were treated with **8** for four hours, the boundary between the nucleus and the cytoplasm disappeared, and most of the GFP fluorescence aggregated to be granular splotches. These results suggested that **8** also depolymerized F-actin in *situ* and caused rapid disassembly of the actin cytoskeleton in HEp-2 cells.

Above results indicates that **8** holds potent bioactivities of the natural ligand, ApA.
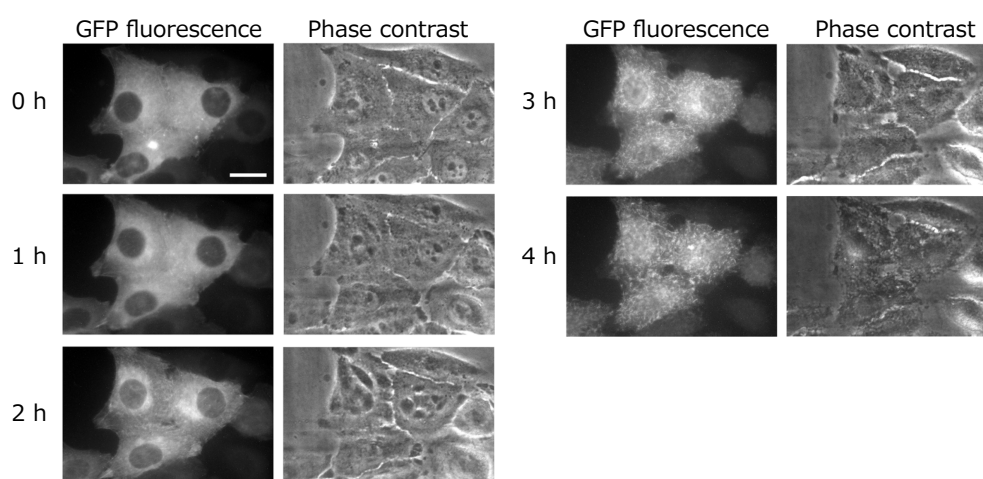
Figure 2-7. Time-lapse analysis of the HEp-2 cells treated with ApA-FL. ApA-FL (**8**) (3 μM) was applied to HEp-2 cells that expressed GFP-tagged actin. After 30 min, cells were washed with buffer and incubated further at 37 °C. Scale bar: 20 μm.

2-2-3. Accumulations of Fluorescent Probes in Living Cells

To approach the relationship of cell-growth inhibitory activities of probes with cell accumulation, probes **8**, **9**, **15**, and **16** were added to HeLa S3 cells and their TAMRA fluorescences were compared. After incubation for 30 min, red fluorescence were observed in either cell by fluorescence microscopy. These observations revealed that the fluorescent probes **8**, **9**, **15**, and **16** were all readily (less than 30 min) incorporated into HeLa S3 cells. Notably, ApA-FL (**8**) and ApC-FL (**9**) were retained well and distributed through the cytoplasm even after cells were washed with culture medium and incubated for an additional hour (Figure 2-8). MyB-FL (**15**) was also retained as much as before washing. In contrast, model probe **16** was almost completely excluded from the cells under the same treatments. The initial cellular incorporations of MyB-FL (**15**) and model **16** were less than that of **8** or **9**.
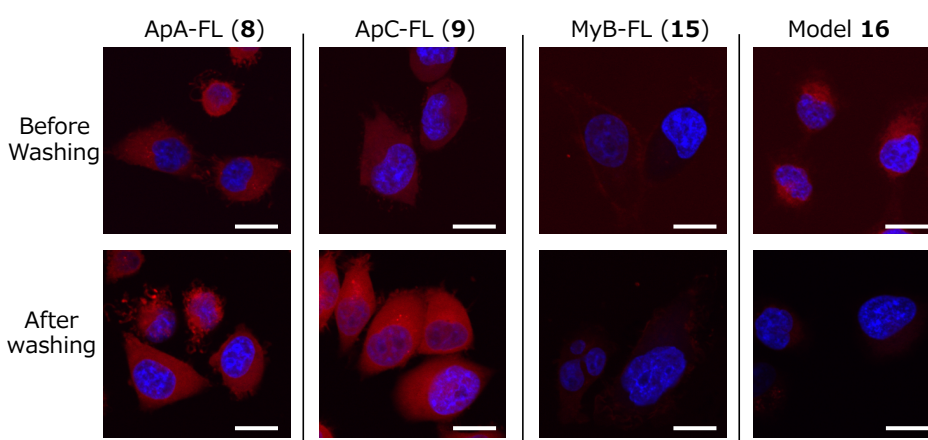
Figure 2-8. Confocal fluorescence images of HeLa S3 cells treated with fluorescent derivatives (TAMRA, red). After the cells had been preincubated with probes (500 nM) for 30 min, they were washed with culture medium and incubated for an additional hour. Cells were costained with Hoechst 33342 (nuclei, blue) and imaged with differential interference contrast. Scale bars: 20 μm.

To establish the intracellular accumulation of fluorescent probes quantitatively, the flow cytometry (FCM) analysis was performed (Figure 2-9). As with microscopy observations, the fluorescence of the cells treated with **8** and **9** hardly changed after washing the cells. So, both probes were well accumulated in HeLa S3 cells. The cellular fluorescence of MyB-FL (**15**) and model probe **16** was lower than **8** and **9** in first incubation, and fluorescent intensity of the cells treated with **16** significantly decreased by washing.
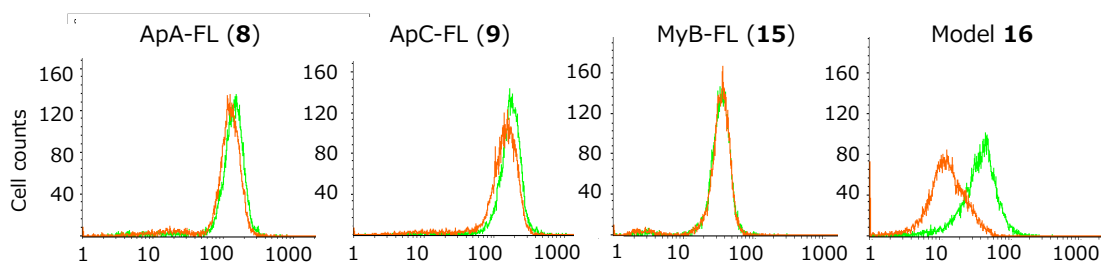
Figure 2-9. Flow cytometry analysis of HEp-2 cells treated with various fluorescent probes. After cells had been incubated with probes (1 μM) for 30 min (green), they were washed with culture medium and incubated for an additional 1.5 h (orange).

On the fluorescence microscope observation and FCM analysis, incorporation of probes **8**, **9**, **15** hardly decreased by washing. These results indicated that each probe binds to abundant actin through natural ligand moiety and is strongly trapped in the cytoplasm. The incorporated amount of MyB probe **15** into the cells was less than **8** even though MyB possesses actin-depolymerizing activity as with ApA, suggesting that low permeability is one reason that MyB shows weaker cell-growth inhibitory activity than ApA.

In an effort to particularly evaluate the cellular accumulation of ApA-FL (**8**) and ApC-FL (**9**), flow cytometry analyses were performed with different treating times (Figure 2-10). Both probes accumulated to HeLa S3 cells in time-dependent manner. ApA-FL seemed to be incorporated slightly less than ApC-FL. However, a little difference in the cellular accumulation between ApA-FL (**8**) and ApC-FL (**9**) could not explain significant difference in cell-growth inhibitory activity. This indicates that the hypothesis 1 described in chapter 1 was wrong.
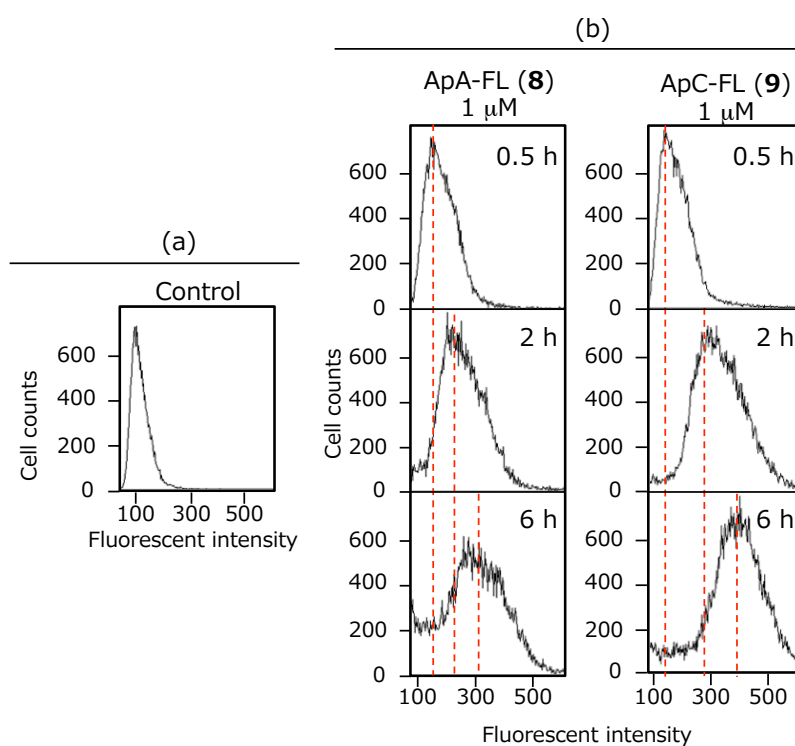
Figure 2-10. Flow cytometry analysis of HeLa S3 cells treated with fluorescent probes **8** and **9** with different times. (a) Control, untreated HeLa S3 cells. (b) HeLa S3 cells were treated with **8** or **9** (1 µM) for 0.5, 2, and 6 h.

2-2-4. Stain of Actin in the Cells Treated with Aplyronines

In order to investigate the difference in bioactivity between ApA and ApC, the author examined the relationships between the cell-growth inhibitory activity and actin-destabilizing properties by fluorescence microscopy observation. F-actin and nucleus were stained with rhodaine-phalloidin and 4',6-diamidino-2-phenylindole (DAPI), respectively. Both 100 nM ApA and ApC caused rapid disassembly of the actin cytoskeleton in HeLa S3 cells (Figure 2-11). These effects on HeLa S3 cells were similar to those of typical actin-targeting agents (e.g., 100−1000 nM latrunculin A, cytochalasin D, and mycalolide B) [9,10]. Meanwhile, treatment with 100-fold more diluted samples (1 nM) of ApA or ApC induced no detectable alteration of the actin cytoskeleton although ApA showed strong cell-growth inhibitory activity at this concentration. These results suggest that the potent cell-growth inhibitory activity of ApA may not be due solely to its F-actin severing properties. Furthermore, only ApA morphologically changed the cells, and constriction of the proximal cytoplasm was observed. Therefore, ApA obviously has the morphologic effect, which ApC lacks, on tumor cells, and this effect might be involved with potent cell-growth inhibitory activity of ApA (IC_{50} = 0.010 nM). Then, in order to analyze the mode of action of ApA in more detail, the author planned to search other target proteins of ApA than actin on the basis of the second hypothesis as shown in chapter 1 from next section.
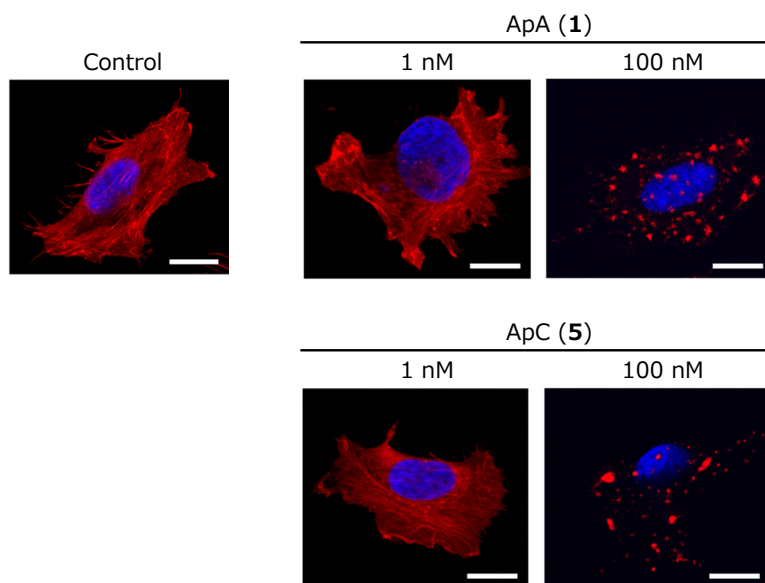
Figure 2-11. Confocal fluorescence images of HeLa S3 cells treated with aplyronines for 2 h. Cells were stained with rhodamine-phalloidin (red, F-actin) and DAPI (blue, nucleus). Scale bars: 20 μm.

2-3. Identification of the Second Target Protein of Aplyronine A with Photoaffinity Probes

2-3-1. Designs and Syntheses of Photoaffinity Probes[11]

It was predicted that C7 trimethylserine ester moiety of ApA is important for the interaction with the second target protein (the hypothesis 2 described in chapter 1). To identify additional target proteins of ApA, the author designed aplyronine A photoaffinity biotin probe (**17**, ApA-PB) possessing ApA moiety as a ligand, and ApC photoaffinity biotin probe (ApC-PB, **18**) as a negative control (Figure 2-12). These probes have a photoreacting group, a diazirine group to form a covalent bond with target proteins, and a biotin group to purify and detect the target proteins.
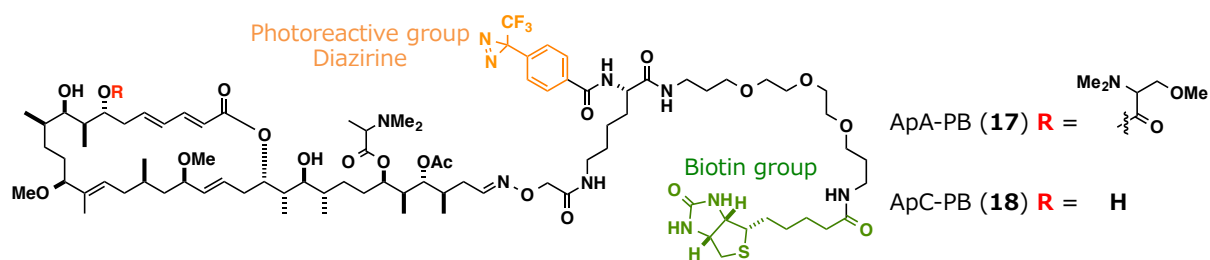
Figure 2-12. Structure of photoaffinity biotin probes.

As with fluorescent probes, C34 enamide moiety would be modified to convert into photoaffinity derivatives. Aldehyde **10** resulted from ApA was condensed with oxyamine **19**[12] in the presence of 0.1 M acetate buffer (pH 4.0) to give ApA-PB (**17**, 69% in 2 steps, Scheme 2-5). Similarly, ApC photoaffinity biotin probe (ApC-PB, **18**) was converted from ApC in 2 steps.
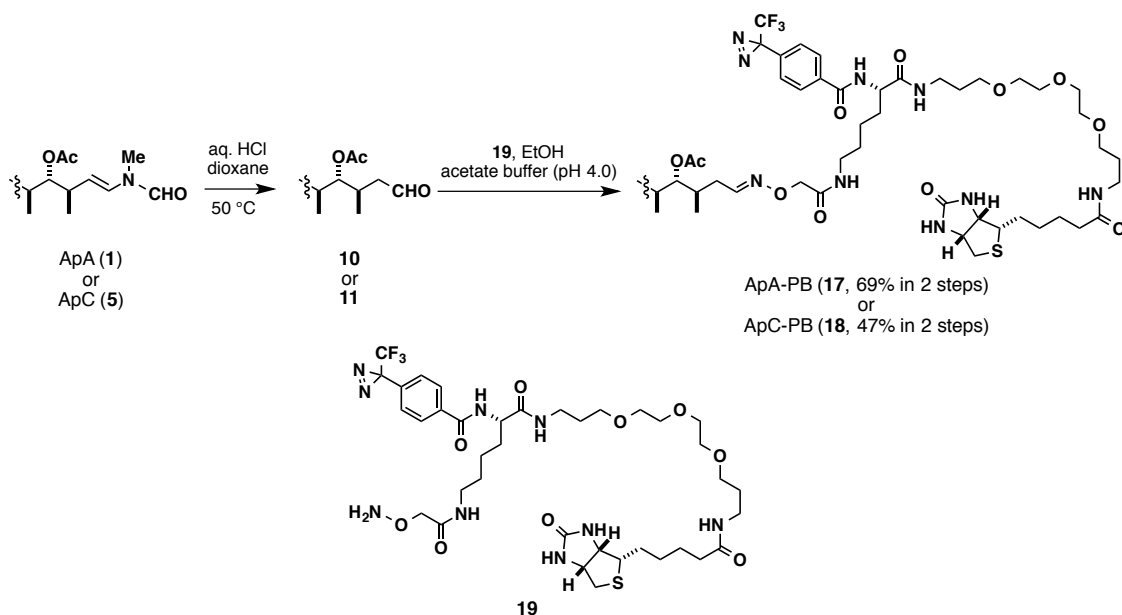
Scheme 2-5. Synthesis of ApA-PB (**17**) and ApC-PB (**18**).

2-3-2 Cytotoxicity of Photoaffinity Probes[11]

Cell-growth inhibitory activities of probes were examined (Table 2-2). ApA-PB (**17**) showed a potent activity against HeLa S3 cells (IC$_{50}$ 3.0 nM). This activity was 300 times weaker than the natural product but approximately 100-fold more potent than ApC-PB (**18**). Therefore, it was thought that ApA-PB (**17**) possesses binding properties of target proteins that are important for potent cell-growth inhibitory activity of ApA. And the second target protein of ApA as described in hypothesis 2 (Figure 1-19) was expected to be purified by using ApA-PB.

Table 2-2. Cell-growth inhibitory activity of biotin probes.

Compound	IC$_{50}$ against HeLa S3 cells (nM)
ApA-PB (**17**)	3.0
ApA (**1**)	0.010
ApC-PB (**18**)	320
ApC (**5**)	17

2-3-3. Purification of the Target Proteins of Aplyronine A from Living Cells[11]

The author performed photolabeling experiments with the whole cell lysate and living tumor cells (Figure 2-13). First, to the whole cell lysate of HeLa S3 cells was added the NeutrAvidin agarose pretreated with ApA-PB or ApC-PB. After incubation and photoreaction, the resin was washed and the target proteins were eluted by boiling in SDS (sodium dodecyl sulfate) buffer. The eluent was applied to SDS-PAGE (poly-acrylamide gel electrophoresis), and the purified proteins were detected by silver stain and Western blotting. Purifying target proteins from lysate has the merit that tiny proteins can be detected because the high concentration lysate can be prepared and proteins can be stably treated at high concentration. Next, to conduct photolabeling experiment in living tumor cells, probes were added to the HeLa cells and incubated. After *in situ* photoreaction, the cells were extracted and photolabeled products were purified by using NeutrAvidin agarose, and analyzed similarly as mentioned above. This purification from living cells is able to label the cellular target proteins specifically, and to detect the unstable target proteins derived from cell lysate.
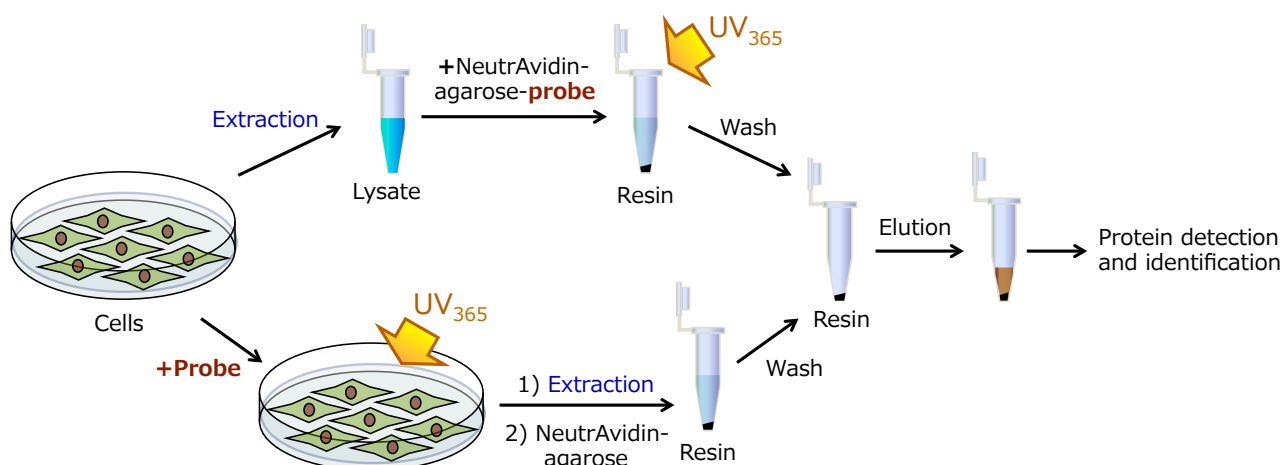
Figure 2-13. Outline of the purification of target proteins using photoaffinity biotin probes from the whole cell lysate (top) and living cells (bottom).

When the target proteins of ApA were purified from cell lysate using ApA-PB (**17**) and ApC-PB (**18**), the proteins purified with **17** specifically were not detected. This result suggested that the second target proteins, which are the cause of antitumor activity of ApA, were not purified. The reason was expected that the target proteins of ApA were unstable *in vitro*, and denaturalized during the lysate preparation. Then, target proteins of ApA were purified from living cells by using ApA-PB (**17**) (Figure 2-14). As the results of silver stain and Western blotting, 43 kDa protein (actin) was detected in both cases using **17** and **18** (*Lane 1,2,4,5*, Figure 2-14). And biotinylated bands at 55 and 58 kDa were detected only by using ApA-PB (**17**) (*Lane 4*). These proteins were never detected with ApC-PB (**18**). Thus, 55 and 58 kDa proteins were predicted to be the second target proteins of ApA. The author predicted that 55 and 58 kDa proteins were not purified from cell lysate due to instability *in vitro*, but the functions and structures of these proteins were retained in cells until photoreaction. So, it was thought that these proteins could be purified from living cells. In addition, 70, 72 and 120 kDa proteins were detected in both cases of ApA-PB (**17**) and ApC-PB (**18**). These three proteins were presumed to intrinsic biotin-binding proteins (propionyl-CoA carboxylase, methylcrotonyl-CoA carboxylase, and pyruvate carboxylases, respectively),[13] because they were detected even at the control (*lanes 3* and *6*).

Figure 2-14. Purification of target proteins of ApA from living HeLa S3 cells.

2-3-4. PMF Analysis of 55, 58 kDa Proteins Purified by Using ApA-PB[11]

   To identify the 55 and 58 kDa Proteins, peptide mass fingerprinting (PMF) analysis was performed. The purified proteins in Figure 2-14 were applied to SDS-PAGE and detected by silver stain without glutaraldehyde fixation[14]. The stained 55 and 58 kDa bands were cut and in-gel tryptic digestion was performed. The tryptic peptides were analyzed by MALDI-TOF MS (matrix-assisted laser desorption/ionization time of flight mass spectrometry) (Figure 2-15, 2-16). Detected peaks were analyzed by a PMF search program MS-Fit (University of California, http://prospector.ucsf.edu/prospector/cgi-bin/msform.cgi?form=msfitstandard). Then PMF analysis revealed that the 55 kDa protein contains five peptides (K1-5) of α-tubulin and twelve peptides (K1-4, K6-13) of β-tubulin (Table-2-3, Figure 2-17). And the 58 kDa protein contained eleven peptides (K1-11, K13) of β-tubulin (Table-2-4). Therefore it was established that the 55 and 58 kDa proteins are composed of α- and β- tubulin as major constituents.
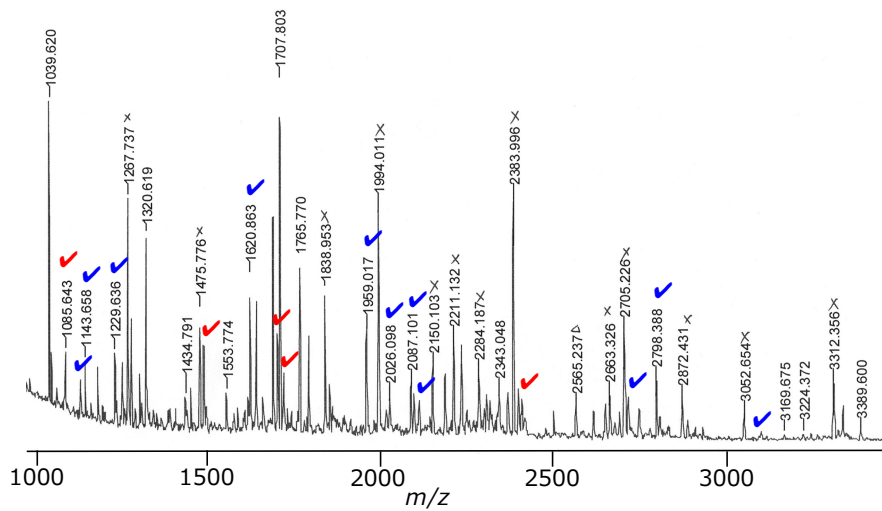
Figure 2-15. MALDI-TOF MS analysis of the tryptic peptides derived from the 55 kDa proteins. Check marks in red and blue represent the peptide ions that were identified as human α- and β-tubulin, respectively. "x" represents the peptides derived from non-specific contaminants (trypsin, keratin, etc.).

Table 2-3. Tryptic peptides of the 55 kDa protein detected by MALDI-TOF MS.

human α-tubulin (accession No. Q9BQE3)

	Observed (m/z)[a]	calcd (m/z)	Start		End	Sequence
K1	1085.64	1085.62	113	-	121	EIIDLVLDR
K2	1487.90	1487.88	230	-	243	LISQIVSSITASLR
K3	1701.93	1701.91	65	-	79	AVFVDLEPTVIDEVR
K4	1718.90	1718.88	216	-	229	NLDIERPTYTNLNR
K5	2409.23	2409.21	244	-	264	FDGALNVDLTEFQTNLVPYPR

[a] The data represent the monoisotopic ion peak [M+H]$^+$ values.

human β-tubulin (accession No. P07437)

|	Observed (m/z)[a]	calcd (m/z)	Start		End	Sequence
K1	1039.62	1039.59	310	-	318	YLTVAAVFR
K2	1130.61	1130.60	242	-	251	FPGQLNADLR
K3	1143.66	1143.63	253	-	262	LAVNMVPFPR
K4	1229.64	1229.60	381	-	390	ISEQFTAMFR
K6	1620.86	1620.84	263	-	276	LHFFMPGFAPLTSR
K7	1959.02	1958.98	104	-	121	GHYTEGAELVDSVLDVVR
K8	2026.10	2026.08	363	-	380	MAVTFIGNSTAIQELFKR
K9	2087.10	2087.08	104	-	122	GHYTEGAELVDSVLDVVRK
K10	2110.09	2110.06[b]	1	-	19	MREIVHIQAGQCGNQIGAK
K11	2708.44	2708.34[b]	217	-	241	LTTPTYGDLNHLVSATMSGVTTCLR
K12	2798.39	2798.34	78	-	103	SGPFGQIFRPDNFVFGQSGAGNNWAK
K13	3102.47	3102.41	20	-	46	FWEVISDEHGIDPTGTYHGDSDLQLDR

[a] The data represent the monoisotopic ion peak [M+H]$^+$ values.

[b] Putative values indicating that the Cys residue(s) in the sequences are carbamidomethylated.
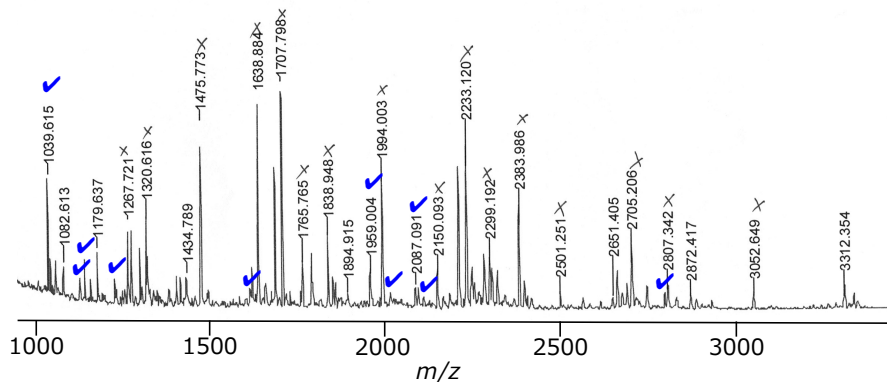

Figure 2-16. MALDI-TOF MS analysis of the tryptic peptides derived from the 58 kDa proteins; Check marks in blue represent the peptide ions that were identified as human β-tubulin. "x" represents the peptides derived from non-specific contaminants (trypsin, keratin, etc.).

Table 2-4. Tryptic peptides of the 58 kDa protein detected by MALDI-TOF MS.

human β-tubulin (accession No. P07437)

	Observed (m/z)[a]	calcd (m/z)	Start		End	Sequence
K1	1039.62	1039.59	310	-	318	YLTVAAVFR
K2	1130.61	1130.60	242	-	251	FPGQLNADLR
K3	1143.65	1143.63	253	-	262	LAVNMVPFPR
K4	1229.63	1229.60	381	-	390	ISEQFTAMFR
K5	1615.86	1615.84	63	-	76	AILVDLEPGTMDSVR
K6	1620.86	1620.84	263	-	276	LHFFMPGFAPLTSR
K7	1959.00	1958.98	104	-	121	GHYTEGAELVDSVLDVVR
K8	2026.10	2026.08	363	-	380	MAVTFIGNSTAIQELFKR
K9	2087.09	2087.08	104	-	122	GHYTEGAELVDSVLDVVRK
K10	2110.09	2110.06[b]	1	-	19	MREIVHIQAGQCGNQIGAK
K12	2798.36	2798.34	78	-	103	SGPFGQIFRPDNFVFGQSGAGNNWAK

[a] The data represent the monoisotopic ion peak [M+H]$^+$ values.

[b] Putative values indicating that the Cys residue(s) in the sequences are carbamidomethylated.

human α-tubulin (accession No. Q9BQE3)

```
1     MRECISIHVG  QAGVQIGNAC  WELYCLEHGI  QPDGQMPSDK  TIGGGDDSFN  TFFSETGAGK  HVPRAVFVDL  EPTVIDEVRT
                                                                                            K3
81    GTYRQLFHPE  QLITGKEDAA  NNYARGHYTI  GKEIIDLVLD  RIRKLADQCT  GLQGFLVFHS  FGGGTGSGFT  SLLMERLSVD
                                         K1
161   YGKKSKLEFS  IYPAPQVSTA  VVEPYNSILT  THTTLEHSDC  AFMVDNEAIY  DICRRNLDIE  RPTYTNLNRL  ISQIVSSITA
                                                                              K4          K2
241   SLRFDGALNV  DLTEFQTNLV  PYPRIHFPLA  TYAPVISAEK  AYHEQLTVAE  ITNACFEPAN  QMVKCDPRHG  KYMACCLLYR
                  K5
321   GDVVPKDVNA  AIATIKTKRT  IQFVDWCPTG  FKVGINYQPP  TVVPGGDLAK  VQRAVCMLSN  TTAVAEAWAR  LDHKFDLMYA

401   KRAFVHWYVG  EGMEEGEFSE  AREDMAALEK  DYEEVGADSA  DGEDEGEEY
```

human β-tubulin (accession No. P07437)

```
1     MREIVHIQAG  QCGNQIGAKF  WEVISDEHGI  DPTGTYHGDS  DLQLDRISVY  YNEATGGKYV  PRAILVDLEP  GTMDSVRSGP
                  K10                    K13                                             K5
81    FGQIFRPDNF  VFGQSGAGNN  WAKGHYTEGA  ELVDSVLDVV  RKEAESCDCL  QGFQLTHSLG  GGTGSGMGTL  LISKIREEYP
                  K12                    K7  K9
161   DRIMNTFSVV  PSPKVSDTVV  EPYNATLSVH  QLVENTDETY  CIDNEALYDI  CFRTLKLTTP  TYGDLNHLVS  ATMSGVTTCL
                                                                                        K11
241   RFPGQLNADL  RKLAVNMVPF  PRLHFFMPGF  APLTSRGSQQ  YRALTVPELT  QQVFDAKNMM  AACDPRHGRY  LTVAAVFRGR
      K2          K3          K6                                                         K1
321   MSMKEVDEQM  LNVQNKNSSY  FVEWIPNNVK  TAVCDIPPRG  LKMAVTFIGN  STAIQELFKR  ISEQFTAMFR  RKAFLHWYTG
                                                     K8                      K4
401   EGMDEMEFTE  AESNMNDLVS  EYQQYQDATA  EEEEDFGEEA  EEEA
```

Figure 2-17. Amino acid sequences of human α- and β-tubulin. The sequences of the tryptic fragments (K1–K5 for α-tubulin and K1–K13 for β-tubulin) identical to the MS data are indicated by solid underlines.

2-3-5. Purification of the Target Proteins of Aplyronine A from Cell Lysate

The reason why tubulin was not specifically purified from cell lysate using biotin probe **17** is expected that tubulin denatured in the process of cell lysis, and did not interact with ApA moiety of **17**. The author thought that tubulin might be purified form cell lysate by optimizing the condition to prepare cell lysate. When the lysate was prepared by using general cell lysis buffer [10 mM Tris·HCl (pH 7.4), 0.15 M NaCl, 10 μg/mL leupeptin and 1% triton-X 100] and target proteins were photolabeled and affinity-purified with ApA-PB (**17**), tubulin was slightly detected by silver stain, but not specific for **17** (*Lane 1* and *2*, Figure 2-18). The reason is anticipated that tubulin denatured and non-specifically interacted with the resin. And, only actin was specifically detected by Western blotting as the target protein of ApA. Additionally, Arp2,3, which were also purified by biotin probe **7**[2], were detected by silver stain, but not detected by Western blotting (*Lane 9* and *10*), suggesting that Arp2 and Arp3 were not labeled by ApA-PB (**17**) at this condition. These results indicated that general cell lysis buffer was unsuitable for the purification of tubulin. So, RBR80 buffer [80 mM PIPES·Na (pH 6.9), 1 mM MgCl₂, 1 mM EGTA, 1 mM GTP], which is suitable for tubulin, was next examined for the purification of the target proteins. Furthermore, the effects of surfactant, 1% triton-X 100, on the purification of tubulin were checked.
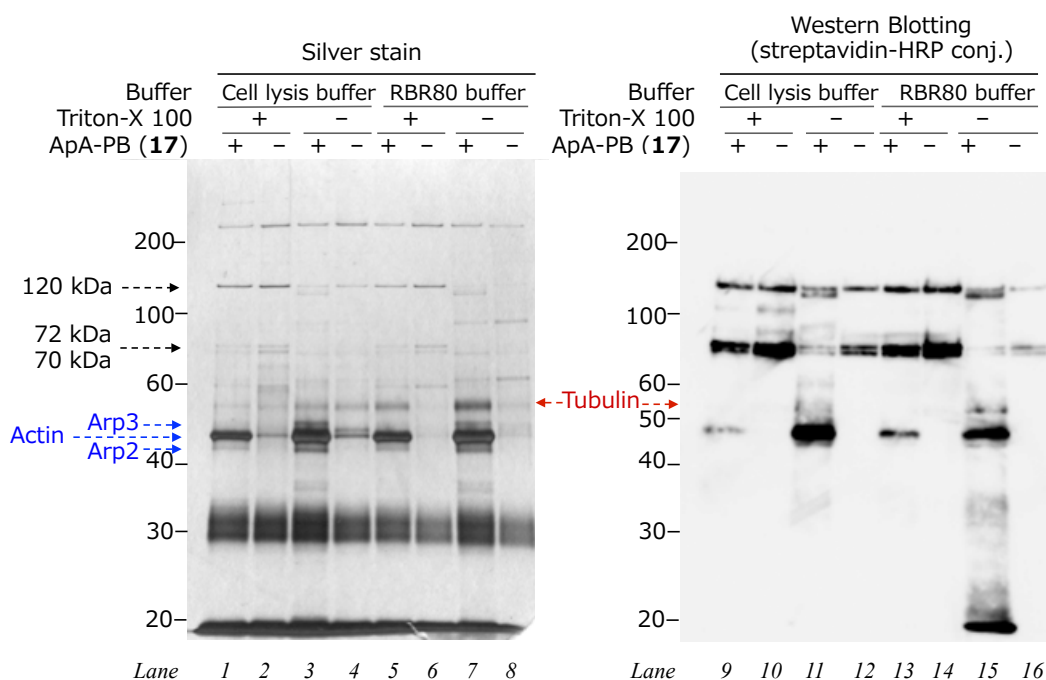

Figure 2-18. Purification of target proteins of ApA from cell lysate.

The target proteins of ApA were purified using ApA-PB (**17**) from cell lysate prepared with BRB80 buffers and detected by silver stain and Western blotting (*Lanes 5-8,13-16*, Figure 2-18). As a result, tubulin was specifically purified by using ApA-PB (**17**) (*Lanes 5,7*) along with actin and also detected by Western blotting (*Lane 15*). So, specific photolabeling with ApA-PB (**17**) occurred. Additionally, when triton-X 100 was not used, the purified amount of intrinsic biotin-binding proteins (70, 72, and 120 kDa) decreased compared with the use of triton-X 100 (*Lanes 5-8,13-16*), and the amount of actin, Arp2, 3 and tubulin purified by using ApA-PB (**17**) increased (*Lanes 5,7,13,15*). In the condition of the absence of triton-X 100, crushing of cellular and mitochondrial membranes were expected to be insufficient. Since biotin-binding proteins (70-72 and 120 kDa)

were highly contained in mitochondria,[13] the extracted amount of intrinsic biotin-binding proteins were thought to decrease without surfactant. Therefore, it was thought that the capacity of NeutrAvidin-resin to bind to ApA-PB (**17**) increased, and target proteins of ApA were more efficiently purified in absence of triton-X 100. Actually, in the cases of using cell lysis buffer, the detected amount of biotin-binding proteins also decreased (*lane 3,4,11,12*), and the amount of tubulin increased to the detectable level of Western blotting (*lane 11*). This result suggested that a few tubulin molecules were labeled with ApA-PB (**17**) even in the unsuitable condition for tubulin.

Based on above experiments, the author verified that tubulin was specifically purified from the cell lysate as the target protein of ApA.

As the result of Western blotting analysis with anti-tubulin by co-worker[15], the 55 kDa protein was identified as α- and β-tubulin, and 58 kDa was β-tubulin. Additionally co-worker established that ApA formed an 1:1:1 complex of actin−ApA−tubulin heterodimer by gel permeation HPLC analysis. And it was shown that ApA has synergistic inhibitory effect on tubulin polymerizing in the presence of actin. In contrast, ApC rarely showed these effects on tubulin. These results suggested that ApA induces the protein-protein interaction between actin and tubulin through the C7 trimethylserine moiety, followed by the inhibition of tubulin polymerization.

2-4. Analysis of the Effects of Aplyronine A on Microtubule Dynamics *in situ*

The interaction between actin-ApA complex and tubulin was expected to closely relate to the potent anti-tumor activity of ApA. So, in this section, the effect of ApA on cellular microtubule dynamics was examined.

Microtubule-targeting compounds, such as taxol, colchicine, and vinblastine, generally affect microtubule dynamics and inhibit the formation of bipolar (normal) spindles that are assemble forms of microtubule in metaphase cells, followed by inducing mitotic block. So, the author first tried to check the effect of aplyronines on spindles in tumor cells.

2-4-1. The Effect on Spindle Formation

Immunostaining experiments showed that HeLa S3 cells treated with 100 pM ApA had irregular multipolar spindle structures with unaligned chromosomes (Figure 2-19). Treatment with 1 nM ApA strongly inhibited spindle formation and induced abnormal spindle formation as with 10 nM vinblastine. At the same concentration, microtubule structures in interphase cells were partially disrupted but actin filaments were hardly affected, comparable to the effects of the treatment with 10 nM vinblastine.
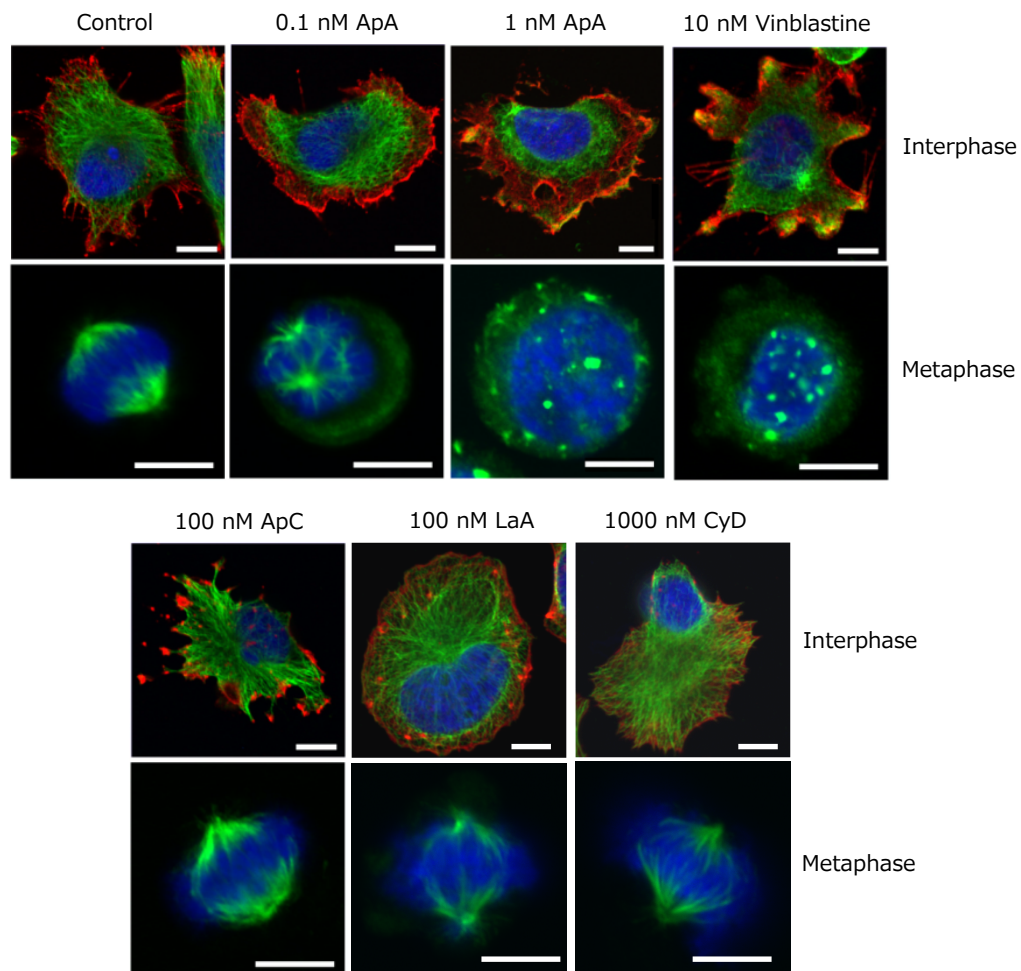

Figure 2-19. Confocal fluorescence images of HeLa S3 cells treated with various compounds for 6 h. Interphase cells were immunostained with anti-α-tubulin (green), anti-β-actin (red) and costained with DAPI (blue). In metaphase cells, only α-tubulin (green) and DAPI (blue) were shown. Scale bars: 10 μm.

To evaluate the effects on the spindle formation statistically, the author counted irregular (multipolar and abnormal) spindles and normal spindles on mitotic cells that were synchronized with hydroxyurea (HU)[16]. Irregular spindles were observed in 36%, 52%, and 91% of synchronized mitotic cells by treatment with 0.1, 1, and 10 nM ApA, respectively, but in only 13% of control cells (Figure 2-20). So, ApA induced the irregular spindle formation in a dose-dependent manner. The result of treatment with 10 nM ApA was comparable to 10 nM vinblastine (VBL).
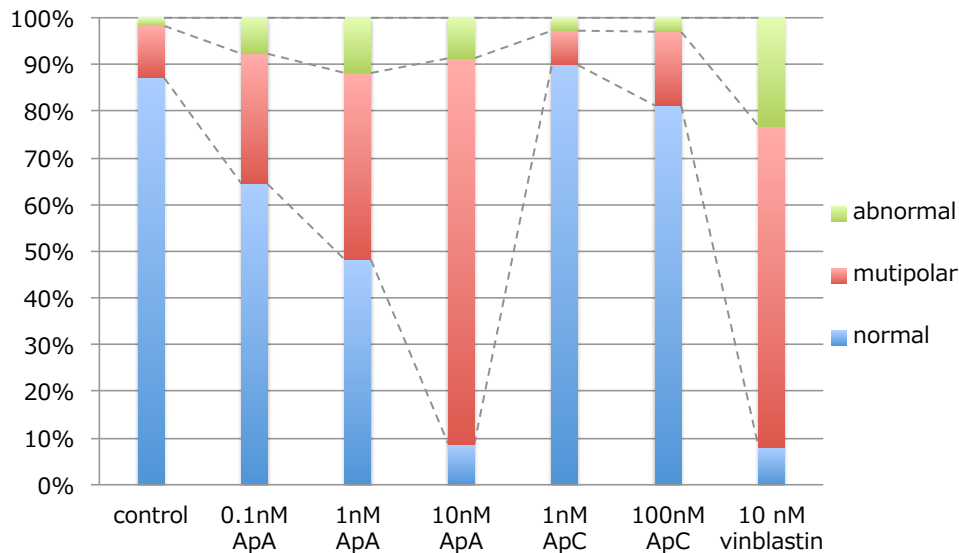

Figure 2-20. Classification of metaphase cells based on their spindle structures. HeLa S3 cells were synchronized with 0.1 mM HU, and samples were treated for 3 h. At least 120 mitotic cells were counted for each sample.

In contrast, treatment with ApC had no effects on spindle formation in metaphase cells even at 100 nM, the same concentration that caused complete disassembly of the actin cytoskeleton in interphase cells (Figure 2-19). Moreover, there were little difference between 1-100 nM ApC and control in ratio of irregular spindles (Figure 2-20).

The author also observed the cells treated with two actin-targeting agents that bind to the different sites of actin from aplyronines, latrunculin A (LaA) and cytochalasin D (CyD). Each agent showed the cell-growth inhibitory activity against HeLa S3 cells (IC$_{50}$ 94 and 34 nM, respectively). As shown in Figure 2-19, both compounds partially disrupted actin cytoskeleton in interphase cells at the cell-growth inhibitory concentration (100 nM and 1000 nM, respectively). They, however, affected neither microtubule dynamics in interphase cells nor spindle formation in metaphase cells. These results suggested that the effect of sub-nM ApA on spindle, which is cell-growth inhibitory concentration, was attributed to the disruption of microtubule dynamics, not of actin cytoskeleton.

2-4-2. Cell Cycle Analysis

Microtubule-targeting compounds generally inhibit cell cycle progression. Cell cycle is divided to four periods[17] (Figure 2-21a). The three periods are interphase, and each is referred to G1, S, and G2 phases. G1 phase extends from the end of cell division to the beginning of DNA replication. During the second period, S phase, DNA replication takes place. G2 phase is the stage from the end of DNA replication to the early stage of the division into two daughter cells. Fourth period is metaphase and is referred to M phase. Mitosis and cytokinesis occur at M phase. Aside from these four phases, G0 phase exists. Non-proliferative cells enter the quiescent G0 phase from G1 phase in general. Cell cycle can be analyzed by the measurement of fluorescent intensity of the cells in which DNA were stained with a fluorophore, propidium iodide (PI), since each phase cell has different amounts of DNA. FCM analysis of the HeLa S3 cells stained with PI gives the histogram as shown in Figure 2-21b. G0/G1 cells generally exist at a higher ratio than S and G2/M phase.
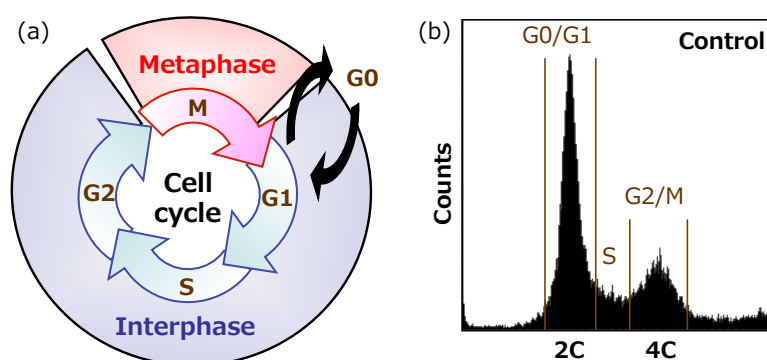

Figure 2-21. Cell cycle. (a) Outline of cell cycle. (b) Flow cytometry analysis of HeLa S3 cells stained by PI. G0 and G1 phase cells have diploid chromosome (2C), G2 and M phase cells contain tetraploid chromosome (4C). The value of chromosome at S phase cells shows between 2C and 4C.

ApA induced G2/M arrest against HeLa S3 cells in a dose-dependent manner (Figure 2-22), and most of HeLa S3 cells were arrested at G2/M phase with ApA at 1 nM, the same concentration as that in the spindle formation inhibition, and this effect was comparable to 10 nM vinblastine. The same treatment of 1 nM ApC hardly affected cell cycle. G2/M arrest seemed to occur when HeLa S3 cells were treated with 100 nM ApC. The treatment of HeLa S3 cells with ApC at this concentration results in the disruption of actin filament as described in section 2-2-4. And 100 nM ApC hardly inhibited spindle formation as shown above. So, the author presumed that 100 nM ApC blocked cytokinesis, but not mitosis. This means that ApC did not inhibit cell cycle progression. If only cytokinesis is blocked, binucleated cells are thought to generate. Actually, it was reported that the binucleation of the cells is caused by the treatment with an actin-binding compound, cytochalasin B, which is the analog of cytochalasin D.[18] The author found that binucleated cells were also formed by treating with 100 nM LaA for 24 h (Figure 2-23). When HeLa S3 cells treated with 100 nM ApC, binucleated cells were observed as with LaA. It was confirmed that ApC did not inhibit cell cycle progression, but blocked cytokinesis.

These results indicated that ApA induces G2/M arrest by the abnormal spindle formation at very low concentration (0.1-1 nM), and these effects were thought to be deeply related to the interaction with tubulin through the C7 trimethylserine moiety of ApA.
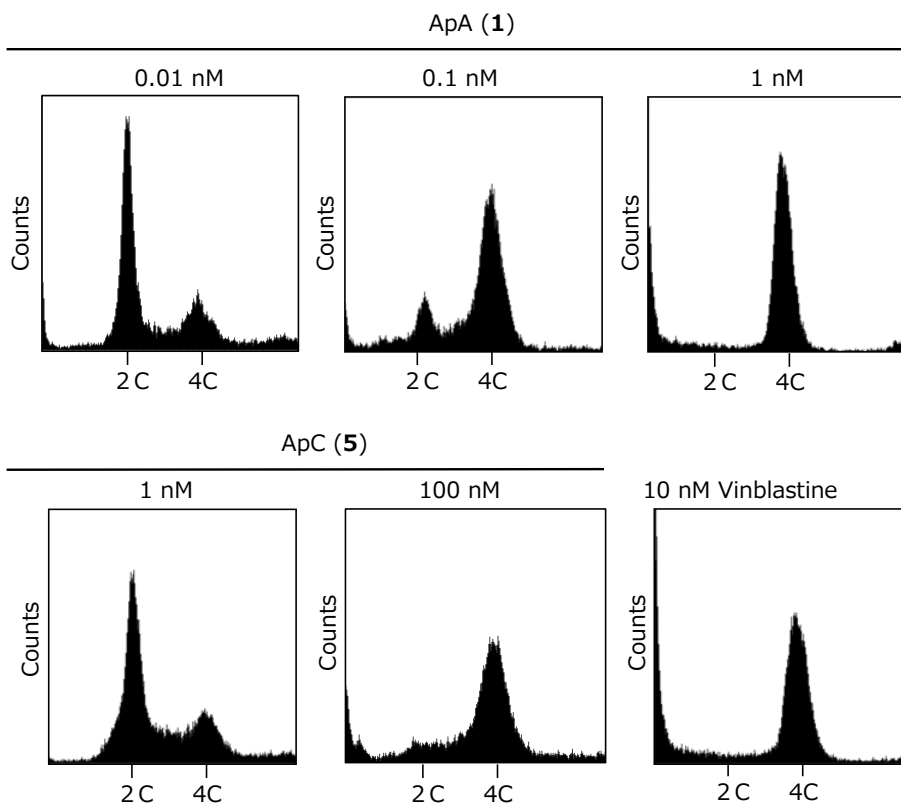

Figure 2-22. Cell cycle analysis. HeLa S3 cells were treated with compounds for 18 h followed by PI staining.
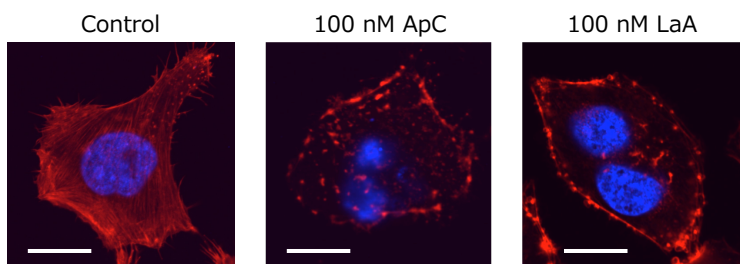

Figure 2-23. Confocal fluorescence images of HeLa S3 cells treated with ApC and LaA for 24 h. Cells were stained with rhodamine-phalloidin (red, F-actin) and DAPI (blue, nucleus). Scale bars: 20 μm.

2-4-3. Apoptosis Inducing Activity

The inhibitory effects of ApA on spindle formation and mitosis might be essential for its antitumor activity. Generally, microtubule-targeting compounds induce G2/M arrest of cell cycle, resulting in the cellular death (apoptosis) in many cases.[19] In this section, the assay about death of cells is presented.

To check dead cells, cell viability assay based on trypan blue dye exclusion was performed. Dead cells treated with compounds were selectively stained with trypan blue. ApA-induced cell death was approximately 1000-fold stronger than other actin-targeting agents, such as latrunclin, MyB and ApC, and also more potent than an antitumor agent, vinblastine (Figure 2-24).
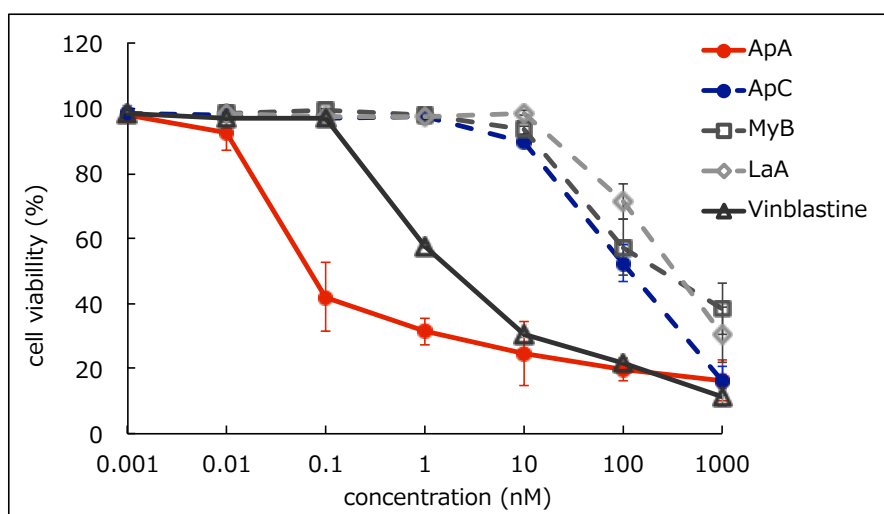

Figure 2-24. Cell viability assay based on trypan blue dye exclusion. After HeLa S3 cells were treated with compounds for 96 h, trypan blue was added to the cells. Nonstained cells (alive) and stained (dead) cells were counted. Values are the means ±SD of independent experiments, n = 4 (ApA and ApC) and 2 (MyB, LaA and vinblastine).

Cell death is typically subdivided into apoptosis and necrosis.[20] Apoptosis is the process of programmed cell death executed by intrinsic cellular machinery, and characterized by morphological changes, such as cell rounding, membrane blebbing, and DNA fragmentation. Necrosis is unregulated cell death and is induced by overwhelming stress, which is incompatible with cell survival. Programmed process of apoptosis is mainly orchestrated by caspases, a family of cysteine proteases. Among caspases family, caspase-3 is activated in the later phase of apoptosis (Figure 2-25a) and DNA fragmentation occurs in the downstream step of caspase-3 activation.[21] So, caspase-3 is activated in many cases that apoptosis occurs. Therefore, enzymatic activity of activated caspase-3 was examined to study on cell death induced by ApA in more detail. Activated caspase-3 specifically recognizes a particular peptide sequence, DEVD, and then the C-terminus of aspartic acid residue is hydrolyzed. Activated caspase-3 hydrolyzes Ac-DEVD-pNA to release p-nitroaniline (pNA), the quantity of which was determined by its absorbance at 405 nm (Figure 2-25b). Based on the colorimetric assay, enzymatic activity of caspase-3 was established.
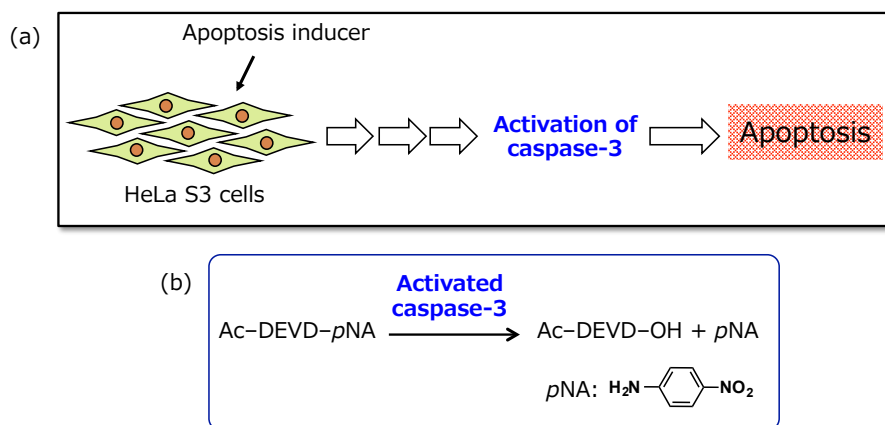
Figure 2-25. Outline of caspase-3 assay. (a) The relationship of caspase-3 with apoptosis. (b) The reaction of activated caspase-3 with Ac-DEVD-*p*NA.

Caspase-3 assay of HeLa S3 cells treated with compounds was tested. The caspase-3 activity significantly increased (> 250%) by 1 nM ApA on HeLa S3 cells (Figure 2-26). This effect of ApA was stronger than a positive control, 135 nM corcemide. In the cases of aplyronine C (ApC) and mycalolide B (MyB), caspase-3 activities were almost same level as a control (−) even at 100 nM that is the concentration to disrupt cellular actin cytoskeleton. Additionally, DNA fragmentation was also detected by treatment of HeLa S3 cells with 1 nM ApA.[22] So, it was found that ApA surely induced caspase-3 dependent apoptosis in HeLa S3 cells.
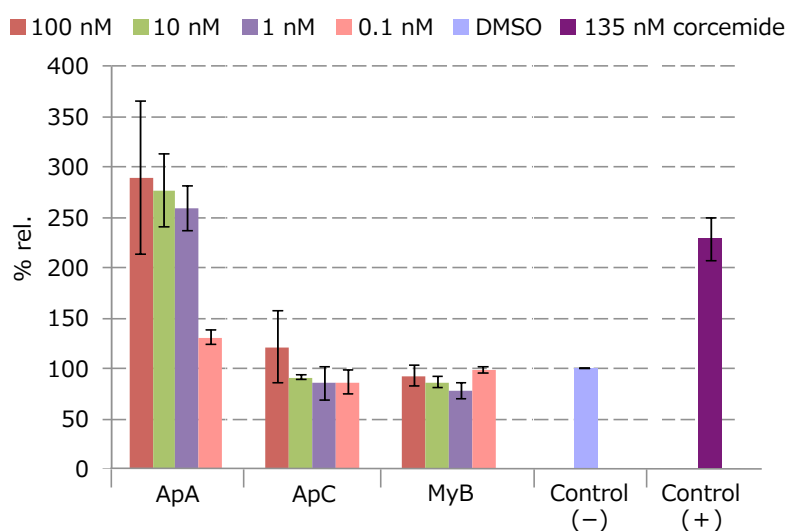
Figure 2-26. Enzymatic assay of caspase-3. After treating with each compound for 24 h incubation, HeLa S3 cells were lysed and capase-3 activities were measured.

As described above, ApA inhibited microtubule dynamics by the formation of ternary complex with actin and tubulin. And this effect on tubulin was thought to be important for the spindle formation inhibition and cell cycle arrest induced by 1 nM ApA. Because this concentration was the same as that induces the caspase-3 activation of HeLa S3 cells, the effects of ApA on tubulin, spindle and cell cycle were expected to be closely related to the apoptosis induced by ApA.

2-4. Summary

To analyze the mode of action of anti-tumor macrolide aplyronine A (ApA, **1**), fluorescent probes and photoaffinity biotin probes were synthesized. It was indicated that ApA binds to cytoplasmic actin and accumulates into HeLa S3 cells by the fluorescent observation and flow cytometry analysis using ApA fluorescent probe (ApA-FL, **8**). On the photolabeling experiment with ApA photoaffinity biotin probe (ApA-PB, **17**), tubulin was specifically purified along with actin. And tubulin was not detected by the experiment with ApC-PB (**18**), suggesting that the second target protein of ApA was tubulin, and C7 trimethylserine moiety plays an important role for the interaction between tubulin and ApA.

Co-worker has clarified that ApA forms the 1:1:1 complex with actin and tubulin, followed by inhibiting microtubule dynamics. And the author showed that ApA inhibits normal spindle formation of HeLa S3 cells and causes G2/M arrest at only 0.1-1 nM, which is just same as the cell-growth inhibitory concentration, but does not affect actin cytoskeleton. Additionally, 1 nM ApA caused the apoptosis of HeLa S3 cells.

From the above experiments, the author hypothesized that the potent antitumor activity of ApA is deeply related to the a series of effects as follows: (1) An actin‑tubulin‑ApA ternary complex affects microtubule dynamics but not actin cytoskeleton. (2) Irregular spindles are formed and cell cycle progression is inhibited. (3) Apoptosis is induced.

Anti-tumor activity of ApA is stronger than many tubulin-targeting compounds, and the protein-protein interaction between actin and tubulin by small molecules has not been reported. So clarifying the binding mode of actin-ApA complex with tubulin may lead to the discovery of new pharmaceutical lead compounds and new tools that induce new PPIs. Therefore, the author next tried to develop novel chemical probes to analyze the binding mode of ApA on target proteins. These results and discussions are presented at the next chapter.

2-6. Experimental

2-6-1. General

NMR spectra were recorded on a Bruker Biospin AVANCE 600 spectrometer (600 MHz for ^{1}H). Chemical shifts are reported in parts per million (ppm) with coupling constants (J) in hertz relative to the solvent peaks, δ_H 3.31 (residual CHD_2OD). For the quantification of minute amounts of specimens by ^{1}H NMR analyses, dichloromethane (10-50 mM in CD_3OD) or benzene (8.3-20 mM in CD_3OD) was added to the sample solutions as a standard (1:60-120, v/v). Fluorescence spectra were measured on a Hitachi F-4500 spectrofluorophotometer with H_2O as solvents. High-resolution electrospray ionization mass spectra (HR-ESIMS) were measured on an AccuTOF CS spectrometer (JEOL). Matrix-assisted laser desorption/ionization with time-of-flight mass spectra (MALDI-TOF MS) were measured using a Bruker ultrafleXtreme spectrometer with α-cyano-4-hydroxycinnamic acid (CHCA) as a matrix.

Chemicals and solvents were the best grade available and were used as purchased with following experiment. Synthetic and biological experiments using aryl diazirine derivatives were conducted with light-shaded glass or plastic tube, and under a yellow-filtered light hood.

For the bioassays, TAMRA derivatives and biotin derivatives were all stored in DMSO at 1 mM.

2-6-2. Cell Culture and Cell-growth Inhibitory Assay

HeLa S3 cells (suspension culture-adapted human cervical carcinoma cell line, ATCC CCL-2.2) were cultured in Eagle's minimal essential medium (E-MEM) supplemented with fetal bovine serum (FBS, 10%) in a humidified atmosphere containing CO_2 (5%) at 37 °C. The cell-growth inhibitory activities of the probes and model compounds were measured by the 3-(4,5-dimethylthiazol-2-yl)-2,5-diphenyltetrazolium bromide (MTT) method. HeLa S3 cells were seeded at 2×10^4 cells per well in 96-well plates. After incubation for 1 day at 37 °C, compounds (1 pM – 5 μM) were added, and the cells were incubated for 96 h at 37 °C. After MTT was added, the mixtures were incubated for 3 h to give an insoluble formazan derivative. The medium was removed, and the formazan derivative was dissolved in DMSO, followed by the absorbance measurement at 540 nm on Immuno MiniNJ-2300 spectrometer (BioTec) or Infinite F200 PRO spectrofluorophotometer (TECAN). The IC_{50} values (concentrations required for 50% inhibition of cell growth) were determined using a growth curve by comparison of negative control wells.

2-6-3. Recovery of ApA-FL (**8**) from HeLa S3 Cells

ApA-FL (**8**, 5 μM) was added to HeLa S3 cells in a 6-well plate [90% confluent, culture medium was replaced with Hank's balanced saline solution (HBSS, Nakalai Tesque) before 24 h]. After the cells were incubated for 30 min at 37 °C, cells were washed four times with HBSS. DMSO (600 μL) was added to the cells and shaken for 1 h to crush the cells. After centrifugation, the supernatant was lyophilized and analyzed by HPLC [Develosil ODS-HG-5 (φ 4.6 mm I.D. × 250 mm), MeOH/20 mM ammonium acetate (80/20), 1 mL/min, UV 254 nm, λ_{ex} 565 nm, λ_{em} 580 nm].

2-6-4. *In vitro* Actin-depolymerizing Activity Assay

The actin-depolymerizing activities were measured on the basis of their abilities to attenuate the fluorescence of pyrene-conjugated (pyrenyl) actin. A 0.15 M $MgCl_2$ solution (3.3 μL) was added to a 3 μM solution of actin (from rabbit skeletal muscle, Cytoskeleton Inc., containing 10% pyrenyl actin) in G-buffer [2 mM Tris·HCl (pH8.0), 0.2 mM $CaCl_2$, 0.2 mM ATP, 0.5 mM 2-mercaptoethanol] (500 μL), and the mixture was stirred at room temperature for 1 h to polymerize G-actin to F-actin. The fluorescent derivatives were added to the solution of F-actin with stirring, and the time course of depolymerization was continuously monitored by measuring fluorescence of pyrenyl actin with a fluorometer with a magnetic stirrer at 25 °C at 365 nm excitation and 407 nm emission wavelengths. The EC_{50} values mean the concentration required to depolymerize F-actin to 50% of its control amplitude.

2-6-5. Fluorescence Microscopy Observations

HEp-2 cells (human laryngeal epithelial carcinoma cells) were cultured in Eagle's minimal essential medium (E-MEM) supplemented with 10% FBS in a humidified atmosphere containing CO_2 (5 %). Enhanced green fluorescent protein (EGFP)-actin-expressing[23] Epstein−Barr virus (EBV)-based vector[24], pEB6CAGFPAct, was introduced into HEp-2 cells with Lipofectamine LTX (Life Technologies). After four days selection with G418 (1 mg/mL), cells were stained with ApA-FL (**8**, 3 μM) for 30 min and imaged with a Sensys[TM] CCD camera attached to an Olympus IX70 inverted fluorescent microscope with filters for excitation 495/20 and emission 535/30 on GFP-actin observation.

HeLa S3 cells were cultured in E-MEM supplemented with 10% FBS in a humidified atmosphere containing CO_2 (5 %). Cells (1.5×10^4 cells per 150 μL) were seeded on a glass-bottomed dish (φ 12 mm, Asahi Glass) and incubated at 37 °C for 12 h. After the addition of culture medium (2 mL), cells were incubated for an additional 12 h. After the culture medium had been replaced with fresh medium (300 μL), fluorescent probes (500 nM) were added. After incubation for 1 h, cells were washed with the culture medium (twice) and incubated for an additional hour. Cells were treated with the culture medium containing Hoechst 33342 (10 μg/mL) before observation. Fluorescence and bright-field images of living cells were captured by use of an Olympus FV1000-D laser scanning confocal microscope.

2-6-6. Flow Cytometry Analyses for Cellular Accumulation

Fluorescent probes in DMSO were added to the HEp-2 cells in a 24-well plate (90% confluent) or HeLa S3 cells in a 6-well plate. After 0.5, 2 or 6 h, cells were washed with PBS (three times) and treated with trypsin/EDTA (0.05 %). The cells were resuspended in PBS, and the cellular TAMRA fluorescence was immediately measured with a FACSCalibur flow cytometer (BD Biosciences) or an Attune[TM] Acoustic Focusing Cytometer (Life Technologies) with argon laser excitation (488 nm). Alternatively, after the incubation with fluorescent probes for 30 min, cells were washed with the culture medium (twice) and further incubated for 1.5 h, and the flow cytometry analyses were then conducted as above.

2-6-7. Immunofluorescence Staining

Exponentially growing HeLa S3 cells were seeded on an 8-well glass chamber slide coated with collagen (Lab-Tek[TM], Nunc) at 1.2×10^4 cells per 0.25 mL. The cells were incubated for 24 h at 37 °C, prior to addition of samples.

For F-actin staining, the cells were incubated for 2 h at 37 °C, washed twice with phosphate buffer saline (PBS), fixed with 4% paraformaldehyde in PBS for 20 min, washed three times with PBS, and then permeabilized for 5 min with PBS containing 0.25% Triton X-100. The cells were washed three times with PBS, and blocked for 1 h with 0.1% Tween 20 in PBS (PBS-T) containing 1% bovine serum albumin (BSA). The cells were then incubated in rhodamine-phalloidin (Molecular Probes) at 0.14 μM, and the mixture was left to stand for 1 h. The cells were washed three times with PBS-T, then 4',6-diamidino-2-phenylindole (DAPI, DOJINDO) at 0.5 μg/mL in PBS was added, and the mixture was left to stand for 1 h. The cells were again washed with PBS, the polystyrene chambers were removed, and slides were mounted with SlowFade® Gold antifade reagent (Invitrogen). Fluorescence and bright-field images of fixed cells were captured using an Olympus FV1000-D laser scanning confocal microscope.

For microtubule staining, cells that had been treated with samples for 6 h at 37 °C were washed with PBS, and fixed with MeOH (0.25 mL) for 30 min at –20 °C. After washing with PBS, the cells were blocked with 0.5% BSA in PBS for 1 h at room temperature. The cells were then incubated in anti-α-tubulin monoclonal antibody DM1A (cat. no. sc-32293, Santa Cruz Biotechnology) at 0.8 μg/mL and anti-β-actin polyclonal antibody (cat. no. ab8227, Abcam) at 0.63 μg/mL, diluted in the blocking buffer, for 1 h at room temperature. The cells were washed with 0.5% BSA/PBS, and incubated in Alexa Fluor® 488 anti-mouse IgG (cat. no. 4408S, Cell Signaling Technology) at 2 μg/mL and Alexa Fluor® 568 goat anti-rabbit IgG (cat. no. A-11011, Invitrogen) at 2 μg/mL, diluted in 0.5% BSA/PBS. The mixture was left to stand for 1 h at room temperature. The mixture was washed four times with PBS, then DAPI at 0.5 μg/mL in PBS was added, and the mixture was left to stand for 1 h. After washing three times with PBS, the polystyrene chambers were removed, slides were mounted, and fluorescent microscopy observations were carried out as described above.

To classify the M-phase cells treated with samples based on their spindle structures, HeLa S3 cells were synchronized at the G1/S phase by a double-hydroxyurea (HU) block. Exponentially growing cells were seeded on an 8-well glass chamber slide coated with collagen at 2.5×10^4 cells per 0.25 mL. After the incubation for 24 h at 37 °C, the cells were cultured in E-MEM supplemented with 10% FBS containing 0.1 mM HU for 24 h. The wells were washed with culture medium and were incubated for 10 h in medium lacking HU. Medium was exchanged with the medium containing 0.1 mM HU, and cells were incubated an additional 15 h. Cells were then incubated for 6 h to reach a peak in mitosis. After the treatment with samples for 3 h at 37 °C, the cells were fixed and immunostained as described above.

2-6-8. Cell Cycle Analyses

HeLa S3 cells were seeded at 3×10^4 cells/mL in 6-well plates. Samples were added after incubation overnight at 37 °C. The cells were incubated for 18 h at 37 °C, then treated with 0.05% trypsin–EDTA. The collected cells were washed with PBS, resuspended in 500 μL of cooled 70% EtOH aq., and left to stand for 30 min at −20 °C. The fixed cells were collected by centrifugation, washed with PBS, and stained with PI solution (50 μg/mL propidium iodide, 1 mg/mL sodium citrate, 2 mg/mL NP40, 20 μg/mL RNase A) overnight at 4 °C. The amount of cellular DNA was measured by an Attune™ Acoustic Focusing Cytometer with argon laser excitation (488 nm).

2-6-9. *In situ* Photolabeling Assay

Aplyronine photoaffinity derivatives (2.5 μM) were added to the HeLa S3 cells in a 6-well plate (80% confluent). After incubation for 2 h at 37 °C, the cells were cooled on ice and irradiated with UV light (365 nm) for 15 min, using a handheld UV lamp (0.8 mW/cm^2). The culture medium was removed, and the cells were scraped and lysed in 200 μL of lysis buffer [80 mM PIPES (pH 6.9), 1 mM EGTA, 1 mM MgCl$_2$, 1 mM GTP]. After the freeze-thawing process, which was repeated five times, the lysate were filtered (Millipore 0.45 μm centrifugal filter), and treated with NeutrAvidin agarose resin (40 μL), equilibrated with lysis buffer. After incubation with a rotator for 1 h at 4 °C, the resins were washed four times with PBS-T, three times with 0.1% Tween 20 in 1 M KCl, and twice with PBS, then resuspended in 2×SDS buffer (40 μL). The binding proteins were eluted by boiling for 5 min at 95 °C. SDS-PAGE was performed by using a precast 10% polyacrylamide gel, and the gels were stained with a Silver Stain Kit for Protein (GE Healthcare).

For immunoblot analyses, proteins in the gels after electrophoresis were transferred to PVDF membranes, using the Trans-Blot® SD semi-dry blotting system (Bio-Rad), according to the manufacturer's instructions. Proteins were detected with HRP-conjugated streptavidin (1:3000, cat. no. RPN1231v, GE Healthcare). The HRP-conjugated bands were visualized with an ECL-prime system (GE Healthcare), and detected by a Fujifilm LAS-4000 MINI imaging scanner. Densitometry of Western blots and CBB-stained proteins were performed using ImageJ software.

2-6-10. In-gel Digestion and PMF Analyses

After SDS-PAGE, gels were silver-stained in a mass-compatible manner as follows[14]. The gel was fixed by 5% acetic acid in 50% methanol for 0.5 h. After the gel was washed with water twice, sensitized in 0.02% sodium thiosulfate for 2 min. After washing with water for 1 min twice, the gel was shaken in 0.25% silver nitrate solution for 30 min. and washed with water for 1 min twice. Then stained bands were developed in 0.004% formaldehyde, 2% sodium carbonate, followed by removal of the developing solution and washing the gel with 1% acetic acid. Stained spots were excised from the PAGE gel. The gels were desilverized by vortexing in 30 mM potassium ferricyanide / 100 mM sodium thiosulfate (v/v = 1/1) and dehydrated in acetonitrile. And the proteins in the gels were reduced by 10 mM dithiotreitol (DTT) in 25 mM ammonium bicarbonate for 45 min at 56 °C, and then carbamidomethylated by vortexing in 55 mM iodoacetamide, 25 mM ammonium bicarbonate for 30 min under light shielding. After washing the gel with 50% acetonitrile in 25 mM ammonium bicarbonate three times and dehydration in acetonitrile, the gels were incubated with a sequence-grade, modified trypsin (1:100 w/w, #V5111, Promega) in 25 mM ammonium bicarbonate for 19 h at 37 °C. The tryptic peptides were extracted from the gel by 5% trifluoroacetic acid in 50% acetonitrile and desalted using a prespotted Anchorchip[TM] (PAC 384/96 CHCA, Bruker Daltonics), according to the manufacturer's instruction for MS analyses. Detected peaks were transferred into the peptide mass fingerprint search program, MS fit in ProteinProspector (http://prospector.ucsf.edu/prospector/mshome.htm). SwissProt was used as Database, and the search of proteins were conducted by the condition including partial methionine oxidation, N-terminal acetylation, conversion of N-terminal glutamine to pyroglutamic acid residue, complete cysteine carbamidomethylation, and one missed trypsin cleavages.

2-6-11. Photolabeling and Affinity Purification of Aplyronine Binding Proteins in HeLa S3 Cell Lysate

HeLa S3 cells (3.4×10^7 cells) in culture were washed twice with phosphate-buffered saline (PBS), and treated with 0.05% trypsin–EDTA. Suspended cells were collected by spin-down and washed with PBS. The cells were divided into four equal parts. To each cells were added 1.0 mL of cell lysis buffer (10 mM Tris·HCl [pH 7.4], 0.15 M NaCl, 10 μg/mL leupeptin) with or without 1% Triton X-100, or BRB80 buffer (80 mM PIPES·Na [pH 6.9], 1 mM $MgCl_2$, 1 mM EGTA, 1 mM GTP) with or without 1% Triton X-100. And, the cells were lysed in the buffers with a pestle at 4 °C and filtered by using Centrifugal Filter Unit with Durapore® PVDF Membrane (pore size: 0.45 μm, Millipore) to give the cell lysate. All of the following experiments using cell lysate were conducted at 4 °C unless otherwise noted.

Solution of photoaffinity biotin probes in DMSO (1 mM, 5 μL) and PBS-T (240 μL) were added to the 1:1 suspension (20 μL) of PBS-T and NeutrAvidin agarose resin (Pierce) in 1.5 mL Eppendorf tubes. After the incubation with a rotator shielded from light for 2 h, the pretreated resin was collected by filtration. To the pretreated resin was added four kinds of the cell lysate prepared above, and incubated for additional 2 h. Then the resulting mixture was irradiated with UV light (365 nm) by handheld UV lamp (0.8 mW/cm^2) on ice for 15 min. For the direct elution by boiling, the resins were thoroughly washed four times with PBS-T followed by PBS and resuspended in 2×SDS buffer (30 μL). The binding proteins were eluted by boiling at 95 °C for 5 min. SDS-PAGE was performed by using a precast 10% polyacrylamide gel, and the gels were stained with a Silver Stain Kit, Protein. For the immunoblot analyses, proteins in the gels after electrophoresis were transferred to PVDF membranes using the Trans-Blot® SD semi-dry blotting system (Bio-Rad) according to the manufacturer's instructions. Proteins were detected with HRP-conjugated streptavidin (1:3000, GE Healthcare). The HRP-conjugated bands were visualized with an ECL-prime system (GE Healthcare), and detected by a Fujifilm LAS-4000 MINI imaging scanner.

2-6-12. Trypan Blue Exclusion Test

HeLa S3 cells were seeded at 1×10^4 cells/mL in 6-well plates and incubated for 1 day at 37 °C. After adding the compounds at 1 pM-1 μM, the cells were incubated for additional 96 h. Both the cells in supernatant and the suspended cells (treated with 0.05% trypsin–EDTA) were collected by spin-down and washed with PBS. After adding the E-MEM containing FBS, the cells were treated with trypan blue solution (8 mg/mL trypan blue (Wako), 18 mg/mL NaCl), and the number of stained cells was counted. The cell viability was calculated by comparison with unstained cells and total cells.

2-6-13. Caspase 3 (DEVDase) Activity Assay

Caspase 3 (DEVDase) activity was measured using the CaspACE™ Assay System, Colorimetric (Promega). HeLa S3 cells were seeded on a 6-well plate at 5×10^5 cells/mL. After cells were incubated for 4 h at 37 °C, compounds in DMSO solution were added at several concentrations. After the incubation for additional 24 h, the cells were scraped and collected. After washing with PBS, cell lysis buffer (included in the above kit, 30 μL) were added to the cells. After freeze-thawing of suspension, the residue was incubated on ice for 15 min, and then the supernatant was collected by centrifugation (15,000 rpm, 4 °C, 20 min). The lysate (24 μL) was mixed with caspase assay buffer (included in the above kit, 32 μL), DMSO (2 μL), 1 M DTT (1 μL), H_2O (39 μL) and 10 mM Ac-Asp-Glu-Val-Asp-pNA (Ac-DEVD-pNA) in DMSO (2 μL), and incubated at 37 °C for 4 h, according to the manufacturer's protocol. The free p-nitroaniline was measured by the absorbance at 405 nm. The relative activity was calculated by comparison with a control (DMSO) based on the average of three experiments.

2-6-14. Synthesis and Spectroscopic Data of Compounds

Aplyronine C (**5**)
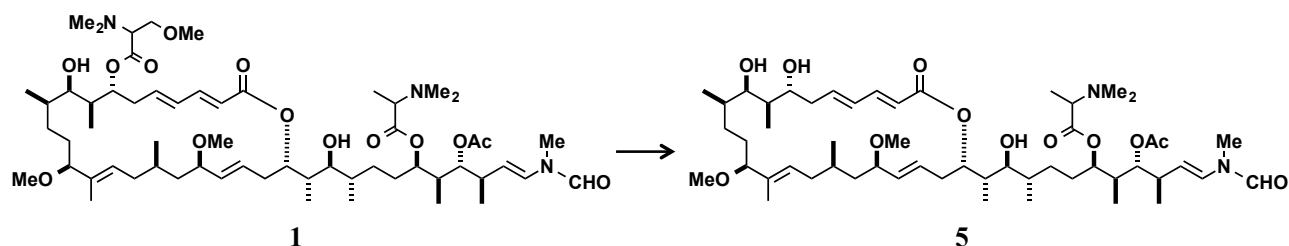
A solution of ApA (**1**) (0.70 mg, 660 nmol) in 0.1% triethylamine–MeOH (14 mL) was stirred at 50 °C for 12 days. The reaction mixture was concentrated and applied to a Develosil ODS-HG-5 HPLC column (20 mm I.D. × 250 mm), and eluted with MeOH / 20 mM ammonium acetate (80:20) at a flow rate of 5 mL/min, with monitoring at 254 nm (t_R = 24–26 min), followed by freeze drying to give ApC (**5**) (0.37 mg, 394 nmol, 60%, based on NMR quantification) as a white powder. Compound **5**: t_R = 7.4 min [Develosil ODS-HG-5 (4.6 mm I.D. × 250 mm), MeOH/20 mM ammonium acetate (80/20), 1 mL/min, UV 254 nm, λ_{ex} 565 nm, λ_{em} 580 nm]; ^{1}H NMR (600 MHz, CD$_3$OD) δ 8.33 [8.08][1] (s, 1H), 7.24 (dd, J = 15.3, 10.5 Hz, 1H), 6.77 [7.14] (d, J = 14.2 Hz, 1H), 6.38 (ddd, J =15.2, 9.5, 4.8 Hz, 1H), 6.31 (dd, J = 15.2, 10.5 Hz, 1H), 5.92 (d, J = 15.3 Hz, 1H), 5.65 (ddd, J = 14.9, 10.9, 4.0 Hz, 1H), 5.54 (br d, J = 11.2 Hz, 1H), 5.16 (br dd, J = 14.7, 9.4 Hz, 1H), 5.09 (dd, J = 14.2, 9.5 Hz, 1H), 5.01-4.98 (m, 1H), 4.95-4.91 (m, 1H), 4.82-4.75 (m, 1H), 3.45-3.18 (m, 5H), 3.18 (s, 3H), 3.16 (s, 3H), 3.07 (dd, J = 9.5, 2.3 Hz, 1H), 3.01 [3.10][1] (s, 3H), 2.68-2.61 (m, 1H), 2.46-2.38 (m, 1H), 2.35 [2.33][2] (s, 6H), 2.29-2.25 (m, 1H), 2.21-2.14 (m, 1H), 2.06 [2.06][1] [2.05][2] [2.05][1,2] (s, 3H), 2.02-1.89 (m, 3H), 1.81-1.76 (m, 1H), 1.74-1.48 (m, 9H), 1.35-1.31 (m, 1H), 1.30 [1.30][1] [1.29][2] [1.29][1,2] (d, J = 7.1 Hz, 3H), 1.24-1.06 (m, 5H), 1.02-0.96 (m, 15H), 0.90 (br d, J = 6.7 Hz, 3H), 0.82 (d, J = 6.0 Hz, 3H) Chemical shifts of the minor diastereomers are within parentheses as follows: [ ][1], 7:3 at C34 stereoisomers; [ ][2], 3:1 at C7 trimethylserine moiety; [ ][3], 1.4:1 at C29 dimethylalanine moiety; MS (ESI) m/z 946.6 [M+H]$^+$.

Aldehyde 10
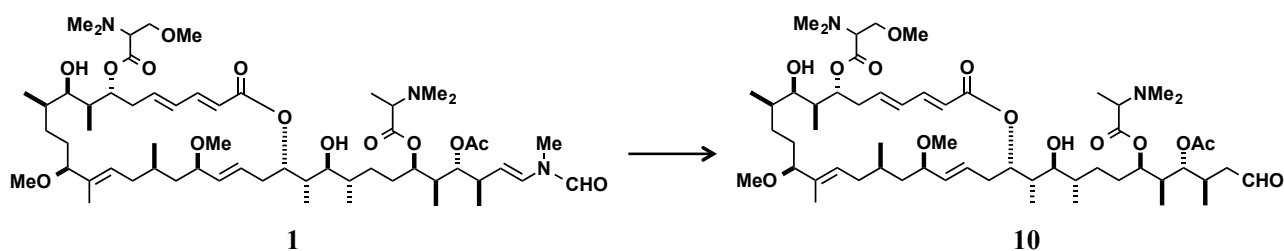
A solution of aplyronine A (0.32 mg, 0.30 μmol) in a 3:1 mixture of 1,4-dioxane (300 μL) and 2 M aq. HCl (100 μL) was stirred for 80 min at 50 °C. The resulting mixture was diluted with sat. NaHCO$_3$ aq. (250 μL) and water (2 mL), and extracted with CHCl$_3$ (1 mL × 5). The combined extracts were washed with brine and concentrated *in vacuo* to give an aldehyde **10**, which was used for the next step without further purification.

Aplyronine A fluorescent probe (8)
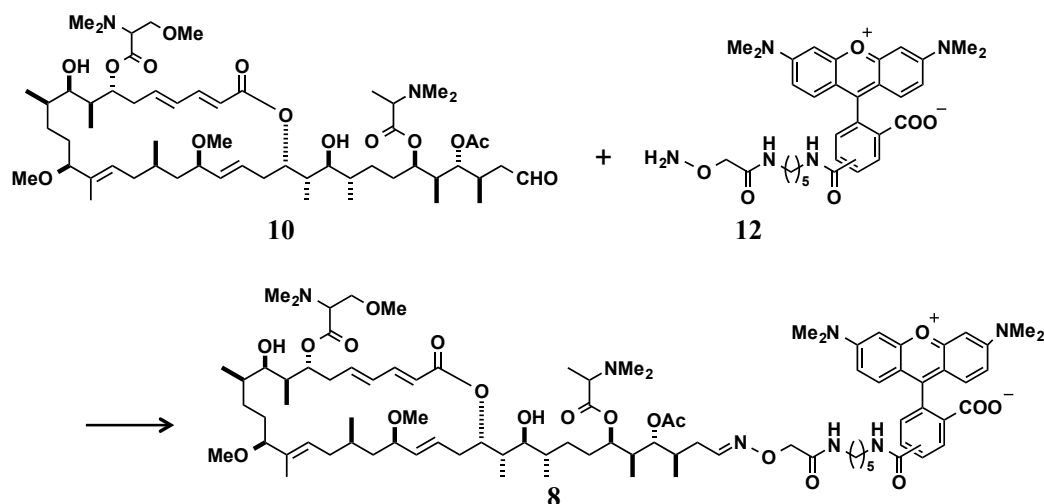
To the stirred solution of aldehyde **10** in EtOH (400 μL) was added the 100 mM solution of aminooxy-5(6)-TAMRA (**12**) in DMSO (15 μL, 1.5 μmol, 2:1 mixture of 6/5-TAMRA derivatives, commercially available material from Biotium Inc.). After being stirred for 5 days at room temperature, the reaction mixture was concentrated *in vacuo* and applied to a Develosil ODS-HG-5 HPLC column (20 mm I.D. × 250 mm). Samples were eluted with MeCN / 20 mM ammonium acetate (50:50) at a flow rate of 5 mL/min and with monitoring at 254 nm (t_R = 35–45, 45–56 min). Resulted mixture was purified by HPLC again under same condition to give ApA–FL (**8**) (0.50 mg, 66% based on NMR quantification as a 2:1 mixture of 6/5-TAMRA derivatives). Compound **8** (6-TAMRA isomer): t_R = 7.7 min [Develosil ODS-HG-5 (4.6 mm I.D. × 250 mm), MeOH/20 mM ammonium acetate (80/20), 1 mL/min, UV 254 nm, λ_{ex} 565 nm, λ_{em} 580 nm]; ^{1}H NMR (600 MHz, CD$_3$OD) δ 8.13 (d, J = 8.2 Hz, 1H), 8.07 (dd, J = 8.2 Hz, J = 1.7 Hz, 1H), 7.69 (d, J = 1.7 Hz, 1H), 7.54 [6.82][1] (t, J = 6.4 Hz, 1H), 7.26 (d, J = 9.4 Hz, 2H), 7.19 (dd, J = 16.1, 10.7 Hz, 1H), 7.02 (dd, J = 9.4, 2.6 Hz, 2H), 6.93 (d, J = 2.6 Hz,

2H), 6.39-6.34 (m, 1H), 6.24-6.18 (m, 1H), 5.96 (d, J = 16.1 Hz, 1H), 5.65-5.60 (m, 1H), 5.54-5.52 (m, 1H), 5.12-5.07 (m, 1H), 4.95-4.73 (m, 4H), 4.36 [4.42][1] (s, 2H), 3.69-3.65 (m, 2H), 3.56-3.45 (m, 2H), 3.46-3.43 (m, 1H), 3.38-3.36 (m, 2H), 3.33-3.32 (m, 1H), 3.29 (s, 3H), 3.28 (s, 12H), 3.25-3.20 (m, 3H), 3.17 (s, 3H), 3.14 (s, 3H), 3.09-3.05 (m, 1H), 2.50-2.25 (m, 5H), 2.37 [2.38][2] (s, 6H), 2.33 [2.34][1] [2.32][3] [2.32][1,3] (s, 6H), 2.17-2.12 (m, 1H), 2.09-1.92 (m, 3H), 2.02 [2.03][1] [2.01][3] [2.02][1,3] (s, 3H), 1.75-1.08 (m, 22H), 1.50 [1.51][2] (s, 3H), 1.30 [1.29][3] (d, J = 7.2 Hz, 3H), 1.04-0.94 (m, 12H), 0.92-0.86 (m, 6H), 0.76 [0.75][2] (d, J = 5.9 Hz, 3H) Chemical shifts of the minor diastereomers are within parentheses as follows: [ ][1], 8:2 at C34 stereoisomers; [ ][2], 3:1 at C7 trimethylserine moiety; [ ][3], 1.4:1 at C29 dimethylalanine moiety; HRMS (ESI) m/z 824.9712 (calcd for ($C_{88}H_{130}N_7Na_2O_{19}$)/2 [M+2Na]$^{2+}$, Δ −1.4 mmu). Compound **8** (5-TAMRA isomer): t_R = 9.0 min [Develosil ODS-HG-5 (4.6 mm I.D. × 250 mm), MeOH/20 mM ammonium acetate (80/20), 1 mL/min, UV 254 nm, λ_{ex} 565 nm, λ_{em} 580 nm]; ^{1}H NMR (600 MHz, CD$_3$OD) δ 8.49 (d, J = 1.6 Hz, 1H), 8.04 (dd, J = 7.9, 1.6 Hz, 1H), 7.58 [6.88][1] (t, J = 6.4 Hz, 1H), 7.35 (d, J = 7.9 Hz, 1H), 7.24 (d, J = 8.5 Hz, 2H), 7.19 (dd, J = 16.1, 10.7 Hz, 1H), 7.02 (dd, J = 8.5, 3.0 Hz, 2H), 6.92 (d, J = 3.0 Hz, 2H), 6.39-6.34 (m, 1H), 6.24-6.18 (m, 1H), 5.96 (d, J = 16.1 Hz, 1H), 5.65-5.60 (m, 1H), 5.54-5.52 (m, 1H), 5.12-5.07 (m, 1H), 4.95-4.73 (m, 4H), 4.42 [4.36][1] (s, 2H), 3.69-3.65 (m, 2H), 3.56-3.45 (m, 2H), 3.46-3.43 (m, 1H), 3.38-3.36 (m, 2H), 3.33-3.32 (m, 1H), 3.29 (s, 3H), 3.28 (s, 12H), 3.25-3.20 (m, 3H), 3.17 (s, 3H), 3.14 (s, 3H), 3.09-3.05 (m, 1H), 2.50-2.25 (m, 5H), 2.37 [2.38][2] (s, 6H), 2.33 [2.34][1] [2.32][3] [2.32][1,3] (s, 6H), 2.17-2.12 (m, 1H), 2.09-1.92 (m, 3H), 2.04 [2.04][1] [2.03][3] [2.03][1,3] (s, 3H), 1.75-1.08 (m, 22H), 1.50 [1.51][2] (s, 3H), 1.30 [1.29][3] (d, J = 7.2 Hz, 3H), 1.04-0.94 (m, 12H), 0.92-0.86 (m, 6H), 0.76 [0.75][2] (d, J = 5.9 Hz, 3H) Chemical shifts of the minor diastereomers are within parentheses as follows: [ ][1], 8:2 at C34 stereoisomers; [ ][2], 3:1 at C7 trimethylserine moiety; [ ][3], 1.4:1 at C29 dimethylalanine moiety; HRMS (ESI) m/z 824.9712 (calcd for ($C_{88}H_{130}N_7Na_2O_{19}$)/2 [M+2Na]$^{2+}$, Δ −1.4 mmu).

Aldehyde 11

5 → **11**
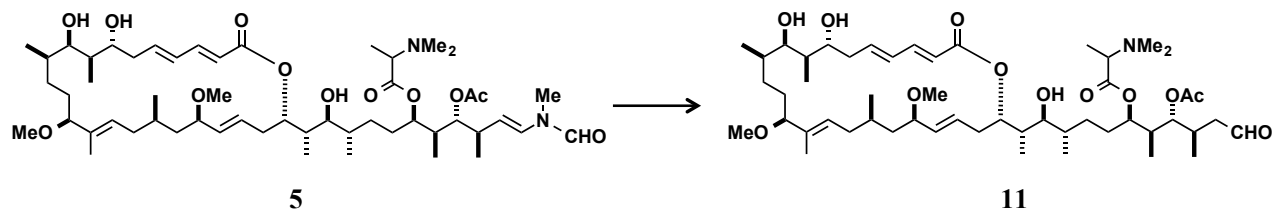
A solution of Aplyronine C (**5**) (0.10 mg, 0.10 μmol) in a 3:1 mixture of 1,4-dioxane (150 μL) and 2 M aq. HCl (50 μL) was stirred for 80 min at 50 °C. The resulting mixture was diluted with sat. NaHCO₃ aq. (250 μL) and water (2 mL), and extracted with CHCl₃ (1 mL × 4). The combined extracts were washed with brine and concentrated *in vacuo* to give an aldehyde **11**, which was used for the next step without further purification.
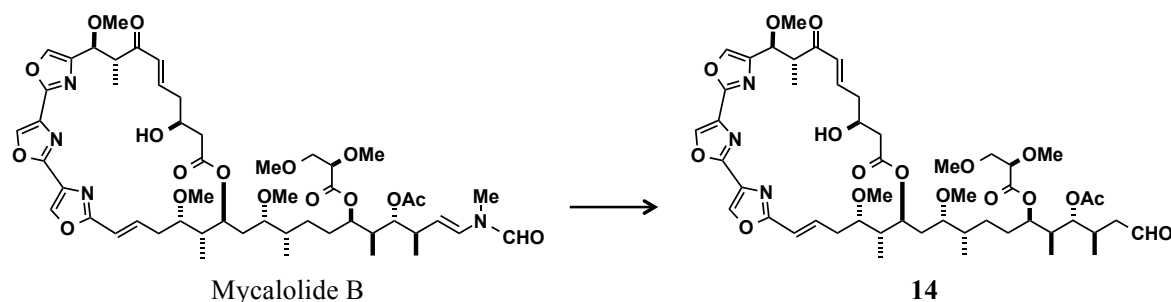
Aplyronine C fluorescent probe (9)

11 + **12** → **9**
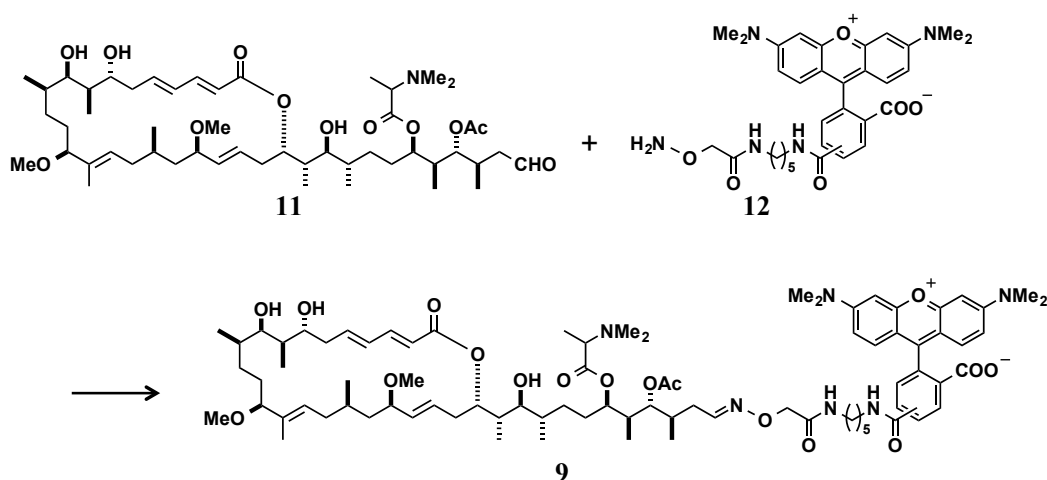
To the stirred solution of aldehyde **11** in EtOH (300 μL) was added the 100 mM solution of aminooxy-5(6)-TAMRA (**12**) in DMSO (5.0 μL, 0.50 μmol). After being stirred for 4 days at room temperature, the reaction mixture was concentrated *in vacuo* and applied to a Develosil ODS-HG-5 HPLC column (20 mm I.D. × 250 mm). Samples were eluted with MeCN / 20 mM ammonium acetate (50:50) at a flow rate of 5 mL/min and with monitoring at 254 nm (t_R = 30–34, 38–42 min) to give ApC–FL (**9**) (38 μg 26 nmol, 26% based on NMR quantification as a 2:1 mixture of 6/5-TAMRA derivatives). Compound **9** (6-TAMRA isomer): t_R = 12.3 min [Develosil ODS-HG-5 (4.6 mm I.D. × 250 mm), MeOH/20 mM ammonium acetate (75/25), 1 mL/min, UV 254 nm, λ_{ex} 565 nm, λ_{em} 580 nm]; ^{1}H NMR (600 MHz, CD₃OD) δ 8.13 (d, *J* = 8.3 Hz, 1H), 8.07 (dd, *J* = 8.3, 2.1 Hz, 1H), 7.69 (d, *J* = 2.1 Hz, 1H), 7.54 [6.81][1] (t, *J* = 6.0 Hz, 1H), 7.26 (d, *J* = 9.4 Hz, 2H), 7.25-7.16 (m, 1H), 7.02 (dd, *J* = 10.0, 3.1 Hz, 2H), 6.93 (d, *J* = 1.9 Hz, 2H), 6.40-6.28 (m, 2H), 5.91 (d, *J* = 13.7 Hz, 1H), 5.66-5.61 (m, 1H), 5.56-5.53 (m, 1H), 5.16-5.12 (m, 1H), 5.09-4.50 (m, 3H), 4.36 [4.42][1] (s, 2H), 3.57-3.41 (m, 3H), 3.37-3.36

(m, 2H), 3.28 (s, 12H), 3.20-3.25 (m, 3H), 3.19-3.18 (m, 1H), 3.17 (s, 3H), 3.15 (s, 3H), 3.09-3.05 (m, 1H), 2.25-2.50 (m, 5H), 2.33 [2.34][1] [2.32][2] [2.32][1,2] (s, 6H), 2.17-2.12 (m, 1H), 2.08-1.92 (m, 3H), 2.02 [2.03][1] [2.01][2] [2.02][1,2] (s, 3H), 1.75-1.08 (m, 22H), 1.45 (s, 3H), 1.31-1.29 (m, 3H), 1.02-0.86 (m, 18H), 0.82 (d, J = 6.0 Hz, 3H). Chemical shifts of the minor diastereomers are within parentheses as follows: [ ][1], 8:2 at C34 stereoisomers; [ ][2], 3:1 at C7 trimethylserine moiety; [ ][3], 1.4:1 at C29 dimethylalanine moiety; HRMS (ESI) m/z 738.4521 (calcd for $(C_{83}H_{124}N_6O_{17})/2$ [M+2H]$^{2+}$, Δ +0.9 mmu). Compound **9** (5-TAMRA isomer): t_R = 15.5 min [Develosil ODS-HG-5 (4.6 mm I.D. × 250 mm), MeOH/20 mM ammonium acetate (75/25), 1 mL/min, UV 254 nm, λ_{ex} 565 nm, λ_{em} 580 nm]; ^{1}H NMR (600 MHz, CD$_3$OD) δ 8.49 (d, J = 2.4 Hz, 1H), 8.04 (dd, J = 7.0 Hz, J = 2.4 Hz, 1H), 7.59 [6.87][1] (t, J = 6.8 Hz, 1H), 7.35 (d, J = 7.0 Hz, 1H), 7.24 (d, J = 8.9 Hz, 2H), 7.25-7.16 (m, 1H), 7.01 (dd, J = 9.5 Hz, J = 2.6 Hz, 2H), 6.93 (d, J = 4.0 Hz, 2H), 6.40-6.28 (m, 2H), 5.91 (d, J = 13.7 Hz, 1H), 5.66-5.61 (m, 1H), 5.56-5.53 (m, 1H), 5.16-5.12 (m, 1H), 5.09-4.50 (m, 3H), 4.42 [4.36][1] (s, 2H), 3.57-3.41 (m, 3H), 3.37-3.36 (m, 2H), 3.28 (s, 12H), 3.20-3.25 (m, 3H), 3.19-3.18 (m, 1H), 3.17 (s, 3H), 3.15 (s, 3H), 3.09-3.05 (m, 1H), 2.25-2.50 (m, 5H), 2.33 [2.34][1] [2.32][2] [2.32][1,2] (s, 6H), 2.17-2.12 (m, 1H), 2.08-1.92 (m, 3H), 2.04 [2.04][1] [2.03][2] [2.03][1,2] (s, 3H), 1.75-1.08 (m, 22H), 1.45 (s, 3H), 1.31-1.29 (m, 3H), 1.02-0.86 (m, 18H), 0.82 (d, J = 6.0 Hz, 3H) Chemical shifts of the minor diastereomers are within parentheses as follows: [ ][1], 8:2 at C34 stereoisomers; [ ][2], 3:1 at C7 trimethylserine moiety; [ ][3], 1.4:1 at C29 dimethylalanine moiety; HRMS (ESI) m/z 738.4521 (calcd for $(C_{83}H_{124}N_6O_{17})/2$ [M+2H]$^{2+}$, Δ +0.9 mmu).

Aldehyde **14**

Mycalolide B → **14**

A solution of Mycalolide B (0.10 mg, 0.097 μmol) in a 1:1 mixture of acetonitrile (100 μL) and 1 M aq. HCl (100 μL) was stirred for 70 min at 60 °C. The resulting mixture was diluted with brine (2 mL), and extracted with EtOAc (1 mL × 4). The combined extracts were dried with sodium sulfate and concentrated *in vacuo* to give an aldehyde **14**, which was used for the next step without further purification.

Mycalolide B fluorescent probe (MyB-FL, **15**)


14 + **12** → **15**
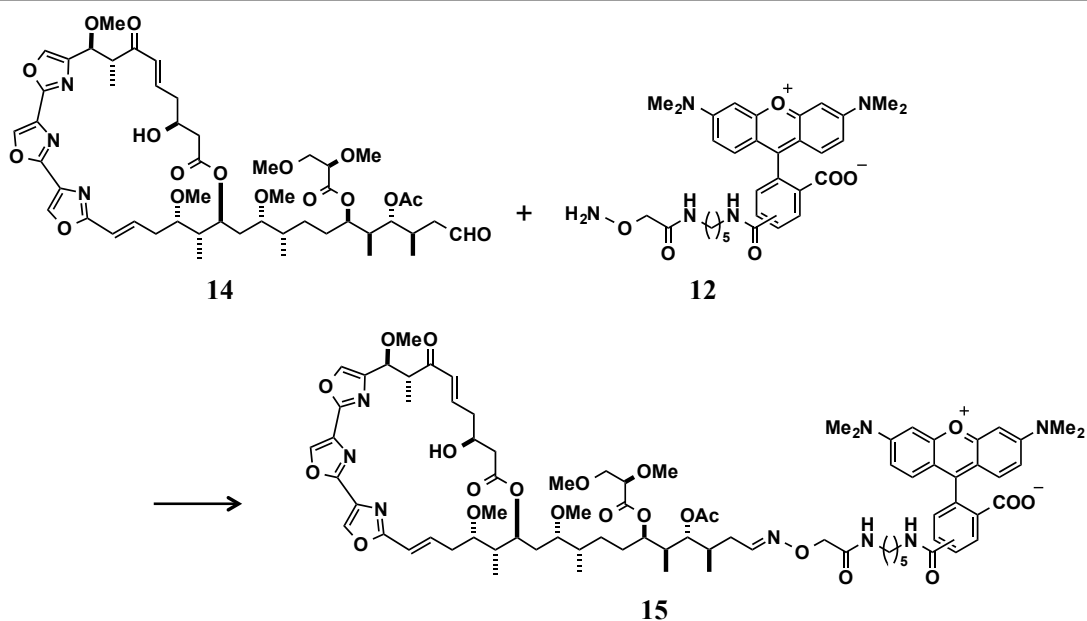
To the stirred solution of aldehyde **14** in EtOH (250 μL) was added the 100 mM solution of aminooxy-5(6)-TAMRA (**12**) in DMSO (3.0 μL, 0.30 μmol). After being stirred for 5 days at room temperature, the reaction mixture was concentrated *in vacuo* and applied to a Develosil ODS-HG-5 HPLC column (20 mm I.D. × 250 mm). Samples were eluted with MeCN / 20 mM ammonium acetate (50:50) at a flow rate of 5 mL/min and with monitoring at 254 nm to give MyB–FL (**15**) (23 μg, 15 nmol, 15% based on fluorescent intensity as a 2:1 mixture of 6/5-TAMRA derivatives). Compound **15** (6-TAMRA isomer): t_R = 9.6 min [Develosil ODS-HG-5 (4.6 mm I.D. × 250 mm), MeOH/20 mM ammonium acetate (75:25), 1 mL/min, UV 254 nm, λ_{ex} 565 nm, λ_{em} 580 nm], HRMS (ESI) *m/z* 800.3629 (calcd for $(C_{82}H_{106}N_8Na_2O_{22})/2$ $[M+2Na]^{2+}$, Δ +2.0 mmu). Compound **15** (5-TAMRA

isomer)**:** t_R = 11.5 min [Develosil ODS-HG-5 (4.6 mm I.D. × 250 mm), MeOH/20 mM ammonium acetate (75:25), 1 mL/min, UV 254 nm, λ_{ex} 565 nm, λ_{em} 580 nm]; HRMS (ESI) *m/z* 800.3629 (calcd for $(C_{82}H_{106}N_8Na_2O_{22})/2$ [M+2Na]$^{2+}$, Δ +2.0 mmu).

Model compound **16**

3-phenylpropanal   **12**   **16**
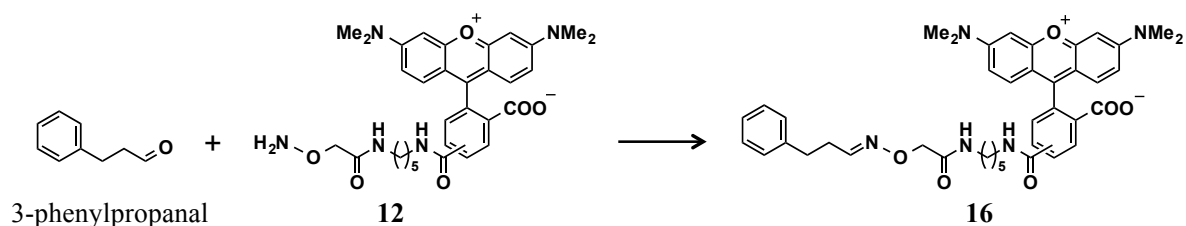
To the stirred solution of 3-phenylpropanal (20 μL, 148 μmol) in EtOH (400 μL) was added the 100 mM solution of aminooxy-5(6)-TAMRA (**12**) in dimethylformamide (DMF) (2.0 μL, 0.20 μmol). After being stirred for 70 min at room temperature, the reaction mixture was concentrated *in vacuo*. The crude sample was applied to SiO_2 column ($CHCl_3$/methanol = 9/1 to 0/1) and a Develosil ODS-HG-5 HPLC column (20 mm I.D. × 250 mm). Samples were eluted with 70% MeOH at a flow rate of 5 mL/min and with monitoring at 254 nm (t_R = 20–24, 25-30 min) to give model (**16**) (120 μg, 0.17 mmol, 85% based on NMR quantification as a 2:1 mixture of 6/5-TAMRA derivatives). Compound **16** (6-TAMRA derivative): t_R = 9.7 min [Develosil ODS-HG-5 (4.6 mm I.D. × 250 mm), 70% MeOH, 1 mL/min, UV 254 nm, λ_{ex} 565 nm, λ_{em} 580 nm]; ^{1}H NMR (600 MHz, CD_3OD) δ 8.13 (d, *J* = 8.1 Hz, 1H), 8.07 (dd, *J* = 8.1, 1.7 Hz, 1H), 7.68 (d, *J* = 1.7 Hz, 1H), 7.51 [6.73] (t, *J* = 5.9 Hz, 1H), 7.25 (d, *J* = 9.5 Hz, 2H), 7.26-7.11 (m, 5H), 7.00 (dd, *J* = 9.5, 2.5 Hz, 2H), 6.93 (d, *J* = 2.5 Hz, 2H), 4.30 [4.33] (s, 2H), 3.39-3.36 (m, 2H), 3.27 (s, 12H), 3.24-3.19 (m, 2H), 2.76 (t, *J* = 7.7 Hz, 2H), 2.45 (td, *J* = 8.1, 5.9 Hz, 2H), 1.68-1.60 (m, 2H), 1.54-1.50 (m, 2H), 1.40-1.34 (m, 2H). Chemical shifts of the minor diastereomers are within parentheses as follows: [ ], 7:3 at C34 stereoisomers; HRMS (ESI) *m/z* 704.3456 (calcd for $C_{41}H_{46}N_5O_6$ [M+H]$^+$, Δ +0.8 mmu). Compound **16** (5-TAMRA derivative): t_R = 13.2 min [Develosil ODS-HG-5 (4.6 mm I.D. × 250 mm), 70% MeOH, 1 mL/min, UV 254 nm, λ_{ex} 565 nm, λ_{em} 580 nm]; ^{1}H NMR (600 MHz, CD_3OD) δ 8.49 (d, *J* = 1.8 Hz, 1H), 8.03 (dd, *J* = 7.9, 1.8 Hz, 1H), 7.51 [6.73] (t, *J* = 5.9 Hz, 1H), 7.33 (d, *J* = 7.9 Hz, 1H), 7.24 (d, *J* = 9.5 Hz, 2H), 7.26-7.11 (m, 5H), 7.00 (dd, *J* = 9.5, 2.4 Hz, 2H), 6.92 (d, *J* = 2.5 Hz, 2H), 4.30 [4.33] (s, 2H), 3.39-3.36 (m, 2H), 3.27 (s, 12H), 3.24-3.19 (m, 2H), 2.76 (t, *J* = 7.7 Hz, 2H), 2.45 (td, *J* = 8.1, 5.9 Hz, 2H), 1.68-1.60 (m, 2H), 1.54-1.50 (m, 2H), 1.40-1.34 (m, 2H). Chemical shifts of the minor diastereomers are within parentheses as follows: [ ], 7:3 at C34 stereoisomers; HRMS (ESI) *m/z* 704.3456 (calcd for $C_{41}H_{46}N_5O_6$ [M+H]$^+$, Δ +0.8 mmu).
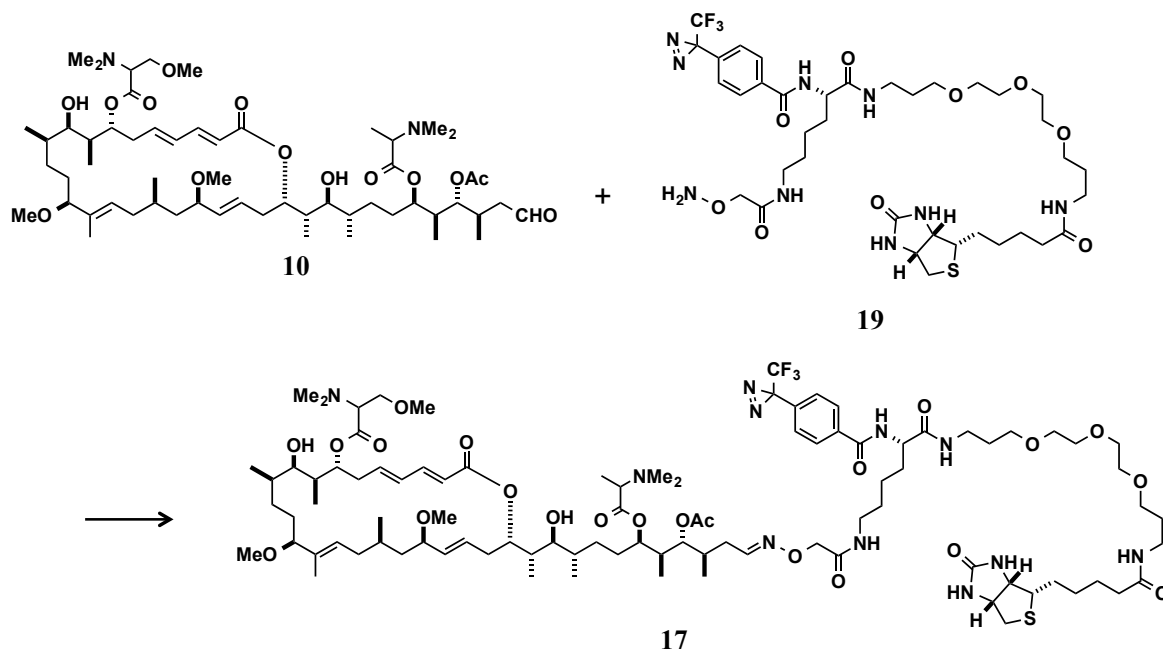
A solution of the aldehyde **10** prepared from ApA (0.16 mg, 150 nmol) as described above and the alkoxyamine **19** (1.6 mg, 1.4 μmol)[12] in a 10:1 mixture of EtOH and 100 mM acetate buffer (pH 4.0) (0.22 μL) was stirred at room temperature for 22 h. The reaction mixture was concentrated *in vacuo* and applied to a Develosil ODS-HG-5 HPLC column (20 mm I.D. × 250 mm). Samples were eluted with MeOH / 20 mM ammonium acetate (80:20) at a flow rate of 5 mL/min, with monitoring at 254 nm (t_R = 49–55 min) to give ApA–PB (**17**) (103 nmol, 69%, based on NMR quantification, E/Z = 7/3 for the C34 isomers). Compound **17**: t_R = 14.3 min [Develosil ODS-HG-5 (4.6 mm I.D. × 250 mm), MeOH/20 mM ammonium acetate (80/20), 1 mL/min, UV 254 nm]; ^{1}H NMR (600 MHz, CD$_3$OD) δ 7.97 (d, J = 8.7 Hz, 2H), 7.54 [6.80][1](t, J = 6.0 Hz, 1H), 7.35 (d, J = 8.7 Hz, 2H), 7.20 (dd, J = 10.8, 15.1 Hz, 1H), 6.38 [6.39][2](dd, J = 10.8, 15.3 Hz, 1H), 6.25-6.20 (m, 1H), 5.97 (br d, J = 14.8 Hz, 1H), 5.63 (ddd, J = 4.0, 10.6, 14.8 Hz, 1H), 5.55 (br d, J = 11.2 Hz, 1H), 5.12-5.07 (m, 1H), 4.95 (s, 2H), 5.0-4.8 (m, 3 H), 4.79 [4.78][2] (d, J = 10.0 Hz, 1H), 4.48 (dd, J = 4.9, 7.9 Hz, 1H), 4.45 (dd, J = 5.3 Hz, 9.0 Hz, 1H), 4.29 (dd, J = 4.4, 7.9 Hz, 1H), 3.70-3.52 (m, 16H), 3.51 (t, J = 6.0 Hz, 2H), 3.50 (t, J = 6.1 Hz, 2H), 3.38 [3.34][2] (s, 3H), 3.38-3.32 (m, 3H), 3.24 (t, J = 6.7 Hz, 2H), 3.21-3.16 (m, 1H), 3.18 (s, 3H), 3.15 (s, 3H), 3.07 (br d, J = 9.9 Hz, 1H), 2.91 (dd, J = 4,9, 12.7 Hz, 1H), 2.69 (d, J = 12.7 Hz, 1H), 2.54-2.25 (m, 5H), 2.38 [2.39][2] (s, 6H), 2.34 [2.34][1] [2.32][3] [2.33][1,3](s, 6H), 2.17 (t, J = 7.2 Hz, 2H), 2.20-2.10 (m, 1H), 2.04 [2.04][1] [2.02][3] [2.03][1,3] (s, 3H), 2.10-1.90 (m, 3H), 1.84-1.56 (m, 29H), 1.50 [1.51][2] (s, 3H), 1.30 [1.29][3] (d, J = 6.9 Hz, 3H), 1.18-1.06 (m, 3H), 1.04-0.95 (m, 12H), 0.91 (d, J = 6.9 Hz, 3H), 0.89 (d, J = 6.8 Hz, 3H), 0.76 [0.75][2] (d, J = 5.8 Hz, 3H). Chemical shifts of the minor diastereomers are within parentheses as follows: [ ][1], 7:3 at C34 stereoisomers; [ ][2], 1:1 at C7 trimethylserine moiety; [ ][3], 3:1 at C29 dimethylalanine moiety; HRMS(ESI) m/z 961.0323 (calcd for [C$_{94}$H$_{152}$F$_3$N$_{11}$Na$_2$O$_{22}$S]/2 [M+2Na]$^{2+}$, Δ +3.2 mmu).
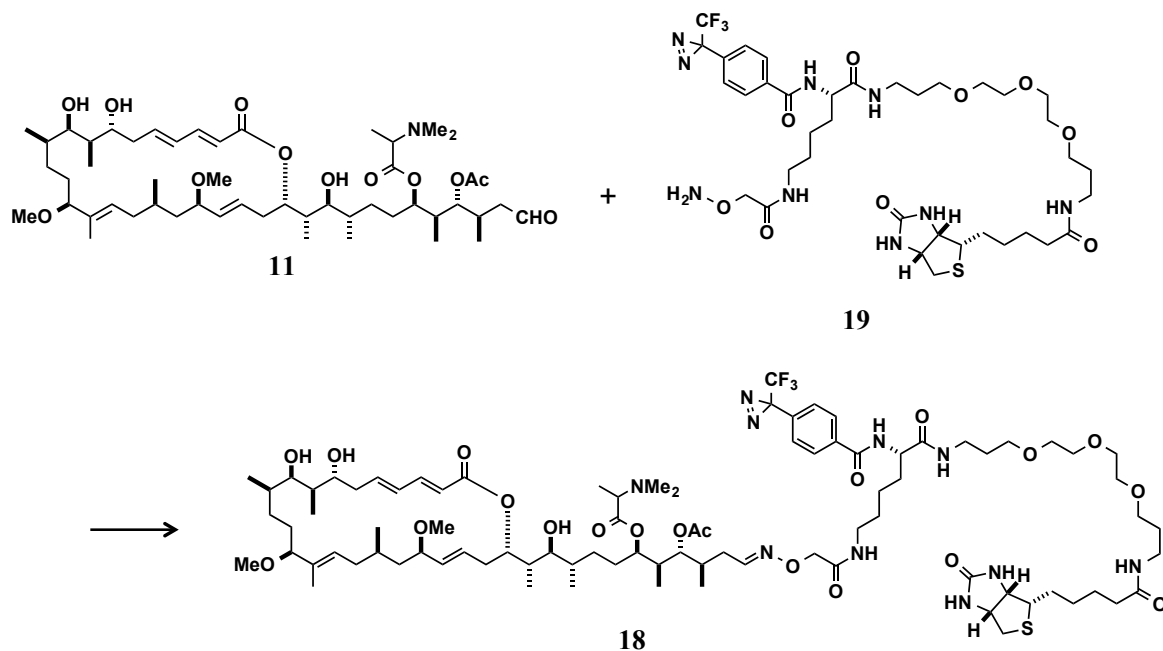
A solution of the aldehyde **11** prepared from ApC (0.17 mg, 180 nmol) as described above and the alkoxyamine **19** (0.95 mg, 1.1 μmol) in a 10:1 mixture of EtOH and 100 mM acetate buffer (pH 4.0) (0.22 μL) was stirred at room temperature for 2 h. After adding 100 mM acetate buffer (pH 4.0) (0.05 μL), the reaction mixture was stirred at room temperature for additional 10 h and concentrated *in vacuo* and applied to a Develosil ODS-HG-5 HPLC column (20 mm I.D. × 250 mm). Samples were eluted with MeOH / 20 mM ammonium acetate (80:20) at a flow rate of 5 mL/min, with monitoring at 254 nm (t_R = 41–46 min) to give ApC-PB (**18**) (82 nmol, 47%, based on NMR quantification, *E/Z* = 7/3 for the C34 isomers). Compound **18**: t_R = 10.8 min [Develosil ODS-HG-5 (4.6 mm I.D. × 250 mm), MeOH/20 mM ammonium acetate (80/20), 1 mL/min, UV 254 nm]; ^{1}H NMR (600 MHz, CD$_3$OD) δ 7.96 (d, *J* = 8.5 Hz, 2H), 7.54 [6.80][1] (t, *J* = 6.4 Hz, 1H), 7.34 (d, *J* = 8.5 Hz, 2H), 7.24 (dd, *J* = 10.4, 15.3 Hz, 1H), 6.38 (ddd, *J* = 5.0, 9.8, 15.0 Hz, 1H), 6.31 (dd, *J* = 15.0, 10.4 Hz, 1H), 5.92 (d, *J* = 15.3 Hz, 1H), 5.65 (ddd, *J* = 5.0, 10.4, 14.8 Hz, 1H), 5.55 (br d, *J* = 11.4 Hz, 1H), 5.14 (m, 1H), 5.10 (m, 1H), 5.00–4.77 (m, 2H), 4.48 (dd, *J* = 4.4, 7.5 Hz, 1H), 4.46 (dd, *J* = 4.4, 8.0 Hz, 1H), 4.39 [4.44] [1] (s, 2H), 4.29 (dd, *J* = 4.5, 7.8 Hz, 1H), 3.70–3.45 (m, 3H), 3.62-3.49 [4.21-3.95] (m, 16H), 3.33 (m, 1H), 3.24 (t, *J* = 6.8 Hz, 2H), 3.20 (m, 1H), 3.18 (s, 3H), 3.16 (s, 3H), 3.08 (dd, *J* = 2.8, 11.6 Hz, 1H), 2.91 (dd, *J* = 5.0, 12.8 Hz, 1H), 2.69 (d, *J* = 12.8 Hz, 1H), 2.47–2.41 (m, 1H), 2.37–2.27 (m, 5H), 2.34 [2.35][1] [2.33][2] [2.33][1,2] (s, 6H), 2.20–1.95 (m, 9H), 1.93–1.52 (m, 29H), 1.45 (s, 3H), 1.31 [1.30][2] (d, *J* = 6.7 Hz, 3H), 1.22–1.08 (m, 3H), 1.01–0.87 (m, 18H), 0.82 (d, *J* = 5.9 Hz, 3H). Chemical shifts of the minor diastereomers are within parentheses as follows: [ ][1], 7:3 at C34 stereoisomers; [ ][2], 3:1 at C29 dimethylalanine moiety; HRMS (ESI) *m/z* 885.4984 (calcd for [C$_{88}$H$_{142}$F$_3$N$_{10}$NaO$_{20}$S]/2 [M+H+Na]$^{2+}$, Δ –0.2 mmu).

References

1. Kuroda, T.; Suenaga, K.; Sakakura, A.; Hanada, T.; Okamoto, H.; Kigoshi, H. *Bioconjugate Chem*. **2006**, *17*, 524–529.

2. Kita, M.; Hirayama, Y.; Sugiyama, M.; Kigoshi, H. *Angew. Chem. Int. Ed.* **2011**, *50*, 9871–9874.

3. Hirata, K.; Muraoka, S.; Suenaga, K.; Kuroda, T.; Kato, K.; Tanaka, H.; Yamamoto, M.; Tanaka, M.; Yamada, K. *J. Mol. Biol.* **2006**, *356*, 945–954.

4. Kigoshi, H.; Suenaga, K.; Mutou, T.; Ishigaki, T.; Atsumi, T.; Ishiwata, H.; Sakakura, A.; Ogawa, T.; Ojika, M.; Yamada, K. *J. Org. Chem.* **1996**, *61*, 5326–5351.

5. Ojika, M.; Kigoshi, H.; Yoshida, Y.: Ishigaki, T.; Nishiwaki, M.; Tsukada, I.; Arakawa, M.; Ekimoto, H.; Yamada, K. *Tetrahedron* **2007**, *63*, 3138–3167.

6. Wada, S.; Matsunaga, S.; Saito, S.; Fusetani, N.; Watabe, S. *J. Biochem.* **1998**, *123*, 946–952.

7. Kouyama, T.; Mihashi, K. *Eur. J. Biochem.* **1981**, *114*, 33–38.

8. Kita, M.; Yoneda, K.; Hirayama, Y.; Yamagishi, K.; Saito, Y.; Sugiyama, Y.; Miwa, Y.; Ohno, O.; Morita, M.; Suenaga, K.; Kigoshi, H. *ChemBioChem* **2012**, *13*, 1754–1758.

9. Sumiya, E.; Shimogawa, H.; Sasaki, H.; Tsutsumi, M.; Yoshita, K.; Ojika, M.; Suenaga, K.; Uesugi, M. *ACS Chem. Biol.* **2011**, *6*, 425–431.

10. Spector, I.; Shochet, N. R.; Kashman, Y.; Groweiss, A. *Science* **1983**, 219, 493−495.

11. The experiments were conducted in cooperation with Dr. Y. Hirayama.

12. Kita, M.; Hirayama, Y.; Yamagishi, K.; Yoneda, K.; Fujisawa, R.; Kigoshi, H. *J. Am. Chem. Soc*. **2012**, *134*, 20314–20317.

13. (a) Chandler, C. S.; Ballard, F. B. *Biochem. J.* **1985**, *232*, 385−393. (b) Ahmad, P. M.; Ahmad, F. *FASEB J.* **1991**, *5*, 2482−2485.

14. Shevchenko, A.; Wilm, M.; Vorm, O.; Mann, M. *Anal. Chem.* **1996**, *68*, 850–858.

15. (a) Hirayama, Y. *PhD Thesis* **2014**, University of Tsukuba, Tsukuba, Japan. (b) Kita, M.; Hirayama, Y.; Yoneda, K.; Yamagishi, K.; Chinen, T.; Usui, T.; Sumiya, E.; Uesuigi, M.; Kigoshi, H. *J. Am. Chem. Soc.* **2013**, *135*, 18089–18095.

16. Byfield, J. E.; Scherbaum, O. H. *Nature* **1967**, *216*, 1017−1018.

17. Cooper, G. M. "Chapter 14: The Eukaryotic Cell Cycle". in *The cell: a molecular approach* (2nd ed.), Washington, D.C: ASM Press. **2000**, ISBN 0-87893-106–6.

18. Hoehn, H.; Sprague, C. A.; Martin, G. M. *Exp. Cell Res.* **1973**, *76*, 170–174.

19. (a) Schmidt, M.; Bastians, H. *Drug Resistance Updates* **2007**, *10*, 162–181. (b) Bhalla, K. N. *Oncogene* **2003**, *22*, 9075–9086. (c) Wang, L. G.; Liu, X. M.; Kreis, W.; Budman, D. R. *Cancer Chemother. Pharmacol.* **1999**, *44*, 355–361.

20. (a) Degterev, A.; Yuan, J. *Nat. Rev. Mol. Cell Biol*. **2008**, *9*, 378–390. (b) Kurokawa, M.; Kornbluth, S. *Cell*

2009, *138*, 838–854.

21. (a) Porter, A. G.; Janicke, R. U. *Cell Death Differentiation* **1999**, *6*, 99–104. (b) Elmore, S. *Toxicol Pathol.* **2007**, *35*, 495–516.

22. Ohno, O.; Morita, M.; Kitamura, K.; Teruya, T.; Yoneda, K.; Kita, M.; Kigoshi, H.; Suenaga, K. *Bioorg. Med. Chem. Lett.* **2013**, *23*, 1467–1471.

23. Westphal, M.; Jungbluth, A.; Heidecker, M.; Mühlbauer, B.; Heizer, C.; Schwartz, J. M.; Marriott, G.; Gerisch, G. *Curr. Biol.* **1997**, *7*, 176–183.

24. Tanaka, J.; Miwa, Y.; Miyoshi, K.; Ueno, A.; Inoue, H. *Biochem. Biophys. Res. Commun.* **1999**, *264*, 938–943.

Chapter 3.

Development of Novel Chemical Probes to Analyze

Protein-ligand Interactions

Abstract

The aim of this study is the development of novel chemical probes of aplyronine A (ApA) to analyze the binding sites of protein-ligand interactions. These probes were designed to possess a pyrene or amidopyrene group and reacting group. After the labeling of target proteins with (amido)pyrene probes and enzymatic digestion, peptides labeled with the probes would be selectively detected by label-assisted laser desorption ionization mass spectrometry (LA-LDI MS) without purification. Here, the author synthesized several pyrene and amidopyrene probes, and an ApA amidopyrene probe including *N*-hydroxysuccinimide ester moiety as a detecting group efficiently bound to the target protein actin. After enzymatic digestion of the actin–probe complex, the binding position of the probe on actin was established by LA-LDI MS analysis. This amidopyrene probe method can be applied for various ligands as well as ApA, and is expected to be more convenient than current chemical probe methods because of the omission of purification process. Therefore, a useful analytical method for the binding mode analysis was established by this study.

3-1. Introduction

3-1-1. Binding Mode Analyses of Protein-ligand Interactions

The elucidation of protein-ligand interactions at a molecular level should provide insight for the design and development of new pharmacological tools and drug leads.[1] X-ray crystallographic analysis and NMR spectroscopy is very useful and have been widely used to analyze protein-ligand interactions because the complete structures of their complexes could be provided. However, due to the weak interactions and thermal instability of the target proteins, and for other reasons, the interactions with many ligands (especially for natural products and their derivatives) have not been fully established.

Another approach to solve the difficulty in the above cases is through the use of chemical probes[2]. In the case of the chemical probe with diazirine group, it covalently binds to the amino acid residues by photoreaction, which are close to the binding sites of a ligand on the target proteins (Figure 3-1). Next, the complex is digested by enzyme such as trypsin. Labeled peptides are subsequently purified based on the detecting group of chemical probe, and analyzed by mass spectrometry. Then, peptide-mass fingerprint (PMF) analysis or Edman degradation of labeled peptides can establish the binding positions of ligands. Finally, the whole structure of protein-ligand complex is estimated by computational approach, such as docking simulation of the ligand with the target protein. This method is even applicable for the weak protein-ligand interaction since a covalent bond is formed between the ligand and the target protein with retaining their complex structure.

And, the binding mode analysis of ligands with proteins can be examined even in the cases of minor cellular proteins because of the high sensitivity on MS analysis.
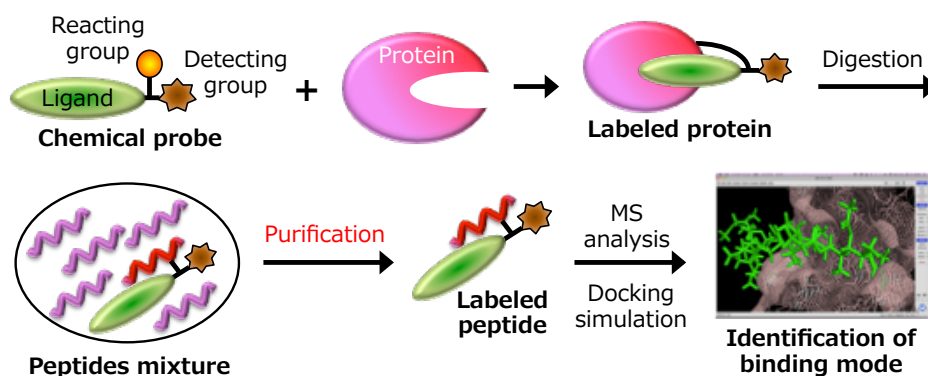

Figure 3-1. Current chemical probe method for the binding mode analysis of protein−ligand interaction.

3-1-2. Demerit of Current Chemical Probe Method

In the case of the chemical probes that are not labeled with radioactive groups, such as tritium, it is generally difficult to purify small quantities of labeled peptides from a mixture of unreacted ligands and other degraded products. For example, when a detecting group is a fluorescent group, the labeled peptides could be purified by HPLC based on the fluorescence. But optimization of the purification method of labeled peptides is needed. When a detecting group is a biotin group, the labeled peptides could be affinity-purified by using avidin-loaded resin. But vigorous condition is needed to elute the labeled peptides from the resin. In both cases, the amount of the labeled peptides decreases during the purification. In this chapter, the author proposed the novel chemical probe method to detect the labeled peptides without purification.

3-1-3. Label-assisted Laser Desorption/ionization Mass Spectrometry (LA-LDI MS)

To selectively detect labeled peptides from the peptide mixture, laser desorption/ionization mass spectrometry (LDI MS) was focused. MALDI MS is the method to indirectly ionize organic and organometallic compounds by matrix when UV laser is irradiated. Meanwhile, LDI MS without matrixes is another method to detect the molecular ions of compounds that are directly irradiated by UV laser. For example, LDI MS analysis of dipeptides containing aromatic amino acids[3] and polycyclic aromatic hydrocarbons (PAHs)[4], such as pyrene and anthracene, have been reported. In 2013, Kozmin and co-workers reported that pyrene-conjugated compounds were selectively detected by LDI MS from the mixture of reactants and reagents, and named this method as label-assisted laser desorption/ionization (LA-LDI) MS.[5] Since then, several examples related to LA-LDI MS have been reported, which used PAHs or rhodamine fluorophores as detection tags.[6] On these LA-LDI MS analysis, the molecular ions of organic compounds were detected as H^+, Na^+, K^+ adducts or radical cations as with MALDI MS. Due to the direct ionization by UV laser irradiation on LA-LDI MS, samples receive high energy. So, LA-LDI MS is a hard ionization process compared with the soft ionization process on MALDI MS. Therefore, fragmentation of compounds is expected during the measurement of LA-LDI MS. Still, it was expected that various kinds of compounds possessing PAHs (such as pyrene) as a detection tag are only detected by LA-LDI MS. Based on this assumption, the author thought that LA-LDI MS analysis is also useful for the selective detection of labeled peptides from peptide mixture.

3-1-4. Proposal of Novel Chemical Probe Method

        To detect labeled peptides without purification, a novel chemical probe possessing a reacting group and a pyrene group was designed based on the property of ionization of LA-LDI MS. After the labeling of target proteins by reacting group and subsequent enzymatic digestion, pyrene-labeled peptides could be solely detected on LA-LDI MS (Figure 3-2). If this approach is successful, the purification of labeled peptides could be omitted, and the binding positions of ligands might be analyzed more efficiently.
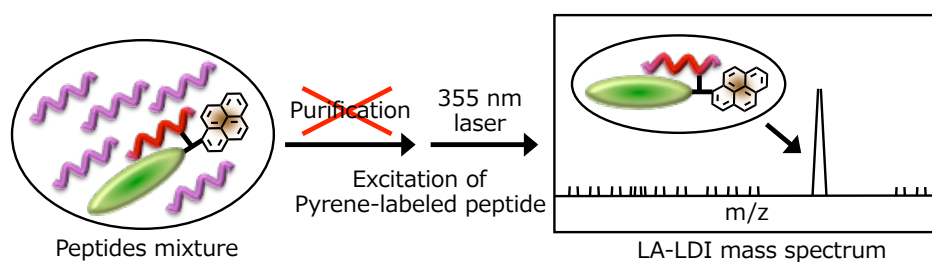
Figure 3-2. Pyrene probe method for binding mode analysis.

        Because protein−probe complex is generally digested at µg~ng scale, the labeled peptides are obtained at sub-nano mol order. However, according to Kozmin and co-workers, simple pyrene compounds, such as 1-pyrenebutyric acid, were detected at 35 nmol by the LA-LDI MS instrument equipped with a 355 nm Nd:YAG laser (UltraXtreme-TN, Bruker).[5] This amount was used to selectively detect pyrene derivatives with sufficient S/N (signal-to-noise) ratio from the mixture of unlabeled compounds. However, this amount is too much to be applicable for the detection of labeled proteins. To achieve my proposed methods as mentioned above, pyrene derivatives that are detectable at pico-mol order by LA-LDI MS should be developed.

        Therefore, the author planned to check the detection limit of pyrene derivatives and the newly designed pyrene probes in the next section.

3-2. Photoaffinity Probe

3-2-1. Pyrene Compounds for a LA-LDI Tag

To verify the usefulness of pyrene groups as a detecting group, the detectability of two simple pyrene compounds on LA-LDI MS were examined (Figure 3-3). The first one is 1-pyrenebutyric acid, the same compound that Kozmin's group reported. The second one is methyl 4-(1-pyrenyl)butyrate (**20**), which was prepared from 1-pyrenebutyric acid.
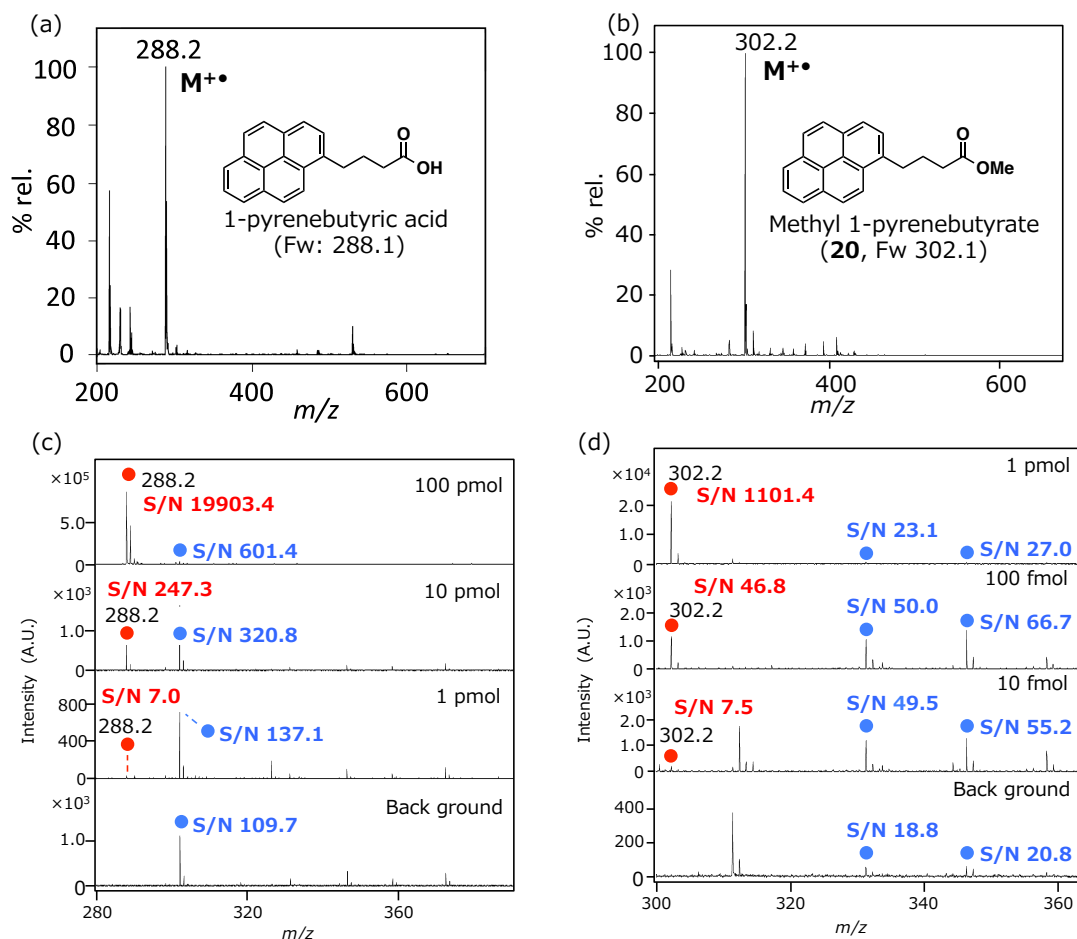

Figure 3-3. LA-LDI MS of pyrene compounds. The whole mass spectra of (a) 1-pyrenebutyric acid at 100 pmol and (b) methyl 4-(1-pyrenyl)butyrate (**20**) at 1 pmol. Magnified mass spectrum of the molecular ion of (c) 1-pyrenebutyric acid (100-1 pmol) and (d) **20** (1 pmol-10 fmol). Red circles indicate the molecular ion peaks of pyrene derivatives and blue circles indicate representative background peaks.

The molecular ion peak (m/z 288.2, M$^{\bullet+}$) of 1-pyrenebutyric acid was dominantly observed as a radical cation at 100 pmol (Figure 3-3a), while the S/N ratio of this peak at 10 pmol was same as those of background peaks, and the molecular ion peak was hardly detected at 1 pmol (Figure 3-3c). So, LA-LDI MS of a pyrene compound was observed at lower amount (pico-mol order) than Kozimins' experiment (nano-mol order). Meanwhile, the molecular ion peak (m/z 302.2, M$^{\bullet+}$) of **20** was clearly detected at 1 pmol with sufficient S/N ratio (Figure 3-3b), and also detected even at 10 fmol (Figure 3-3d). Therefore, the protection of carboxylic acid moiety highly improved the detectability on LA-LDI MS. These results indicated that pyrene is a useful detecting group for chemical probes.

3-2-2. Design and Synthesis of Pyrene Probes

      To validate my new chemical probe method, the author chose aplyronine A (ApA) as a ligand, which forms a 1:1 complex with actin as mentioned in chapter 1. A photoaffinity biotin probe, ApA-PB (**17**) was synthesized as a chemical probe, and was shown to possess cell-growth inhibitory activity. So ApA PEG-linker photoaffinity pyrene probe (ApA-PP, **21**) was designed on the basis of the structure of **17** (Figure 3-4). Additionally, the author designed ApA-AP (**22**), in which a pyrene group is conjugated though an alkyl-linker with ApA moiety.
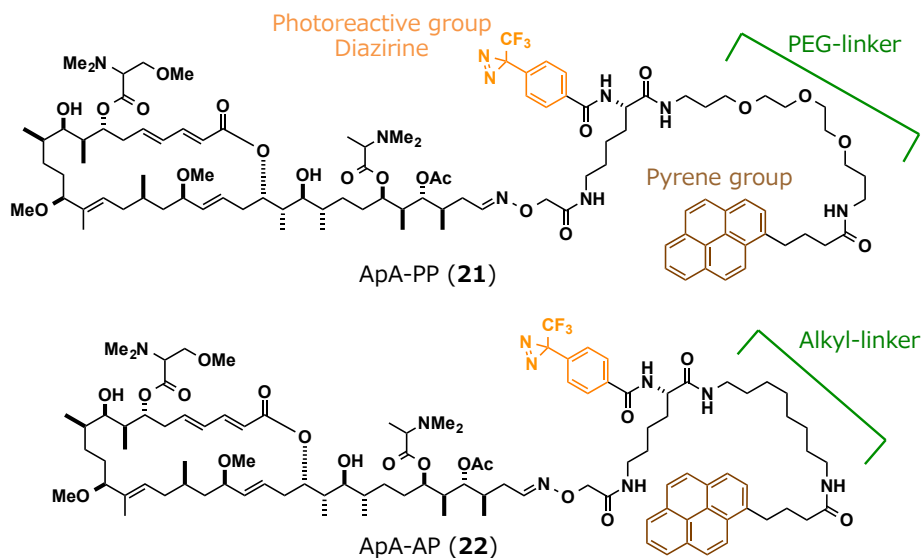

Figure 3-4. The structures of ApA-PP (**21**) and ApA-AP (**22**).

      First, alkoxyamines **33** and **34** possessing a diazirine group and a pyrene group were synthesized (Scheme 3-1). Condensation of 1-pyrenebutyric acid with amine **23**[7] or **24**[8] prepared from 1,8-diaminooctane in the presence of *N*-(3-dimethylaminopropyl)-*N'*-ethylcarbodiimide hydrochloride (EDC·HCl) and 1-hydroxy-benzotriazole (HOBt) gave amide **25** (84%) or **26** (76%). Deprotection of the Boc group of amides **25** and **26** followed by the coupling with carboxylic acid **27**[9] gave amides **28** (81%) and **29** (76%). In the same way, deprotection of the Boc group of amides **28** and **29** and subsequent coupling with succinimidyl ester **30**[10] gave amides **31** (51%) and **32** (41%), respectively. Removal of the phthalimide (phth) group in **31** and **32** yielded alkoxyamines **33** and **34** (quant, respectively).
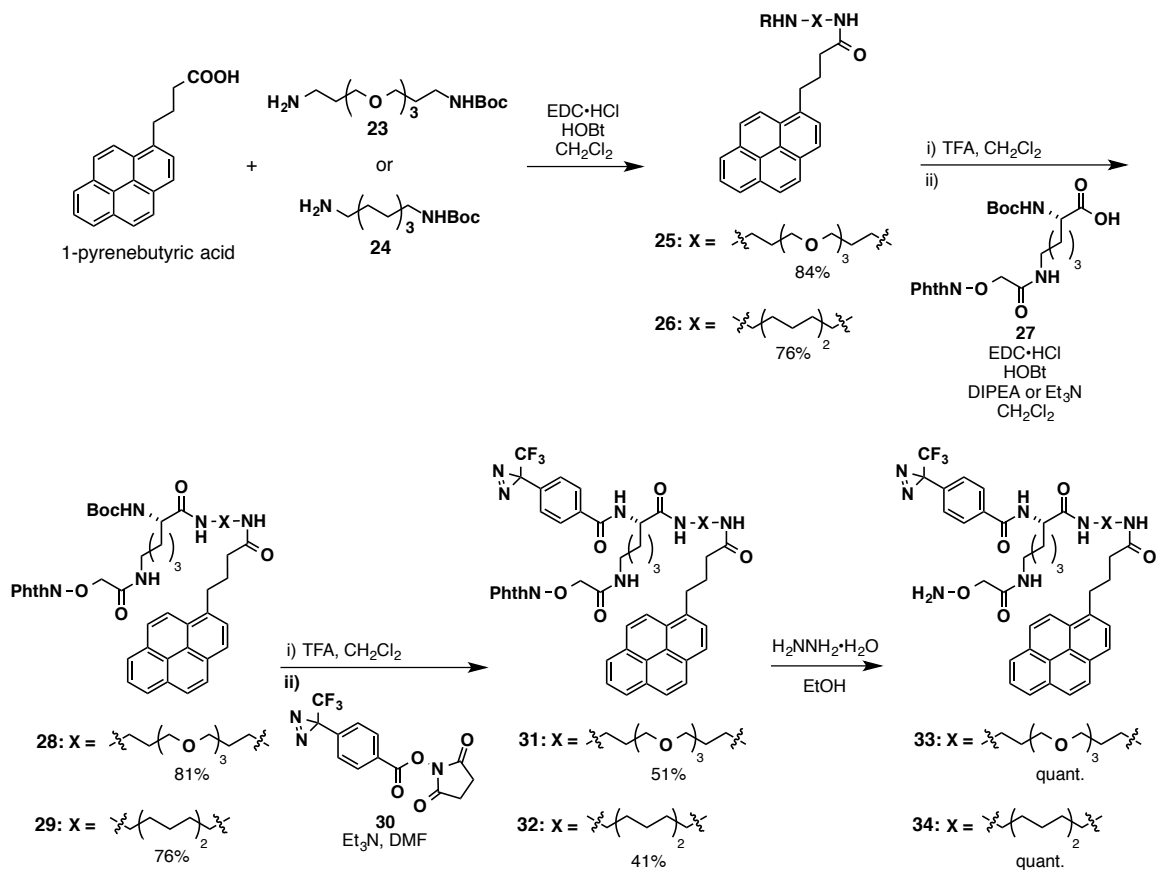
Scheme 3-1. Synthesis of alkoxyamines **33** and **34**.

ApA-PP (**21**) and ApA-AP (**22**) were synthesized from ApA (Scheme 3-2). As shown in chapter 2, aldehyde **10** was obtained by the acidic hydrolysis of ApA. Oximation of aldehyde **10** with alkoxyamines **33** and **34** gave ApA-PP (**21**) and ApA-AP (**22**) (46% and 66% from **1**), respectively.
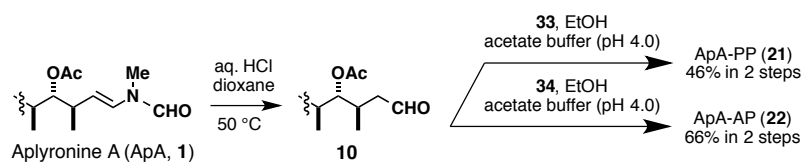
Scheme 3-2. Synthesis of ApA-PP (**21**) and ApA-AP (**22**).

3-2-3. LA-LDI MS of Pyrene Probes

　　　　To check the detectability of photolabeled pyrene derivatives on LA-LDI MS, ApA-PP (**21**) was reacted with MeOH by the irradiation with UV_{365} at 0 °C for 15 min. As a result, a MeOH-adduct **35** was afforded in 8% yield (Scheme 3-3). Since carbenes generated from trifluoromethylaryldiazirines are known to insert into the O–H bond of MeOH in preference to the C–H and C–O bonds,[11] the planar structure of **35** was estimated as methyl ether, not primary or tertiary alcohols.
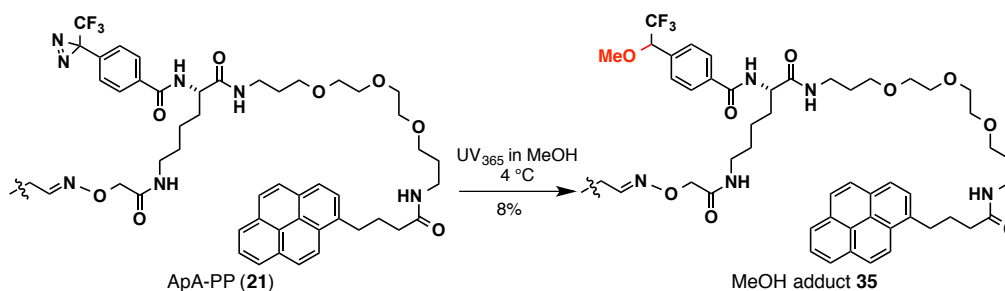
Scheme 3-3. Synthesis of MeOH-adduct **35**

　　　　LA-LDI MS analysis of the MeOH-adduct **35** was conducted. The molecular ion (m/z 1947.0, $[M+Na]^+$) of **35** was observed as a sodium ion adduct at 10 pmol but not detected at 1 pmol (Figure 3-5a,b). At 1 pmol, two major fragment ions were observed at m/z 915.4 and 491.3 along with several minor unassignable fragment ions. The former ion corresponded to the fragment cleaved at the oxime N–O bond. The latter ion was assigned as the fragment cleaved at the amide C–N bond of the C-terminus of the Lys group. Due to the direct excitation by UV laser, LA-LDI is relatively hard ionization process. So, it was thought that the fragmentation occurred similarly as EI (electron ionization) methods when the MeOH-adduct **35** was measured by LA-LDI MS. And, no fragment ions generated by the cleavage of the PEG C–O bonds, other amide C–N bonds, or the photoreacted sites were observed.

　　　　The fragment ion (m/z 915.4), which has the photoreacted moiety (MeOH), was not detected 0.1 pmol (Figure 3-5c). Because the molecular ion of **20** was detected at 0.1 pmol (Figure 3-3d), the detectability of **35** on LA-LDI MS was lower than **20**. This reason was supposed to be due to the fragmentation at the amide C–N bond of the lysine C-terminus on the linker moiety in **35**.
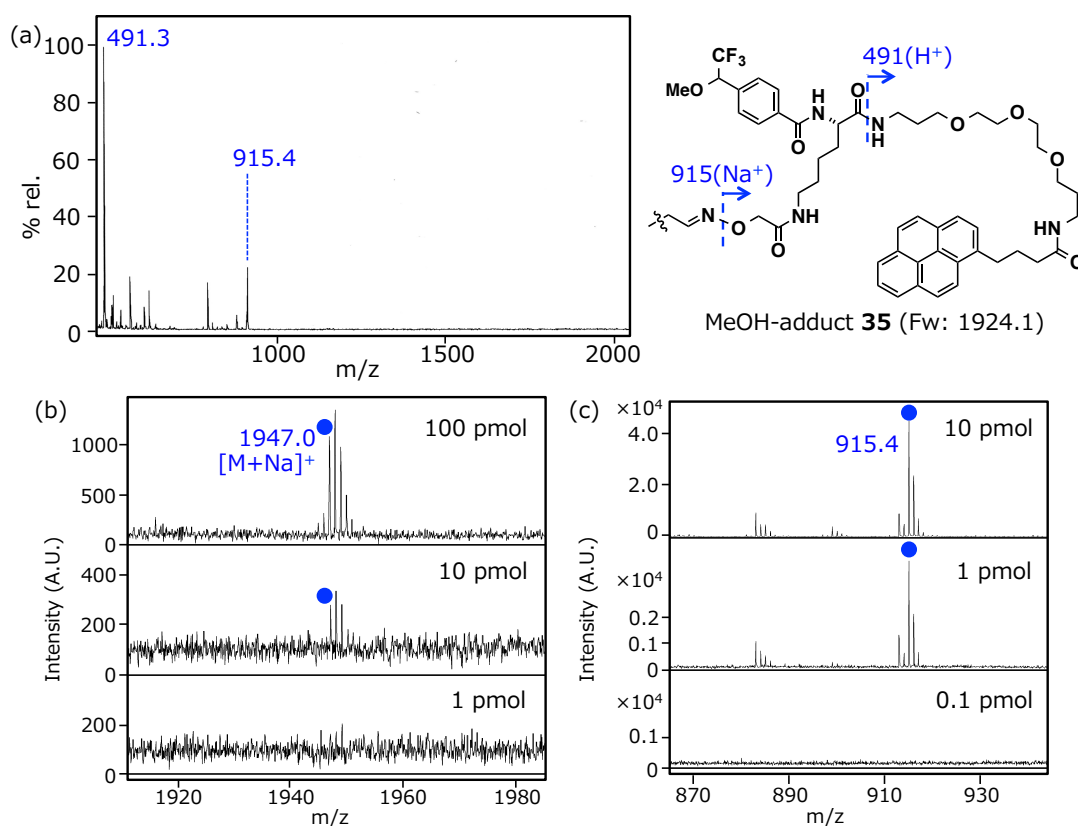
Figure 3-5. LA-LDI MS of MeOH-adduct **35** prepared by the photoreaction of **21** with MeOH. (a) The whole mass spectrum of **35** at 1 pmol. Fragment ion peaks were assigned as shown in the right chemical structure. Magnified mass spectra of (b) the molecular ion (100-1 pmol) and (c) the fragment ion (*m/z* 915.4, 10-0.1 pmol).

To establish the structure of the LA-LDI MS fragment **35a** (*m/z* 915.4) generated from **35**, MS/MS analysis was performed at 1 pmol (Figure 3-6). Four ion peaks at *m/z* 857.4, 513.2 (base peak), 271.0, and 217.0 were detected, all of which were cleaved at the amide C–N bonds. Meanwhile, a number of unassigned ion peaks were also observed in the MS/MS analysis of **35a**. But, since the fragment ion that includes the photoreacted moiety (MeOH) was detected, LA-LDI MS/MS was found to be useful to analyze the internal structure of the compound labeled by pyrene probe **21**.
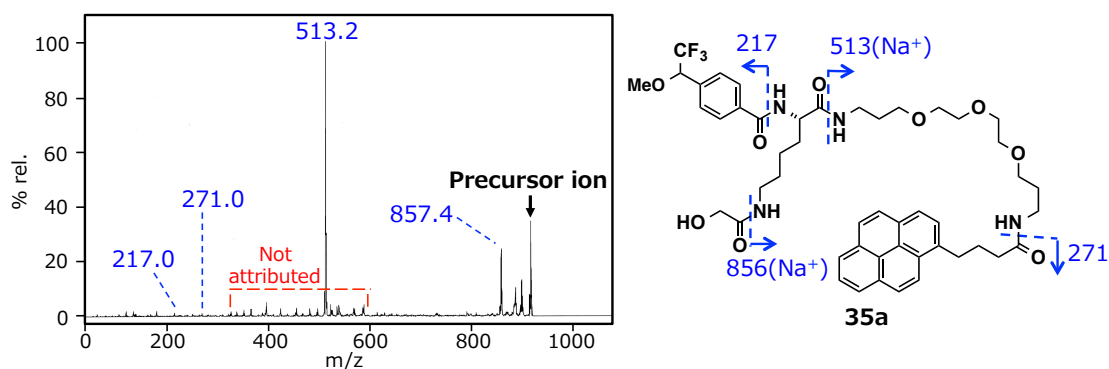

Figure 3-6. MS/MS analysis of the fragment **35a** generated from **35** (1 pmol), precursor ion: *m/z* 915.4. The fragmentation mass peaks were assigned as shown in the right chemical structure.

67

3-2-4. Bioactivities of Pyrene Probes

   With respect to the biological activity of ApA-PP (**21**) having a PEG-linker, and ApA-AP (**22**) having an alkyl-linker, *in vitro* F-actin sedimentation assay[12] was performed. On ultracentrifugation, actin in G-buffer was detected in the supernatant as a monomer (G-actin) (Figure 3-7, lane 1). In the presence of Mg^{2+}, actin was polymerized to F-actin and detected in the precipitate (lane 2). Because ApA inhibits actin polymerization, the F-actin treated with ApA (1.7 eq. against 3 μM G-actin) was detected in the supernatant (lane 3). In both cases of probes **21** and **22** (1.7 eq.), actin was mainly detected in the precipitate, comparable to lane 2 (lanes 5, 4). Because of the hydrophobicity of pyrene group, probes **21** and **22** were expected to non-specifically interact with hydrophobic amino acid residues in actin or self-assemble by the stacking of pyrenes. Therefore, probes **21** and **22** might hardly show inhibitory effects on actin-polymerization.

   When actin was treated with ApA-PP (**21**), actin in the supernatant was detected slightly more than that treated with ApA-AP (**22**) (Lanes 4, 5). This difference in activity between **21** and **22** may be due to the difference in the linker structure: more hydrophilic nature of the linker results in more potent effect activity on actin-polymerization. The increase of hydrophilicity of pyrene group was thought to be necessary for the probes that retain the bioactivity of ApA. Also, the PEG-linker like **21** seemed to be better for the activities of ApA derivatives. Therefore, in next section, the modification of a pyrene group of **21** was examined.
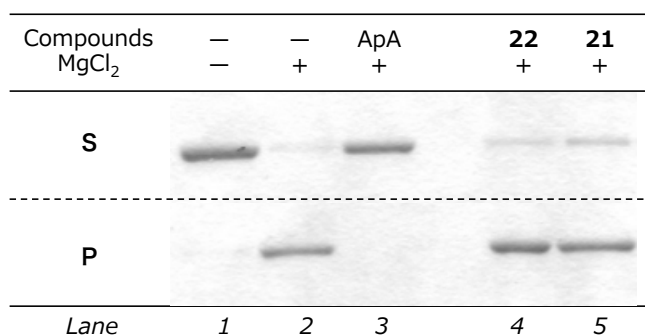

Figure 3-7. Inhibitory effects of ApA, ApA-AP (**22**) and, ApA-PP (**21**) on actin polymerization. Polymerized actin with $MgCl_2$ (except for lane 1) was incubated with each sample, and the F-actin was precipitated by ultracentrifugation. The proteins in supernatant (S) and precipitate (P) were detected by CBB stain.

3-2-5. Synthesis and LA-LDI MS of Aminopyrene and Amidopyrene

      To increase the hydrophilicity of the pyrene group, aminopyrene **37** and amidopyrene **38** were synthesized as shown in Scheme 3-4. Nitration of **20** with 44% aqueous nitric acid resulted in a 1:1:1 mixture of regioisomers of nitropyrene **36** (quant.). Catalytic hydrogenation of nitropyrene **36** gave aminopyrenes, which were separated by SiO_2 column chromatography to give 6-aminopyrene **37** as a single isomer (28%) and a 1:1 mixture of two isomers (59%). Acetylation of **37** afforded amidopyrene **38** in 93% yield. Finally, hydrolysis of **38** gave carboxylic acid **39** (86%).
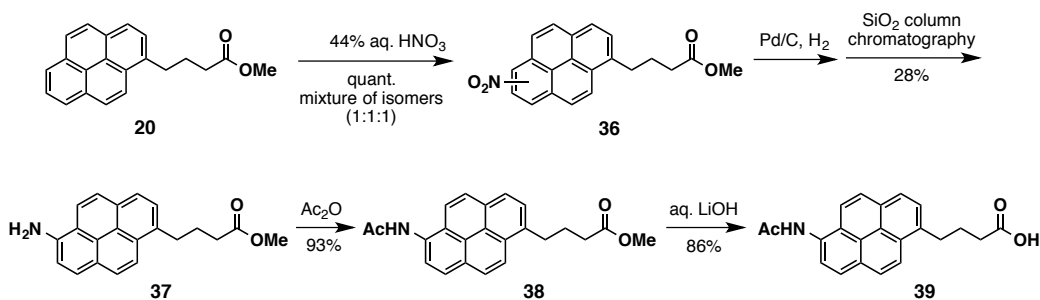
Scheme 3-4. Synthesis of amidopyrene **39**.

      To evaluate aminopyrene and amidopyrene as LA-LDI MS tags, the author compared the UV–Vis absorbance spectra (Figure 3-8) and LA-LDI MS (Figure 3-9) of **37** and **38**, with those of unmodified pyrene compounds. Because compounds are excited by UV laser (355 nm) on LA-LDI MS, the absorbance of LA-LDI MS tags at 355 nm are thought to be important. Compared with the UV absorbance of 1-pyrenebutyric acid (λ_{max} 340 nm), the maximum absorbances of both **37** and **38** shifted to longer wavelength (λ_{max} 362 and 346 nm, respectively), with substantial absorption at 355 nm. On the other hand, 1-pyrenebutyric acid had little absorption at 355 nm. These results suggested that both aminopyrene and amidopyrene were better than the unmodified pyrene as LA-LDI MS tags.
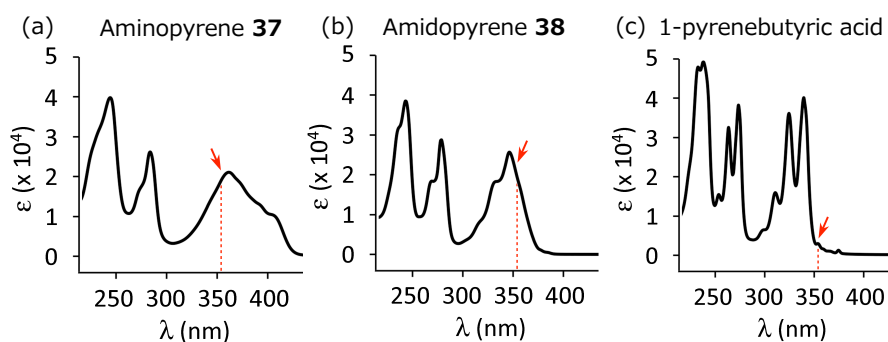

Figure 3-8. UV–Vis absorbance spectra of pyrene derivatives **37**, **38**, and 1-pyrenebutyric acid. A red arrow suggests the absorption at 355 nm.

      In the LA-LDI mass analysis of **37**, a molecular ion peak at *m/z* 317.2 [M]$^{+\bullet}$ was observed as a radical cation, with a base peak at *m/z* 632.3 (Figure 3-9a). The latter peak was assigned to be a homodimer (radical) cation [2M–2H]$^{+\bullet}$. Aniline and related aromatic amines are known to dimerize with acidic treatment or UV irradiation to give hydrazines and other compound mixtures.[13] Thus, **37** was thought to be oxidatively-dimerized

by UV laser irradiation on LA-LDI MS. Due to the complexity of mass spectra, aminopyrene was thought to be unsuitable for LA-LDI MS tags. In contrast, in the case of amidopyrene **38**, a molecular ion peak at *m/z* 359.2 ([M]$^{+\bullet}$, base peak) and a fragment ion at *m/z* 317.2 [M–42]$^{+\bullet}$ were solely detected with no dimerized ion peaks (Figure 3-9b). Acetanilide is known to fragment by losing ketene (CH$_2$=C=O), producing the peak of aniline on EI (electron ionization) MS analysis[14]. Thus, the latter peak corresponding to the aminopyrene generated *in situ* by the removal of ketene from **38**. And these two peaks were not detected at 1 fmol. Compared with LA-LDI MS of pyrene **20** (Fig. 3-3b), the molecular ion and the fragment ion of **38** were detected at 10 fmol with ca. 3 times higher S/N ratios (Figure 3-10).

Thus, amidopyrene **38** was detected much more than **20** on LA-LDI MS, and the most useful LA-LDI tag from the viewpoint of detectability, compared with other synthetic compounds on this study.
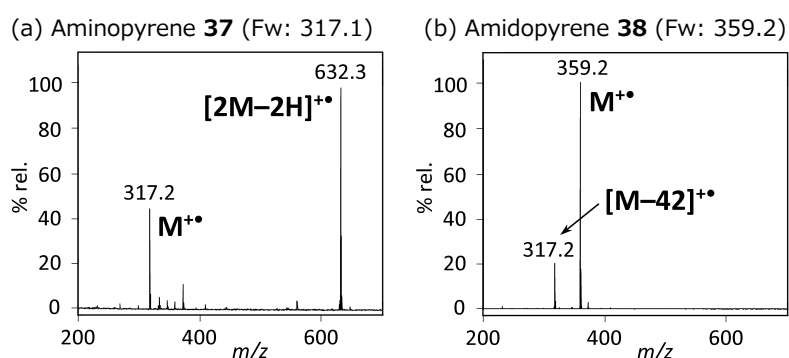

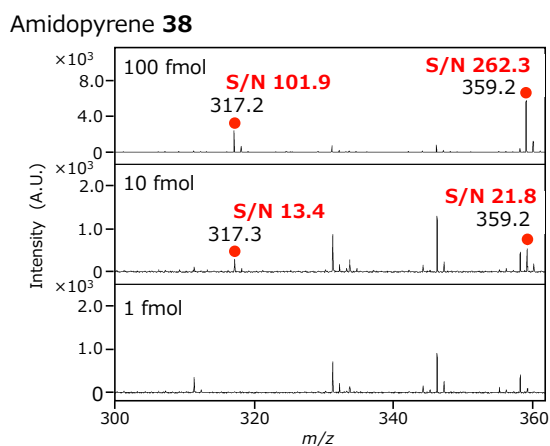Figure 3-9. LA-LDI mass spectra of (a) **37** and (b) **38** (5 pmol each).

Figure 3-10. LA-LDI mass spectra of (a) amidopyrene **37** in amounts of 100 to 1 fmol. Signal-to-noise (S/N) ratios of the ion peaks at *m/z* 317.2 [M–42]$^{+\bullet}$ and 359.2 [M]$^{+\bullet}$ are shown in red.

3-2-6. Synthesis of an Amidopyrene Probe

In the preceding section, amidopyrene group was found to be a desirable LA-LDI MS tag. So, an ApA PEG-linker photoaffinity amidopyrene probe (ApA-PaP, **40**), which has the same PEG-linker of ApA-PB (**17**) and ApA-PP (**21**), was designed (Figure 3-11). Amidopyrene **39** was converted to an alkoxyamine derivative (Scheme 3-5). Condensation of amidopyrene **39** with amine **23** gave amide **41** (98%). Deprotection of the Boc group of amide **41** followed by the coupling with carboxylic acid **27** in the presence of EDC·HCl and HOBt gave amide **42** (76%). In the same way, deprotection of the Boc group of amide **42** followed by the coupling with succinimidyl ester **30** gave amide **43** (84%). Removal of the Phth group in **43** yielded alkoxyamine **44** quantitatively. Coupling of alkoxyamine **44** with aldehyde **10** prepared from ApA (**1**) afforded ApA-PaP (**40**) in 68% yield (Scheme 3-6).
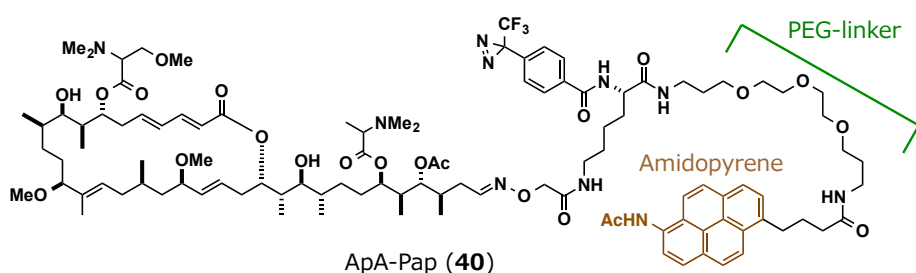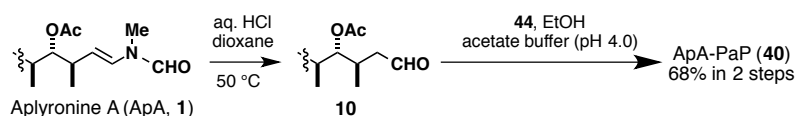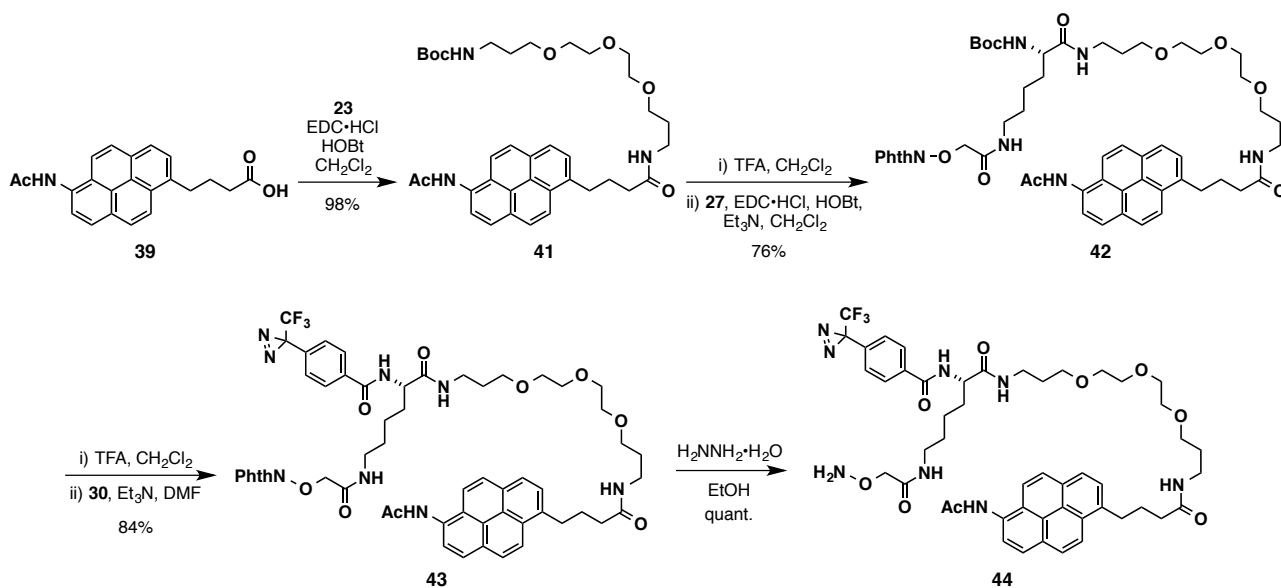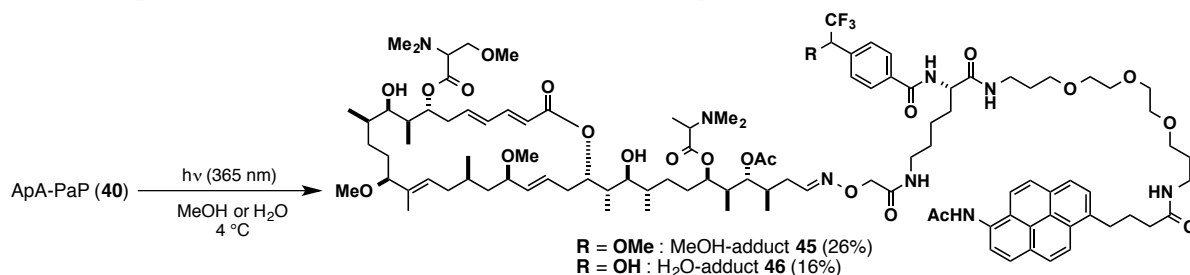

Figure 3-11. Structure of ApA-PaP (**40**).

Scheme 3-5. Synthesis of alkoxyamine **44**.

Scheme 3-6. Synthesis of ApA-PaP (**40**).

3-2-7. LA-LDI MS of Amidopyrene Probes

As a model experiment, a MeOH-adduct **45** and an H$_2$O-adduct **46** were prepared by the UV$_{365}$ irradiation of ApA-PaP (**40**) in MeOH or H$_2$O (26% and 16%, respectively) (Scheme 3-7).

Scheme 3-7. Syntheses of MeOH-adduct **45** and H$_2$O-adduct **46**.

On the LA-LDI MS analysis of the MeOH-adduct **45** (1 pmol), the molecular ion peak [M+Na]$^+$ was not detected as with the MeOH-adduct **35** (Figure 3-12a), but two pairs of characteristic fragment ions with differences of 42 mu were mainly observed at *m/z* 573.3/531.3 and 949.4/907.4. The former ion peaks were assigned as the fragment cleaved at the C–C bond of carbonyl α position of a Lys group, not at the amide C–N bond. This fragment pattern differed from the case of ApA-PP (**21**). These results suggested that pyrene moieties of **45** would have a certain role to stabilize the *N*-carbonyl cations generated *in situ*. The latter ion peaks (*m/z* 949.4/907.4) were assumed to be the fragments cleaved at the oxime N–O bond as in the case of MeOH-adduct **35**. Another peak at *m/z* 875.4 was assigned as the fragment cleaved at the ε-amino group. On the same condition, no fragment ions were observed, which were generated by the cleavage of the PEG C–O bonds, other amide C–N bonds, or the photoreacted sites. The molecular ion [M+Na]$^+$ and a fragment ion [M+Na–CH$_2$CO]$^+$ were slightly observed in an amount of more than 100 pmol (Figure 3-12b). Meanwhile, the fragment ion that includes the photoreacted moiety (MeOH), especially *m/z* 907.4, was observed even at 0.1 pmol (Figure 3-12c). LA-LDI MS using amidopyrene probe **40** would enable the author to detect photoreacted compounds at a very small amount such as sub-pmol.

Additionally, the fragment pattern of MeOH-adduct **45** of ApA-PaP on LA-LDI MS was obviously simpler than that of **35**. The reason is thought that the amidopyrene or the aminopyrene formed *in situ* retained positive charge desirable for LA-LDI MS. Therefore, the S/N ratio of mass peaks of the compounds labeled with ApA-PaP (**40**) was higher than those with ApA-PP (**21**) on LA-LDI MS, and peaks are expected to be easily analyzed and assigned.

As for the H$_2$O-adduct **46**, two fragment ions at *m/z* 893.4 and 861.4 were observed in an amount of 10 pmol, which were 14 mu (CH$_2$) smaller than those observed in the MeOH-adduct **45**, while the peaks at *m/z* 573.3/531.3 were same (Figure 3-12d). These results using ApA-PaP (**40**) strongly suggested that the amide C–C bond of the carbonyl α position of an amidopyrene and the oxime N–O bonds were preferentially cleaved to generate aminopyrene fragments *in situ*, regardless of the structures and sizes of the adducts of photoreactions.
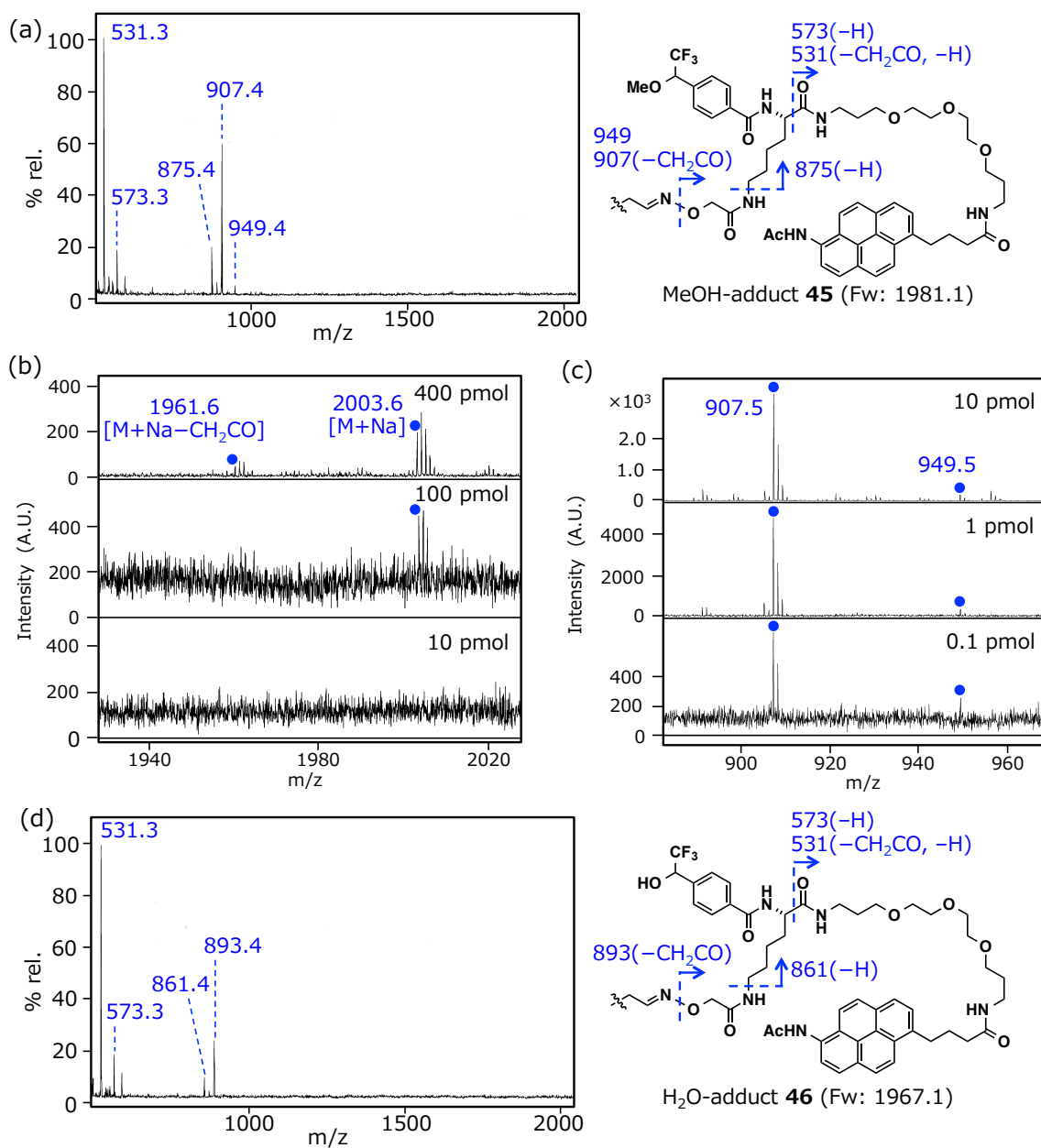
Figure 3-12. LA-LDI MS of (a-c) the MeOH-adduct **45** and the (d) H₂O-adduct **46** prepared by the photoreaction of **40**. (a) The whole mass spectrum of **45** at 1 pmol. Fragmentation mass peaks are assigned as right chemical structure. Magnified mass spectra of (b) the molecular ion of **45**, and (c) the fragment ion (*m/z* 907.5). (d) The whole mass spectrum of **46** at 10 pmol. Assigned fragmentation mass peaks are shown in right chemical structure.

To establish the structure of the major LA-LDI MS fragment **45a** (*m/z* 907.5) generated from **45**, MS/MS analysis was performed (Figure 3-13a). As in a typical MALDI-TOF MS/MS analysis, the amide C–N bonds and PEG C–O bonds were cleaved, which were surely assigned by the comparison with those of **46a** (*m/z* 893.4) generated from **46** (Figure 3-13b). Among them, two pairs of peaks at *m/z* 403.2/505.3 in **45a** and *m/z* 389.3/505.4 in **45a** were assigned as the acylium and ammonium fragment ions, respectively, which were generated by the cleavage at the Lys C-terminus amides, respectively. Unlike the case of LA-LDI MS analysis, no peaks derived from the cleavage at the C–C bond of carbonyl α position of a Lys group were observed. Notably, a fragment ion at *m/z* 243.2 was predominantly observed in both MS/MS analyses and was assigned as 6-amino-1-vinylpyrene cation formed by the McLafferty rearrangement at the 1-pyrenebutylamide moiety. In contrast to the LA-LDI MS/MS analysis of the MeOH-adduct **35** of ApA-PP, fragment pattern of **45a** was simpler than **35a**, and most peaks were surely assigned, probably due to the stable positive charge of an aminopyrene group.
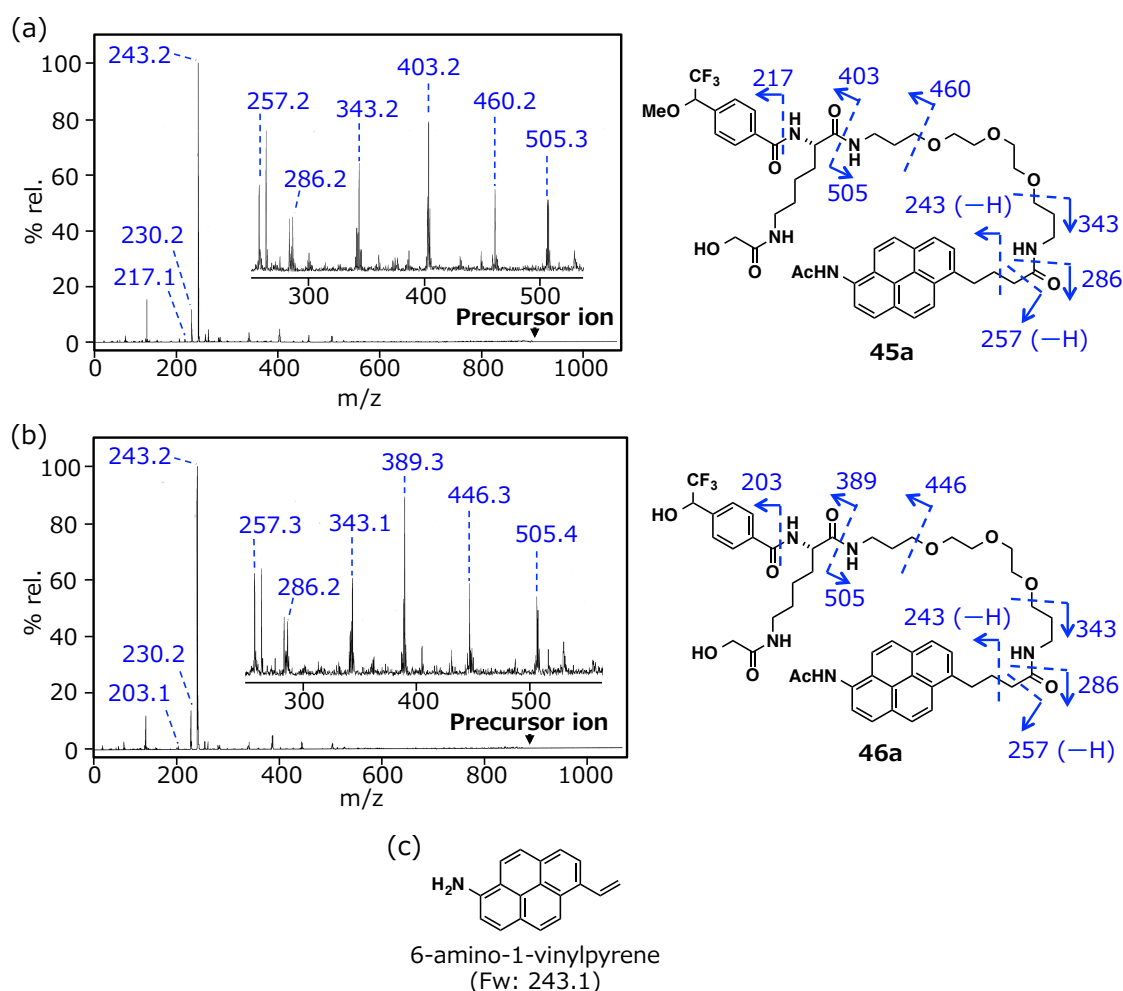

Figure 3-13. MS/MS analysis. (a) Fragment **45a** generated from **45** (1 pmol). Precursor ion: *m/z* 907.4. (b) Fragment **46a** generated from **46** (10 pmol). Precursor ion: *m/z* 893.4. The assigned fragmentation mass peaks are shown in each right chemical structure. (c) Structure of 6-amino-1-vinylpyrene, a McLafferty rearrangement product on MS/MS analysis.

To address the difference in the detectability and fragmentation patterns between 6-amidopyrene and unmodified pyrene compounds on LA-LDI MS, the author considered the weak interactions such as hydrogen bonding on the excited states. It has been shown that electronic excited-state hydrogen bonding dynamics have important roles on internal conversion, electronic spectral shifts, photoinduced electron transfer (PET), intramolecular charge transfer (ICT), and so on.[15] For example, the fluorescence quenching of the oxazine 750 dye in protic solvents is caused by the solute–solvent intermolecular PET from protic alcohols to the chromophore via intermolecular hydrogen bonds.[16] In fact, in comparison with the almost same fluorescence of pyrene **20** in MeCN and MeOH, significant fluorescence quenching for amidopyrene **38** was observed in the protic solvent (~50% reduce) (Figure 3-14). Thus, even under the highly vacuum and solid conditions, intra- or intermolecular hydrogen bonds could facilitate the PET or ICT of amidopyrene moieties, which might contribute to the unique fragmentation and stabilization of the fragments possessing amidopyrene (and aminopyrene generated *in situ*) tags on the LA-LDI MS.
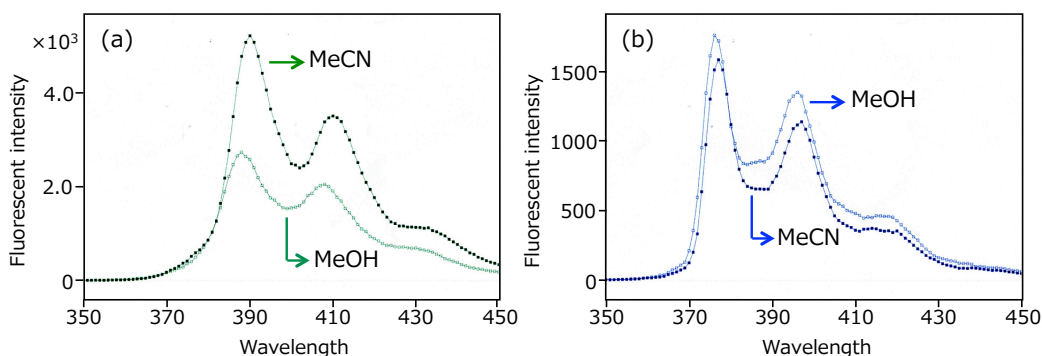

Figure 3-14. Fluorescence spectra of pyrenes. (a) Amidopyrene **38** and (b) pyrene **20** in MeCN and MeOH, excitation wavelength: 337 nm, concentration: 2.5 µM.

As shown the above experiments with ApA-PaP (**40**), an amidopyrene group absorbs 355 nm laser more strongly than a pyrene group, and enables to stabilize the cations detectable by LA-LDI MS. So, LA-LDI MS analyses of the compounds photolabeled with **40** were thought to be detectable with better S/N ratio and clearer than the MeOH-adduct **35** of ApA-PP. Therefore, an amidopyrene group is better than a pyrene group as a LA-LDI MS tag, and ApA-PaP (**40**) was expected to be useful for the binding mode analysis with the target proteins of ApA.

3-2-8. Bioactivity of Photoaffinity Amidopyrene Probe

The biological activity of ApA-PaP (**40**) was next evaluated. When an *in vitro* F-actin sedimentation assay was conducted, actin treated with **40** was detected in both supernatant and precipitate at 1:1 ratio (Figure 3-15, lane 4). So, **40** showed weaker inhibitory activity on actin polymerization than ApA (Lane 3). Compared with ApA-PP (**21**, Lane 5), the activity of **40** was obviously more potent. This difference between **40** and **21** was thought to attribute the higher hydrophilicity of **40** than **21**. Additionally, ApA-PaP (**40**) showed only 15-fold less cell-growth inhibitory activity (IC_{50} 0.27 nM, against HeLa S3 cells) than ApA. As mentioned in chapter 2, ApA prevented spindle formation in metaphase tumor cells. The effect on spindle formation of ApA-PaP (**40**) was also examined. As a result, HeLa S3 cells treated with 1 nM ApA-PaP (**40**) had abnormal multipolar spindles, as in the case of 0.1 nM ApA (Figure 3-16). These results suggested that the amidopyrene group had little effect on the bioactivity of ApA.
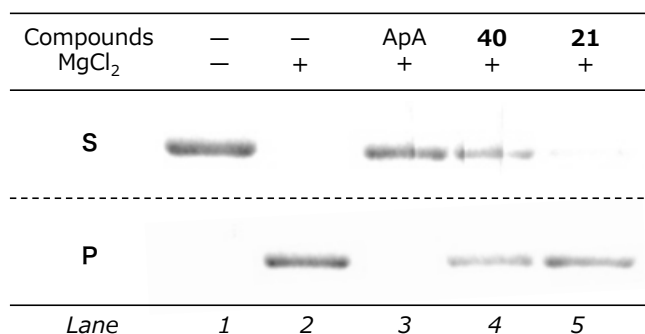

Compounds	—	—	ApA	**40**	**21**
$MgCl_2$	—	+	+	+	+
S					
P					
Lane	*1*	*2*	*3*	*4*	*5*

Figure 3-15. Inhibitory effect of ApA, ApA-PaP (**40**) and ApA-PP (**21**) on actin polymerization. G-actin (3 μM) was incubated with samples (1.7 eq), and $MgCl_2$, then F-actin was precipitated by ultracentrifugation. The proteins in the supernatant (S) and the precipitate (P) were detected by CBB stain.

Control   ApA (**1**)   ApA-PaP (**40**)
                 0.1 nmol   1 nmol
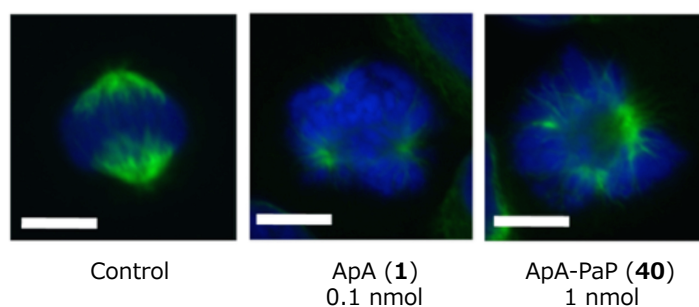
Figure 3-16. Confocal fluorescence images of HeLa S3 cells (metaphase) treated with ApA or probe **40** for 6 h. Cells were immunostained with anti-α-tubulin (green) and costained with DAPI (blue). Scale bars: 10 μm.

3-2-9. Actin-labeling by Photoaffinity Amidopyrene Probe

Actin-labeling experiments were next examined by using ApA-PaP (**40**). The G-actin (8.1 μM, Fw: 42,024) was photolabeled with **40** (10 μM, Fw: 1,977) in G-buffer by UV$_{365}$ irradiation, then the photoreacted products were directly analyzed by MALDI-TOF MS with sinapic acid as a matrix. Although the predicted exact mass of the actin−probe complex is 43,973, the corresponding peak was very weak (Figure 3-17, *m/z* 43,549), and still the actin peak (*m/z* 41,822) was a major one. These results showed that ApA-PaP (**40**) scarcely formed the covalent bond with actin while it maintains the bioactivity of ApA. This result suggested that carbene species generated by photoirradiation might mainly react with solvent molecules such as water but little with actin. The tryptic peptides of the photo-irradiated actin with **40** were analyzed by LA-LDI MS analysis. But the peptides labeled with ApA-PaP (**40**) were not detected. This result could be due to the low labeling efficiency of **40** on actin. Therefore, the new probe, which forms a covalent bond with actin more efficiently, was needed. The author next considered reacting groups other than diazirine.
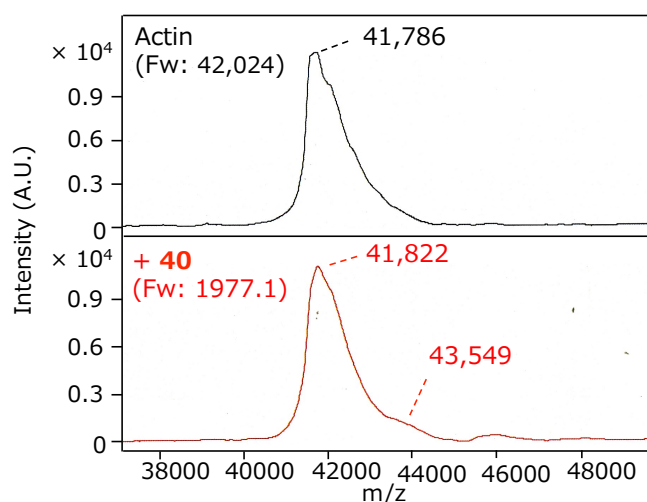

Figure 3-17. MALDI-TOF MS analysis of the actin photoreacted by ApA-PaP (**40**). Top figure shows the untreated actin. Bottom one shows the photoreacted actin with ApA-PaP (**40**, 12.5 eq) by UV$_{365}$ irradiation (on ice for 15 min). Detected peaks were shown as the average one.

3-3. Succinimide Probe

3-3-1. Consideration of the Suitable Reacting Group for LA-LDI MS

While photoreacting group such as diazirine is useful for chemical probes because of the high reactivity toward various molecules, the labeling efficiency of **40** was too low to detect the labeled peptides of actin by an ApA probe. To improve the labeling efficiency of reacting group, *N*-hydroxysuccinimide (NHS) ester was tried. This group is known to selectively react with nucleophilic functional group in amino acid residues such as lysine ε-amino group or serine hydroxy group. To check the reactivity of NHS ester toward actin and the detectability of its digested peptides on LA-LDI MS, amidopyrene succinate (Apy-Su, **47**) was prepared from carboxylic acid **39** and NHS in 66% yield. Apy-Su was reacted with actin (Scheme 3-8), which was digested with trypsin to give a mixture of amidopyrene-labeled peptides and unlabeled peptides.
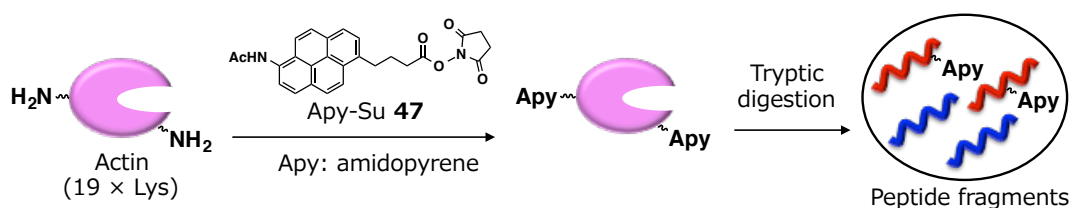
Scheme 3-8. Preparation of amidopyrene-labeled peptide fragments.

In the MALDI MS analysis, eight amidopyrene-labeled peptides and twelve unlabeled peptides were detected (Figure 3-18a). Most of the peaks were observed as H$^+$ adducts as shown in Table 3-1. Trypsin generally does not recognize acylated lysine residues. The C-termini of most amidopyrene-labeled lysine were not cleaved (No. 1, 8, 15, 26, 27). However, several peptides cleaved at the C-termini of labeled lysine residues were also detected (No. 4, 5). Additionally, serine or tyrosine residue was labeled with **47** and its ion peak was detected (No. 9). The Lys ε-amino groups in detected peptides were all located on the surface of actin. The author confirmed that these amino acids were sufficiently labeled with **47** and NHS ester moiety could be useful for the reacting group of amidopyrene probe.

In contrast to MALDI MS, ten amidopyrene-labeled peptides were selectively detected by LA-LDI MS (Figure 3-18b). Two representing peptides on MALDI MS, *m/z* 1483.6 (No. 16) and 1790.8 (No. 20) in Figure 3-18a were not detected by LA-LDI MS, while two unlabeled peptides at *m/z* 1130.5 (No. 9) and 1515.7 (No. 18) were slightly detected. Since No. 9 and No. 18 peptides include aromatic amino acid residues, such as tyrosine, phenylalanine, and tryptophan, they might be directly excited by UV laser irradiation and their ion peaks could be observed by LA-LDI MS. Surprisingly, two amidopyrene-labeled peptides at *m/z* 1937.9 (No. 19) and 2452.0 (No. 23) were detected only by LA-LDI MS. This suggested that there is the difference of ionization pattern between MALDI and LA-LDI MS methods. Additionally, several fragment ion peaks that lost ketene (CH$_2$=C=O) was observed at *m/z* 1044.5 (No. 1), 1230.6 (No. 5) and 1895.9 (No. 19) by LA-LDI MS as with the experiments for amidopyrene derivatives **38**, **45**, and **46**.
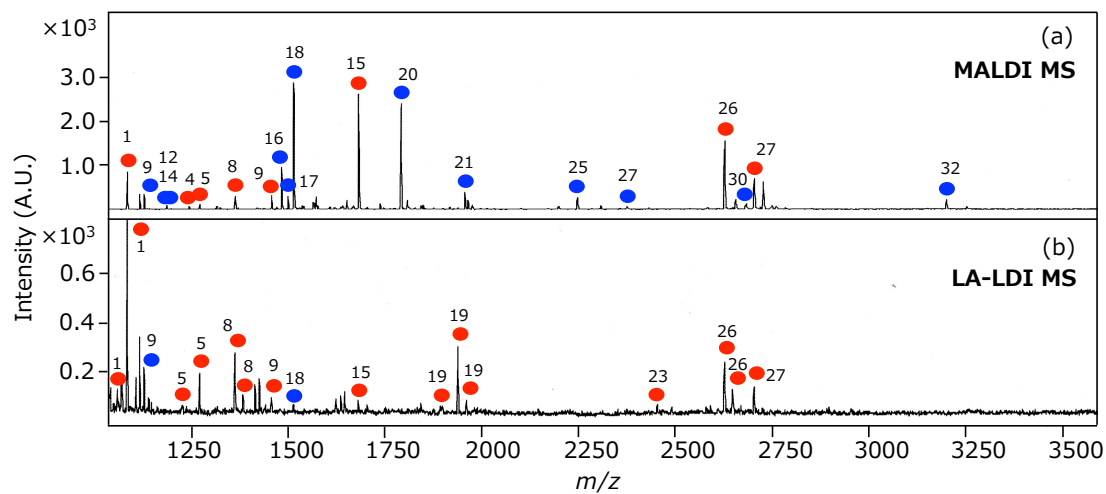
Figure 3-18. MS analysis of the mixture of unlabeled actin peptides and the peptides labeled with Apy-Su (**47**). (a) MALDI MS analysis. (b) LA-LDI MS analysis. Blue circles indicate unlabeled actin peptides. Red circles show amidopyrene-labeled peptides.

Table 3-1. Detected actin peptids labeled with Apy-Su.

No	m/z (calculated)[a]		m/z (observed)[b]		Peptide sequence
	(peptide+H⁺)	(peptide+Apy+H⁺)	MALDI	LA-LDI	
1	759.5	1086.6	1086.6	1044.5[d] 1086.6	**K**ILTER[e]
2	791.4				*C*DIDIR[f]
3	795.5				IIAPPER
4	919.5	1245.6	1246.6		*C*DIDIR**K**[e,f]
5	923.6	1250.7	1272.6[c]	1230.6[d] 1272.6[c]	IIAPPER**K**[e]
6	976.4				AGFAGDDAPR
7	998.5	1325.6			DLTDYLMK
8	1036.7	1363.8	1363.7	1363.7 1385.7[c]	I**K**IIAPPER[e]
9	1130.5	1457.6	1130.5	1130.5 1457.6	G**YS**FVTTAER[g]
10	1161.6	1488.7			EITALAPSTMK
11	1171.6	1498.7			HQGVMVGMGQK
12	1187.6		1187.5		HQGVMVGmGQK[h]
13	1198.5	1525.6			DSYVGDEAQSK
14	1198.7		1198.7		AVFPSIVGRPR
15	1354.6	1681.7	1681.7	1681.7	DSYVGDEAQS**K**R[e]
16	1483.7		1483.6		QEYDEAGPSIVHR[i]
17	1500.7		1500.7		QEYDEAGPSIVHR
18	1515.7		1515.7	1515.7	IWHHTFYNELR
19	1610.8	1937.9		1895.9[d] 1937.9 1959.9[c]	DLTDYLM**K**ILTER[e]
20	1790.9		1790.8		SYELPDGQVITIGNER
21	1956.0	2283.1	1956.0		VAPEEHPTLLTEAPLNPK
22	1960.9	2288.0			YPIEHGIITNWDDMEK
23	2124.9	2452.0		2452.0	M*C*DEDETTALV*C*DNGSGLV**K**[e,f,j]
24	2213.9	2541.0			M*C*DEDETTALV*C*DNGSGLVK[f]
25	2246.0		2246.0		DLYANNVMSGGTTMYPGIADR
26	2297.2	2624.3	2624.2	2624.2 2646.2[c]	VAPEEHPTLLTEAPLNP**K**ANR[e]
27	2374.1	2701.2	2374.0 2701.1	2701.1	**K**DLYANNVMSGGTTMYPGIADR[e]
28	2536.2	2863.3			L*C*YVALDFENEMATAASSSSLEK
29	2616.4	2943.5			YSVWIGGSILASLSTFQQMWITK
30	2681.2	3008.3	2681.3		DLYANNVmSGGTTmYPGIADRmQK[h]
31	3188.5	3515.6			*C*PETLFQPSFIGMESAGIHETTYNSIMK
32	3196.6		3196.5		TTGIVLDSGDGVTHNVPIYEGYALPHAIMR
33	3251.6				MTQIMFETFNVPAMYVAIQAVLSLYASGR

(a) Calculated *m/z* value (monoisotopic) of tryptic peptides of unlabeled or labeled actin. (b) Observed peptides corresponding to the calculated ones. (c) Na⁺ adduct. (d) Fragment ion by losing ketene ($CH_2=C=O$) from amidopyrene. (e) "**K**" means amidopyrene-labeled lysine residue. (f) "*C*" means carbamidomethylated cysteine residue. (g) "**YS**" means that either amino acid was labeled with amidopyrene. (h) Methionines of the peptides were oxidized. (i) N-terminus glutamine was converted into pyroglutamic acid. (j) N-terminus methionine was lost and *N*-acetylation occurred.

To determine the sequence and the labeling site of amidopyrene-labeled peptides, LA-LDI MS/MS analysis of the detected peak (*m/z* 2624.3, No. 26 in Figure 3-18) was performed (Figure 3-19a, Table 3-2). A number of detected peaks corresponded to the calculated values of the fragment ion peaks cleaved at the amide C–N bonds as with typical MALDI MS/MS analysis. Interestingly, amidopyrene-containing fragment ions, y4-y6, y8-y10, y15 and y16 ions, were surely assigned. Additionally, the amide bond between the lysine residue and amidopyrene moiety was cleaved on MS/MS analysis, and amidopyrene units were detected as fragment ions (*m/z* 328.1 and 286.1). So, the author determined that the detected peak (*m/z* 2624.3) was of the amidopyrene-labeled peptide as shown in Figure 3-19b. Thus, LA-LDI MS/MS analysis was found to be useful to analyze the labeled position of amidopyrene group on target proteins.
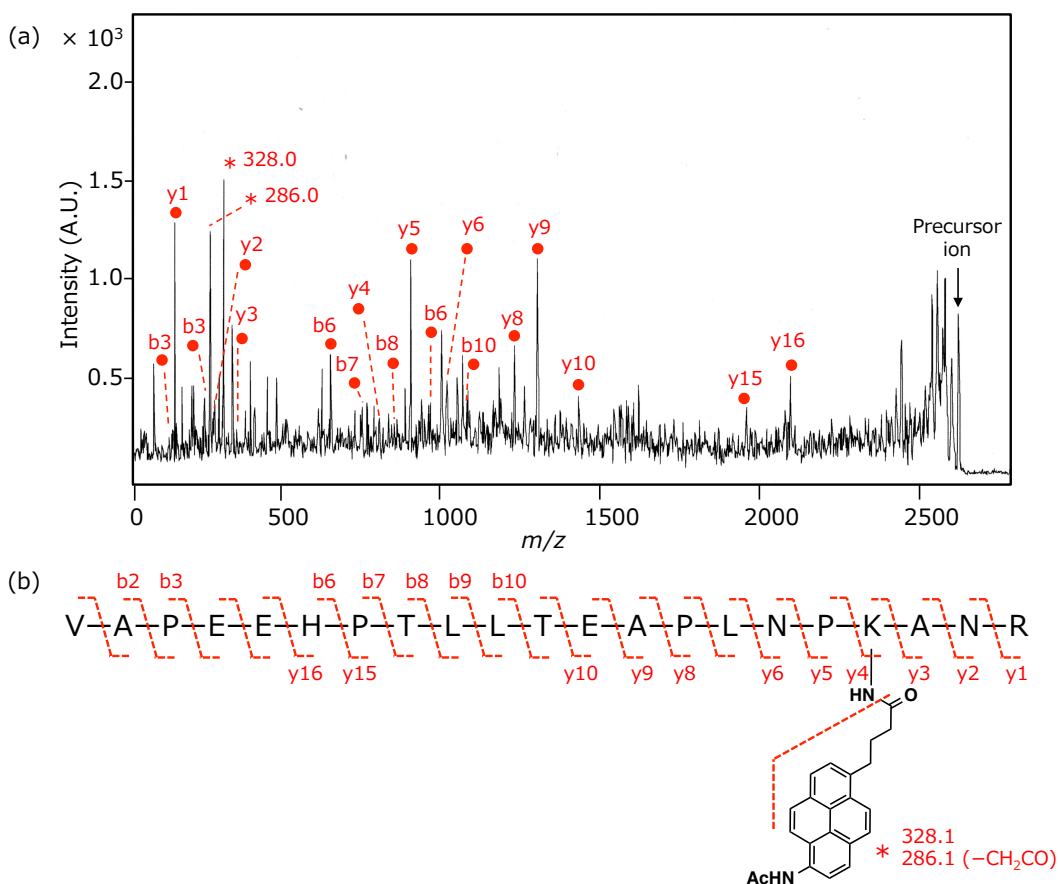

Figure 3-19. LA-LDI MS/MS of an amidopyrene-labeled peptide (precursor ion: *m/z* 2624.3). (a) LA-LDI MS/MS spectrum. Red circles show the corresponding peaks to the b or y fragment ions. Numerals of peptide peaks correspond to the data in Table 3-2. (b) Structure of an amidopyrene-labeled peptide (*m/z* 2624.3 for [M+H]$^{+}$). Red asterisk shows the fragment ion cleaved at the amide bond between the lysine residue and amidopyrene moiety.

Table 3-2. Assignment of LA-LDI MS/MS analysis (Precursor ion: 2624.2).

b	m/z calculated	m/z observed	y	m/z calculated	m/z observed
1		-	21		-
2	171.1	171.1	20	2525.3	-
3	268.2	268.0	19	2454.2	-
4	397.2	-	18	2357.2	-
5	526.3	-	17	2228.1	-
6	663.3	663.2	16	2099.1	2099.0
7	760.4	760.3	15	1962.0	1962.2
8	861.4	861.3	14	1865.0	-
9	974.5	974.4	13	1763.9	-
10	1087.6	1087.4	12	1650.8	-
11	1188.6	-	11	1537.8	-
12	1317.7	-	10	1436.7	1436.7
13	1388.7	-	9	1307.7	1307.6
14	1485.8	-	8	1236.6	1236.6
15	1598.8	-	7	1139.6	-
16	1712.9	-	6	1026.5	1026.4
17	1809.9	-	5	912.4	912.3
18	2265.1	-	4	815.4	815.2
19	2336.2	-	3	360.2	360.2
20	2450.2	-	2	289.2	289.0
21		-	1	175.1	175.0

These results indicated that amidopyrene-peptide conjugates could be selectively detected on LA-LDI MS analysis, and the probe possessing a NHS ester would be applicable for the binding mode analysis using LA-LDI MS.

In order to try other functional groups as a reacting group, model probe **48,** which has a maleimide group that can specifically react with the thiol groups of cysteine residues, was also synthesized (Figure 3-20).
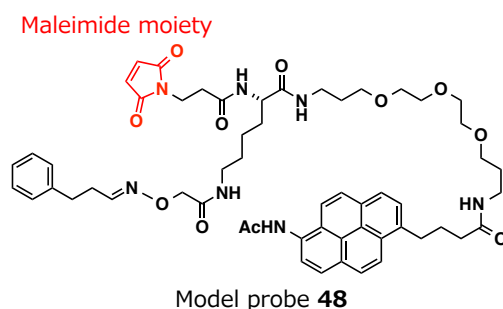

Figure 3-20. Structure of model probe **48**

First, oxyamine **49** was synthesized from **42** by the deprotection of Boc group and the removal of Phth group (Scheme 3-9). The oximation of 3-phenylpropanal with **49** gave amine **50** (79%) (Scheme 3-10). Then, amine **50** was condensed with *N,N'*-disuccinimidyl glutarate to yield model probe **48** (70%). Before LA-LDI MS analysis, model probe **48** was reacted with glutathione to afford glutathione-adduct **51**.
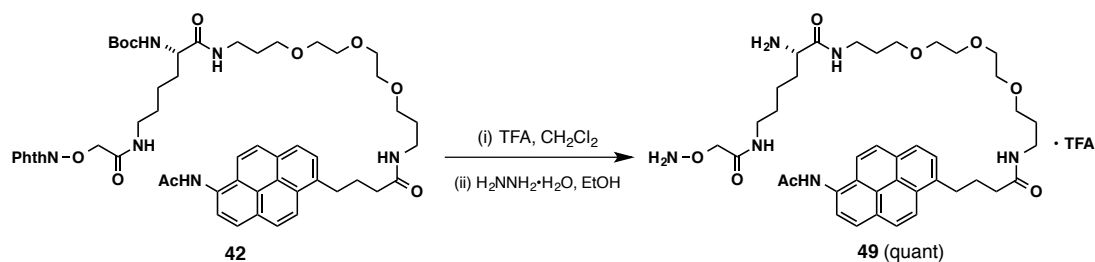
Scheme 3-9. Synthesis of oxyamine **49**.
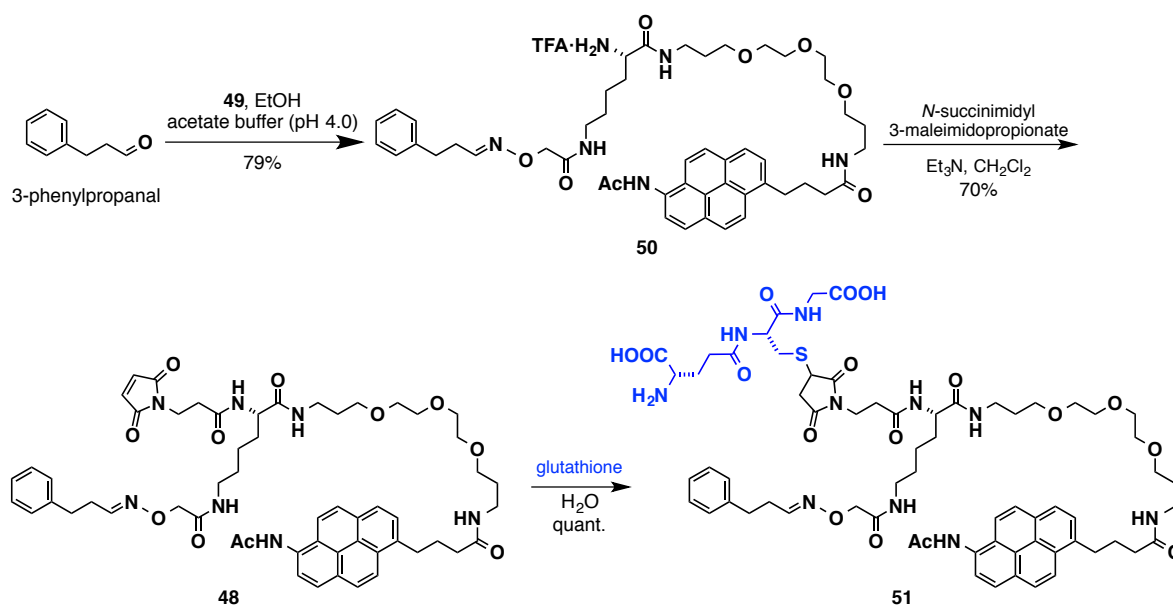
Scheme 3-10. Synthesis of model probe **48** and glutathione-adduct **51**.

The molecular ion peak of glutathione-adduct **51** was not detected by LA-LDI MS (Figure 3-21). As with MeOH-adduct **45** or H$_2$O-adduct **46** of ApA-PaP, the fragment ion cleaved at the C−C bond of Lys carbonyl α position was mainly detected at *m/z* 531.3. In addition, a fragment ion was also detected at *m/z* 975.5. This ion was assigned to the compound where the thioether C−S bond connecting **48** and glutathione was cleaved. The thioether C−S bond of carbonyl α position was expected to be easily cleaved by LA-LDI MS analysis. Furthermore, as in the cases of **45** and **46**, the oxime N−O bond was also cleaved to give major fragment ions at *m/z* 844.4, 867.4 and 909.4. These results suggested that amidopyrene probe with maleimide as a reacting group was not suitable for the LA-LDI MS analysis because the target molecule part of a probe conjugate cannot be analyzed by LA-LDI MS.
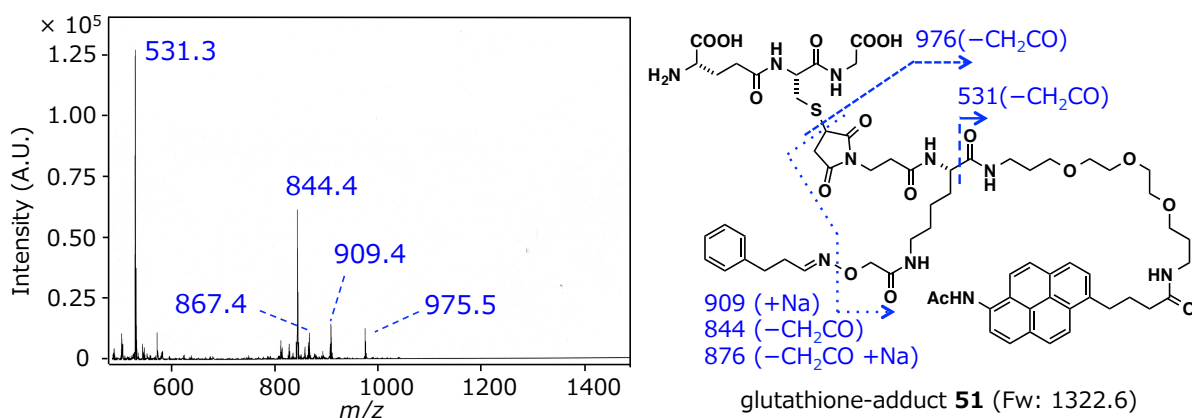
Figure 3-21. LA-LDI MS of glutathione adduct **51**. The assigned fragmentation mass peaks are shown in the right chemical structure.

3-3-2. Design and Synthesis of Aplyronine A NHS Ester Amidopyrene Probe

Next, ApA amidopyrene probe **52** possessing an NHS ester moiety was designed and synthesized (Figure 3-22, Scheme 3-11). Oximation of aldehyde **10** prepared from ApA with alkoxyamine **49** gave oxime **53** (63% from ApA). Oxime **53** was reacted with *N, N'*-disuccinimidyl glutarate to yield NHS ester amidopyrene probe **52** (quant.). Probe **52** was used for the following experiments without purification because of the instability of NHS ester structure. To check whether **52** was surely formed, **52** was condensed with glycine under basic aqueous condition. As a result, the Gly-adduct **54** was obtained in 68% yield, which was confirmed by HPLC and MALDI MS analyses.
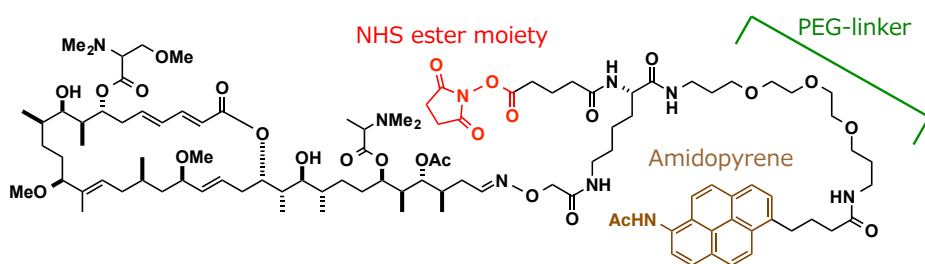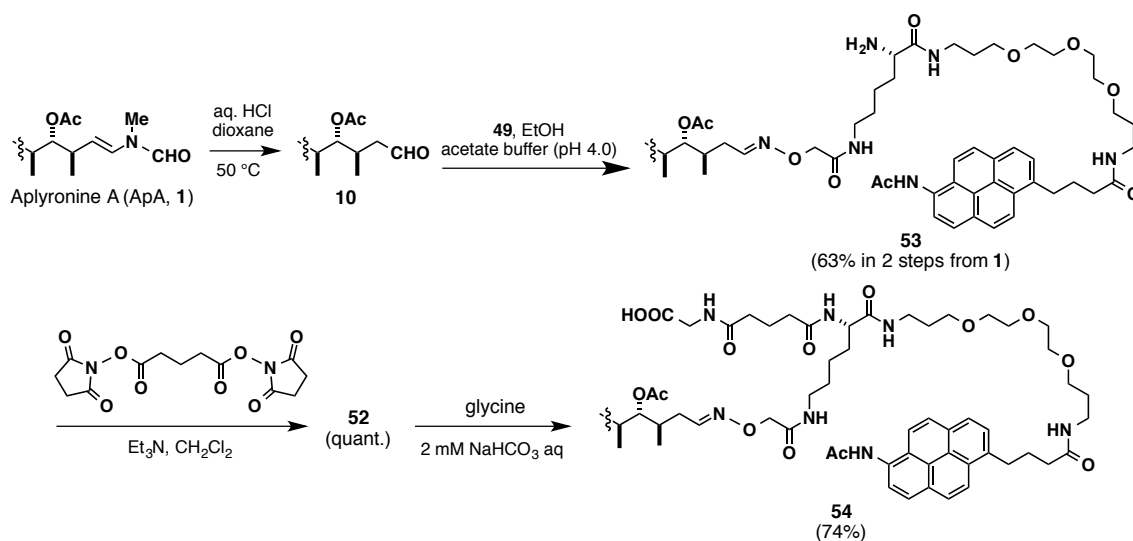

Figure 3-22. Structure of ApA amidopyrene probe **52** possessing an NHS ester moiety

Scheme 3-11. Synthesis of probe **52** and its Gly-adduct **54**

3-3-3. Actin-labeling with ApA NHS Ester Amidopyrene Probe

   To check the labeling efficiency of ApA NHS ester amidopyrene probe **52** toward actin, G-actin was labeled with probe **52** (Fw: 1,977) at 4 °C for 3 h. MALDI-TOF MS of an actin−probe **52** complex (Fw: 43,885) showed the main mass peak (*m/z* 43,875) along with two small peaks at *m/z* 45,704 and 47,559 (Figure 3-23b). These average mass values corresponded to the actin labeled with one, two, and three probe molecules, respectively. Thus, although the excess amount (3.5 eq) of probe **52** was used for the labeling with actin, the actin labeled with one molecule of probe was mainly detected. Additionally, these three peaks clearly disappeared when ApA (10 eq) was added (Figure 3-23c). These results suggested that probe **52** preferentially interacted with a specific site of actin and labeled to form a 1:1 complex of actin and **52**, and two small peaks (*m/z* 45,704 and 47,559) were the actin that non-specifically bound to probe **52** along with specific labeling.

   When ApA was added, unlabeled actin peak was shifted by 277 mu than untreated actin (Figure 3-23a, c). This reason could be due to the non-specific labeling of *N,N'*-disuccinimidyl glutarate (Fw: 270.1), since probe **52** used for these experiments contained unreacted *N,N'*-disuccinimidyl glutarate in the preparation. Because the specific labeling with **52** occurred sufficiently in spite of the actin-modification with the contaminant, it was not disadvantage for this purpose. Furthermore, by SDS-PAGE analysis, the band of actin−probe complex was shifted to higher molecular weight than actin (Figure 3-24). Therefore, it was clearly showed that probe **52** quantitatively bound to actin.
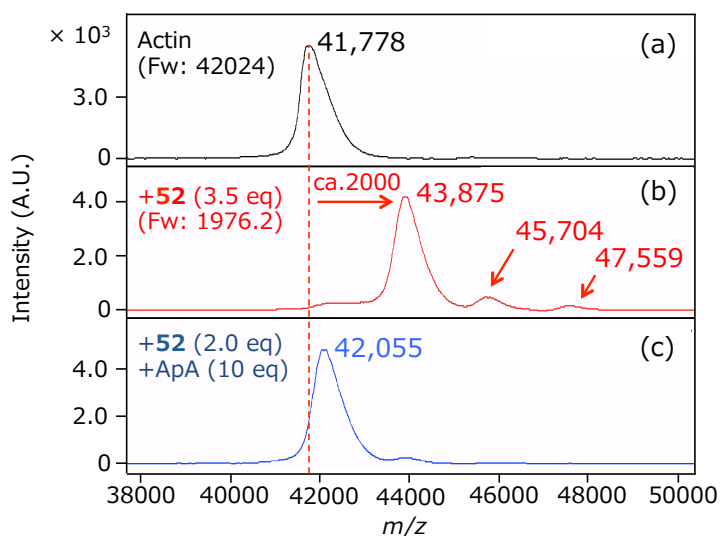

Figure 3-23. MALDI-TOF MS analysis of the actin reacted with probe **52**. (a) Untreated actin. Labeled actin with probe **52** (3.5 eq or 2.0 eq) for 3 h at 4 °C in the absence (b) or presence (c) of ApA (**1**, 10 eq). Detected peaks were shown as average mass values.

SDS-PAGE
CBB stain
Actin 100 pmol

Actin —

50 kDa
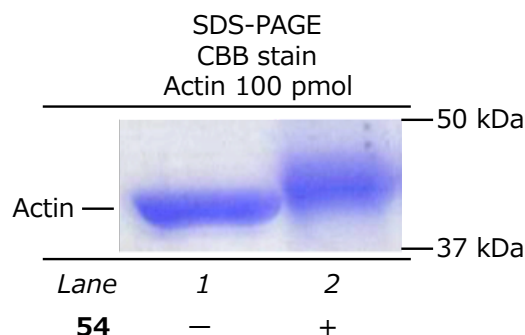
37 kDa

| Lane | 1 | 2 |
| **54** | — | + |

Figure 3-24. SDS-PAGE analysis of the labeled actin with probe **52**.

3-3-4. LA-LDI MS of the Actin Peptides Labeled with ApA NHS Ester Amidopyrene Probe

Actin−probe **52** complex was digested by the mixture of trypsin and Glu-C, the former which selectively cleaves the C-termini of lysine and arginine residues, the latter which selectively cleaves the C-termini of glutamic acid and aspartic acid residues. Then, LA-LDI MS analysis of the peptide mixture (ca. 200 pmol) was examined (Figure 3-25, Table 3-3). A molecular ion peaks of the labeled peptides were detected at m/z 2841.5 (No. 19) and 2799.5 (No. 18) along with unlabeled actin-derived peptides (No. 2−17). The m/z value of the peak (No. 19) corresponded to the conjugate of A108−R116 peptide (Fw: 979.5) with probe **52** (Fw: 1976.2) as $[M+H]^+$ (exact mass = 2841.6). This ion peak was detectable up to 20 pmol peptide mixture, but not with 2 pmol. The peak (No. 18) corresponded to the compound generated by ketene elimination from the peptide−probe conjugate. Additionally, the base peak was the fragment ion (No. 1, m/z 531.2) by the cleavage at the C−C bond of the Lys carbonyl α position as with the previous experiments (Fig. 3-12a,d and Fig. 3-21).
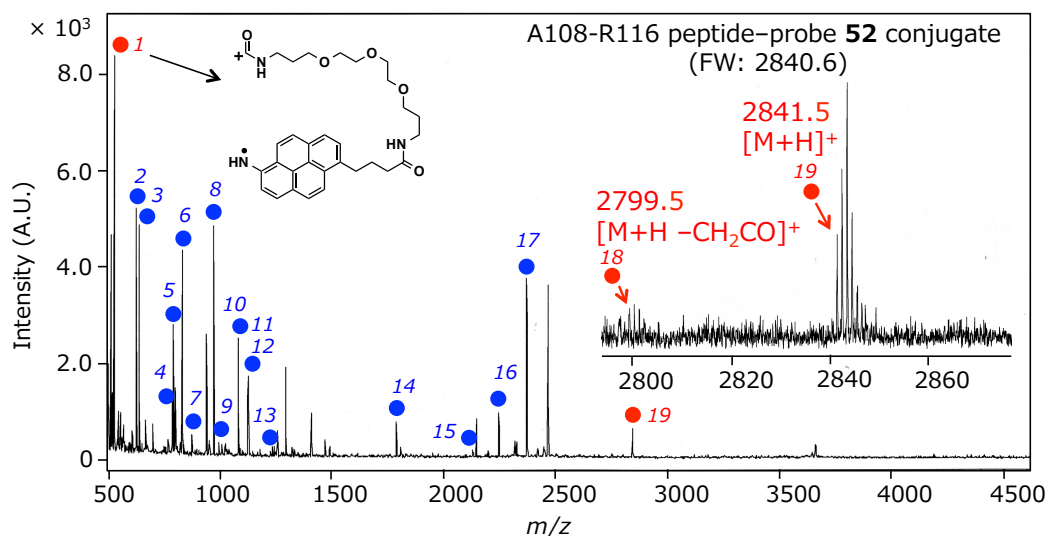
Figure 3-25. LA-LDI MS analysis of the digested peptides of actin labeled with probe **52** at 200 pmol. Blue circles indicate unlabeled actin peptides. Red circles indicate the compound possessing an amidopyrene moiety. Numerals of the peptide peaks correspond to the data in Table 3-3.

Table 3-3. LA-LDI MS analysis of the digested peptides of actin labeled with probe **52**.

No.	m/z (obs.)[a]	m/z (calc.)[b]	Position of actin	Peptide sequence	No.	m/z (obs.)[a]	m/z (calc.)[b]	Position of actin	Peptide sequence
1	531.2[c]				11	1128.6	1128.6	160 - 169	GVTHNVPIYE
2	631.3	631.4	194 - 198	ILTER			1128.6	170 - 179	GYALPHAIMR
3	644.3	644.4	180 - 185	LDLAGR	12	1130.5	1130.5	198 - 207	RGYSFVTTAE
			65 - 70	GILTLK			1130.5	199 - 208	GYSFVTTAER
4	791.3	791.4	287 - 292	CDIDIR[d]	13	1246.5	1246.6	87 - 95	IWHHTFYNE
5	795.4	795.5	331 - 337	IIAPPER	14	1790.9	1790.9	241 - 256	SYELPDGQVITIGNER
6	836.4	836.5	367 - 374	AGPSIVHR	15	2130.9	2131.0	295 - 314	LYANNVMSGGTTMYPGIADR
7	880.2	880.5	329 - 336	IKIIAPPE	16	2245.9	2246.0	294 - 314	DLYANNVMSGGTTMYPGIADR
8	976.4	976.4	21 - 30	AGFAGDDAPR	17	2371.2	2371.2	128 - 149	TFNVPAMYVAIQAVLSLYASGR
9	998.4	998.5	186 - 193	DLTDYLMK	18	2799.5	2799.6	108 - 116	APLNP**K**ANR[e] + probe **52** − CH₂CO
10	1086.6	1086.6	247 - 256	GQVITIGNER	19	2841.5	2841.6	108 - 116	APLNP**K**ANR[e] + probe **52**

(a) Observed mass numbers of the peaks in Figure 3-25 as H$^+$ adducts. (b) Calculated mass numbers of peptides as H$^+$ adducts. (c) The fragment ion cleaved at the C−C bond of Lys carbonyl α position from parent ion (No. 18 and 19). (d) "*C*" means a carbamidomethylated cysteine residue. (e) "**K**" means amidopyrene-labeled lysine residue.

In contrast to LA-LDI MS, MALDI MS of an amidopyrene-labeled actin peptide showed a base peak at *m/z* 2841.6 on MALDI MS (Figure 3-26, No. 14). This result indicated that the quantitative labeling of actin with probe **52**, which was shown in Fig. 3-23b, occurred at the A108−R116 peptide on actin. Additionally, a partially digested labeled peptide (No. 15) was also detected at *m/z* 4158.2, which includes the same sequence as the peptide (No. 14), along with unlabeled actin peptides (No. 1-13). In MALDI MS, the fragment ion at *m/z* 531.3 observed by LA-LDI MS was not detected. Therefore, in the case of LA-LDI MS analysis, the lower detectability of amidopyrene-labeled actin peptide than those of unlabeled peptides was explained by the fragmentation at the C−C bond of Lys carbonyl α position.
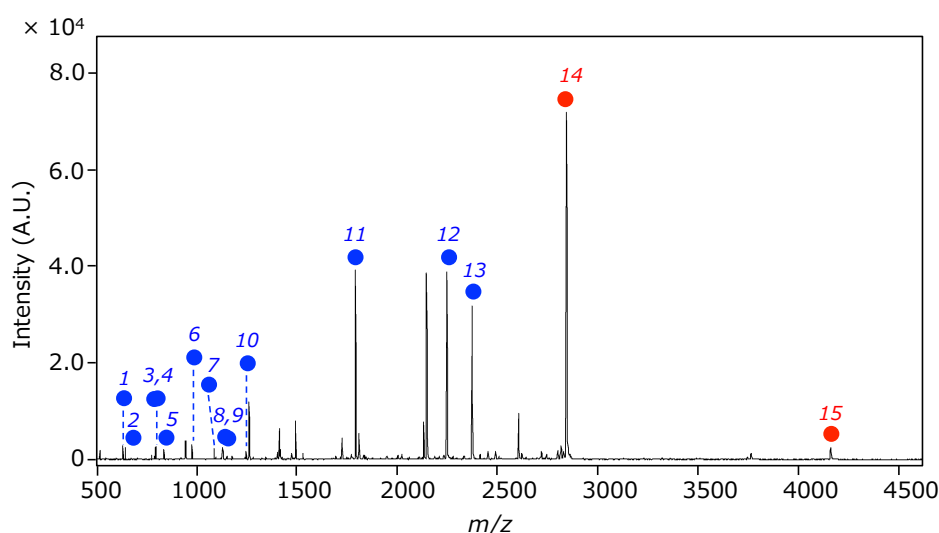

Figure 3-26. MALDI MS of the digested peptides of the labeled actin with probe **52**. Blue circles indicate unlabeled actin peptides. Red circles indicate the compound possessing an amidopyrene moiety. Numerals of the peptide peaks correspond to the data in Table 3-4.

Table 3-4. MALDI MS analysis of the digested peptides of actin labeled with probe **52**.

No.[a]	*m/z* (obs.)[b]	*m/z* (calc.)[c]	Position of actin	Peptide sequence	No.[a]	*m/z* (obs.)[b]	*m/z* (calc.)[c]	Position of actin	Peptide sequence
<u>1</u>	631.3	631.4	194 - 198	ILTER	<u>9</u>	1130.5	1130.5	198 - 207	RGYSFVTTAE
<u>2</u>	644.3	644.4	180 - 185	LDLAGR			1130.5	199 - 208	GYSFVTTAER
		644.4	65 - 70	GILTLK	10	1246.5	1246.6	87 - 95	TLFQPSFIGME
3	791.3	791.4	287 - 292	CDIDIR[d]	<u>11</u>	1790.9	1790.9	241 - 256	SYELPDGQVITIGNER
<u>4</u>	795.4	795.5	331 - 337	IIAPPER	12	2246.0	2246.0	294 - 314	DLYANNVMSGGTTMYPGIADR
<u>5</u>	836.4	836.5	367 - 374	AGPSIVHR	13	2371.2	2371.2	128 - 149	TFNVPAMYVAIQAVLSLYASGR
<u>6</u>	976.4	976.4	21 - 30	AGFAGDDAPR	14	2841.6	2841.6	108 - 116	APLNP**K**ANR[f] + probe **52**
<u>7</u>	1086.5	1086.6	247 - 256	GQVITIGNER[e]	15	4159.2	4159.3	96 - 116	VAPEEHPTLLTEAPLNP**K**ANR[f] + probe **52**
<u>8</u>	1128.6	1128.6	160 - 169	RGYSFVTTAE					
		1128.6	170 - 179	GYSFVTTAER					

(a) Numeral of the peak that appeared in Table 3-3 was underlined. (b) Observed mass numbers of the peaks in Figure 3-26 as H$^+$ adducts. (c) Calculated mass numbers of peptides as H$^+$ adducts. (d) "*C*" means a carbamidomethylated cysteine residue. (e) "**K**" means probe-labeled lysine residue.

Furthermore, the author anticipated that amidopyrene plays a role as the matrix to facilitate the ionization of unlabeled peptides since several unlabeled actin peptides were detected in the presence of amidopyrene probe on LA-LDI MS (Fig. 3-25). To confirm this, actin alone was digested by the mixture of trypsin and Glu-C and analyzed by LA-LDI MS (Figure 3-27, Table 3-5).
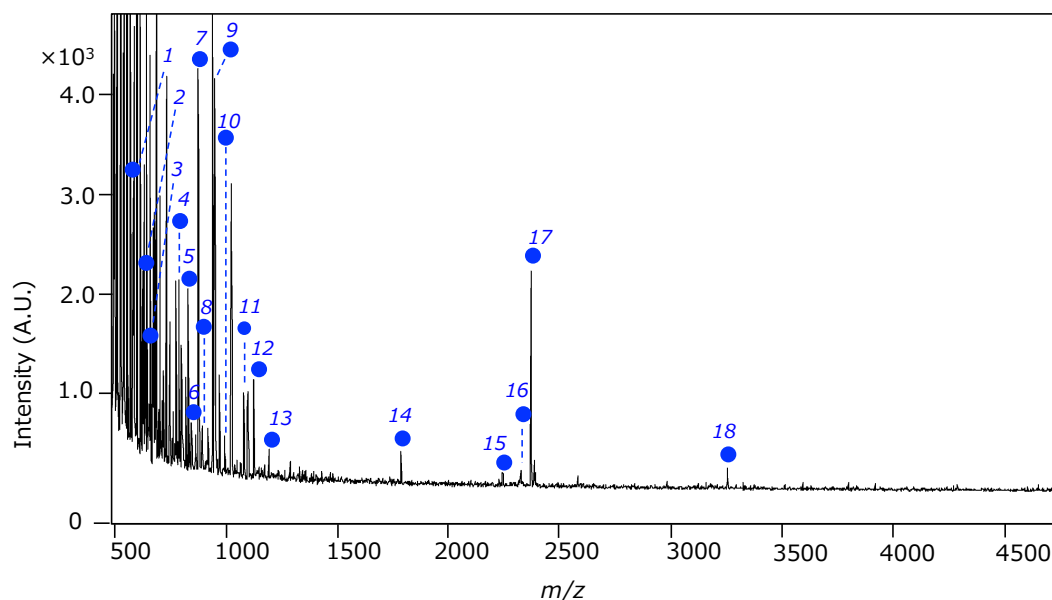

Figure 3-27. LA-LDI MS of the digested peptides of unlabeled actin (20 pmol). Blue circles indicate unlabeled actin peptides. Numerals of the peptide peaks correspond to the data in Table 3-5.

Table 3-5. LA-LDI MS analysis of digested peptides of unlabeled actin.

No.[a]	m/z (obs.)[b]	m/z (calc.)[c]	Position of actin	Peptide sequence[d]	No.[a]	m/z (obs.)[b]	m/z (calc.)[c]	Position of actin	Peptide sequence[d]
1	589.4	589.3	60 - 64	AQSKR	10	976.4	976.4	21 - 30	AG**F**AGDDAPR
2	631.4	631.4	194 - 198	ILTER	11	1086.6	1086.6	247 - 256	GQVITIGNER
3	644.4	644.4	180 - 185	LDLAGR	12	1130.5	1130.5	198 - 207	RG**YSF**VTTAE
		644.4	65 - 70	GILTLK			1130.5	199 - 208	G**YSF**VTTAER
4	795.4	795.5	331 - 337	IIAPPER	13	1198.7	1198.6	229 - 240	mATAASSSSLEK[f]
5	836.4	836.5	367 - 374	AGPSIVHR			1198.7	31 - 41	AV**F**PSIVGRPR
6	851.2	851.4	6 - 13	ETTALV**C**D[e]	14	1790.9	1790.9	241 - 256	S**Y**ELPDGQVITIGNER
7	880.2	880.6	329 - 336	IKIIAPPE	15	2246.0	2246.0	294 - 314	DL**Y**ANNVMSGGTTM**Y**PGIADR
8	899.5	899.4	121 - 127	MTQIMFE	16	2371.2	2371.2	128 - 149	T**F**NVPAMYVAIQAVLSL**Y**ASGR
		899.5	187 - 193	LTD**Y**LMK	17	2387.2	2387.2	128 - 149	T**F**NVPAm**Y**VAIQAVLSL**Y**ASGR[f]
9	955.2	955.5	75 - 82	HGIITN**W**D	18	3251.5	3251.6	121 - 149	MTQIMFET**F**NVPAM**Y**VAIQAVLSL**Y**ASGR

(a) Numeral of the peak that appeared in Table 3-3 was shown with underline. (b) Observed mass numbers of the peaks in Figure 3-27 as H^{+} adducts. (c) Calculated mass numbers of peptides as H^{+} adducts. (d) "**F**", "**Y**" and "**W**" means aromatic amino acid (e) "*C*" means a carbamidomethylated cysteine residue. (e) "**K**" means probe-labeled lysine residue. (f) "m" means oxidated methionine.

As a result, a number of peaks of actin peptides were detected by LA-LDI MS. Most of them corresponded to the peaks of unlabeled actin peptides as observed in Fig. 3-25. Furthermore, peptides (No. 8-10, 12-18) included aromatic amino acids. So, it was suggested that unlabeled peptides with aromatic amino acids were directly excited by 355 nm laser on LA-LDI MS. When the amount of actin is small (1 pmol), the peaks of unlabeled peptides were not clearly observed. Therefore, in order to selectively detect the peptides labeled with amidopyrene probe, it is necessary for amidopyrene-labeled peptides to be detected at pico-mol amount.

To ensure whether the detected peak at m/z 2841.5 on LA-LDI and MALDI MS (Figure 3-25, 3-26) was a labeled peptide with probe **52**, the digested peptide mixture of actin reacted with **52** was analyzed by HPLC based on the fluorescence of amidopyrene group (λ_{ex} 337 nm, λ_{em} 409 nm) (Figure 3-28). The major fluorescent peak was detected at 23.5 min, while a number of actin peptide peaks were observed by UV detection. Additionally, when the peak (23.5 min) was collected and analyzed by MALDI-TOF MS, the desired peak at m/z 2841.7 was observed as an almost single component (Figure 3-29). These results indicated that actin quantitatively labeled with probe **52** at the specific site, and this result was corresponded to LALDI or MALDI MS analysis, in which an amidopyrene-labeled peptide was observed as an almost single component.
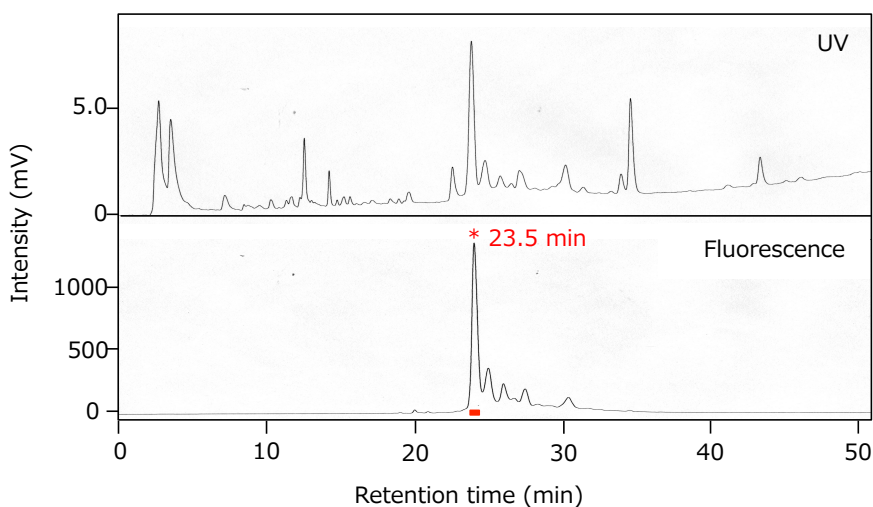

Figure 3-28. HPLC analysis of the digested peptides of actin labeled with probe **52**. Column: Develosil RP-Aqueous AR-5 (1.5 mm I.D. × 150 mm), buffer: a linear gradient of 10% to 100% aq. MeCN containing 0.05 % TFA for 60 min, temperature: 25 °C, flow rate: 100 μL/min, detection: UV 254 nm (top), fluorescence λ_{ex} 337 nm and λ_{em} 409 nm (bottom). Collected area is shown in red.
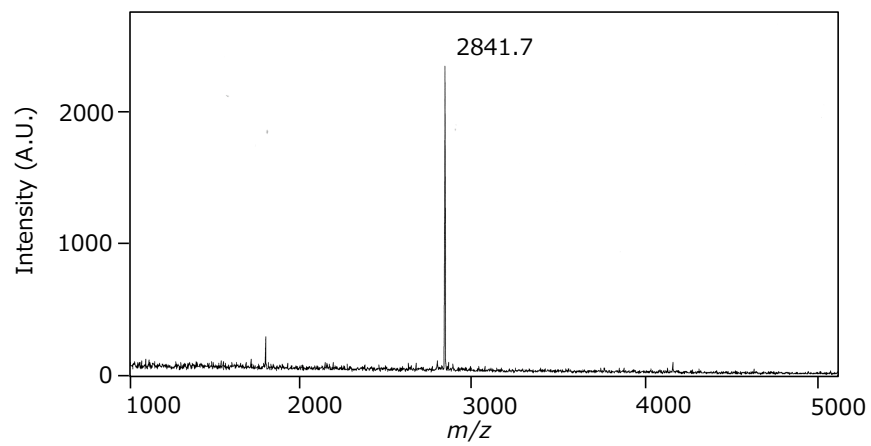
Figure 3-29. MALDI MS of the purified peptide labeled with probe **52** (retention time: 23.5 min in Fig. 3-28).

Additionally, MALDI MS/MS analysis of the purified peptide (precursor ion: *m/z* 2841.7) showed several b and y fragment ions (Figure 3-30), suggesting that this fragment was the A108-R116 peptide of actin that was labeled with **52**. However, there were some uncharacterizable peaks on MALDI MS/MS analysis. They might be the fragment ions generated by the cleavage of the internal probe structure.
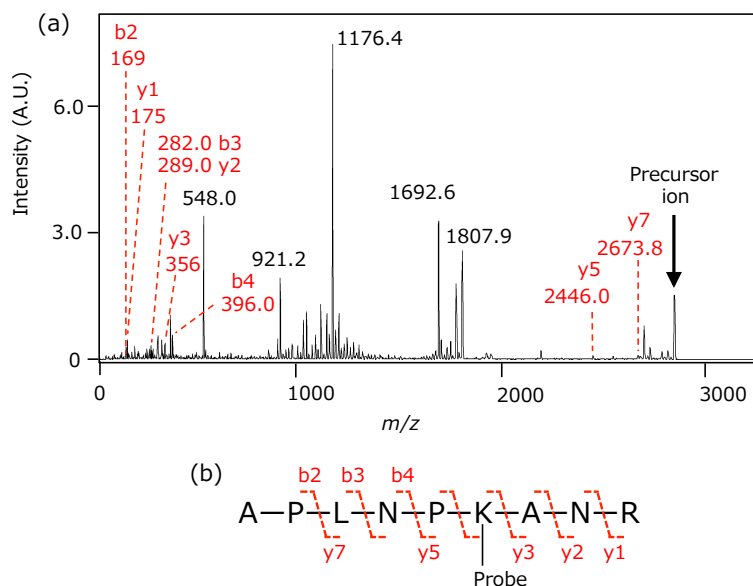

Figure 3-30. MALDI-TOF MS/MS of the labeled nonapeptide with probe **52** (precursor ion: *m/z* 2841.7 [M+H]$^+$). (a) MALDI MS/MS analysis. Red numbers correspond to the b or y fragment ion peaks. Black numbers are the peaks not to be determined. (b) Structure of the probe-labeled peptide (*m/z* 2841.6 for [M+H]$^+$).

Finally, position of the A108−R116 peptide established by the LA-LDI MS analysis was considered in the X-ray crystal structure of actin−ApA complex (Figure 3-31a). Additionally, conformational search of probe **52** on actin was performed (Figure 3-31b).
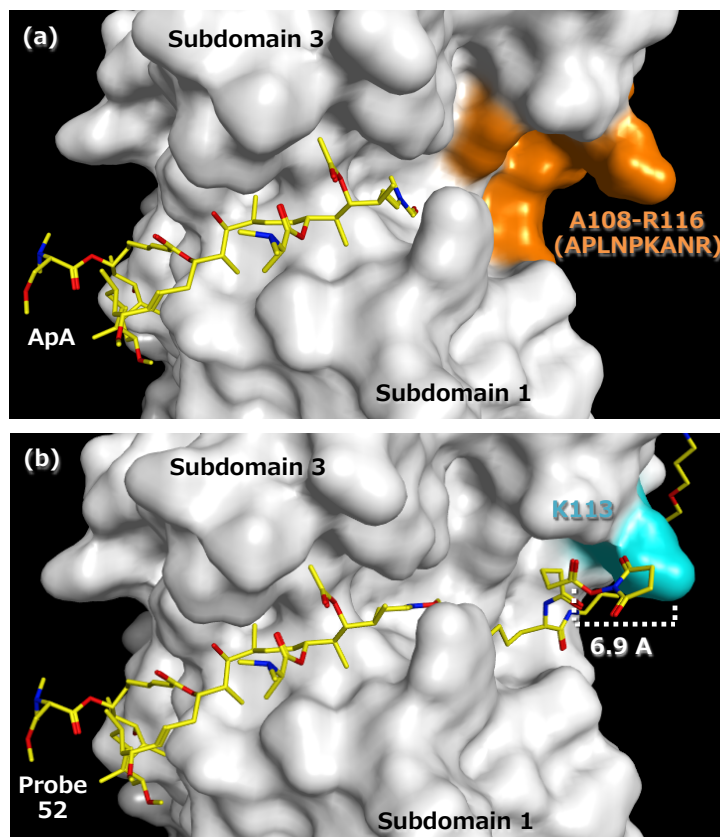

Figure 3-31. Structures of an actin−ApA complex and an actin−probe **52** complex. (a) X-ray crystal structure of actin−ApA complex (1WUA), A108−R116 peptide is indicated in orange. (b) The most stable conformation of the probe **52** on actin, which was calculated by MOE software. The initial structure of the actin−probe **52** complex was constructed by replacing the C24-C34 side-chain part of ApA in (a). Conformational search of probe **52** was performed using the Amber12-EHT force-field, in which both actin and the ApA moiety (C1-C34) of **52** were fixed. The lysine residue (K113) is indicated in cyan.

In the case of actin-ApA complex (Figure 3-31a), A108−R116 peptide is located behind the hydrophobic cleft interacting with the side-chain of ApA. Additionally, as shown in Figure 3-31b, the conformation of probe **52** on actin was the most stable when the linker part of **52** faced to the position of A108−R116 peptide. In this case, the NHS ester moiety of **52** got close to the ε−amino group of K113 at 6.9 Å. Therefore, it is reasonable that K113 was specifically labeled with probe **52** as shown in the MALDI MS/MS analysis (Fig. 3-30). Also, the binding mode analysis of target protein−ligand complex was successfully demonstrated by the proposed method shown in Scheme 3-2.

3-4. Summary

To analyze the binding mode of the protein-ligand interaction readily, novel chemical probes were developed. These probes were designed to hold pyrene or amidopyrene group in order that digested peptides of the probe‑protein complex are selectively detected by LA-LDI MS. The author synthesized two photoaffinity probes, ApA-PP (**21**) and ApA-PaP (**40**), and analyzed their interactions with actin. However, ApA-PP (**21**) did not inhibit actin-polymerization. ApA-PaP (**40**) showed similar activity as ApA, but hardly photolabeled actin since it might react with water molecules.

ApA NHS ester probe **52** was next synthesized, which was expected to preferentially react with the lysine residue of actin than water. In contrast to ApA-PaP (**40**), actin was quantitatively labeled with probe **52**. When the peptide mixture was analyzed by LA-LDI MS, which was prepared by the digestion of the probe **52**−actin complex with trypsin and Glu-C, the A108−R116 peptide labeled with **52** was detected as an almost single labeled peptide. The probe-binding position, A108−R116 peptide, was close to the ApA-binding site of actin. Therefore, the author succeeded to confirm the binding position of ApA on actin by LA-LDI MS analysis.

On the other hand, the fragment ion peak (*m/z* 531), which was cleaved at the Lys C−C bond of carbonyl α position of probe **52**, was observed as a base peak by LA-LDI MS (Fig. 3-25). This fragmentation led to the decrease of detectability of amidopyrene-labeled peptide. Thus, much amount of peptide mixture (200 pmol) was required for LA-LDI MS. In these conditions, several unlabeled peptides including aromatic amino acids were also directly excited by UV laser and detected by LA-LDI MS. To solve the problem that unlabeled peptides were non-selectively detected, the detectability of labeled peptides should be increased. Because unlabeled peptides were not detected at 1 pmol, selective detection of labeled peptides would be possible by optimizing an amidopyrene probe structure and increasing the detectability of amidopyrene-labeled compounds up to pico-mol order.

For the future study, the author has two ideas as follows: (1) to change detecting groups more suitable for LA-LDI MS than amidopyrene group, and (2) to design a new probe possessing the linker structure where the fragmentation does not occur by LA-LDI MS.

In the case of (1), functionalized amidopyrene group will be tried (Figure 3-32). On this idea, the author controls an electronic state and an UV absorbance by the introduction of electron withdrawing or electron donating group, such as nitro and amino groups. Since the detection of LA-LDI MS depends on the photoexcitation of compounds, its detectability would be increased by modifying the absorbance intensity of UV laser (355 nm).

R = **NO₂** or **NH₂** etc.

Functionalized amidopyrene group

Figure 3-32. Idea of new detecting groups

In the case of (2), the development of ligand-dissociated-type probe[17] will be tried. In the case of ligand-dissociated-type probe, the LA-LDI tag, such as amidopyrene group, is connected to a ligand via a reacting group (Figure 3-33).

When the target protein is labeled with a ligand-dissociated-type probe, ligand and linker moieties are dissociated, and only amidopyrene moiety would remain on the target protein. So, the labeled peptide is expected to be effectively detected by LA-LDI MS without the fragmentation at the linker moieties.
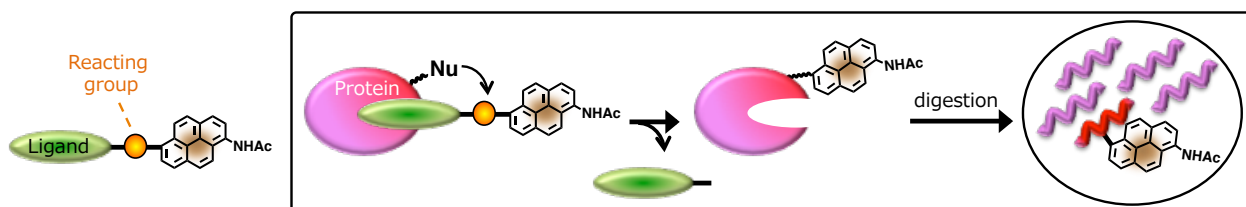

Figure 3-33. Preparation of the labeled peptide with a ligand-dissociated-type probe

This LA-LDI tag method can be applied for various ligands as well as ApA, and seems to be more convenient than current chemical probe methods due to the omission of purification process. So, a useful method for the binding mode analysis would be established by the optimization of amidopyrene probe structure to improve the detectability.

3-5. Experimental

3-5-1. General

NMR spectra were recorded on a Bruker Biospin AVANCE 600 spectrometer (600 MHz for ^{1}H and 150 MHz for ^{13}C) or a Bruker Biospin AVANCE 400 spectrometer (400 MHz for ^{1}H and 100 MHz for ^{13}C). Chemical shifts are reported in parts per million (ppm) with coupling constants (J) in hertz relative to the solvent peaks, δ_H 3.31 (residual CHD$_2$OD), δ_H 7.26 (residual CHCl$_3$) and δ_C 77.16 for CDCl$_3$, δ_H 2.50 (residual CHD$_2$S(O)CD$_3$) and δ_C 39.52 for (CD$_3$)$_2$S=O, respectively. For the quantification of minute amounts of specimens by ^{1}H NMR analyses, benzene (5-10 mM in CD$_3$OD) was added to the sample solutions as a standard (1:60, v/v). Optical rotations were measured with a JASCO DIP-1000 polarimeter. IR spectra were recorded on a JASCO FT/IR-230 spectrometer. UV–Vis absorption spectra were measured on a JASCO V-560 spectrometer with MeOH as a solvent. Fluorescence spectra were measured on a Hitachi F-4500 spectrofluorophotometer with acetonitrile or MeOH as solvents. High-resolution electrospray ionization mass spectra (HR-ESIMS) were measured on an AccuTOF CS spectrometer (JEOL). Fuji Silysia silica gels BW-820MH and FL60D were used for column chromatography.

Chemicals and solvents were the best grade available and were used as purchased with following experiment. Synthetic and biological experiment using aryl diazirine or pyrene deriveatives were conducted with light-shaded glass or plastic tube under a yellow-filtered light hood.

In the case of the synthesis of aplyronine analogs, desalting was conducted by freeze-dry after HPLC purification.

3-5-2. Cell-culture and Immunofluorescence Staining

Culture of HeLa S3 cells and immunofluorescence staining were conducted as shown in chapter 2.

3-5-3. LDI-MS Analysis

Matrix-assisted laser desorption/ionization with time-of-flight mass spectrometry (MALDI-TOF MS) and its tandem MS analyses were performed using a Bruker UltrafleXtreme spectrometer, equipped with a 355 nm Nd:YAG laser, with α-cyano-4-hydroxycinnamic acid or sinapinic acid as a matrix. Label-assisted laser desorption/ionization mass spectrometry (LA-LDI MS) and its tandem MS analyses were performed using the same apparatus as with MALDI-TOF MS. Samples dissolved in 50% aq. MeOH or MeCN/0.1-1% TFA were spotted to an MTP384 ground steel target plate and air-dried according to the manufacturer's instructions. In the case that peptides were measured, the samples were air-dried and washed with water before measurement.

3-5-4. *In vitro* Actin-polymerization Inhibitory Assay

The actin-polymerization inhibitory activities were measured based on F-actin sedimentation (centrifugation method). Samples were added to a solution of rabbit muscle actin (3 µM, cytoskeleton) in G-buffer (100 µL). The mixture was stirred at 25 °C for 30 min and then 0.15 M $MgCl_2$ (0.8 µL) were added, and stirred at 25 °C for 40 min. After ultracentrifugation (150,000 ×*g*, 22 °C, 1 h), The supernatants (lyophilized) and the precipitates were dissolved in 1×SDS buffer (100 µL, Sigma) and boiled at 95 °C for 5 min. SDS-PAGE was performed by using a precast polyacrylamide gel (ATTO, 10%), and the gels were stained with a Quick-CBB kit (Wako).

3-5-5. Labeling Experiments of Actin with Apy-Su (**47**) and Triptic Digestion

The lyophilized actin poder (purchased) contained Tris-HCl as the components of G-buffer. To remove this, 232 µM G-actin (10 µL, 2.3 nmol) in actin buffer was diluted to 500 µL with labeling solution 1 (50 mM NH_4HCO_3, 0.2 mM $CaCl_2$, 0.5 mM 2-mercaptoethanol), and concentrated to 50 µL by ultrafiltration (14,000 ×*g*, 4 °C, 15 min) using a centrifuge tube filter (UFC501096, Millipore). This buffer exchange was conducted additional three times. The solution was diluted by labeling solution 1 to 350 µL, and was mixed with 5 mM Apy-Su (**47**) in DMSO (23 µL). After incubation at room temperature for 17.5 h with a rotater, the solution was exchanged with 50 mM NH_4HCO_3 three times by ultrafiltration to remove unreacted Apy-Su (**47**), and concentrated to 50 µL by ultrafiltration. To the resulting solution was added 45 mM DTT in 25 mM NH_4HCO_3 aq (1.5 µL), and the solution was incubated at 56 °C for 15 min. And then, the solution was reacted with 100 mM iodacetamide in 25 mM NH_4HCO_3 aq 1.5 µL by shaking for 15 min, and a sequence-grade, modified trypsin (100 ng/µL, 4.3 µL, #V5111, Promega) was added, and the resulting mixture was incubated at 37 °C for 20.5 h. After the addition of 10% TFA aq (3 µL), the solution was concentrated *in vacuo*. After dissolving in 50% MeCN containing 0.05% TFA, the mixture was analyzed by LA-LDI MS and MALDI MS.

3-5-6. Labeling Experiments of Actin with Aplyronine Deriveatives

In the case of photolabeling, 5 mM ApA–PaP (**21**) in DMSO (0.5 μL, 2.5 nmol) was mixted with 116 μM G-actin (1.72 μL, 200 pmol) and G-buffer 22 μL in 0.6 mL tubes. After incubation with a rotater at room temperature for 30 min, the solutions were cooled on ice and irradiated with UV light (365 nm) for 15 min, using a handheld UV lamp (0.8 mW/cm^2). The reaction solution was mixed with the saturated solution of the matrix sinapinic acid containing 50% MeCN and 0.1 % TFA in 1:1 ratio, and the solution (1.0 μL) directly spotted to an ground steel plate, and MALDI-TOF MS was measured.

In the case of probe **52**, 232 μM G-actin (43 μL, 10 nmol) in actin buffer was diluted to 500 μL with labeling solution 2 (2 mM NaHCO$_3$, 0.2 mM CaCl$_2$ aq.) and concentrated to 50 μL by ultrafiltration (14,000 ×g, 4 °C, 15 min) using a centrifuge tube filter. This buffer exchange was conducted additional three times. Resulting solution was diluted to 500 μL with labeling solution 2 and the diluted solution was mixed with 2 mM probe **52** (17.5 μL, 35 nmol). After incubation with a rotater at 4 °C for 3 h, 50 mM Tris·HCl (20 μL, pH8.0) was added to the reaction mixture to mask unreacted NHS ester moiety. The 1 μL of the solution was analyzed by MALDI-TOF MS by mixing with saturated sinapinic acid aqueous solution (1 μL). For the competition experimentes, 10 mM ApA (1 μL, 10 nmol) was added simultaneously with 2 mM probe **52** (1 μL, 2 nmol) to 21 μM actin (48 μL, 1 nmol) in labeling solution 2. For SDS-PAGE analysis, labeled actin sample (5 μL) was mixed with water (5 μL) and dissolved in 2×SDS buffer (10 μL, Sigma), and boiled at 95 °C for 5 min. SDS-PAGE was performed by using a 10% precast polyacrylamide gel (ATTO), and the gels were stained with a Quick-CBB kit (Wako).

3-5-7. Enzymatic Digestion of Actin−probe **52** Complex and MS Analysis

The actin−probe **52** complex (ca. 10 nmol, 500 μL), which was prepared as session 3-5-6, or actin in labeling solution 2 was concentrated to 50 μL by ultrafiltration (14,000 ×g, 4 °C, 15 min) using a centrifuge tube filter. Then, the solution was dilluted to 500 μL with 25 mM NH$_4$HCO$_3$ aq., and this exchange of solution was conducted additional three times. After concentration to 100 μL by ultrafiltration, 100 mM DTT in 25 mM NH$_4$HCO$_3$ aq. (5 μL) was added and incubated at 56 °C for 20 min. The solution was reacted with 100 mM iodeacetamide in 25 mM NH$_4$HCO$_3$ aq. (5 μL) by shaking at room temperature for 20 min, followed by incubation with a mixture of sequence-grade, modified trypsin (100 ng/μL, 100 μL) and Glu-C (100 ng/μL, 100 μL, #V1651, Promega) at 37 °C for 15.5 h. After the addition of 10% TFA (20 μL), the solution was freeze-dried. After dissolving in 0.1% TFA, 50% MeCN, the 1/50 amount of the mixture was directly analyzed by LA-LDI MS. To purify labeled peptides, samples were loaded on a Develosil RP-Aqueous AR-5 semi-micro HPLC column (1.5 mm I.D. × 150 mm) at 25 °C. A linear gradient of 10% to 100% aq. MeCN for 60 min containing 0.05 % TFA was applied at a flow rate of 100 μL/min, with monitoring at fluorescence (λ_{ex} 337 nm and λ_{em} 409 nm) to give a labeled peptide (t_R = 23.5 min, m/z 2842), which was analyzed by MALDI-TOF MS analysis.

3-5-8. Quantification Based on Fluorescence Intensity

In the case of photoreaction of pyrene derivatives, the yield was calculated by comparison of the fluorescence intensity of model MeOH-adduct **55** (Figure 3-34). Model MeOH-adduct **55** was synthesized as shown in Scheme 3-12.
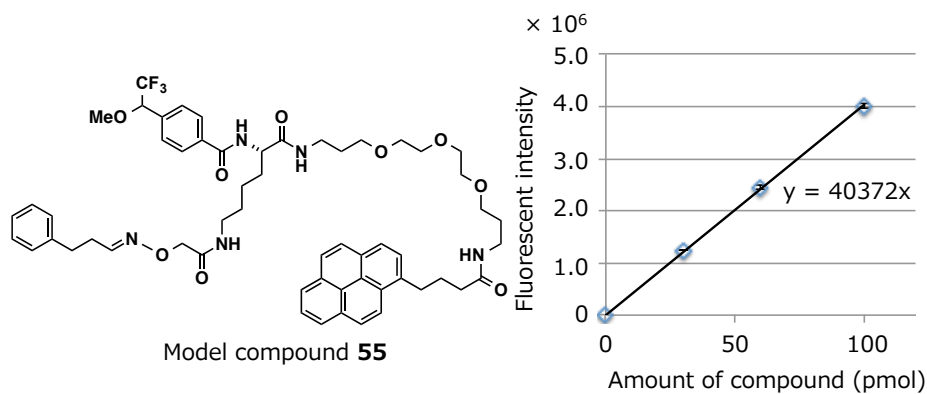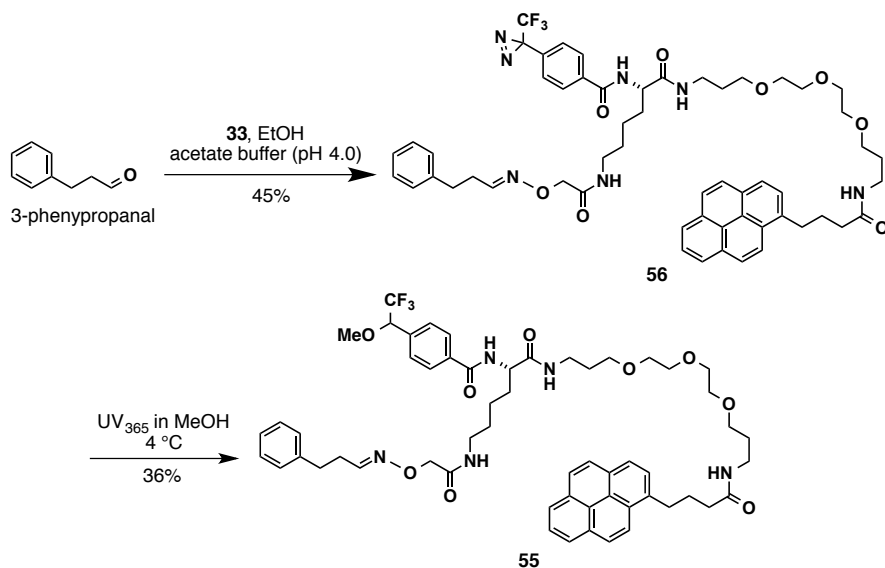

Figure 3-34. Structure of model MeOH-adduct **55** and its standard curve based on fluorescence intensity. Values are the means ± SD of independent experiments (n = 3).

Scheme 3-12. Synthesis of model MeOH-adduct **55**.

In the case of photoreaction of amidopyrene derivatives, the yield was calculated by comparison of the fluorescence intensity of model MeOH-adduct **57** (Figure 3-35). This fluorescence standard curve was drawn up by co-worker. Model MeOH-adduct **57** was synthesized as shown in Scheme 3-13.
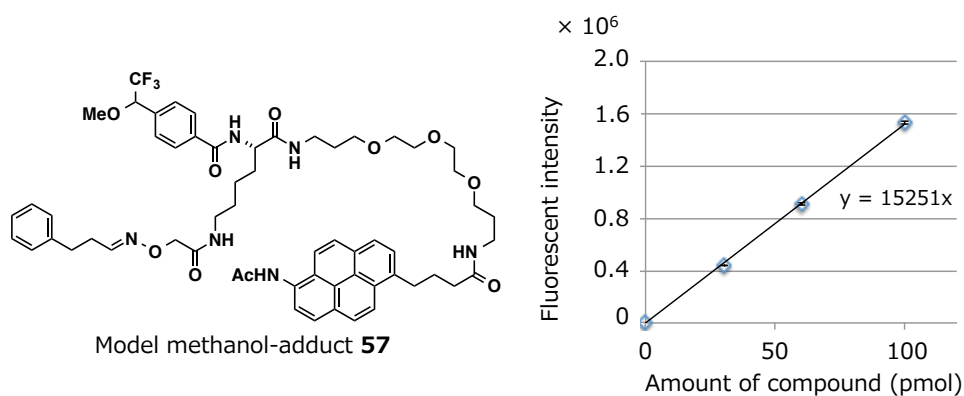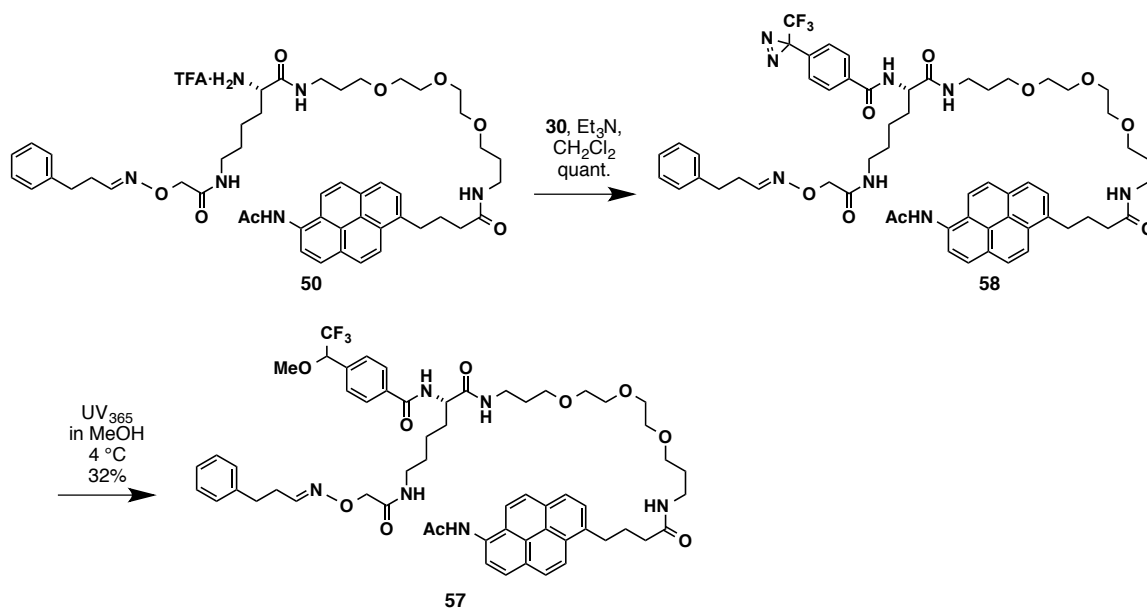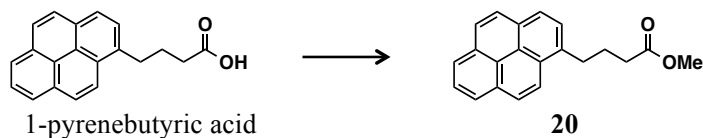

Figure 3-35. Model MeOH-adduct **57** and its standard curve based on fluorescence intensity. Values are the means ±SD of independent experiments (n = 3).


Scheme 3-13. Synthesis of model MeOH-adduct **57**.

Methyl 4-(1-pyrenyl)butyrate (**20**)

1-pyrenebutyric acid   **20**

To a stirred solution of 1-pyrenebutyric acid (102 mg, 0.356 mmol) in dry CH_2Cl_2 (2 mL) were added thionyl chloride (0.20 mL, 2.8 mmol) and MeOH (1.0 mL, 25 mmol) dropwise at −8 °C. After being stirred at room temperature for 1.5 h, the reaction mixture was concentrated *in vacuo*. The crude material was purified with a SiO_2 column (3.0 g, $CHCl_3$/acetone = 1/0 to 0/1) to give methyl ester **20** (105 mg, 98%) as light yellow solid needles. Compound **20**: R_f = 0.55 ($CHCl_3$); mp. 46.8–47.1 °C; ^{1}H NMR (400 MHz, $CDCl_3$) δ 8.31 (d, J = 9.3 Hz, 1H), 8.18 (dd, J = 7.6, 1.1 Hz, 1H), 8.17 (dd, J = 7.6, 1.1 Hz, 1H), 8.12 (d, J = 9.3 Hz, 1H), 8.11 (d, J = 7.8 Hz, 1H), 8.04 (d, J = 9.2 Hz, 1H), 8.03 (d, J = 9.2 Hz, 1H), 8.00 (t, J = 7.6 Hz, 1H), 7.86 (d, J = 7.8 Hz, 1H), 3.71 (s, 3H), 3.40 (t, J = 7.7 Hz, 2H), 2.48 (t, J = 7.3 Hz, 2H), 2.21 (tt, J = 7.7, 7.3 Hz, 2H); ^{13}C NMR (100 MHz, $CDCl_3$) δ 174.1, 135.8, 131.6, 131.0, 130.1, 128.9, 127.6, 127.5, 127.4, 126.8, 126.0, 125.2, 125.1, 125.0, 124.9, 124.9, 123.4, 51.7, 33.8, 32.9, 26.9; IR ($CHCl_3$) 3043, 3011, 2952, 1731, 1604, 1588, 1509, 848 cm^{-1}; HRMS (ESI) *m/z* 325.1209 (calcd for $C_{21}H_{18}NaO_2$ [M+Na]$^+$, Δ +0.5 mmu).

1-pyrenebutyric acid   **23**   **25**
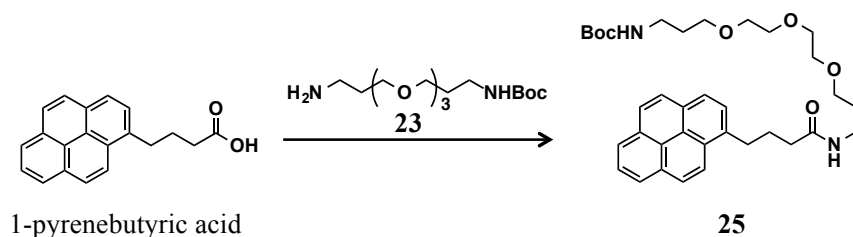
To a solution of 1-pyrenebutylic acid (29.2 mg, 101 μmol) in dry CH_2Cl_2 (2 mL) were added HOBt (21.2 mg, 157 μmol), EDC·HCl (39.0 mg, 203 μmol), and a solution of amine **23**[7] (45.7 mg, 143 μmol) in dry CH_2Cl_2 (3 mL). After being stirred for 4 h, the reaction mixture was washed with sat. NH_4Cl aq. (2 mL × 2) and brine (10 mL), dried with Na_2SO_4, and concentrated *in vacuo*. The crude material was purified with a SiO_2 column (1.5 g, $CHCl_3$/acetone = 1/0, 9/1 to 1/1) to give amide **25** (49.4 mg, 84%) as a yellow oil. Compound **25**: R_f = 0.46 ($CHCl_3$/acetone = 2/1); ^1H NMR (600 MHz, $CDCl_3$) δ 8.30 (d, J = 9.3 Hz, 1H), 8.16 (dd, J = 1.3, 7.5 Hz, 1H), 8.15 (dd, J = 1.3, 7.5 Hz, 1H), 8.10 (d, J = 9.3 Hz, 1H), 8.10 (d, J = 7.7 Hz, 1H), 8.02 (d, J = 9.0 Hz, 1H), 8.01 (d, J = 9.0 Hz, 1H), 7.98 (dd, J = 7.6, 7.6 Hz, 1H), 7.86 (d, J = 7.7 Hz, 1H), 6.24 (br s, 1H), 4.88 (br s, 1H), 3.56–3.48 (m, 6H), 3.44–3.34 (m, 10H), 3.15 (m, 2H), 2.27 (t, J = 7.2 Hz, 2H), 2.20 (tt, J = 7.2, 7.2 Hz, 2H), 1.76 (tt, J = 6.0, 6.0 Hz, 2H), 1.66 (tt, J = 6.2, 6.2 Hz, 2H), 1.48 (s, 9H); ^{13}C NMR (150 MHz, $CDCl_3$) δ 172.7, 156.1, 136.2, 131.5, 131.0, 130.0, 128.9, 127.6, 127.5, 127.4, 126.8, 126.0, 125.2, 125.1, 125.0, 124.9, 124.9, 123.6, 79.1, 70.5, 70.5, 70.3, 70.2, 70.2, 69.5, 38.6, 38.2, 36.2, 33.0, 29.7, 29.1, 28.6 (3C), 27.6; IR ($CHCl_3$) 3452, 3399, 3007, 2950, 2931, 2873, 1705, 1658, 1510, 1455, 848, 766 cm^{-1}; HRMS (ESI) *m/z* 613.3241 (calcd for $C_{35}H_{46}N_2NaO_6$ $[M+Na]^+$, Δ −0.7mmu).

1-pyrenebutyric acid   **24**   **26**
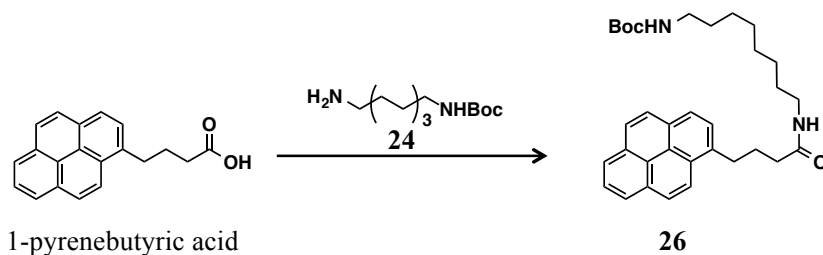
To a solution of 1-pyrenebutylic acid (50 mg, 0.17 mmol) in dry CH_2Cl_2 (5 mL) were added HOBt (35 mg, 0.26 mmol), EDC·HCl (66 mg, 0.35 mmol), and a solution of amine **24**[8] (62 mg, 0.26 mmol) in dry CH_2Cl_2 (3 mL). After being stirred for 9 h, the reaction mixture was washed with sat. NH_4Cl aq. (5 mL × 4) and brine (10 mL), dried with Na_2SO_4, and concentrated *in vacuo*. The crude material was purified with a SiO_2 column (2.2 g, $CHCl_3$/acetone = 9/1 to 1/1) to give amide **26** (67 mg, 76%) as a yellow oil. Compound **26**: R_f = 0.35 ($CHCl_3$/MeOH = 9/1); ^{1}H NMR (400 MHz, $CDCl_3$) δ 8.30 (d, J = 9.3 Hz, 1H), 8.16 (br d, J = 7.6 Hz, 1H), 8.16 (br d, J = 7.6 Hz, 1H), 8.10 (d, J = 9.3 Hz, 1H), 8.10 (d, J = 7.8 Hz, 1H), 8.02 (s, 2H), 7.99 (dd, J = 7.6, 7.6 Hz, 1H), 7.85 (d, J = 7.8 Hz, 1H), 5.40 (br t, J = 6.7 Hz, 1H), 4.48 (br t, J = 6.4 Hz, 1H), 3.38 (t, J = 7.1 Hz, 2H), 3.20 (td, J = 6.7, 6.7 Hz, 2H), 3.06 (td, J = 6.4, 6.4 Hz, 2H), 2.28−2.16 (m, 4H), 1.44 (s, 9H), 1.28−1.22 (m, 12H); ^{13}C NMR (100 MHz, $CDCl_3$) δ 172.7, 156.1, 136.0, 131.6, 131.0, 130.0, 129.0, 127.6, 127.5, 127.5, 126.8, 125.9, 125.2, 125.1, 125.0, 124.9 (2C), 123.5, 79.2, 40.7, 39.6, 36.2, 32.8, 30.0 29.6, 29.2 (2C), 28.5 (3C), 27.5, 26.9, 26.7; IR ($CHCl_3$) 3451, 3009, 2950, 2932, 2858, 1708, 1662, 1510, 1455, 848, 766 cm^{-1}; HRMS (ESI) *m/z* 537.3069 (calcd for $C_{33}H_{42}N_2NaO_3$ [M+Na]$^+$, Δ+1.9 mmu).

Lysine amide **28**
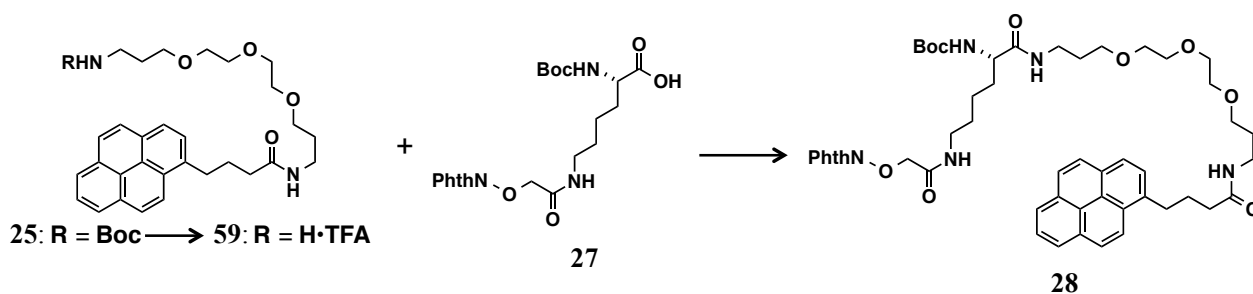
A solution of amide **25** (16.4 mg, 27.8 μmol) in a 1:1 mixture of dry CH_2Cl_2 and trifluoroacetic acid (1 mL) was stirred for 40 min at room temperature, and azeotropically concentrated with toluene *in vacuo* to give an amine TFA salt **59**.

To a solution of carboxylic acid **27**[9] (19.6 mg, 43.6 μmol), HOBt (6.5 mg, 48 μmol) and EDC·HCl (9.9 mg, 52 μmol) in dry CH_2Cl_2 (1 mL) were added a solution of the above amine TFA salt **59** in dry CH_2Cl_2 (3 mL) and *N,N*-diisopropylethylamine (DIPEA) (9.5 μL, 56 μmol). After being stirred for 6 h, DIPEA (9.5 μL, 56 μmol) was additionally added. After being stirred for 25 h, the reaction mixture was washed with sat. $NaHCO_3$ aq and brine, dried with Na_2SO_4, and concentrated. The crude material was purified with a SiO_2 column (0.7 g, $CHCl_3$/acetone = 9/1, 4/1, 2/1 to 0/1) to give amide **28** (20.7 mg, 81%) as a yellow oil. Compound **28**: R_f = 0.20 ($CHCl_3$/acetone = 2/1); $[\alpha]_D^{29}$ –0.13 (*c* 0.59, $CHCl_3$); ^{1}H NMR (400 MHz, $CDCl_3$) δ 8.29 (d, *J* = 9.3 Hz, 1H), 8.15 (d, *J* = 7.6 Hz, 1H), 8.14 (d, *J* = 7.6 Hz, 1H), 8.09 (d, *J* = 9.3 Hz, 1H), 8.09 (d, *J* = 7.8 Hz, 1H), 8.01 (d, *J* = 9.2 Hz, 1H), 7.99 (d, *J* = 9.2 Hz, 1H), 7.97 (dd, *J* = 7.6, 7.6 Hz, 1H), 7.86 (d, *J* = 7.8 Hz, 1H), 7.79 (dd, *J* = 3.1, 5.5 Hz, 2H), 7.70 (dd, *J* = 3.1, 5.5 Hz, 2H), 6.74 (br s, 1H), 6.37 (br s, 1H), 5.29 (br d, *J* = 7.4 Hz, 1H), 4.65 (s, 2H), 4.01 (br s, 1H), 3.55–3.51 (m, 6H), 3.50–3.20 (m, 15H), 2.29 (t, *J* = 7.2 Hz, 2H), 2.20 (tt, *J* = 7.2, 7.2 Hz, 2H), 1.82 (m, 2H), 1.77 (tt, *J* = 6.2, 6.2 Hz, 2H), 1.70 (tt, *J* = 6.1, 6.1 Hz, 2H), 1.58 (m, 2H), 1.41 (s, 9H), 1.39 (m, 2H); ^{13}C NMR (100 MHz, $CDCl_3$) δ 172.9, 172.1, 167.1, 163.8 (2C), 155.8, 136.2, 135.1 (2C), 131.5, 131.0, 130.0, 128.9, 128.5 (2C), 127.6, 127.5, 127.5, 126.8, 126.0, 125.2, 125.1, 125.0, 124.9, 124.9, 124.1 (2C), 123.6, 79.9, 77.4, 76.9, 70.5, 70.2, 70.0, 69.8, 69.7, 54.6, 38.9, 37.9, 36.2, 33.0, 32.4, 29.4, 29.2, 29.1, 29.0, 28.5 (3C), 27.7, 22.9; IR ($CHCl_3$) 3432, 3376, 3009, 2977, 2931, 2893, 1734, 1716, 1706, 1669, 1657, 1540, 1522, 1370, 848, 707 cm^{-1}; HRMS (ESI) *m/z* 944.4423 (calcd for $C_{51}H_{63}N_5NaO_{11}$ [M+Na]$^+$, Δ +0.7 mmu).
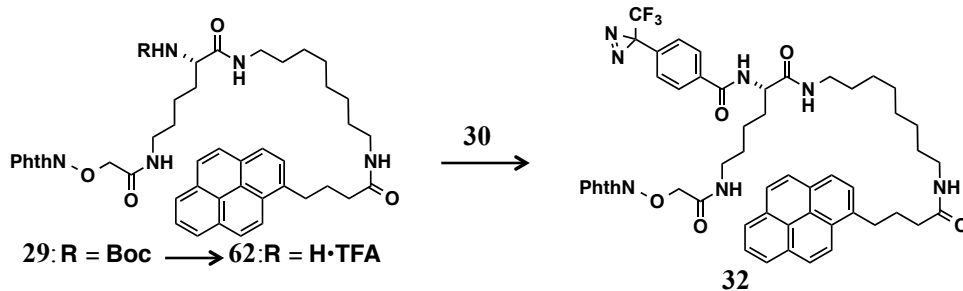
26: R = Boc ⟶ 60: R = H·TFA
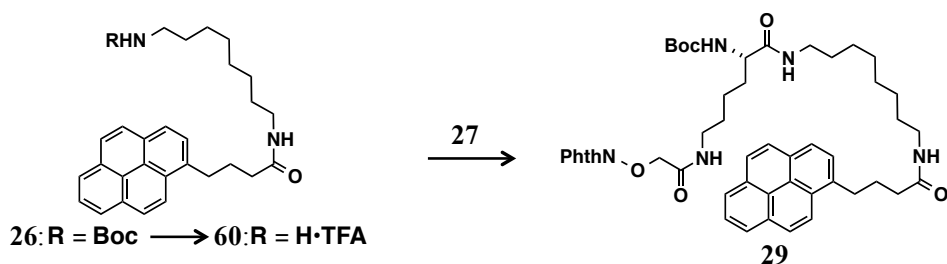
A solution of amide **26** (39.4 mg, 76.7 μmol) in a 1:1 mixture of dry CH$_2$Cl$_2$ and trifluoroacetic acid (1.0 mL) was stirred for 30 min at room temperature, and azeotropically concentrated with toluene *in vacuo* to give crude amine as a TFA salt **60**.

To a solution of carboxylic acid **27** (52.2 mg, 0.116 mmol), HOBt (20.3 mg, 0.150 mmol) and EDC·HCl (25.4 mg, 0.133 mmol) in dry CH$_2$Cl$_2$ (3 mL) were added a solution of the crude amine TFA salt **60** in dry CH$_2$Cl$_2$ (3 mL) and triethylamine (Et$_3$N, 50 μL, 0.36 mmol). After being stirred for 12 h, the reaction mixture was washed with sat. NaHCO$_3$ aq (5 mL × 3) and brine (10 mL), dried with Na$_2$SO$_4$, and concentrated. The crude material was purified with a SiO$_2$ column (2.1 g, CHCl$_3$/acetone) to give amide **29** (49.3 mg, 76%) as a yellow oil. Compound **29**: R_f = 0.56 (CHCl$_3$/MeOH = 5/1); ^{1}H NMR (400 MHz, CDCl$_3$) δ 8.28 (d, J = 9.2 Hz, 1H), 8.15 (br d, J = 7.6 Hz, 1H), 8.14 (br d, J = 7.6 Hz, 1H), 8.08 (d, J = 7.8 Hz, 1H), 8.08 (d, J = 9.2 Hz, 1H), 8.00 (s, 2H), 7.97 (dd, J = 7.6, 7.6 Hz, 1H), 7.84 (d, J = 7.8 Hz, 1H), 7.81–7.77 (m, 2H), 7.73−7.69 (m, 2H), 6.22 (br t, J = 5.5 Hz, 1H), 5.55 (br t, J = 5.3 Hz, 1H), 5.18 (br d, J = 6.3 Hz, 1H), 4.68 (s, 2H), 3.99 (m, 1H), 3.39–3.30 (m, 2H), 3.37 (t, J = 7.1 Hz, 2H), 3.21 (t, J = 6.8 Hz, 2H), 3.18 (td, J = 6.3, 5.3 Hz, 2H), 2.29−2.16 (m, 4H), 1.89−1.80 (m, 2H), 1.67–1.55 (m, 4H), 1.42 (s, 9H), 1.28−1.21 (m, 12H) . One proton signal (NH) was not detected; ^{13}C NMR (100 MHz, CDCl$_3$) δ 172.7, 172.0, 167.1, 163.8 (2C), 155.9 136.1, 135.2 (2C), 131.5, 131.0, 130.0, 128.9, 128.5 (2C), 127.6, 127.5 (2C), 126.8, 126.0, 125.2, 125.1, 125.0, 124.9 (2C), 124.1 (2C), 123.5, 80.1, 54.7, 39.6, 39.5, 38.7, 36.3, 32.9, 31.9, 29.8, 29.7, 29.5, 29.1, 29.1, 28.9, 28.4 (3C), 27.6, 26.8, 26.7, 22.8; IR (CHCl$_3$) 3438, 3370, 3009, 2932, 2858, 1735, 1708, 1667, 1545, 1519, 1369, 848, 706 cm^{-1}; HRMS (ESI) *m/z* 302.1307 (calcd for C$_{49}$H$_{59}$N$_5$NaO$_8$ [M+Na]$^+$, Δ±0.0 mmu).
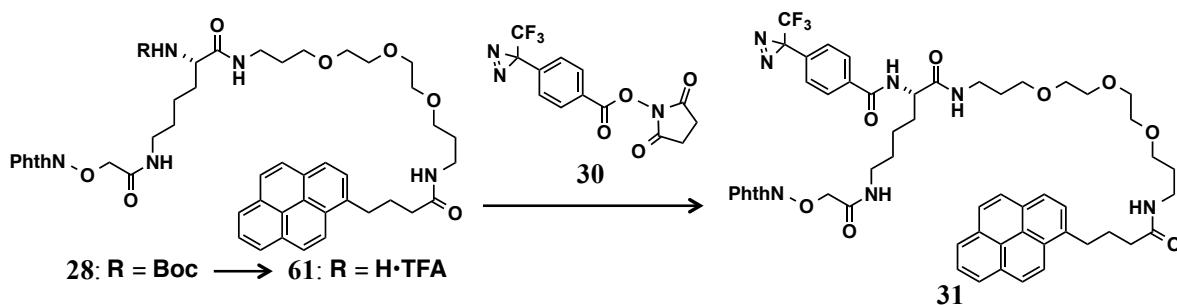
A solution of lysine amide **28** (7.9 mg, 8.6 μmol) in a 1:1 mixture of dry CH_2Cl_2 and trifluoroacetic acid (1 mL) was stirred for 30 min at room temperature, and the resulting solution was azeotropically concentrated with toluene *in vacuo* to give an amine TFA salt **61**. Diazirine succinimidyl ester **30**[10] (6.3 mg, 19 μmol) in dry DMF (0.5 mL) and triethylamine (6.0 μL, 43 μmol) were added to a stirred solution of the above amine TFA salt **61**. After being stirred for 26 h at room temperature, the resulting mixture was concentrated *in vacuo*. The crude material was purified by a reversed-phase HPLC [Develosil ODS-HG-5 (ϕ 20 mm I.D. × 250 mm), 5 mL/min, UV 254 nm, 65% aq. MeCN, t_R = 51–55 min] to give diazirine amide **31** (4.5 mg, 51%) as a yellow oil. Compound **31**: $[\alpha]_D^{30}$ +0.16 (*c* 0.38, CHCl$_3$); ^{1}H NMR (600 MHz, CDCl$_3$) δ 8.26 (d, *J* = 9.2 Hz, 1H), 8.14 (br d, *J* = 7.6 Hz, 1H), 8.14 (br d, *J* = 7.6 Hz, 1H), 8.08 (d, *J* = 9.2 Hz, 1H), 8.08 (d, *J* = 7.7 Hz, 1H), 8.01 (d, *J* = 9.2 Hz, 1H), 8.00 (d, *J* = 9.2 Hz, 1H), 7.97 (dd, *J* = 7.6, 7.6 Hz, 1H), 7.83 (d, *J* = 7.7 Hz, 1H), 7.80 (d, *J* = 8.4 Hz, 2H), 7.74 (dd, *J* = 3.1, 5.5 Hz, 2H), 7.69 (dd, *J* = 3.1, 5.5 Hz, 2H), 7.22 (d, *J* = 6.5 Hz, 1H), 7.15 (d, *J* = 8.4 Hz, 2H), 6.97 (br t, *J* = 5.5 Hz, 1H), 6.44 (br t, *J* = 5.3 Hz, 1H), 4.65 (d, *J* = 16.2 Hz, 1H), 4.60 (d, *J* = 16.2 Hz, 1H), 4.55 (td, *J* = 7.6, 6.5 Hz, 1H), 3.56–3.52 (m, 6H), 3.47–3.26 (m, 15H), 2.27 (t, *J* = 6.8 Hz, 2H), 2.18 (tt, *J* = 7.4, 7.4 Hz, 2H), 1.95 (m, 1H), 1.82–1.75 (m, 3H), 1.71 (tt, *J* = 6.0, 6.0 Hz, 2H), 1,60 (m, 2H), 1.44 (m, 2H); ^{13}C NMR (150 MHz, CDCl$_3$) δ 172.9, 171.3, 167.1, 166.0, 163.7 (2C), 136.2, 135.2, 135.1 (2C), 132.5, 131.5, 131.0, 130.0, 128.9, 128.5 (2C), 127.8 (2C), 127.6, 127.5, 127.5, 126.8, 126.6 (2C), 126.0, 125.2, 125.1, 125.0, 124.9, 124.9, 124.1 (2C), 123.6, 122.0 (q, $^1J_{CF}$ = 273 Hz), 70.5, 70.4, 70.2, 70.1, 70.0, 70.0, 69.9, 53.7, 38.8, 38.2, 37.9, 36.2, 33.0, 32.4, 29.2, 29.1, 28.9, 28.4 (q, $^2J_{CF}$ = 41 Hz), 27.7, 22.6; IR (CHCl$_3$) 3420, 3371, 3004, 2949, 2871, 1734, 1717, 1670, 1654, 1558, 1541, 1523, 1374, 1340, 848, 706 cm^{-1}; HRMS (ESI) *m/z* 1056.4085 (calcd for $C_{55}H_{58}F_3N_7NaO_{10}$ [M+Na]$^+$, Δ − 0.4 mmu).

29: R = Boc ⟶ **62**: R = H·TFA

A solution of amide **29** (8.9 mg, 10 μmol) in a 1:1 mixture of dry CH_2Cl_2 and trifluoroacetic acid (1 mL) was stirred for 1 h at room temperature and azeotropically concentrated with toluene *in vacuo* to give crude amine TFA salt **62**. To the crude amine TFA salt **62** were added diazirine succinimidyl ester **30** (5.9 mg, 18 μmol), dry DMF (0.5 mL) and Et_3N (7.0 μL, 50 μmol). After being stirred for 20 h at room temperature, the resulting mixture was concentrated. The crude material was purified with a recycling HPLC [JAIGEL-1H, JAIGEL-2H (20 mm I.D. × 300 mm), $CHCl_3$, UV254 nm] twice to give diazirine amide **32** (3.6 mg, 41%) as an amorphous yellow solid. Compound **32**: ^1H NMR (400 MHz, $CDCl_3$) δ 8.29 (d, J = 9.3 Hz, 1H), 8.16 (br d, J = 7.6 Hz, 1H), 8.14 (br d, J = 7.6 Hz, 1H), 8.10 (d, J = 7.7 Hz, 1H), 8.09 (d, J = 9.3 Hz, 1H), 8.01 (s, 2H), 7.98 (dd, J = 7.6, 7.6 Hz, 1H), 7.85 (d, J = 7.7 Hz, 1H), 7.82 (d, J = 8.4 Hz, 2H), 7.79−7.75 (m, 2H), 7.74−7.71 (m, 2H), 7.20 (d, J = 8.4 Hz, 2H), 7.11 (d, J = 6.5 Hz, 1H), 6.26 (br t, J = 5.6 Hz, 1H), 5.49 (br t, J = 5.6 Hz, 1H), 4.67 (d, J = 16.2 Hz, 1H), 4.59 (d, J = 16.2 Hz, 1H), 4.52 (td, J = 8.0, 6.5 Hz, 1H), 3.41–3.28 (m, 2H), 3.39 (t, J = 7.1 Hz, 2H), 3.23–3.16 (m, 4H), 2.30−2.17 (m, 4H), 1.97 (m, 1H), 1.84 (m, 1H), 1.66–1.57 (m, 4H), 1.49–1.38 (m, 6H), 1.28−1.22 (m, 6H). One proton signal (NH) was not detected; ^{13}C NMR (100 MHz, $CDCl_3$) δ 172.7, 171.5, 167.3, 166.3, 163.8 (2C), 136.0, 135.2 (2C), 135.0, 132.7, 131.5, 131.0, 130.0, 128.9, 128.5 (2C), 127.8 (2C), 127.6, 127.5 (2C), 126.8, 126.6 (2C), 126.0, 125.2, 125.1 (2C), 124.9 (2C), 124.1 (2C), 123.5, 53.7, 39.6, 39.6, 38.5, 36.3, 32.9, 31.8, 29.7, 29.6, 29.4, 29.0, 29.0, 28.9, 27.6, 26.7, 26.7, 22.6. Two carbon signals [Ar−C(=N$_2$)CF$_3$] were not detected; MS (ESI) m/z 980.5092 ([M+Na]$^+$).

Alkoxyamine **33**

31 → **33**
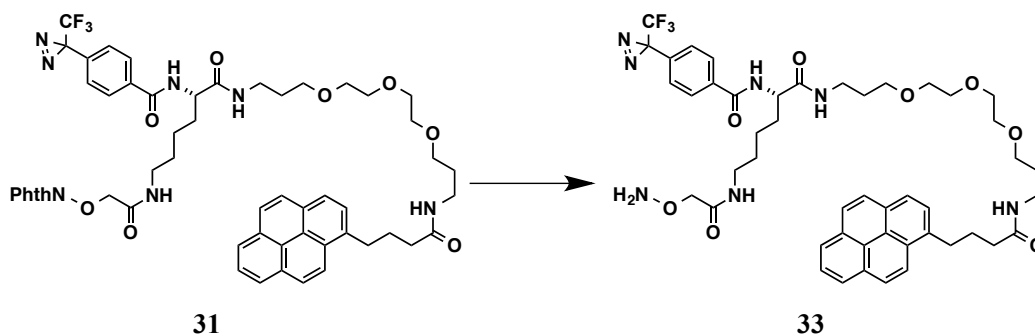
Diazirine amide **31** (1.0 mg, 0.92 μmol) was dissolved in a 21 mM solution of hydrazine monohydrate in EtOH (1.0 mL, 21 μmol). After being stirred at room temperature for 50 min, the resulting mixture was azeotropically concentrated with toluene *in vacuo* to give alkoxyamine **33** (quant. monitored by TLC analysis: R_f = 0.20, CHCl$_3$/acetone = 1/4), which was immediately used for the next step without further purification.
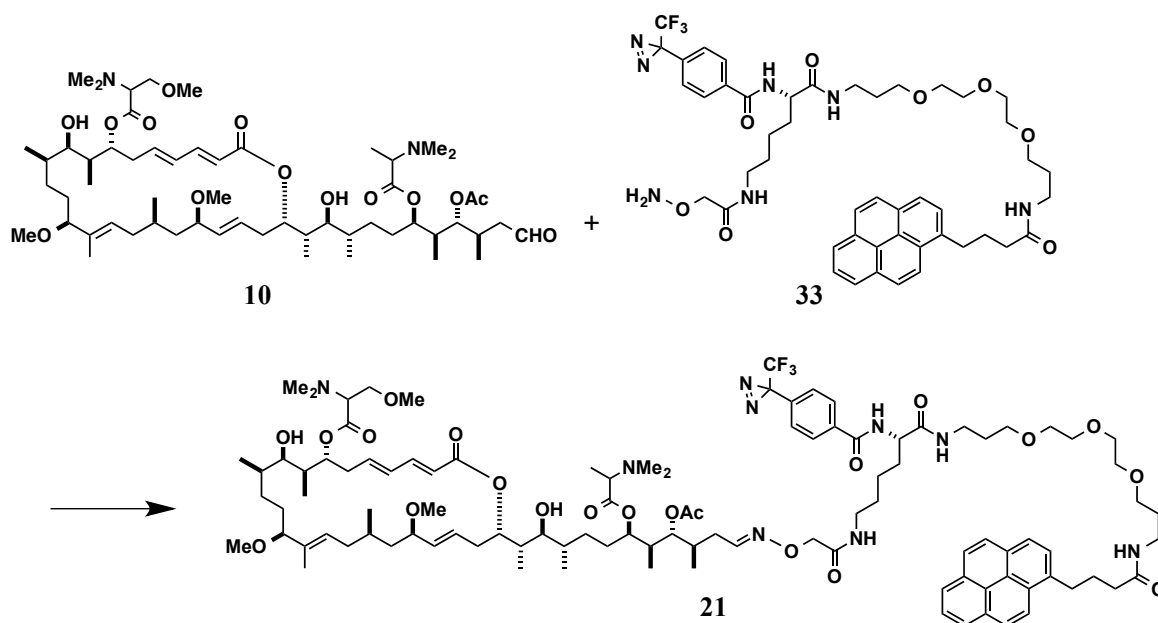
Alkoxyamine **34**

32 → **34**
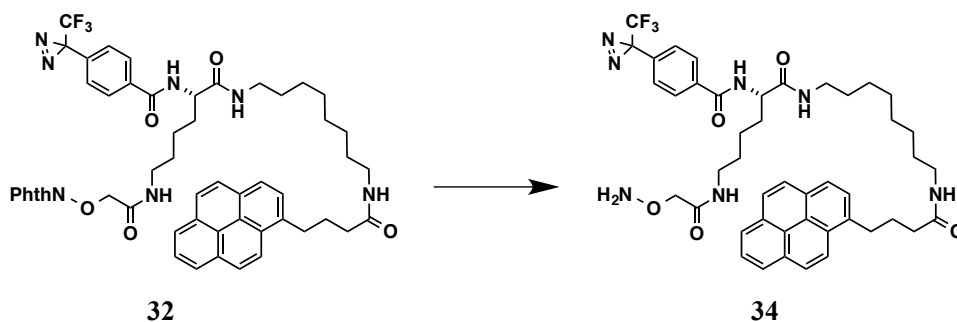
Diazirine amide **32** (1.9 mg, 2.0 μmol) was dissolved in a 21 mM solution of hydrazine monohydrate in EtOH (1.0 mL, 21 μmol). After being stirred at room temperature for 60 min, the resulting mixture was azeotropically concentrated with toluene *in vacuo* to give alkoxyamine **34** (quant. monitored by TLC analysis: R_f = 0.10, CHCl$_3$/acetone = 4/1), which was immediately used for the next step without further purification.

ApA PEG-linker photoaffinity probe (ApA-PP, **21**)

A solution of the aldehyde **10** prepared from ApA (323 μg, 300 nmol) and the alkoxyamine **33** (0.83 mg, 0.92 μmol) in a 3:1 mixture of EtOH and 100 mM acetate buffer (pH 4.0) (0.4 mL) was stirred at room temperature for 106 h. The reaction mixture was concentrated *in vacuo* and applied to a Develosil ODS-HG-5 HPLC column (20 mm I.D. × 250 mm). Samples were eluted by MeOH / 20 mM NH$_4$OAc (90:10) at a flow rate of 5 mL/min, with monitoring at 254 nm to give ApA–PP (**21**) (139 nmol, 46%, based on NMR quantification, t_R = 39–43 min, *E/Z* = 7/3 for the C34 isomers). Compound **21**: t_R = 11.8 min [Develosil ODS-HG-5 (4.6 mm I.D. × 250 mm), MeOH/20 mM NH$_4$OAc (90/10), 1 mL/min, UV 254 nm, λ$_{ex}$ 337 nm, λ$_{em}$ 409 nm];^{1}H NMR (600 MHz, CD$_3$OD) δ 8.34 (d, *J* = 9.3 Hz, 1H), 8.19 (br d, *J* = 7.1 Hz, 1H), 8.18 (br d, *J* = 7.1 Hz, 1H), 8.14 (d, *J* = 9.3 Hz, 1H), 8.14 (d, *J* = 7.7 Hz, 1H), 8.05 (d, *J* = 8.9 Hz, 1H), 8.03 (d, *J* = 8.9 Hz, 1H), 7.99 (dd, *J* = 7.1, 7.1 Hz, 1H), 7.92 (d, *J* = 8.4 Hz, 2H), 7.90 (d, *J* = 7.7 Hz, 1H), 7.51 [6.78][1] (dd, *J* = 6.4, 6.4 Hz, 1H), 7.30 (d, *J* = 8.4 Hz, 2H), 7.18 (dd, *J* = 11.1, 15.1 Hz, 1H), 6.33 (m, 1H), 6.19 (m, 1H), 5.94 (d, *J* = 15.1 Hz, 1H), 5.59 (m, 1H), 5.53 (br d, *J* = 10.7 Hz, 1H), 5.08 (m, 1H), 4.96 (m, 1H), 4.80 (m, 1H), 4.75 (m, 1H), 4.65 (m, 1H), 4.43 (m, 1H), 4.37 [4.42][1] (s, 2H), 3.66–3.62 (m, 2H), 3.56–3.46 (m, 7H), 3.49 (t, *J* = 6.2 Hz, 2H), 3.43–3.32 (m, 8H), 3.36 [3.36][2] (s, 3H), 3.27–3.18 (m, 7H), 3.17 (s, 3H), 3.13 [3.12][2] (s, 3H), 3.06 (dd, *J* = 9.6, 2.7 Hz, 1H), 2.52–2.28 (m, 4H), 2.36 [2.37][2] (s, 6H), 2.32 [2.30][1] [2.33][3] [2.31][1,3] (s, 6H), 2.34–2.30 (m, 2H), 2.26–2.20 (m, 1H), 2.16 (t, *J* = 7.6, *J* = 7.6 Hz, 2H), 2.18–2.08 (m, 1H), 2.05–1.96 (m, 4H), 2.01 [2.03][1] [2.00][3] [2.02][1,3] (s, 3H), 1.84 (m, 1H), 1.79–1.48 (m, 11H), 1.74 (tt, *J* = 6.4, 6.4 Hz, 2H), 1.70 (tt, *J* = 6.4, 6.4 Hz, 2H), 1.62–1.57 (m, 2H), 1.49 [1.50][2] (s, 3H), 1.43–1.21 (m, 11H), 1.31 (d, *J* = 6.8 Hz, 3H), 1.17–1.07 (m, 3H), 1.02 (d, *J* = 6.7 Hz, 3H), 0.99 (d, *J* = 6.8 Hz,

3H), 0.96 (d, J = 7.0 Hz, 3H), 0.89 [0.86][2] (d, J = 6.9 Hz, 3H), 0.75 [0.73][3] (d, J = 5.7 Hz, 3H). Chemical shifts of the minor diastereomers are within parentheses as follows: [][1], 7:3 at C34 stereoisomers; [][2], 3:1 at C7 trimethylserine moiety; [][3], 1.4:1 at C29 dimethylalanine moiety; HRMS (ESI) m/z 983.0446 (calcd for $(C_{104}H_{152}F_3N_9Na_2O_{21})/2$ [M+2Na]$^{2+}$, Δ+2.6 mmu).

ApA alkyl-linker photoaffinity probe (ApA-AP, **22**)
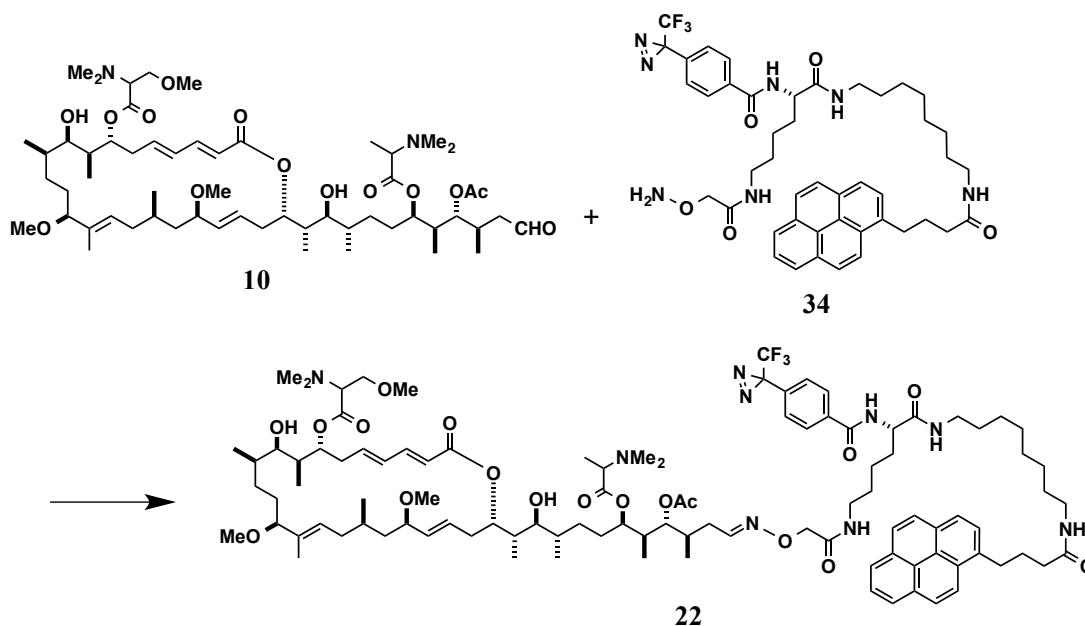
A solution of the aldehyde **10** prepared from ApA (215 μg, 200 nmol) and alkoxyamine **34** (1.6 mg, 2.0 μmol) in a 3:1 mixture of EtOH and 100 mM acetate buffer (pH 4.0) (0.4 mL) was stirred at room temperature for 38 h. The reaction mixture was concentrated *in vacuo* and applied to a Develosil ODS-HG-5 HPLC column (20 mm I.D. × 250 mm). Samples were eluted by MeOH / 20 mM NH$_4$OAc (90:10) at a flow rate of 5 mL/min, with monitoring at 254 nm to give ApA-AP (**22**) (131 nmol, 66%, based on NMR quantification, t_R = 42–45 min, *E/Z* = 7/3 for the C34 isomers). Compound **22**: t_R = 13.5 min [Develosil ODS-HG-5 (4.6 mm I.D. × 250 mm), MeOH/20 mM NH$_4$OAc (90/10), 1 mL/min, λ_{ex} 337 nm, λ_{em} 409 nm]; ^{1}H NMR (600 MHz, CD$_3$OD) δ 8.33 (d, *J* = 9.3 Hz, 1H), 8.18 (br d, *J* = 7.4 Hz, 1H), 8.18 (br d, *J* = 7.4 Hz, 1H), 8.14 (d, *J* = 9.3 Hz, 1H), 8.14 (d, *J* = 7.7 Hz, 1H), 8.05 (d, *J* = 8.0 Hz, 1H), 8.04 (d, *J* = 8.0 Hz, 1H), 7.99 (dd, *J* = 7.4, 7.4 Hz, 1H), 7.93 (d, *J* = 8.5 Hz, 2H), 7.90 (d, *J* = 7.7 Hz, 1H), 7.51 [6.78][1] (dd, *J* = 6.4, 6.4 Hz, 1H), 7.32 (d, *J* = 8.5 Hz, 2H), 7.18 (dd, *J* = 12.4, 13.4 Hz, 1H), 6.34 (m, 1H), 6.19 (m, 1H), 5.94 (d, *J* = 15.1 Hz, 1H), 5.59 (ddd, *J* = 15.0, 10.8, 4.1 Hz, 1H), 5.53 (br d, *J* = 11.0 Hz, 1H), 5.08 (m, 1H), 4.92−4.82 (m, 2H), 4.76 (dd, *J* = 10.2, 2.7 Hz, 1H), 4.65 (m, 1H), 4.44 (m, 1H), 4.37 [4.43][1] (s, 2H), 3.66–3.62 (m, 2H), 3.56–3.46 (m, 2H), 3.38–3.10 (m, 12H), 3.36 [3.35][2] (s, 3H), 3.17 (s, 3H), 3.13 [3.13][2] (s, 3H), 3.06 (dd, *J* = 9.7, 2.3 Hz, 1H), 2.58–2.27 (m, 6H), 2.36 [2.37][2] (s, 6H), 2.32 [2.31][1] [2.33][3] [2.31][1,3] (s, 6H), 2.25–2.20 (m, 1H), 2.18−1.95 (m, 7H), 2.02 [2.03][1] [2.01][3] [2.01][1,3] (s, 3H), 1.80−1.41 (m, 13H), 1.49 [1.50][2] (s, 3H), 1.38–1.21 (m, 26H), 1.14–1.06 (m, 3H), 1.02 (d, *J* = 6.6 Hz, 3H), 0.98 (d, *J* = 6.8 Hz, 3H), 0.96 (d, *J* = 6.9 Hz, 3H), 0.89 [0.86][2] (d, *J* = 6.9 Hz, 3H), 0.75−0.73 (m, 3H). Chemical shifts of the minor diastereomers are within parentheses as follows: [][1], 7:3 at C34 stereoisomers; [][2], 3:1 at C7 trimethylserine moiety; [][3], 1.4:1 at C29 dimethylalanine moiety; HRMS (ESI) *m/z* 923.0550 (calcd for (C$_{102}$H$_{150}$F$_3$N$_9$O$_{18}$)/2 [M+2H]$^{2+}$, Δ −3.0 mmu).
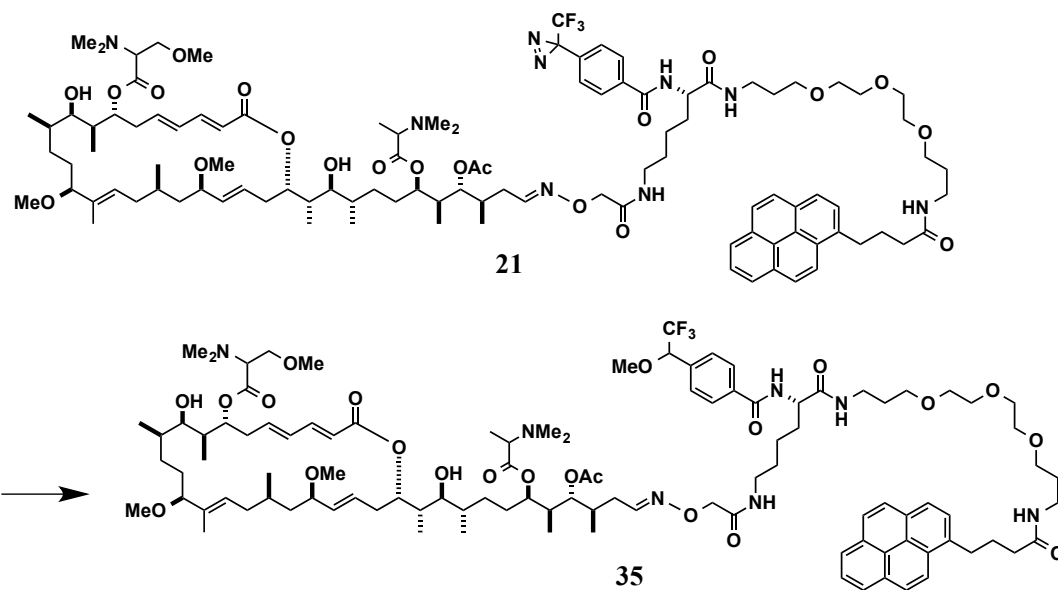
1 mM ApA–PP (**21**) in DMSO (20 µL, 20 nmol), was mixed with MeOH (1 mL) in two 1.5 mL plastic tubes. The solutions were cooled on ice and irradiated with UV light (365 nm) for 15 min, using a handheld UV lamp (0.8 mW/cm^2). The reaction mixture was concentrated *in vacuo* and applied to a Develosil ODS-HG-5 HPLC column (4.6 mm I.D. × 250 mm). Samples were eluted with MeOH / 20 mM NH$_4$OAc (88:12) at a flow rate of 1 mL/min and with monitoring by fluorescence (λ_{ex} 337 nm and λ_{em} 409 nm) to give the MeOH-adduct **35** in 8% yield each (based on the fluorescence in HPLC analysis). Compound **35**: t_R = 10.2 min [Develosil ODS-HG-5 (4.6 mm I.D. × 250 mm), MeOH / 20 mM NH$_4$OAc (88:12), 1 mL/min, λ_{ex} 337 nm, λ_{em} 409 nm]; HRMS (ESI) *m/z* 963.0726 (calcd for C$_{105}$H$_{158}$F$_3$N$_7$O$_{22}$ [M+2H]$^{2+}$, Δ +2.3 mmu).

20 → **36**
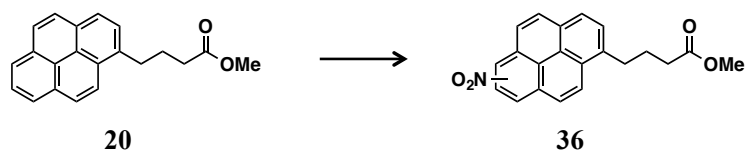
To a stirred solution of methyl ester **20** (105 mg, 0.347 mmol) in acetic anhydride (2.2 mL) was added 44% aqueous nitric acid (22 μL, 0.20 mmol). The mixture was stirred at room temperature for 12.5 h. After the addition of a second quantity of 44% aqueous nitric acid (22 μL, 0.20 mmol), the mixture was stirred at room temperature for an additional 30 min. After being concentrated *in vacuo*, the crude material was purified with a SiO$_2$ column (2.2 g, CHCl$_3$) to give a 1:1:1 regioisomer mixture of nitropyrene **36** (128 mg, quant.) as an yellow oil. Compound **36**: R_f = 0.54–0.40 (CHCl$_3$); ^{1}H NMR (400 MHz, CDCl$_3$) δ 8.83 (d, J = 9.4 Hz, 1H), 8.50 (d, J = 9.1 Hz, 1H), 8.36–8.22 (m, 4H), 8.13 (d, J = 9.0 Hz, 1H), 7.97 (d, J = 7.8 Hz, 1H), 3.71 (s, 3H), 3.43 (t, J = 7.7 Hz, 2H), 2.49 (t, J = 7.3 Hz, 2H), 2.20 (tt, J = 7.7, 7.3 Hz, 2H) [6-isomer was only described]; ^{13}C NMR (100 MHz, CDCl$_3$) δ 173.9 (1/3C), 173.8 (1/3C), 173.7 (1/3C), 142.8 (1/3C), 142.6 (1/3C), 142.5 (1/3C), 139.0 (1/3C), 138.6 (1/3C), 135.5 (1/3C), 135.4 (1/3C), 134.8 (1/3C), 133.0 (1/3C), 131.7 (1/3C), 131.0 (1/3C), 130.8 (2/3C), 130.7 (1/3C), 130.4 (1/3C), 129.7 (1/3C), 129.0 (1/3C), 128.6 (1/3C), 128.6 (1/3C), 128.5 (1/3C), 127.9 (1/3C), 127.7 (1/3C), 127.6 (1/3C), 127.5 (1/3C), 127.2 (1/3C), 127.1 (1/3C), 127.1 (1/3C), 126.9 (1/3C), 126.7 (1/3C), 126.2 (1/3C), 125.5 (1/3C), 125.2 (1/3C), 125.2 (1/3C), 124.7 (1/3C), 124.2 (2/3C), 124.1 (1/3C), 124.0 (1/3C), 123.9 (1/3C), 123.5 (1/3C), 123.4 (2/3C), 122.9 (1/3C), 122.8 (1/3C), 122.7 (1/3C), 121.7 (1/3C), 121.6 (1/3C), 121.0 (1/3C), 51.8, (1/3C), 51.8 (2/3C), 33.7 (2/3C), 33.6 (1/3C), 33.1 (1/3C), 32.8 (1/3C), 32.8 (1/3C), 27.1 (2/3C), 26.3 (1/3C); IR (CHCl$_3$) 3027, 2953, 1732, 1587, 1550, 1542, 1509, 1337, 849, 727 cm^{-1}; HRMS (ESI) *m/z* 370.1029 (calcd for C$_{21}$H$_{17}$NNaO$_4$ [M+Na]$^+$, Δ −2.1 mmu).
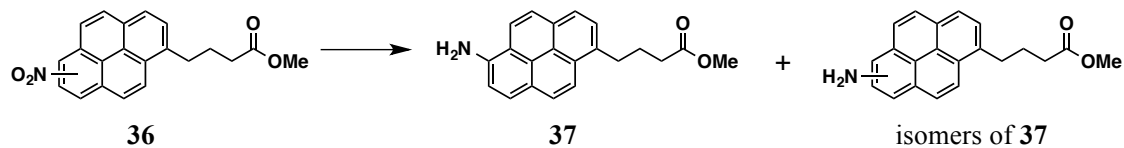
To a stirred solution of nitropyrene **36** (141 mg, 0.406 mmol) in EtOAc (3.2 mL) were added acetic acid (0.26 mL) and palladium 10% on carbon (46.1 mg). The mixture was stirred under a hydrogen atmosphere at room temperature for 2 h. After the reaction mixture was filtered through a pad of Celite, the residue was washed with EtOAc. The filtrate and the washings were combined and concentrated *in vacuo*. The crude material was purified twice with a SiO_2 column (3.1 g, toluene / EtOAc = 100/1 to 0/1) to give 6-aminopyrene **37** (35.8 mg, 28%) as a yellow oil and the 1:1 mixture of two isomers (76.8 mg, 59%). Compound **37**: R_f = 0.57 (CHCl$_3$/acetone = 9/1); ^{1}H NMR (400 MHz, CDCl$_3$) δ 8.05–7.99 (br s, 2H), 8.02 (d, J = 9.2 Hz, 1H), 7.97 (d, J = 7.5 Hz, 1H), 7.96 (d, J = 8.1 Hz, 1H), 7.95 (d, J = 9.2 Hz, 1H), 7.93 (d, J = 9.2 Hz, 1H), 7.90 (d, J = 9.2 Hz, 1H), 7.78 (d, J = 7.5 Hz, 1H), 7.37 (d, J = 8.1 Hz, 1H), 3.69 (s, 3H), 3.33 (t, J = 7.7 Hz, 2H), 2.46 (t, J = 7.3 Hz, 2H), 2.19 (tt, J = 7.7, 7.3 Hz, 2H); ^{13}C NMR (100 MHz, CDCl$_3$) δ 174.2, 140.9, 134.7, 130.6, 129.8, 128.5, 127.8, 127.6, 126.4, 126.3, 126.0, 124.3, 123.5, 119.8, 119.5, 117.2, 114.2, 51.7, 33.8, 33.0, 26.6; IR (CHCl$_3$) 3404, 3016, 2976, 2895, 1733, 1624, 1507, 1498, 877, 843, 789 cm^{-1}; UV (MeOH) λ$_{max}$ 362 (ε 21000), 284 (ε 26000), 244 (ε 40000) nm; HRMS (ESI) *m/z* 340.1322 (calcd for C$_{21}$H$_{19}$NNaO$_2$ [M+Na]$^+$, Δ +1.4 mmu).
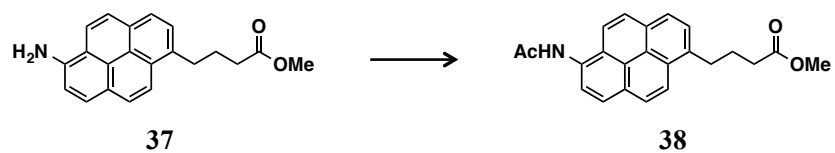
To a solution of 6-aminopyrene **37** (16.8 mg, 52.9 μmol) in dry CH_2Cl_2 (2 mL) was added acetic anhydride (8.0 μL, 84 μmol). After being stirred at room temperature for 10 h, the reaction mixture was neutralized with sat. $NaHCO_3$ aq. The organic layer was washed with sat. $NaHCO_3$ aq. and brine, dried with Na_2SO_4, and concentrated *in vacuo*. The crude material was purified with a SiO_2 column (0.6 g, $CHCl_3$) to give amidopyrene **38** (17.1 mg, 93%) as a colorless amorphous solid. Compound **38**: R_f = 0.32 ($CHCl_3$/acetone = 9/1); mp. 196.5–209.0 °C; ^{1}H NMR (600 MHz, pyridine-d_5) δ 11.22 (s, 1H), 8.72 (d, J = 8.2 Hz, 1H), 8.60 (d, J = 9.1 Hz, 1H), 8.36 (d, J = 9.2 Hz, 1H), 8.26 (d, J = 8.2 Hz, 1H), 8.14 (d, J = 9.2 Hz, 1H), 8.11 (d, J = 9.1 Hz, 1H), 8.11 (d, J = 7.7 Hz, 1H), 7.86 (d, J = 7.7 Hz, 1H), 3.64 (s, 3H), 3.33 (t, J = 7.5 Hz, 2H), 2.51 (s, 3H), 2.48 (t, J = 7.5 Hz, 2H), 2.18 (tt, J = 7.5, 7.5 Hz, 2H); ^{13}C NMR (150 MHz, pyridine-d_5) δ 174.2, 170.1, 137.1, 136.3, 133.6, 130.7, 129.9, 129.6, 128.5, 128.2 (2C), 126.6, 126.2, 125.8, 125.6, 124.7, 123.6, 122.5, 51.9, 34.2, 33.4, 27.7, 24.6; IR ($CHCl_3$) 3427, 3030, 3009, 2953, 1731, 1685, 1550, 1519, 1484, 847, 720 cm^{-1}; UV (MeOH) λ_{max} 346 (ε 26000), 279 (ε 29000), 243 (ε 38000) nm; HRMS (ESI) *m/z* 382.1439 (calcd for $C_{23}H_{21}NNaO_3$ [M+Na]$^+$, Δ +2.5 mmu).
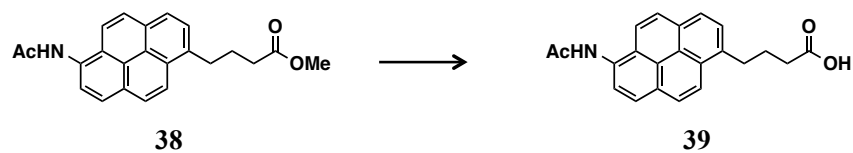
To a solution of amidopyrene **38** (12.5 mg, 34.5 μmol) in dry THF (1 mL) was added 1 M LiOH aq. (1 mL). After being stirred at room temperature for 3.5 h, the reaction mixture was acidified with 1 M HCl aq. and extracted with EtOAc (2 mL × 2) and CHCl$_3$ (2 mL). The combined extracts were washed with brine, dried with Na$_2$SO$_4$, and concentrated *in vacuo*. The crude material was purified with a SiO$_2$ column (0.6 g, CHCl$_3$/acetone/MeOH = 1/1/0, 1/0/1) to give carboxylic acid **39** (10.4 mg, 86%) as a white powder. Compound **39**: R_f = 0.49 (CHCl$_3$/acetone = 1/1); mp. 252.8–254.0 °C; ^{1}H NMR (600 MHz, DMSO-d_6) δ 12.10 (br s, 1H), 10.29 (s, 1H), 8.34 (d, J = 9.1 Hz, 1H), 8.27–8.22 (m, 3H), 8.21 (d, J = 7.8 Hz, 1H), 8.17 (d, J = 9.3 Hz, 1H), 8.16 (d, J = 9.3 Hz, 1H), 7.93 (d, J = 7.8 Hz, 1H), 3.34 (t, J = 7.4 Hz, 2H), 2.38 (t, J = 7.2 Hz, 2H), 2.27 (s, 3H), 2.00 (tt, J = 7.4, 7.2 Hz, 2H); ^{13}C NMR (150 MHz, DMSO-d_6) δ 174.4, 169.1, 136.4, 131.8, 129.2, 128.4, 128.0, 127.7, 127.2, 127.1, 124.8, 124.7, 124.6, 124.4, 124.0, 123.4, 122.6, 121.5, 33.4, 32.1, 26.8, 23.6; IR (KBr) 3282, 3042, 2952, 1698, 1654, 1604, 1552, 1521, 1499, 844, 715, 682 cm^{-1}; HRMS (ESI) *m/z* 344.1297 (calcd for C$_{22}$H$_{18}$NO$_3$ [M–H]$^-$, Δ +0.5 mmu).
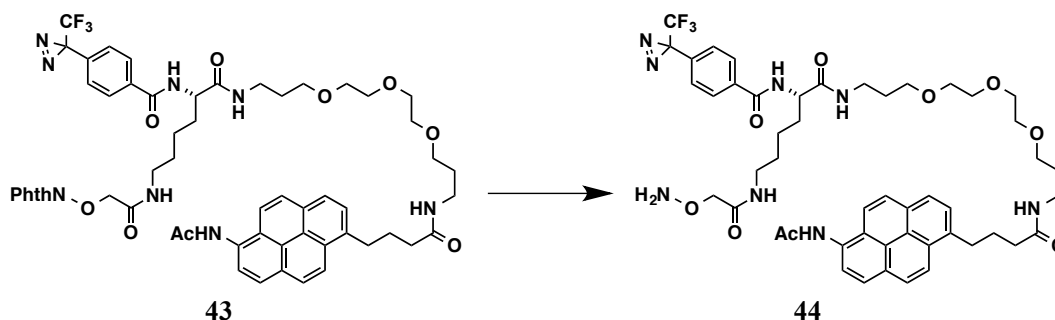
Amide **41**
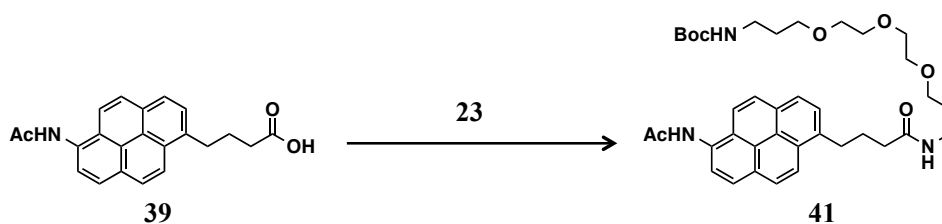
A solution of amine **23** (53.8 mg, 0.168 mmol) in dry CH_2Cl_2 (2 mL) was added to a carboxylic acid **39** (47.9 mg, 0.139 mmol), HOBt (22.5 mg, 0.171 mmol), and EDC·HCl (32.6 mg, 0.170 mmol). After being stirred for 19.5 h, the reaction mixture was washed with sat. NH_4Cl aq. (5 mL × 4) and brine, dried with Na_2SO_4, and concentrated *in vacuo*. The crude material was purified with a SiO_2 column (2.0 g, $CHCl_3$/acetone = 5/1, 4/1, 2/1 to 0/1) to give amide **41** (88.4 mg, 98%) as a yellow amorphous solid. Compound **41**: R_f = 0.36 ($CHCl_3$/acetone = 9/1); mp. 131.9–140.5 °C; ^{1}H NMR (600 MHz, CD_3OD) δ 8.34 (d, J = 9.3 Hz, 1H), 8.20 (d, J = 8.2 Hz, 1H), 8.16 (d, J = 9.1 Hz, 1H), 8.16 (d, J = 7.8 Hz, 1H), 8.14 (d, J = 9.3 Hz, 1H), 8.12 (d, J = 9.1 Hz, 1H), 8.11 (d, J = 8.2 Hz, 1H), 7.93 (d, J = 7.8 Hz, 1H), 3.64 (m, 1H), 3.58 (m, 1H), 3.54 (m, 4H), 3.51 (m, 2H), 3.50 (t, J = 6.1 Hz, 2H), 3.44 (m, 2H), 3.40 (t, J = 6.1 Hz, 2H), 3.28 (t, J = 6.7 Hz, 2H), 3.06 (t, J = 6.8 Hz, 2H), 2.37 (s, 3H), 2.35 (t, J = 7.3 Hz, 2H), 2.17 (tt, J = 7.5, 7.2 Hz, 2H), 1.76 (tt, J = 6.4, 6.4 Hz, 2H), 1.64 (tt, J = 7.3, 7.5 Hz, 2H), 1.40 (s, 9H); ^{13}C NMR (100 MHz, $CDCl_3$) δ 172.7, 169.4, 156.2, 136.7, 130.4, 129.7, 129.2, 129.0, 128.1, 127.8, 127.3, 125.6, 125.3, 125.0 (2C), 124.4, 123.1, 123.0, 120.0, 79.2, 77.4, 70.5, 70.4, 70.4, 70.2 (2C), 70.1, 69.4, 36.2, 33.0, 29.7, 29.0, 28.6 (3C), 27.6, 24.4; IR ($CHCl_3$) 3450, 3009, 2982, 2931, 2872, 1694, 1661, 1655, 1517, 1499, 846, 788 cm^{-1}; HRMS (ESI) *m/z* 670.3485 (calcd for $C_{37}H_{49}N_3NaO_7$ [M+Na]$^+$, Δ +2.2 mmu).
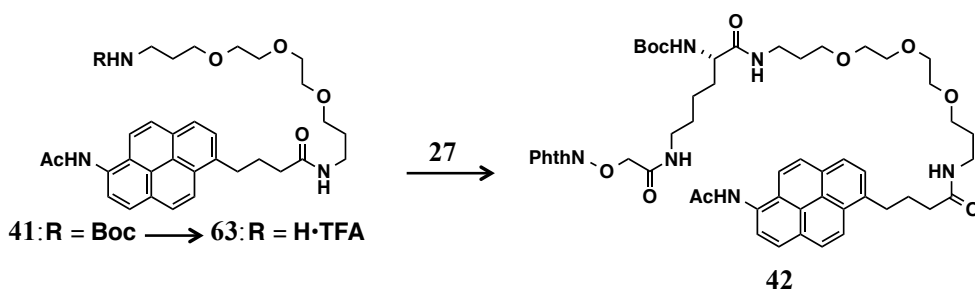
A solution of amide **41** (5.7 mg, 8.8 μmol) in a 1:1 mixture of dry CH_2Cl_2 and trifluoroacetic acid (1 mL) was stirred for 30 min at room temperature, and the resulting mixture was azeotropically concentrated with toluene *in vacuo* to give an amine TFA salt **63**. Triethylamine (4 μL, 29 μmol) was added to a stirred solution of Phth-protected carboxylic acid **27** (7.1 mg, 16 μmol), HOBt (3.1 mg, 23 μmol), EDC·HCl (2.8 mg, 15 μmol), and the above amine TFA salt **63** in dry CH_2Cl_2 (3 mL). After being stirred for 50 h, the reaction mixture was washed with sat. $NaHCO_3$ aq. and brine, dried with Na_2SO_4, and concentrated *in vacuo*. The crude material was purified with a SiO_2 column (0.6 g, $CHCl_3$/acetone = 2/1 to 1/1) to give lysine amide **42** (6.5 mg, 76%) as a yellow oil. Compound **42**: R_f = 0.20 ($CHCl_3$/acetone = 1/1); $[\alpha]_D^{18}$ –0.42 (*c* 0.26, $CHCl_3$); ^{1}H NMR (600 MHz, DMSO-d_6) δ 10.29 (br s, 1 H), 8.31 (d, *J* = 9.1 Hz, 1H), 8.31 (s, 1H), 8.26–8.21 (m, 2H), 8.20 (d, *J* = 7.8 Hz, 1H), 8.17 (d, *J* = 8.9 Hz, 1H), 8.15 (d, *J* = 9.1 Hz, 1H), 8.14 (m, 1H), 8.09 (t, *J* = 5.6 Hz, 1H), 8.03 (t, *J* = 5.5 Hz, 1H), 7.92 (d, *J* = 7.8 Hz, 1H), 7.89–7.84 (m, 2H), 7.83–7.80 (m, 2H), 7.75 (t, *J* = 5.8 Hz, 1H), 4.59 [4.56, 4.53] (s, 2H), 3.80 (m, 1H), 3.50–3.27 (m, 14H), 3.13–2.99 (m, 6H), 2.27 [2.30] (m, 3H), 2.22 [2.21] (t, *J* = 7.3 Hz, 2H), 2.00 (tt, *J* = 7.3, 7.7 Hz, 2H), 1.62 (m, 2H), 1.58 (m, 2H), 1.50–1.37 (m, 2H), 1.32–1.09 (m, 4H), 1.35 (s, 9H); ^{13}C NMR (150 MHz, DMSO-d_6) δ 171.8, 169.1, 168.0, 167.7, 165.7, 162.9, 162.9, 136.6, 134.9 (2C), 134.4, 131.8, 131.6, 129.2, 128.9, 128.5, 128.4, 128.2, 127.7, 127.1 (2C), 124.7, 124.6, 124.4, 123.4, 123.4, 123.1, 122.6, 121.5, 79.2, 75.8, 69.7, 69.7, 69.5, 69.4, 68.5, 68.1, 55.8, 38.2, 35.8, 35.0, 32.4, 32.1, 29.6 (3C), 29.4, 28.6, 28.2, 27.5, 23.5, 22.9, 21.0; IR ($CHCl_3$) 3425, 3378, 3006, 2929, 2868, 1734, 1716, 1670, 1539, 1522, 1370, 846, 703 cm^{-1}; HRMS (ESI) *m/z* 1001.4618 (calcd for $C_{53}H_{66}N_6NaO_{12}$ [M+Na]$^+$, Δ –1.3 mmu).

41: R = Boc ⟶ 64: R = H·TFA

30

43
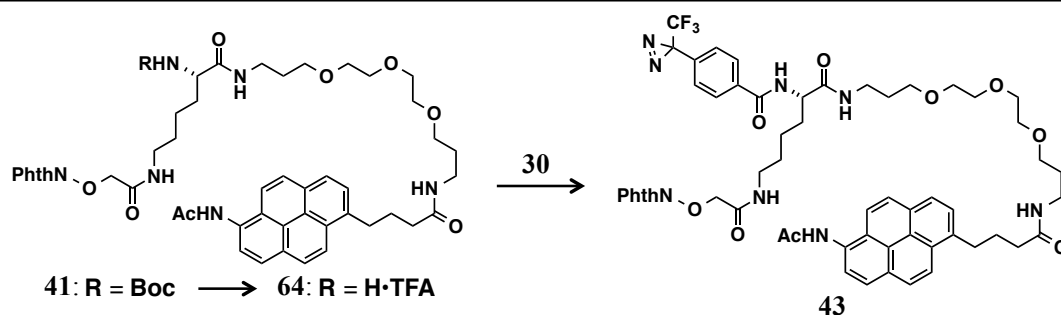
A solution of lysine amide **43** (3.8 mg, 3.9 μmol) in a 1:1 mixture of dry CH_2Cl_2 and trifluoroacetic acid (1 mL) was stirred for 30 min at room temperature, and the resulting mixture was azeotropically concentrated with toluene *in vacuo* to give an amine TFA salt **64**. Diazirine succinimidyl ester **30** (3.2 mg, 9.8 μmol) in dry DMF (0.3 mL) and triethylamine (3.0 μL, 22 μmol) were added to a stirred solution of the above amine TFA salt **64** in dry DMF (0.2 mL). After being stirred for 19 h at room temperature, the resulting mixture was concentrated *in vacuo*. The crude material was purified by a reversed-phase HPLC [Develosil ODS-HG-5 (20 mm I.D. × 250 mm), 5 mL/min, UV 254 nm, 55% aq. MeCN, t_R = 29–32 min] to give diazirine amide **43** (3.6 mg, 84%) as a yellow oil. Compound **43**: t_R = 9.1 min [Develosil ODS-HG-5 (4.6 mm I.D. × 250 mm), MeCN / 0.1% TFA (55:45), 1 mL/min, λ_{ex} 337 nm, λ_{em} 409 nm]; $[\alpha]_D^{18}$ +1.5 (*c* 0.69, CHCl$_3$); ^{1}H NMR (600 MHz, DMSO-d_6) δ 10.29 (s, 1H), 8.55 (d, *J* = 7.8 Hz, 1H), 8.30 (d, *J* = 9.2 Hz, 1H), 8.25–8.21 (m, 3H), 8.19 (d, *J* = 7.8 Hz, 1H), 8.16 (d, *J* = 8.2 Hz, 1H), 8.15 (d, *J* = 9.2 Hz, 1H), 7.99 (d, *J* = 8.2 Hz, 2H), 7.95 (t, *J* = 5.7 Hz, 1H), 7.92 (d, *J* = 7.7 Hz, 1H), 7.85 (s, 4H), 7.82 (t, *J* = 5.6 Hz, 1H), 7.34 (d, *J* = 8.2 Hz, 2H), 4.58 (s, 2H), 4.35 (dt, *J* = 5.4, 8.5 Hz, 1H), 3.85–3.42 (m, 10H), 3.40 (m, 1H), 3.38 (t, *J* = 5.8 Hz, 2H), 3.35 (t, *J* = 6.4 Hz, 2H), 3.28 (t, *J* = 7.6 Hz, 2H), 3.17–3.03 (m, 4H), 2.26 (s, 3H), 2.21 (t, *J* = 7.3 Hz, 2H), 1.99 (tt, *J* = 7.6, 7.3 Hz, 2H), 1.72 (m, 2H), 1.62 (tt, *J* = 6.7, 6.7 Hz, 2H), 1.60 (tt, *J* = 6.7, 6.2 Hz, 2H), 1,46 (m, 2H), 1.37 (m, 1H), 1.29 (m, 1H); ^{13}C NMR (150 MHz, DMSO-d_6) δ 171.8, 171.5, 169.1, 165.7, 165.3, 162.9 (2C), 136.6, 135.8, 134.9 (2C), 131.8, 130.2, 129.2, 128.5, 128.5 (2C), 128.4 (2C), 128.3, 128.0, 127.7, 127.1 (2C), 126.2 (2C), 124.7, 124.6, 124.4, 124.0, 123.4 (2C), 123.4, 122.7, 121.7 (q, $^1J_{CF}$ = 273 Hz), 121.5, 75.8, 69.7, 69.7, 69.5, 69.5, 68.1, 68.0, 53.6, 38.2, 35.9, 35.8, 35.0, 32.3, 31.2, 29.4, 29.2, 28.5, 28.0 (q, $^2J_{CF}$ = 40 Hz), 27.5, 23.5, 23.1; IR (CHCl$_3$) 3421, 3370, 3006, 2944, 2870, 1735, 1669, 1655, 1557, 1541, 1523, 1372, 1344, 846, 705 cm^{-1}; HRMS (ESI) *m/z* 1113.4309 (calcd for $C_{57}H_{61}F_3N_8NaO_{11}$ [M+Na]$^+$, Δ +0.5 mmu).

Diazirine amide **43** (1.1 mg, 1.0 μmol) was dissolved in a 21 mM solution of hydrazine monohydrate in EtOH (1.0 mL, 21 μmol). After being stirred at room temperature for 30 min, the resulting mixture was azeotropically concentrated with toluene *in vacuo* to give alkoxyamine **44** (quant. monitored by TLC analysis: R_f = 0.17, CHCl$_3$/acetone = 1/4), which was immediately used for the next step without further purification.

ApA photoaffinity amidopyrene probe (ApA–PaP, **40**).
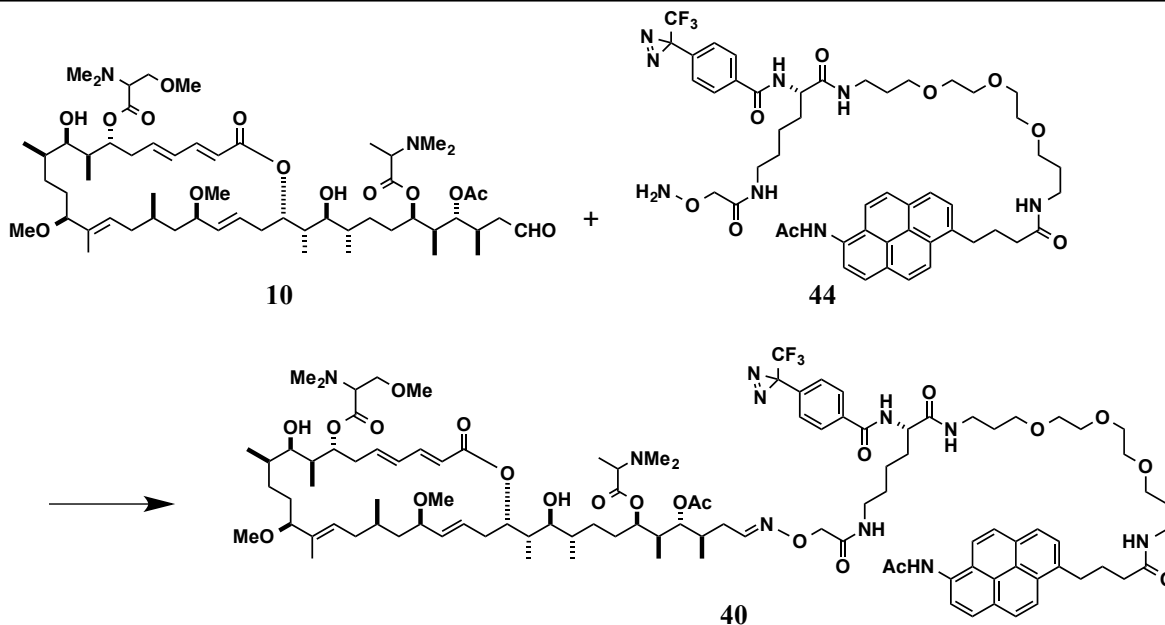
A solution of the aldehyde **10** prepared from ApA (108 μg, 100 nmol) and the whole amount of alkoxyamine **44** prepared as above in a 3:1 mixture of EtOH and 50 mM acetate buffer (pH 4.0) (0.4 mL) was stirred at room temperature for 19 h. The reaction mixture was concentrated and applied to a Develosil ODS-HG-5 HPLC column (20 mm I.D. × 250 mm). Samples were eluted with MeOH / 20 mM NH$_4$OAc (85:15) at a flow rate of 5 mL/min and with monitoring at 254 nm to give ApA–PaP (**40**) (68 nmol, 68%, based on NMR quantification, t_R = 32–35 min, *E/Z* = 7/3 for the C34 isomers). Compound **40**: t_R = 10.1 min [Develosil

ODS-HG-5 (4.6 mm I.D. × 250 mm), MeOH / 20 mM NH$_4$OAc (85:15), 1 mL/min, λ_{ex} 337 nm, λ_{em} 409 nm]; ^{1}H NMR (600 MHz, CD$_3$OD) δ 8.34 (d, J = 9.2 Hz, 1H), 8.20 (d, J = 8.1 Hz, 1H), 8.17 (d, J = 9.4 Hz, 1H), 8.16 (d, J = 7.8 Hz, 1H), 8.14 (d, J = 9.2 Hz, 1H), 8.12 (d, J = 7.8 Hz, 1H), 8.12 (d, J = 9.4 Hz, 1H), 7.93 (d, J = 8.3 Hz, 2H), 7.92 (d, J = 7.9 Hz, 1H), 7.52 [6.79][1] (dd, J = 7.0, 5.7 Hz, 1H), 7.31 (d, J = 8.3 Hz, 2H), 7.19 (br dd, J = 15.2, 11.0 Hz, 1H), 6.36 (m, 1H), 6.20 (m, 1H), 5.96 (d, J = 15.2 Hz, 1H), 5.61 (ddd, J = 14.9, 10.7, 4.1 Hz, 1H), 5.54 (br d, J = 11.2 Hz, 1H), 5.09 (m, 1H), 4.98 (m, 1H), 4.83 (m, 1H), 4.77 (dd, J = 9.7, 2.4 Hz, 1H), 4.67 (m, 1H), 4.43 (m, 1H), 4.38 [4.43][1] (s, 2H), 3.70–3.63 (m, 2H), 3.55–3.47 (m, 7H), 3.50 (t, J = 6.2 Hz, 2H), 3.42 (m, 2H), 3.41 (t, J = 6.4 Hz, 2H), 3.38–3.36 (m, 2H), 3.37 [3.37][2] (s, 3H), 3.34 (m, 2H), 3.27 (t, J = 6.7 Hz, 2H), 3.24–3.19 (m, 5H), 3.18 (s, 3H), 3.14 [3.13][2] (s, 3H), 3.08 (dd, J = 9.4, 2.4 Hz,1H), 2.54–2.41 (m, 2H), 2.38 [2.38][2] (s, 3H), 2.37 [2.38][2] (s, 3H), 2.34 [2.32][1] [2.34][3] [2.34][1,3] (s, 6H), 2.42–2.22 (m, 5H), 2.16 (tt, J = 7.5, 7.5 Hz, 2H), 2.12 (m, 1H), 2.07–1.97 (m, 4H), 2.03 [2.02][1] [2.04][3] [2.02][1,3] (s, 3H), 2.03 (s, 3H), 1.87−1.82 (m, 2H), 1.80–1.64 (m, 5H), 1.75 (tt, J = 6.4, 6.4 Hz, 2H), 1.69 (tt, J = 6.5, 6.5 Hz, 2H), 1.63–1.58 (m, 2H), 1.56–1.48 (m, 5H), 1.51 [1.51][2] (s, 3H), 1.46–1.20 (m, 14H), 1.18–1.08 (m, 3H), 1.03 (d, J = 6.7 Hz, 3H), 1.00−0.95 (m, 6H), 0.90 [0.88][2] (d, J = 6.9 Hz, 3H), 0.76 [0.74][3] (d, J = 5.7 Hz, 3H). Chemical shifts of the minor diastereomers are within parentheses as follows: [][1], 7:3 at C34 stereoisomers; [][2], 3:1 at C7 trimethylserine moiety; [][3], 1.4:1 at C29 dimethylalanine moiety; HRMS (ESI) m/z 1011.5508 (calcd for (C$_{106}$H$_{155}$F$_3$N$_{10}$Na$_2$O$_{22}$)/2 [M+2Na]$^{2+}$, Δ −1.9 mmu).
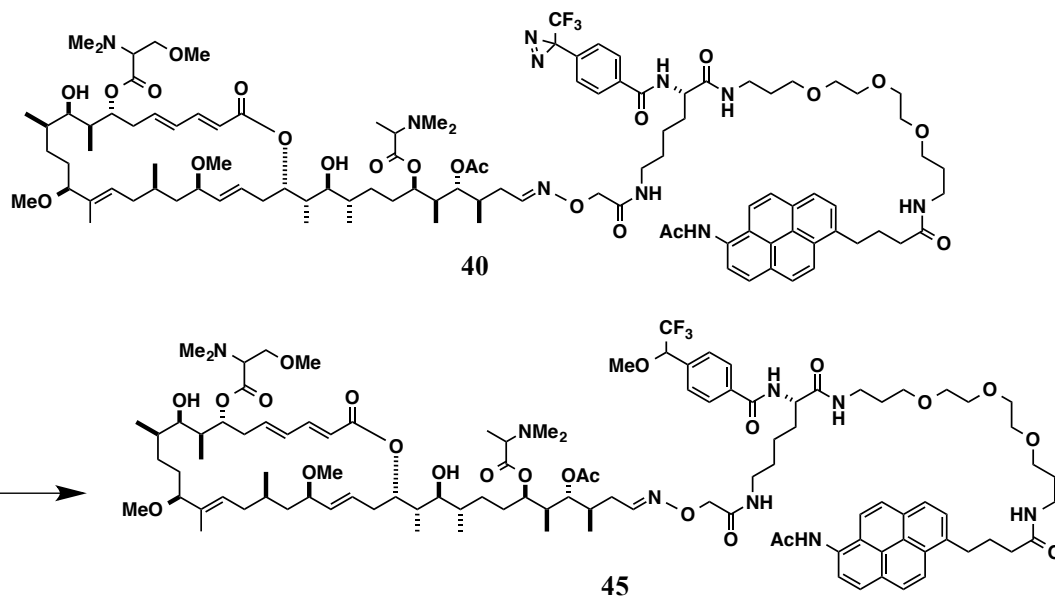
2 mM ApA–PaP (**40**) in DMSO (8 μL), was diluted with MeOH (800 μL). The solution was cooled on ice and irradiated with UV light (365 nm) for 15 min, using a handheld UV lamp (0.8 mW/cm^2). The reaction mixture was concentrated *in vacuo* and applied to a Develosil ODS-HG-5 HPLC column (4.6 mm I.D. × 250 mm). Samples were eluted with MeOH / 20 mM NH$_4$OAc (83:17) at a flow rate of 1 mL/min and with monitoring by fluorescence (λ_{ex} 337 nm and λ_{em} 409 nm) to give the MeOH-adduct **45** in 24% yield (based on the fluorescence in HPLC analysis). Compound **45**. t_R = 8.2 min [Develosil ODS-HG-5 (4.6 mm I.D. × 250 mm), MeOH / 20 mM NH$_4$OAc (83:17), 1 mL/min, λ_{ex} 337 nm, λ_{em} 409 nm]; HRMS (ESI) *m/z* 1013.5618 (calcd for C$_{107}$H$_{159}$F$_3$N$_8$Na$_2$O$_{23}$ [M+2Na]$^{2+}$, Δ +0.9 mmu).
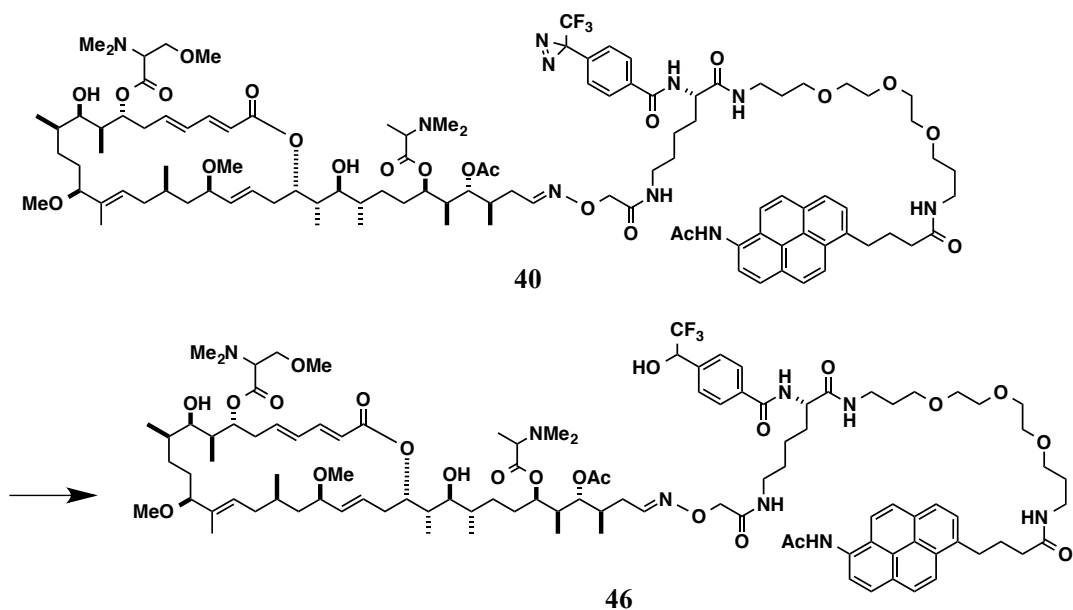
2 mM ApA–PaP (**40**) in DMSO (8 μL), was diluted with H_2O (800 μL). The solution was cooled on ice and irradiated with UV light (365 nm) for 15 min, using a handheld UV lamp (0.8 mW/cm^2). The reaction mixture was concentrated *in vacuo* and applied to a Develosil ODS-HG-5 HPLC column (4.6 mm I.D. × 250 mm). Samples were eluted with MeOH / 20 mM NH_4OAc (81:19) at a flow rate of 1 mL/min and with monitoring by fluorescence (λ_{ex} 337 nm and λ_{em} 409 nm) to give the H_2O-adduct **46** in 16% yield (based on the fluorescence in HPLC analysis). Compound **46**. t_R = 6.8 min [Develosil ODS-HG-5 (4.6 mm I.D. × 250 mm), MeOH / 20 mM NH_4OAc (83:17), 1 mL/min, λ_{ex} 337 nm, λ_{em} 409 nm]; HRMS (ESI) *m/z* 984.5734 (calcd for $C_{106}H_{159}F_3N_8O_{23}$ $[M+2H]^{2+}$, Δ +0.4 mmu).
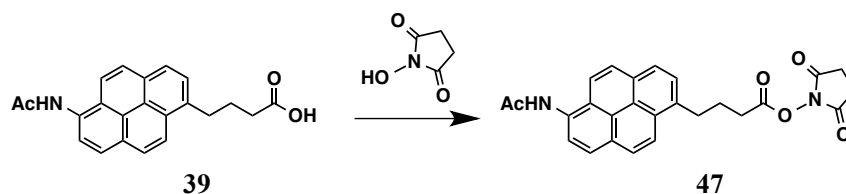
A solution of *N*-hydroxysuccinimide (7.5 mg, 65 μmol) and EDC·HCl (13.8 mg, 72.0 μmol) in dry DMF (0.5 mL) was added to carboxylic acid **39** (18.1 mg, 52.4 μmol). After being stirred for 11.5 h, CHCl$_3$ (4 mL) and MeOH (0.5 mL) were added to the reaction mixture. The solution was washed with sat. NH$_4$Cl aq. (1 mL × 4) and brine (5 mL), dried with Na$_2$SO$_4$, and concentrated *in vacuo*. The crude material was purified by recrystalization (CHCl$_3$/MeOH/hexane) to give Apy-Su (**47**) (15.4 mg, 62%) as a colorless amorphous solid. Compound **47**: R_f = 0.56 (CHCl$_3$/acetone = 1/1); mp. 213.8–214.2 °C; ^{1}H NMR (600 MHz, DMSO-d_6) δ 10.32 (s, 1H), 8.36 (d, J = 9.2 Hz, 1H), 8.27–8.24 (m, 3H), 8.22 (d, J = 7.8 Hz, 1H), 8.18 (d, J = 8.9 Hz, 1H), 8.17 (d, J = 8.9 Hz, 1H), 7.93 (d, J = 7.8 Hz, 1H), 3.42 (t, J = 7.9 Hz, 2H), 2.87 (t, J = 7.1 Hz, 2H), 2.85 (s, 4H), 2.28 (s, 3H), 2.12 (tt, J = 7.9, 7.1 Hz, 2H); ^{13}C NMR (150 MHz, DMSO-d_6) δ 170.4 (2C), 169.1, 169.0, 135.7, 131.9, 129.4, 128.4, 127.9, 127.7, 127.4, 127.1, 124.8, 124.7, 124.7, 124.4, 124.0, 123.4, 122.5, 121.6, 31.6, 30.2, 26.7, 25.5 (2C), 23.6; IR (KBr) 3250, 3041, 2983, 2945, 1671, 1645, 1602, 1546, 1531, 1496, 847, 722, 684 cm^{-1}; HRMS (ESI) *m/z* 465.1421 (calcd for C$_{26}$H$_{22}$N$_2$NaO$_5$ [M+Na]$^+$, Δ ±0.0 mmu).

Alkoxyamine **49**

63 → **49**
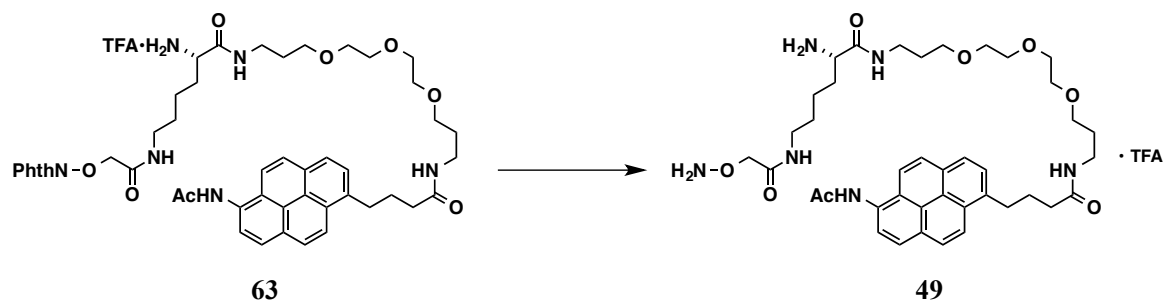
An amine TFA salt **63** (2.3 mg, 2.3 μmol) prepared from lysine amide **42** was dissolved in a 21 mM solution of hydrazine monohydrate in EtOH (2.0 mL, 42 μmol). After being stirred at room temperature for 30 min, the resulting mixture was azeotropically concentrated with toluene *in vacuo* to give alkoxyamine **49** (quant. monitored by TLC analysis: R_f = 0.11, CHCl$_3$/MeOH = 2/1), which was immediately used for the next step without further purification.
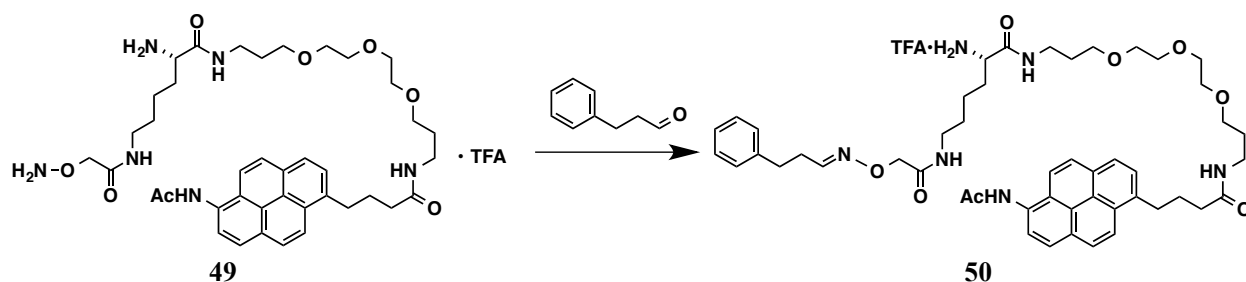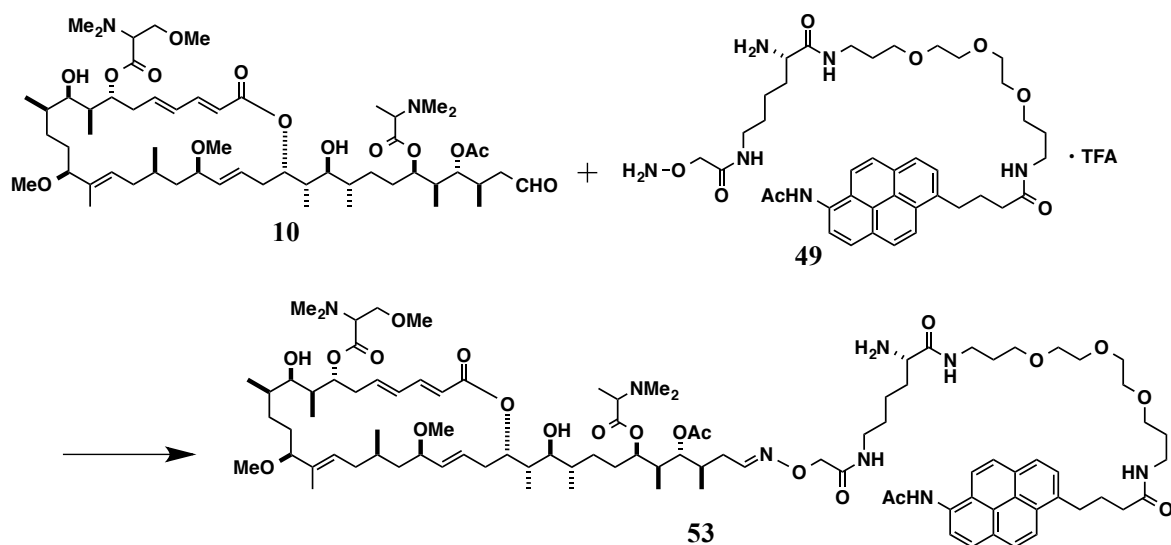
A solution of the alkoxyamine **49** as described above and 3-phenylpropanal (67.1 μg, 500 nmol) in a 3:1 mixture of EtOH and 100 mM acetate buffer (pH 4.0) (0.4 mL) was stirred at room temperature for 18 h. The reaction mixture was concentrated *in vacuo*. The crude sample was applied to a Develosil ODS-HG-5 HPLC column (20 mm I.D. × 250 mm). Samples were eluted with MeOH/0.1% TFA = (65:35) at a flow rate of 5 mL/min and with monitoring at 254 nm (t_R = 45–51 min) to give amine TFA salt **50** (0.447 mg, 465 nmol, 93% based on NMR quantification. *E/Z* = 6/4). Compound **50**: t_R = 5.4 min [Develosil ODS-HG-5 (4.6 mm I.D. × 250 mm), MeOH / 0.1% TFA = (65:35), 1 mL/min, λ_{ex} 337 nm, λ_{em} 409 nm]; ^{1}H NMR (600 MHz, CD$_3$OD) δ 8.34 (d, *J* = 9.2 Hz, 1H), 8.20 (d, *J* = 8.2 Hz, 1H), 8.16 (d, *J* = 9.1 Hz, 1H), 8.16 (d, *J* = 7.7 Hz, 1H), 8.14 (d, *J* = 9.2 Hz, 1H), 8.12 (d, *J* = 9.1 Hz, 1H), 8.11 (d, *J* = 8.2 Hz, 1H), 7.93 (d, *J* = 7.7 Hz, 1H), 7.54 [6.77] (t, *J* = 6.0 Hz, 1H), 7.27−7.14 (m, 5H), 4.37 [4.43] (s, 2H), 3.68 (m, 1H), 3.55–3.38 (m, 14H), 3.29–3.17 (m, 6H), 2.77 (t, *J* = 7.8 Hz, 2H), 2.46 [2.71] (td, *J* = 7.8, 6.0 Hz, 2H), 2.37 (s, 3H), 2.35 (t, *J* = 7.4 Hz, 2H), 2.16 (tt, *J* = 7.4, 7.4 Hz, 2H), 1.86 −1.67 (m, 2H), 1.75 (tt, *J* = 6.4, 6.4 Hz, 2H), 1.69 (tt, *J* = 6.5, 6.5 Hz, 2H), 1.48 (m, 2H), 1.33 (m, 2H). Chemical shifts of the minor *Z*-isomer are within parentheses (square brackets); HRMS (ESI) *m/z* 865.4867 (calcd for C$_{49}$H$_{65}$N$_6$O$_8$ [M+H]$^+$, Δ −0.9 mmu).

Model probe **48**

50 → **48**
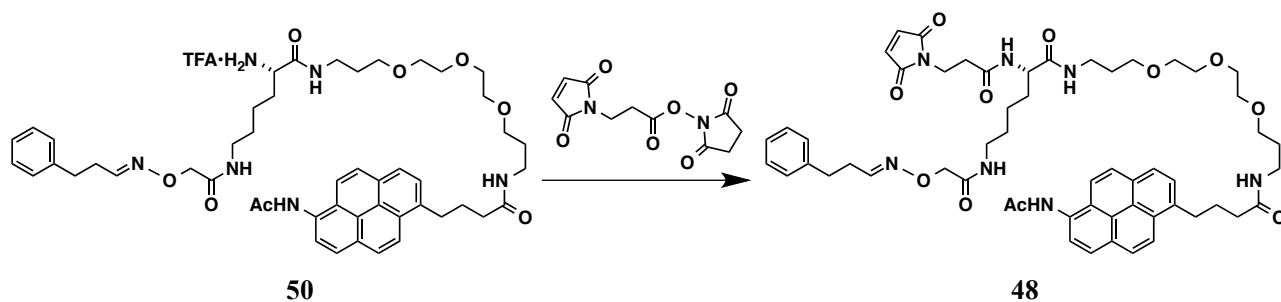
To *N*-succinimidyl 3-maleimidopropionate (0.4 mg, 2 μmol) and amine TFA salt **50** (0.221 mg, 230 nmol) in dry CH_2Cl_2 (0.4 mL) was added a solution of 0.14 M triethylamine in CH_2Cl_2 (2 μL). After being stirred for 20 h at room temperature, the resulting mixture was concentrated *in vacuo* and applied to a reversed-phase HPLC [Develosil ODS-HG-5 (20 mm I.D. × 250 mm), 5 mL/min, UV 254 nm, MeOH / 0.1% TFA (50:50), t_R = 20–23 min] to give model probe **48** (0.165 mg, 162 nmol, 70% based on NMR quantification, *E/Z* = 3/2). Compound **48**: t_R = 10.2 min [Develosil ODS-HG-5 (4.6 mm I.D. × 250 mm), MeOH / 0.1% TFA = (70:30), 1 mL/min, λ_{ex} 337 nm, λ_{em} 409 nm]; ^{1}H NMR (600 MHz, DMSO-d_6) δ 10.27 (s, 1H), 8.31 (d, *J* = 9.2 Hz, 1H), 8.25–8.23 (m, 3H), 8.20 (d, *J* = 7.8 Hz, 1H), 8.17 (d, *J* = 9.3 Hz, 1H), 8.15 (d, *J* = 9.3 Hz, 1H), 8.02 (d, *J* = 7.9 Hz, 1H), 7.92 (d, *J* = 7.8 Hz, 1H), 7.80 (br t, *J* = 4.9 Hz, 1H), 7.79 (br d, *J* = 4.4 Hz, 1H), 7.60 [7.48] (br t, *J* = 5.9 Hz, 1H), 7.54 [6.81] (t, *J* = 5.9 Hz, 1H), 7.29−7.16 (m, 5H), 6.98 (s, 2H), 4.29 [4.34] (s, 2H), 4.09 (td, *J* = 7.4, 7.4 Hz, 1H), 3.60–3.16 (m, 16H), 3.12−3.00 (m, 6H), 2.73 [2.76] (t, *J* = 7.6 Hz, 2H), 2.43 [2.64] (td, *J* = 7.7, 6.2 Hz, 2H), 2.40−2.37 (m, 2H), 2.27 (s, 3H), 2.22 (t, *J* = 7.4 Hz, 2H), 2.00 (tt, *J* = 7.4, 7.4 Hz, 2H), 1.62 (tt, *J* = 66, 6.6 Hz, 2H), 1.58 (tt, *J* = 6.7, 6.7 Hz, 2H), 1.60−1.53 (m, 1H), 1.48 (m, 1H), 1.35 (m, 2H), 1.23−1.12 (m, 2H). Chemical shifts of the minor *Z*-isomer are within parentheses (square brackets); HRMS (ESI) *m/z* 1038.4930 (calcd for $C_{56}H_{69}N_7NaO_{11}$ [M+Na]$^+$, Δ +1.7 mmu).
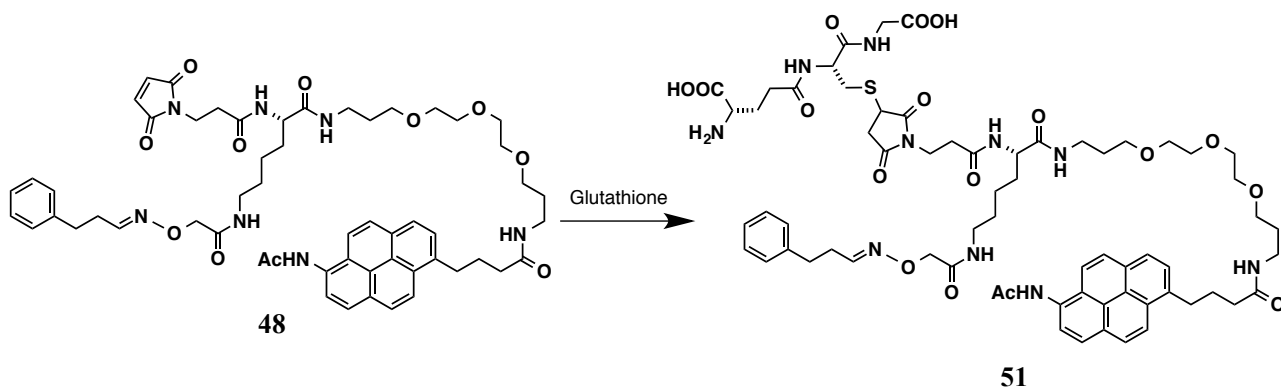
To 1 mM glutathione solution in water (50 μL, 50 nmol) was added 5 mM model probe **48** in DMSO (1 μL, 5 nmol). After incubation for 25.5 h at room temperature, the solution was freeze-dried and applied to a reversed-phase HPLC [Develosil ODS-HG-5 (4.6 mm I.D. × 250 mm), 1 mL/min, λ_{ex} 337 nm, λ_{em} 409 nm, MeCN/0.1% TFA (45:55), t_R = 4.5 min] to give glutathione-adduct **51** (5 nmol, quant., monitored by HPLC analysis). Compound **51**: HRMS (ESI) *m/z* 1323.5999 (calcd for $C_{66}H_{87}N_{10}O_{17}S$ [M+H]$^+$, Δ –3.3 mmu).

A solution of the aldehyde **10** prepared from ApA (466 μg, 433 nmol) and the alkoxyamine **49** (2.1 mg, 2.5 μmol) in a 3:1 mixture of EtOH and 50 mM acetate buffer (pH 4.0) (0.4 mL) was stirred at room temperature for 24.5 h. The reaction mixture was concentrated and applied to a Develosil ODS-HG-5 HPLC column (20 mm I.D. × 250 mm). Samples were eluted with MeOH / 20 mM NH$_4$OAc (80:20) at a flow rate of 5 mL/min and with monitoring at 254 nm to give amine **53** (271 nmol, 63%, based on NMR quantification, t_R = 31–37 min, E/Z = 7/3 for the C34 isomers). Compound **53**: t_R = 9.0 min [Develosil ODS-HG-5 (4.6 mm I.D. × 250 mm), MeOH / 20 mM NH$_4$OAc (80:20), 1 mL/min, λ_{ex} 337 nm, λ_{em} 409 nm]; ^{1}H NMR (600 MHz, CD$_3$OD) δ 8.35 (d, J = 9.3 Hz, 1H), 8.21 (d, J = 8.2 Hz, 1H), 8.17 (d, J = 9.0 Hz, 1H), 8.17 (d, J = 7.8 Hz, 1H), 8.15 (d, J = 9.3 Hz, 1H), 8.12 (d, J = 9.0 Hz, 1H), 8.12 (d, J = 8.2 Hz, 1H), 7.94 (d, J = 7.8 Hz, 1H), 7.55 [6.85][1] (dd, J = 6.4, 6.4 Hz, 1H), 7.19 (dd, J = 15.1, 10.9 Hz, 1H), 6.35 (m, 1H), 6.21 (m, 1H), 5.96 (d, J = 15.1 Hz, 1H), 5.61 (ddd, J = 15.0, 10.7, 3.8 Hz, 1H), 5.54 (br d, J = 11.8 Hz, 1H), 5.09 (m, 1H), 4.97 (m, 1H), 4.88−4.77 (m, 2H), 4.67 (m, 1H), 4.40 [4.45][1] (s, 2H), 3.98 (m, 1H), 3.68–3.64 (m, 2H), 3.56–3.48 (m, 7H), 3.50 (t, J = 6.0 Hz, 2H), 3.45 (m, 2H), 3.43–3.36 (m, 4H), 3.37 [3.38][2] (s, 3H), 3.34–3.17 (m, 9H), 3.18 (s, 3H), 3.14 [3.14][2] (s, 3H), 3.08 (dd, J = 9.2, 2.2 Hz,1H), 2.60–2.40 (m, 2H), 2.37 [2.38][2] (s, 3H), 2.37 [2.38][2] (s, 3H), 2.34 [2.32][1] [2.34][3] [2.33][1,3] (s, 6H), 2.38–2.22 (m, 5H), 2.19−2.13 (m, 3H), 2.06–1.96 (m, 4H), 2.04 [2.02][1] [2.04][3] [2.04][1,3] (s, 3H), 2.04 (s, 3H), 1.90−1.85 (m, 2H), 1.79–1.66 (m, 5H), 1.76 (tt, J = 6.5, 6.5 Hz, 2H), 1.69 (tt, J = 6.4, 6.4 Hz, 2H), 1.64–1.58 (m, 2H), 1.55–1.46 (m, 5H), 1.51 [1.52][2] (s, 3H), 1.46–1.22 (m, 14H), 1.16–1.09 (m, 3H), 1.03 (d, J = 6.7 Hz, 3H), 1.00 (d, J = 6.2 Hz, 3H), 0.97 (d, J = 6.2 Hz, 3H), 0.91 [0.89][2] (d, J = 7.0 Hz, 3H), 0.77−0.74 (m, 3H) Chemical shifts of the minor diastereomers are within parentheses as follows: [][1], 7:3 at C34 stereoisomers; [][2], 3:1 at C7 trimethylserine moiety; [][3], 1.4:1 at C29 dimethylalanine moiety; HRMS (ESI) m/z 883.5625 (calcd for (C$_{97}$H$_{154}$N$_8$O$_{21}$)/2 [M+2H]$^{2+}$, Δ −1.6 mmu).
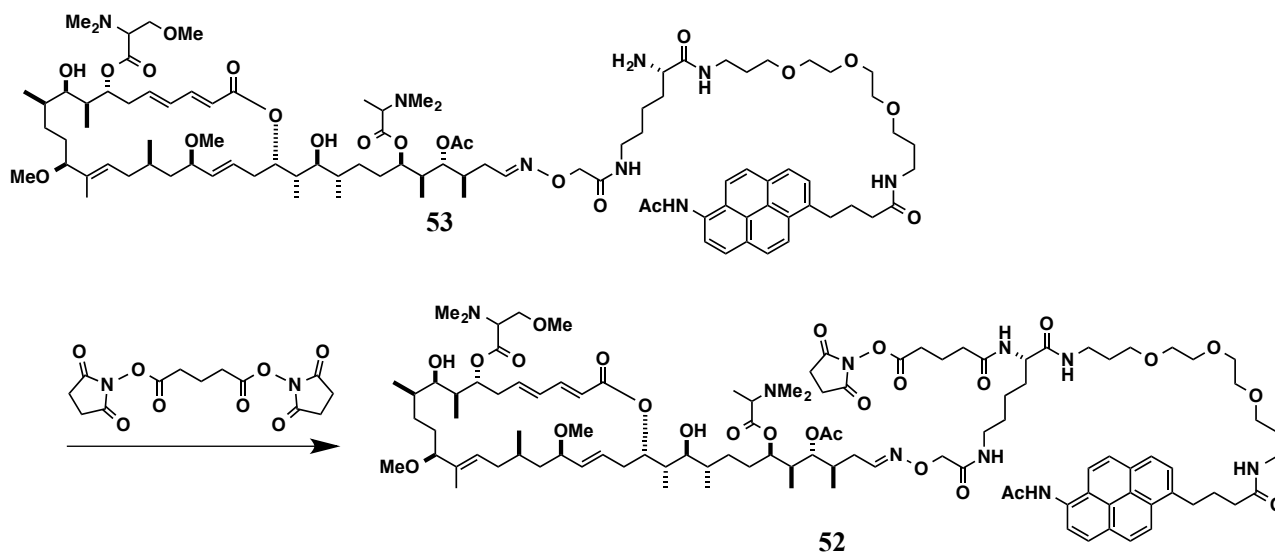
To a solution of amine **53** (99 μg, 50 nmol) in dry CH₂Cl₂ (100 μL) were added 64 mM *N,N'*-disuccinimidyl glutarate solution in dry CH₂Cl₂ (1 μL, 64 nmol) and 54 mM triethylamine in dry CH₂Cl₂ (2 μL, 108 nmol). The solution was stirred at room temperature for 50 min and concentrated *in vacuo* to give crude NHS ester probe **52**. Compound **52**: t_R = 10.7 min [Develosil ODS-HG-5 (4.6 mm I.D. × 250 mm), MeCN / 20 mM NH₄OAc (55:45), 1 mL/min, λ_{ex} 337 nm, λ_{em} 409 nm]; HRMS (ESI) *m/z* 989.0825 (calcd for $C_{106}H_{163}N_9O_{26}$ [M+2H]²⁺, Δ +2.4 mmu).

Compared the HPLC chart of starting material (Figure 3-36a) with the reaction mixture (Figure 3-36b), amine **53** was converted to probe **52** and primary amide **59** (Figure 3-37), which was generated by the reaction of **52** and NH₄⁺ during HPLC analysis. So, this conversion was considered as quantitatively, and protein- or glycine-labeling experiments were conducted without further purification.

Figure 3-36. Reversed-phase HPLC charts of (a) starting material and (b) the reaction mixture. (a) Column: Develosil ODS-HG-5 (4.6 mm I.D. × 250 mm), solvent: MeOH/20 mM NH$_4$OAc = 80/20, 1 mL/min, detection: λ_{ex} 337 nm, λ_{em} 409 nm. (b) Column: Develosil ODS-HG-5 (4.6 mm I.D. × 250 mm), solvent: MeCN/20 mM NH$_4$OAc = 55/45 , 1 mL/min, detection: λ_{ex} 337 nm, λ_{em} 409 nm.
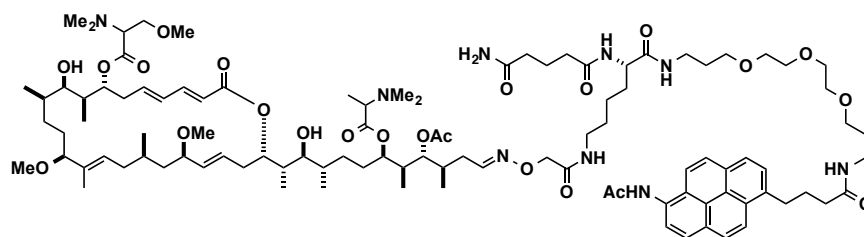
Figure 3-37. Structure of primary amide 59.

Gly-adduct **54**
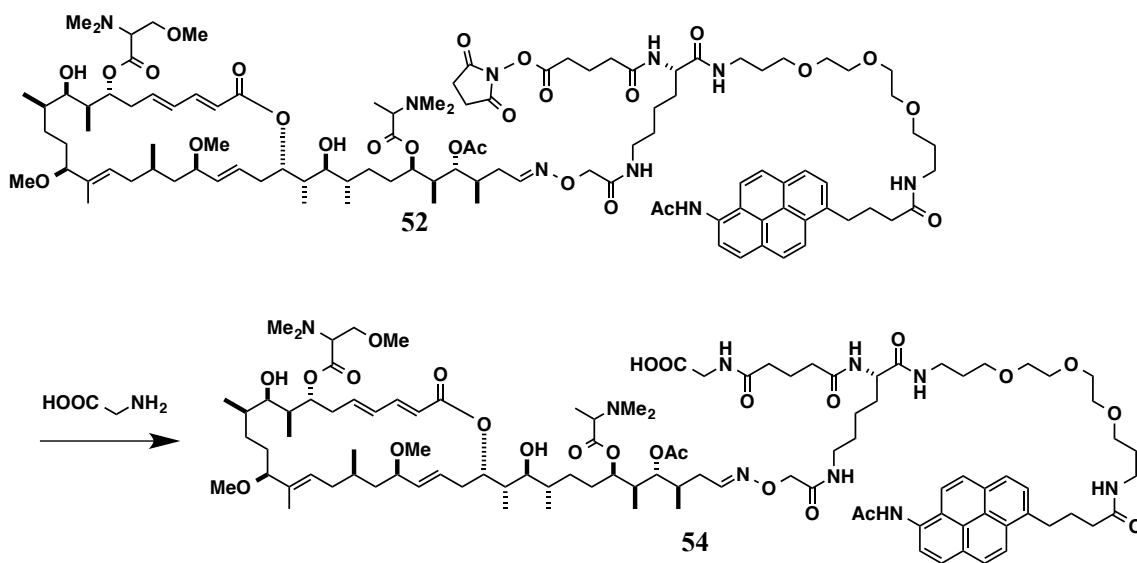
To 0.4 mM solution of glycine in water (50 μL, 20 nmol) was added 2 mM probe **52** in DMSO (1 μL, 2 nmol containing 8% of hydrolyzed product **60** [Figure 3-38]). After incubation for 25.5 h at room temperature, the solution was freeze-dried and applied to a reversed-phase HPLC [Develosil ODS-HG-5 (4.6 mm I.D. × 250 mm), 1 mL/min, λ_{ex} 337 nm, λ_{em} 409 nm, MeCN / 20 mM NH$_4$OAc (50:50), t_R = 5.4 min] to give Gly-adduct **54** (68%, based on the fluorescence in HPLC analysis, Figure 3-39) and **60** (23%). Compound **54**: MS (MALDI) *m/z* 1959.2 ([M+Na]$^+$).

Figure 3-38. Structure of carboxylic acid **60**.
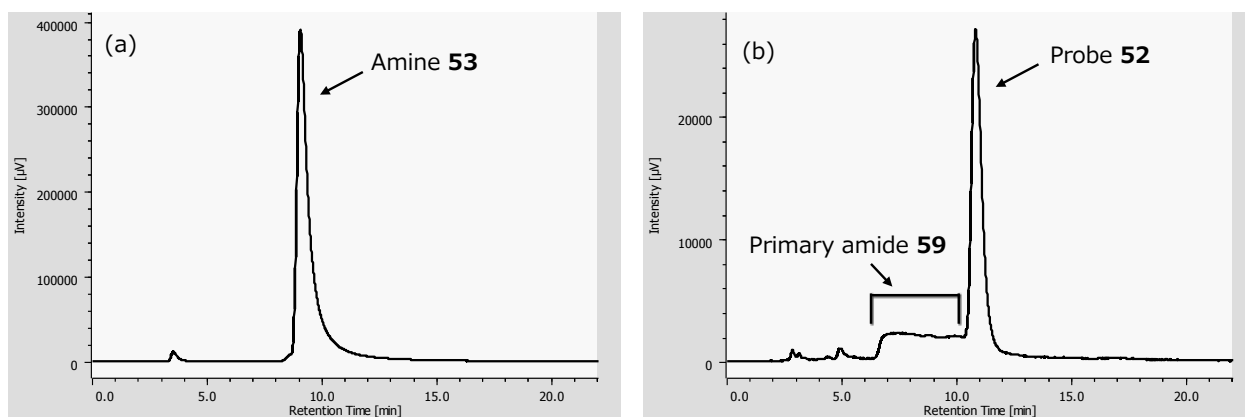

Figure 3-39. Reversed-phase HPLC chart of the reaction mixture. Column: Develosil ODS-HG-5 (4.6 mm I.D. × 250 mm), solvent: MeCN/20 mM NH$_4$OAc = 50/50 , 1 mL/min, detection: λ_{ex} 337 nm, λ_{em} 409 nm.
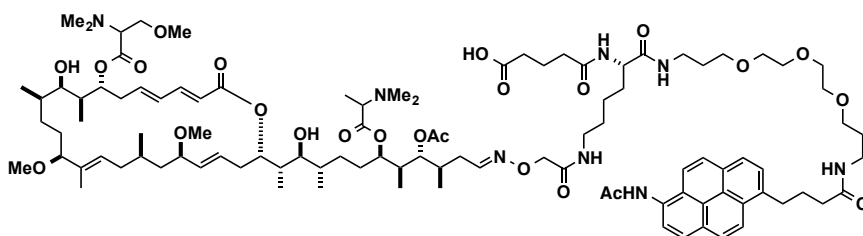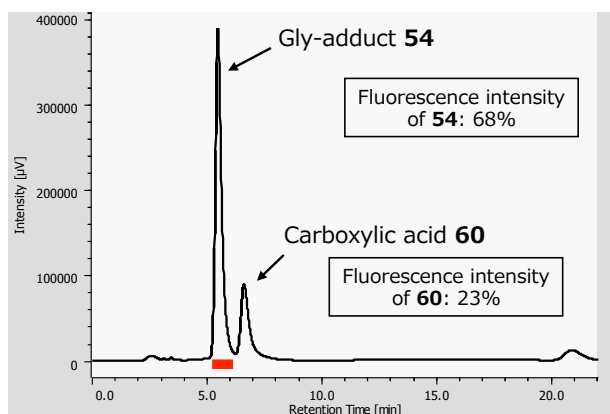
133

Model pyrene probe **56**
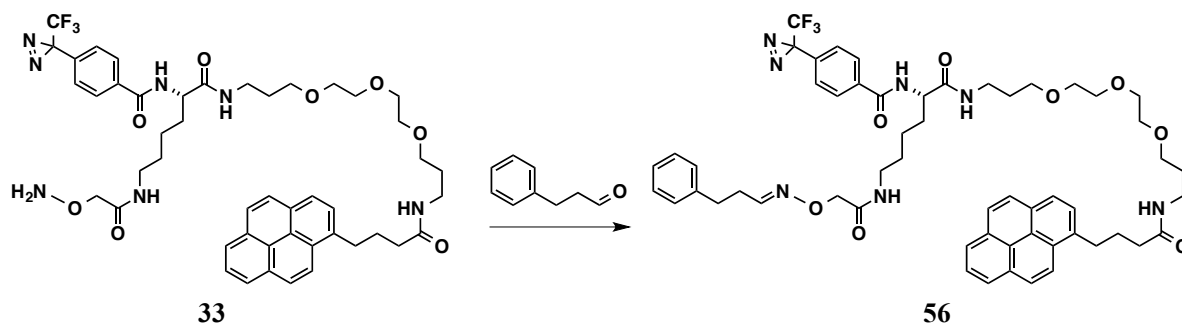
A solution of the alkoxyamine **33** (0.42 mg, 0.46 μmol) and 3-phenylpropanal (1.2 mg, 9.2 μmol) in a 3:1 mixture of EtOH and 100 mM acetate buffer (pH 4.0) (0.4 mL) was stirred at room temperature for 27.5 h. The reaction mixture was concentrated *in vacuo*. The crude sample was applied to a Develosil ODS-HG-5 HPLC column (20 mm I.D. × 250 mm). Samples were eluted with 72% MeCN at a flow rate of 5 mL/min and with monitoring at 254 nm (t_R = 50–54 min) to give model pyrene probe **56** (0.212 mg, 208 nmol, 45% based on NMR quantification). Compound **56**: t_R = 14.0 min [Develosil ODS-HG-5 (4.6 mm I.D. × 250 mm), 72% MeCN, 1 mL/min, λ_{ex} 337 nm, λ_{em} 409 nm]; ^{1}H NMR (400 MHz, CDCl$_3$) δ 8.29 (d, J = 9.3 Hz, 1H), 8.16 (br d, J = 8.0 Hz, 1H), 8.15 (br d, J = 7.8 Hz, 1H), 8.09 (d, J = 9.3 Hz, 1H), 8.09 (d, J = 7.8 Hz, 1H), 8.01 (s, 2H), 7.98 (dd, J = 7.6, 7.6 Hz, 1H), 7.85 (d, J = 8.4 Hz, 2H), 7.84 (d, J = 7.8 Hz, 1H), 7.46 [6.73] (t, J = 5.9 Hz, 1H), 7.30−7.14 (m, 8H), 6.92 (br s, 1H), 6.41 (br t, J = 5.2 Hz, 1H), 6.15 (br t, J = 5.7 Hz, 1H), 4.51 (ddd, J = 7.6, 7.6, 4.9 Hz, 1H), 4.39 [4.40] (d, J = 16.0 Hz, 1H), 4.31 [4.32] (d, J = 16.0 Hz, 1H), 3.54−3.12 (m, 20H), 2.79 (t, J = 7.6 Hz, 2H), 2.50 [2.68] (td, J = 7.7, 6.0 Hz, 2H), 2.27 (t, J = 6.8 Hz, 2H), 2.18 (tt, J = 7.1, 7.1 Hz, 2H), 1.91 (m, 1H), 1.82−1.66 (m, 1H), 1.76 (tt, J = 6.0, 6.0 Hz, 2H), 1.70 (tt, J = 6.0, 6.0 Hz, 2H), 1.51−1.20 (m, 4H). Chemical shifts of the minor *Z*-isomer are within parentheses (square brackets); HRMS (ESI) *m/z* 1042.4681 (calcd for C$_{56}$H$_{64}$F$_3$N$_7$NaO$_8$ [M+Na]$^+$, Δ −2.0 mmu).

56 → **55**
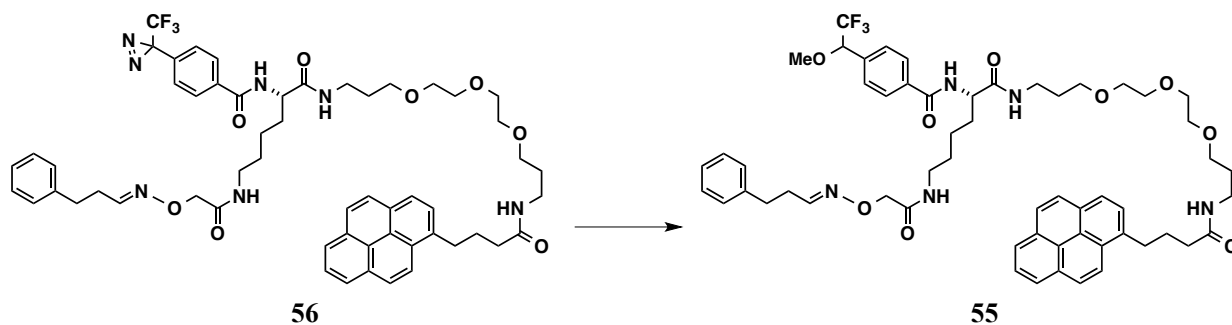
A model probe **56** (0.153 mg, 0.150 μmol) was dissolved in MeOH (6 mL) in two 5 mL glass vials. The solutions were cooled on ice and irradiated with UV light (365 nm) for 15 min, using a handheld UV lamp (0.8 mW/cm^2). The reaction mixtures were combined and concentrated *in vácuo*, and applied to a Develosil ODS-HG-5 HPLC column (20 mm I.D. × 250 mm). Sample was eluted with 85% MeOH at a flow rate of 5 mL/min and with monitoring at 254 nm (t_R = 43-47 min) to give the MeOH-adduct **55** (53.6 nmol, 36% based on the NMR quantification). Compound **55**: t_R = 10.9 min [Develosil ODS-HG-5 (4.6 mm I.D. × 250 mm), 85% MeOH, 1 mL/min, λ_{ex} 337 nm, λ_{em} 409 nm]; ^{1}H NMR (600 MHz, CDCl$_3$) δ 8.29 (d, J = 9.3 Hz, 1H), 8.16 (br d, J = 7.6 Hz, 1H), 8.15 (br d, J = 7.6 Hz, 1H), 8.09 (d, J = 9.3 Hz, 1H), 8.09 (d, J = 7.6 Hz, 1H), 8.02 (d, J = 9.0 Hz, 1H), 8.01 (d, J = 9.0 Hz, 1H), 7.98 (dd, J = 7.6, 7.6 Hz, 1H), 7.88 (d, J = 8.2 Hz, 2H), 7.85 (d, J = 7.6 Hz, 1H), 7.46 (d, J = 8.2 Hz, 2H), 7.46 [6.72][1] (t, J = 5.9 Hz, 1H), 7.29−7.15 (m, 6H), 6.92 (br t, J = 5.3 Hz, 1H), 6.46 (br s, 1H), 6.16 (br t, J = 6.2 Hz, 1H), 4.54 (ddd, J = 7.9, 7.9, 5.3 Hz, 1H), 4.49 [4.48][2] (q, J = 6.2 Hz, 1H), 4.38 [4.39][1] [4.38][2] [4.39][1,2] (d, J = 16.0 Hz, 1H), 4.31 [4.32][1] [4.31][2] [4.32][1,2] (d, J = 16.0 Hz, 1H), 3.55−3.13 (m, 20H), 3.50 [3.49][2] (s, 3H), 2.79 (t, J = 7.6 Hz, 2H), 2.50 [2.67][1] (td, J = 7.6, 6.0 Hz, 2H), 2.27 (t, J = 7.3 Hz, 2H), 2.18 (tt, J = 7.4, 7.4 Hz, 2H), 1.92 (m, 1H), 1.82−1.67 (m, 1H), 1.76 (tt, J = 6.3, 6.3 Hz, 2H), 1.71 (tt, J = 6.0, 6.0 Hz, 2H), 1.51−1.45 (m, 2H), 1.39−1.17 (m, 2H). Chemical shifts of the minor diastereomers are within parentheses as follows: [][1], 7:3 at oxime stereoisomers; [][2], 1:1 at methoxy group; HRMS (ESI) *m/z* 1046.4851 (calcd for C$_{57}$H$_{68}$F$_3$N$_5$O$_9$ [M+Na]^2+, Δ +1.0 mmu).

Model amidopyrene probe **58**

To a solution of diazirine succinyl ester **30** (0.69 mg, 2.1 μmol) in dry CH$_2$Cl$_2$ (0.2 mL) were added 144 mM triethylamine in dry CH$_2$Cl$_2$ (1 μL) and the amine TFA salt **50** (0.048 mg, 50 nmol). After being stirred for 9.5 h at room temperature, 144 mM triethylamine in dry CH$_2$Cl$_2$ (1 μL) was additionally added to the solution and stirred for 4 days and 21 h at room temperature. The resulting mixture was concentrated *in vacuo*. The crude material was purified by a reversed-phase HPLC [Develosil ODS-HG-5 (20 mm I.D. × 250 mm), 5 mL/min, UV 254 nm, MeOH/0.1% TFA (80:20), t_R = 38–41 min] to give model probe **58** (0.054 mg, 54 nmol, quant., based on NMR quantification, E/Z = 3/1). Compound **58**: t_R = 10.3 min [Develosil ODS-HG-5 (4.6 mm I.D. × 250 mm), MeOH / 0.1% TFA = (80:20), 1 mL/min, λ$_{ex}$ 337 nm, λ$_{em}$ 409 nm]; ^{1}H NMR (600 MHz, CD$_3$OD) δ 8.33 (d, J = 9.3 Hz, 1H), 8.19 (d, J = 8.2 Hz, 1H), 8.16 (d, J = 9.1 Hz, 1H), 8.15 (d, J = 7.7 Hz, 1H), 8.13 (d, J = 9.3 Hz, 1H), 8.11 (d, J = 8.2 Hz, 1H), 8.11 (d, J = 9.1 Hz, 1H), 7.92 (d, J = 8.3 Hz, 2H), 7.92 (d, J = 7.7 Hz, 1H), 7.51 [6.72] (t, J = 6.0 Hz, 1H), 7.30 (d, J = 8.3 Hz, 2H), 7.26−7.11 (m, 5H), 4.43 (dd, J = 8.9, 5.6 Hz, 1H), 4.34 [4.37] (s, 2H), 3.52–3.36 (m, 14H), 3.27–3.17 (m, 6H), 2.77 (t, J = 7.5 Hz, 2H), 2.44 [2.68] (td, J = 7.4, 6.0 Hz, 2H), 2.36 (s, 3H), 2.33 (t, J = 7.3 Hz, 2H), 2.15 (tt, J = 7.4, 7.4 Hz, 2H), 1.87−1.72 (m, 2H), 1.75 (tt, J = 6.5, 6.5 Hz, 2H), 1.69 (tt, J = 6.5, 6.5 Hz, 2H), 1.50 (m, 2H), 1.38 (m, 2H). Chemical shifts of the minor isomer are within parentheses (square brackets); HRMS (ESI) *m/z* 1099.4882 (calcd for C$_{58}$H$_{67}$F$_3$N$_8$NaO$_9$ [M+Na]$^+$, Δ −0.7 mmu).

58   **57**

A model amidopyrene probe **58** (65 μg, 60 nmol) was dissolved in MeOH (3 mL) in a 5 mL glass vial. The solutions were cooled on ice and irradiated with UV light (365 nm) for 15 min, using a handheld UV lamp (0.8 mW/cm^2). The reaction mixture was concentrated *in vacuo* and applied to a Develosil ODS-HG-5 HPLC column (20 mm I.D. × 250 mm). Sample was eluted with 80% MeOH at a flow rate of 5 mL/min and with monitoring at 254 nm to give the MeOH-adduct **57** (58.1 nmol, 32% based on the fluorescence in HPLC analysis). Compound **57**: t_R = 7.8 min [Develosil ODS-HG-5 (4.6 mm I.D. × 250 mm), 78% MeOH, 1 mL/min, λ_{ex} 337 nm, λ_{em} 409 nm]; ^{1}H NMR (600 MHz, CD$_3$OD) δ 8.34 (d, *J* = 9.3 Hz, 1H), 8.20 (d, *J* = 8.1 Hz, 1H), 8.16 (d, *J* = 9.2 Hz, 1H), 8.16 (d, *J* = 7.7 Hz, 1H), 8.13 (d, *J* = 9.3 Hz, 1H), 8.11 (d, *J* = 9.2 Hz, 1H), 8.11 (d, *J* = 8.1 Hz, 1H), 7.92 (d, *J* = 7.7 Hz, 1H), 7.92 (d, *J* = 8.2 Hz, 2H), 7.54 (d, *J* = 8.2 Hz, 2H), 7.51 [6.72] (t, *J* = 5.9 Hz, 1H), 7.25−7.13 (m, 5H), 4.87−4.77 (m, 1H), 4.45 (dd, *J* = 9.1, 5.4 Hz, 1H), 4.35 [4.36] (d [s], *J* = 15.8 Hz, 1H), 4.32 [4.36] (d [s], *J* = 15.8 Hz, 1H), 3.52–3.37 (m, 14H), 3.35 (s, 3H), 3.27–3.17 (m, 6H), 2.75 (t, *J* = 7.6 Hz, 2H), 2.44 [2.69] (td, *J* = 7.7, 5.9 Hz, 2H), 2.36 (s, 3H), 2.34 (t, *J* = 7.4 Hz, 2H), 2.15 (tt, *J* = 7.3, 7.3 Hz, 2H), 1.87−1.72 (m, 2H), 1.74 (tt, *J* = 6.5, 6.5 Hz, 2H), 1.69 (tt, *J* = 6.2, 6.2 Hz, 2H), 1.54−1.32 (m, 4H). Chemical shifts of the minor isomer are within parentheses (square brackets); HRMS (ESI) *m/z* 1103.5105 (calcd for C$_{59}$H$_{71}$F$_3$N$_6$NaO$_{10}$ [M+Na]$^+$, Δ −2.9 mmu).

References

1. (a) Deng, Z; Chuaqui, C; Singh, J. *J. Med. Chem.* **2004,** *47,* 337−344. (b) Ueda, M. *Chem. Lett.* **2012**, *41*, 658–666.

2. (a) Das, J. *Chem. Rev.* **2011**, *111*, 4405–4417. (b) Dubinsky, L.; Krom, B. P.; Meijler, M. M. *Bioorg. Med. Chem.* **2012**, *20*, 554–570.

3. Karas, M.; Bachmann, D.; Hillenkamp, F. *Anal. Chem.* **1985**, 57, 2935–2939.

4. (a) Robins, C.; Limbach, P. A. *Rapid Commun. Mass Spec.* **2003**, *17*, 2839–2845. (b) Petroselli, G. Mandal, M. K.; Chen, L. C.; Ruiz, G. T.; Wolcan, E.; Hiraoka, K.; Nonami, H.; Erra-Balsells, R. *J. Mass Spectrom.* **2012**, *47*, 313–321. (c) Martinez–Haya, B.; Hortal, A. R.; Hurtado, P.; Lobato, M. D.; Pedrosa, J. M. *J. Mass Spectrom.* **2007**, *42*, 701–713. (d) Macha, S. F.; McCarley, T. D.; Limbach, P. A. *Anal. Chim. Acta,* **1999** *397*, 235–245.

5. Cabrera–Pardo, J. R.; Chai, D. I.; Liu, S.; Mrksich, M.; Kozmin, S. A. *Nat. Chem.* **2013**, *5*, 423–427.

6. (a) West, R. E. III; Findsen, E. W.; Isailovic, D. *Int. J. Mass Spec.* **2013**, *353*, 54–59. (b) Addy, P. S.; Roy, S. B.; Mandal, S. M.; Basak, A. *RSC Adv.* **2014**, *4*, 23314–23318. (c) Addy, P. S.; Bhattacharya, A.; Mandal, S. M.; Basak, A. *RSC Adv.* **2014**, *4*, 46555–46560.

7. Wilbur, S. D.; Pathare, P. M.; Weerawarna, S. A.; Hamlin, D. K. *PCT Int. Appl.* WO9729114.

8. Tam, T. F.; Karimian, K.; Leung-Toung, R. C. S. H.; Zhao, Y.; Wodzinska, J. M.; Li, W.; Lowrie, J. N. *Eur. Pat. Appl.* EP1348710.

9. Clavé, G.; Boutal, H.; Hoang, A.; Perraut, F.; Volland, H.; Renard, P.; Romieu, A. *Org. Biomol. Chem.* **2008**, *6*, 3065−3078.

10. Strømgaard, K.; Saito, R. D.; Shindou, H.; Ishii, S.; Shimizu, T.; Nakanishi, K. *J. Med. Chem.* **2002**, *45*, 4038−4046.

11. Kanoh, N.; Nakamura, T.; Hondaa, K.; Yamakoshib, H.; Iwabuchi, Y.; Osada, H. *Tetrahedron* **2008**, *64*, 5692–5698.

12. Attri, A. K.; Lewis, M. S.; Korn, E. D. *J. Biol. Chem.* **1991**, *266*, 6815−6824.

13. Boszczyk, W.; Latowski, T. *Z. Naturforsch.* **1989**, *B 44,* 1589–1592.

14. (a) Lee, T. A. in *A Beginner's Guide to Mass Spectral Interpretation*; John Wiley & Sons, Chichester, England **1998**, pp. 106–116. (b) Shapiro, R. H.; Tomer, K. B. *Org. Mass Spectrom.* **1969**, *2*, 579–590. (c) Ohashi, M.; Kizaki, T.; Tsujimoto, K.; Shida, Y.; Yamada, Y. *J. Mass Spectrom. Soc. Jpn.* **1973**, *21*, 85–90.

15. Zhao, G. –J.; Han, K. –L. *Acc. Chem. Res.* **2012**, *45*, 404–413.

16. Zhao, G. –J.; Liu, J. –Y.; Zhou, L. –C.; Han, K. –L. *J. Phys. Chem. B* **2007**, 111, 8940–8945.

17. Tsukiji, S.; Hamachi, I. *Methods in Mol. Biol.* **2015**, *1266*, 243-263.

Chapter 4. Conclusion

Natural products, which show unique bioactivities, are highly useful as medicinal drugs, agrochemicals, and research tools. Antitumor macrolide aplyronine A (ApA) is one of them.

To clarify the mode of action of ApA, the author conducted chemical probe approach in chapter 2. It was revealed that ApA accumulated into the whole cytoplasm and interacted with tubulin as an actin−ApA complex. Furthermore, the author established that ApA caused irregular spindle formation, cell cycle arrest and apoptosis in tumor cells. It was found that the formation of the actin−tubulin−ApA ternary complex inhibited microtubule dynamics. Especially the C7 trimethylserine ester moiety was important for the interaction with tubulin.

Therefore, ApA induces the protein-protein interaction (PPI) of actin and tubulin by the binding to actin through the C24−C34 side chain moiety and by the effect of C7 trimethylserine ester moiety on tubulin (Figure 4-1). This PPI induced by ApA was expected to be important for the potent antitumor activity.
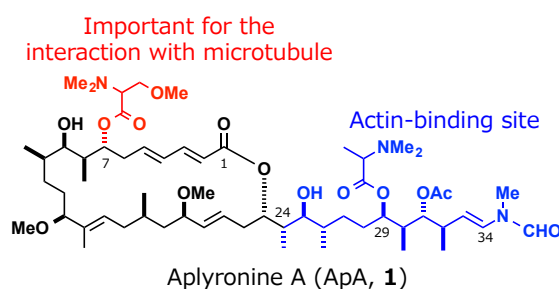

Aplyronine A (ApA, **1**)

Figure 4-1. Important part of ApA for tits unique activity

Microtubule is a typical target of antitumor drug. Several natural products and their derivatives that target microtubule have been approved as medicinal drugs or have undergone clinical evaluation.[1] Vinblastine (Figure 4-2a),[2] one of the vinca alkaloids and microtubule-depolymerizing compounds, binds between two tubulin heterodimer units of microtubule (+) ends (Figure 4-3b), and is approved for lymphomas and various solid tumors. Paclitaxel (Figure 4-2b),[3] a tubulin-polymerizing compound, binds to β-tubulin along the inner side of the microtubules, and is approved for ovarian, breast and non-small cell lung cancers. Many compounds, which show similar binding modes to them, are approved or in clinical trials. Additionally, colchicine (Figure 4-2c),[4] a microtubule-depolymerizing compound, binds between free tubulin heterodimer, which are incorporated in the microtubules, not same as vinblastine and paclitaxel. And, several compounds bound to the same site of tubulin as colchicine are in clinical trials. Thus, microtubule-targeting compounds are known to interact with several sites of tubulin and control microtubule dynamics in several manners. Therefore, these compounds are used as the research tools for molecular and cell biology with tubulin as well as medicinal drugs.
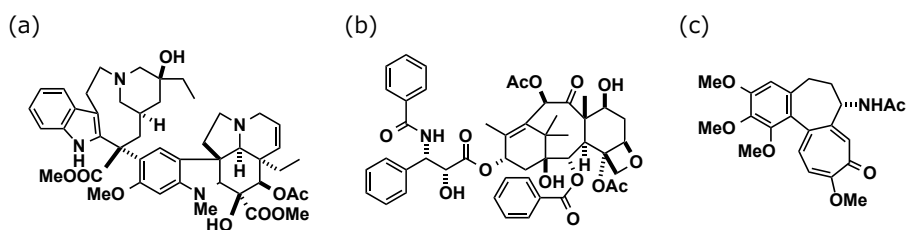
Figure 4-2. Structures of (a) vinblastine, (b) paclitaxel, and (c) colchicine
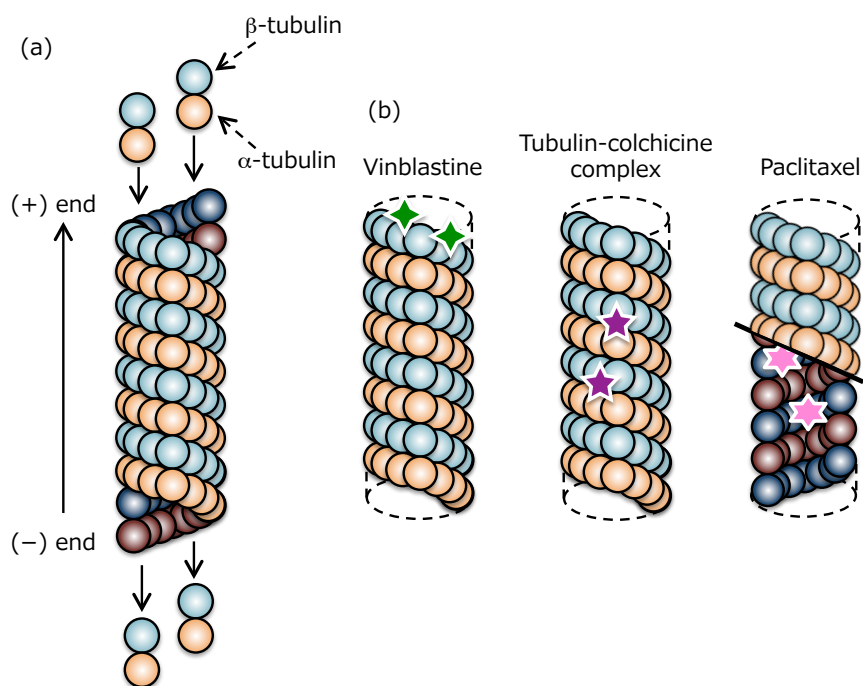

Figure 4-3. Interaction of microtubule-targeting compounds with microtubule. (a) Polymerization and depolymerization of microtubule. (b) Binding modes of compounds with microtubule. Stars show each compound. Light color shows the outside of microtubule, and dark color shows the inner side.

Compared with the cell-growth inhibitory activity against tumor cells, ApA has stronger activity than vinblastine, paclitaxel and colchicine. The reason is not clear yet, but is possibly due to the binding mode of ApA on tubulin and microtubule. Additionally, PPI of two cytoskeletal proteins, actin and tubulin, induced by ApA was a new finding. Therefore, clarification of the binding mode of actin−ApA complex with tubulin would lead to the development of novel antitumor drugs and new research tools that simultaneously control actin and microtubule dynamics.

However, it is thought to be difficult to analyze the binding mode by using the typical methods, such as X-ray and NMR analysis, due to the dynamic instability of actin and tubulin. So, novel chemical probe method that the author described in chapter 3 is expected to be very useful. This probe has an amidopyrene group and an NHS ester moiety, and thus actin was efficiently labeled. Additionally, the author succeeded to determine the ApA-binding position of the actin−probe complex by LA-LDI MS analysis. In the future, further improvement of detectability of an ApA amidopyrene probe would enable the author to clarify the binding modes on the actin−ApA complex with tubulin.

By determination of the detail binding mode of actin−ApA complex on tubulin, conformation of the C7 trimethylserine group and other important groups to interact with tubulin could be clarified. These results provide the author the information to simplify the structure of ApA, and the artificial analogs that induce PPI between actin and tubulin could be designed. These analogs are expected to facilitate the application for medicinal drugs or pharmaceutical tools of ApA.

Based on the above discussion, this study was able to not only show the further possibility of ApA to develop antitumor drugs or research tools, but also provide us novel methods that are available for the analysis of the interaction with target proteins. Therefore, the author expects that this study would contribute to the drug discovery of natural products and the development of chemical biology and molecular biology.

References

1. Dumontet, C.; Jordan, M. A. *Nat. Rev. Drug Discovery* **2010**, *9*, 790–803.

2. Gigant, B.; Wang, C.; Ravelli, R. B. G.; Roussi, F.; Steinmetz, M. O.; Curmi, P. A.; Sobel, A.; Knossow, M. *Nature* **2005**, *435*, 519−522.

3. Nogales, E.; Wolf, S. G.; Khan, I. A.; Luduena, R. F.; Downing, K. H. *Nature* **1995**, *375*, 424−427.

4. Ravelli, R. B. G.; Gigant, B.; Curmi, P. A.; Jourdain, I.; Lachkar, S.; Sobel, A; Knossow, M. *Nature* **2004**, *428*, 198-202.

List of Publications

1) Kita, M.; Yoneda, K.; Hirayama, Y.; Yamagishi, K.; Saito, Y.; Sugiyama, Y.; Miwa, Y.; Ohno, O.; Morita, M.; Suenaga, K.; Kigoshi, H. Fluorescent Aplyronine A: Intracellular Accumulation and Disassembly of Actin Cytoskeleton in Tumor Cells. *ChemBioChem* **2012**, *13*, 1754–1758.

2) Yoneda, K.; Hu, Y.; Kita, M.; Kigoshi, H. 6-Amidopyrene as a label-assisted laser desorption/ionization (LA-LDI) enhancing tag: development of photoaffinity pyrene derivative. *Sci. Rep.* **2015**, *5*, 17853, [DOI: 10.1038/srep17853].

Supplementary List of Publications

1) Kita, M.; Hirayama, Y.; Yamagishi, K.; Yoneda, K.; Fujisawa, R.; Kigoshi, H. Interactions of the Antitumor Macrolide Aplyronine a with Actin and Actin-Related Proteins Established by its Versatile Photoaffinity Derivatives. *J. Am. Chem. Soc.* **2012**, *134*, 20314–20317.

2) Kita, M.; Hirayama, Y.; Yoneda, K.; Yamagishi, K.; Chinen, T.; Usui, T.; Sumiya, E.; Uesuigi, M.; Kigoshi, H. Inhibition of Microtubule Assembly by a Complex of Actin and Antitumor Macrolide Aplyronine A. *J. Am. Chem. Soc.* **2013**, *135*, 18089–18095.

3) Ohno, O.; Morita, M.; Kitamura, K.; Teruya, T.; Yoneda, K.; Kita, M.; Kigoshi, H.; Suenaga, K. Apoptosis-Inducing activity of the actin-depolymerizing agent aplyronine A and its side-chain derivatives. *Bioorg. Med. Chem. Lett.* **2013**, *23*, 1467–1471.